



The
University
Of
Sheffield.

**Breast cancer extracellular vesicles transfer viral cargo following
oncolytic virotherapy**

By: Hyfa Ahmed Alzahrani

A thesis submitted in partial fulfilment of the requirements for the degree of
Doctor of Philosophy

The University of Sheffield
Faculty of Medicine, Dentistry and Health
School of Medicine
Department of Oncology and Metabolism

July 2022

Acknowledgements

To begin with, I give my utmost praise, thankfulness, and gratitude to **ALLAH**, the most merciful, for granting me the delightful opportunity to undertake this research and granting me the set of skills of determination, strength, and patience to persevere until the end of this journey. I could not have done this research without his endless showers of mercy.

Second, I would like to express my gratitude to Dr. Munitta Muthana for all the unconditional support and encouragement she provided me over the course of these years, as well as for serving as a model of what a great supervisor is. In addition, I give my thanks to Dr. Stuart Hunt for the endless support given during the entirety of this research. Thanks to Matthew Fisher for offering to help with the animal work and Dr. Lewis Quayle for help on NanoString analysis and the Muthana team for their support. I appreciate Dr. Haider ALjanabi's constant compassion, generosity, and commitment to bringing light into the shadows.

Third, I thank my husband for his support during my study and my lovely, gorgeous daughters, Remas, and Renad, for accompanying me through life's positive and negative fluctuations and always striving to make the darkest days the brightest ones. There are many reasons why I admire and value my mother, but not enough pages in the world to list them all. Nevertheless, one reason is that she frequently prays for me from the depths of her heart and wishes me the best. In addition, I appreciate my sisters for their love, support and encouragement when I could not give that to myself. I acknowledge that my father could not witness these academic years, but I know that he would be proud of his daughter.

The subsequent names are my companions who aided and comforted me through my battles and kept me steadfast on the path of victory in times I felt retreating. Their words of encouragement and their presence in my life made completing this research more proficient. I am grateful to them: Hanadi, Alaa, Nashwa, Hatoon, Marwa and Ahmed.

To conclude, my final thanks go to Saudi Arabia Cultural Bureau for funding this research and making this study possible.

Table of Contents

ACKNOWLEDGEMENTS	1
TABLE OF CONTENTS	2
LIST OF ABBREVIATIONS	5
LIST OF FIGURES	8
LIST OF TABLES	9
ABSTRACT	10
CHAPTER 1: INTRODUCTION AND LITERATURE REVIEW	11
1.1 BREAST CANCER.....	12
1.1.1 <i>Subtypes of breast cancer</i>	12
1.1.2 <i>Current treatment strategies for breast cancer</i>	13
1.2 OVERVIEW OF ONCOLYTIC VIROTHERAPY	15
1.2.1 <i>The mechanism of action of HSV on tumour cells</i>	16
1.2.2 <i>Development of oncolytic HSV in clinical trials</i>	17
1.2.3 <i>The role of HSV in tumour microenvironment (TME)</i>	18
1.3 EXTRACELLULAR VESICLES.....	21
1.3.1 <i>Biogenesis of the extracellular vesicles</i>	22
1.4 ISOLATION OF EVS.....	26
1.5 UPTAKE OF EXTRACELLULAR VESICLES AND SIGNALLING	28
1.5 ROLE OF EVS IN CANCER AND HEALTH.....	29
1.6 HYPOTHESIS AND AIMS	32
CHAPTER 2: MATERIALS AND METHODS	33
2.1 MATERIALS AND METHODS	34
2.1.1 <i>Chemicals and Reagents</i>	34
2.1.2 <i>Equipment and Apparatus</i>	35
2.1.3 <i>List of Antibodies</i>	36
2.1.4 <i>List of software</i>	37
2.1.5 <i>Culturing of breast cancer cells</i>	38
2.1.6 <i>Passaging of mammalian cells</i>	38
2.1.7 <i>Cryopreservation and retrieval of cells</i>	39
2.1.8 <i>Mycoplasma testing of cell-lines</i>	40
2.1.9 <i>Cell counting</i>	40
2.1.10 <i>Depletion of bovine EVs from FBS</i>	41
2.1.11 <i>Viral infection</i>	42
2.1.12 <i>Extracellular vesicle collection</i>	43
2.1.13 <i>Transmission Electron Microscopy (TEM)</i>	43
2.1.14 <i>Nanoparticle tracking analysis (NTA)</i>	44
2.1.15 <i>Plaque assay</i>	45
2.1.16 <i>Assessment of cell proliferation and survival</i>	46
2.1.17 <i>Scratch (wound healing) assay</i>	47
2.1.18 <i>Cell death and uptake of EVs</i>	48
2.1.19 <i>Western blot analysis</i>	48
2.1.20 <i>Labelling of extracellular vesicles with Alexa fluor 488</i>	51
2.1.21 <i>Label-free mass spectrometry</i>	52
2.1.22 <i>Flow cytometry to assess EVs uptake and cell death in tumour cells MCF-7 and MDA-MB-231</i>	53
2.1.23 <i>In Vivo</i>	53

2.1.24	Statistical analysis.....	58
CHAPTER 3: CHARACTERISATION OF EXTRACELLULAR VESICLES AND EXTRACELLULAR VESICLES DERIVED FROM OV INFECTED TUMOUR CELLS CARRY VIRAL CARGO.....		
59		
3.1	INTRODUCTION.....	60
3.1.1	Hypothesis.....	60
3.1.2	Aims.....	61
3.2	RESULTS.....	61
3.2.1	OV induced breast cancer cell oncolysis.....	61
3.2.2	Characterisation of EVs released from MCF-7 and MDA-MB-231 cells after ultracentrifugation by nanoparticle tracking analysis (NTA).....	64
3.2.3	Characterization of MCF-7 and MDA-MB-231 derived EVs using transmission electron microscopy (TEM).....	67
3.2.4	MCF-7 and MDA-MB-231 derived EV-OV do not contain contaminating free virus.....	68
3.2.5	Characterisation of breast cancer derived extracellular EVs.....	70
3.2.6	Culture of purified EVs with breast cancer cells induces cell death.....	74
3.2.7	EV uptake by breast cancer cells: Flow cytometry.....	76
3.2.8	EV uptake by breast cancer cells: Immunofluorescence.....	80
3.2.9	EV-OV suppress migration of MDA-MB-231.....	82
3.3	DISCUSSION.....	84
3.3.1	OV induced oncolysis of breast cancer cells.....	84
3.3.2	NTA assessment of tumour cell derived EVs size and concentration.....	84
3.3.3	EVs purified from OV infected breast cancer cells express exosome markers and carry viral cargo.....	85
3.3.4	EV-OV are taken up by tumour cells and inhibit tumour cell migration.....	87
CHAPTER 4: MASS SPECTROSCOPY ANALYSIS OF EXTRACELLULAR VESICLES DERIVED FROM HSV1716 INFECTED BREAST CANCER CELLS.....		
89		
4.1	INTRODUCTION.....	90
4.2	RESULTS.....	91
4.2.1	Label-free mass spectrometry.....	91
4.2.2	Proteome profiling of MDA-MB-231 derived EV versus MDA-MB-231 derived EV-OV.....	91
4.2.3	Differential expression of proteins.....	93
4.2.4	Functional Characterisation of Identified Proteins.....	97
4.2.5	Label-free mass-spectrometry validation.....	100
4.3	DISCUSSION.....	102
CHAPTER 5: ANTITUMOUR ACTIVITY OF EXTRACELLULAR VESICLES DERIVED FROM INFECTION BREAST CANCER CELLS.....		
106		
5.1	INTRODUCTION.....	107
5.2	RESULTS.....	108
5.2.1	The antitumour efficacy of EV-OV in the E0771 mammary carcinoma model.....	108
5.2.2	Biodistribution of EV-OV in mice of the harvested tumour and organs.....	110
5.2.3	EV-OV shrinks primary mammary tumours.....	113
5.2.4	EV-OV does not induce changes in pro-inflammatory cytokines and anti-inflammatory cytokines.....	114
5.2.5	EV-OV possess anti-tumour properties.....	118
5.2.6	Successful fluorescent EVs isolation from mice serum.....	120
5.3	DISCUSSION.....	127
5.3.1	Biodistribution of EVs to the tumour.....	127
5.3.2	Extracellular vesicles derived from OV infected cells shrink primary mammary tumours.....	127
5.3.3	EV-OV induces anti-tumour properties.....	128
5.3.4	Successful detection of fluorescent EVs isolation from mice serum after infection with OV.....	129

5.3.5	<i>EV-OV treated tumours induce expression of immune-related genes</i>	129
CHAPTER 6:	SUMMARY OF KEY FINDINGS AND GENERAL CONCLUSION	131
6.1	SUMMARY OF MAIN OUTCOMES AND GENERAL CONCLUSION	132
6.2	LIMITATION OF THE STUDY	141
6.3	FUTURE WORK.....	142
REFERENCES		145

List of Abbreviations

(CAFs)	Cancer-associated fibroblasts
---------------	-------------------------------

(DG)	Density gradient
-------------	------------------

(DCIS)	Ductal carcinoma in situ
---------------	--------------------------

(DMEM)	Dulbecco's Modified Eagle's Medium
---------------	------------------------------------

(DMSO)	Dimethyl Sulfoxide
---------------	--------------------

(DPBS)	Dulbecco's Phosphate Buffered Saline
---------------	--------------------------------------

(dUC)	differential ultracentrifugation
--------------	----------------------------------

(EDTA)	Ethylenediaminetetraacetic acid
---------------	---------------------------------

EVs	Extracellular Vesicles
------------	------------------------

(EGFR)	Epidermal Growth Factor Receptor
---------------	----------------------------------

(ECM)	Extracellular Matrix
--------------	----------------------

(FACS)	Fluorescence-activated cell sorting
---------------	-------------------------------------

(FBS)	Foetal Bovine Serum
--------------	---------------------

(FDA)	Food and Drug Administration
--------------	------------------------------

(FSC)	Forward scatter
--------------	-----------------

(GFP)	Green fluorescent protein
--------------	---------------------------

(GM-CSF)	Granulocyte macrophage-colony stimulating factor
-----------------	--

(HER2)	Human epidermal growth factor
---------------	-------------------------------

(HSV)	Herpes simplex virus
--------------	----------------------

(ILVs)	Intraluminal vesicles
---------------	-----------------------

(IL-12)	Interleukin 12
----------------	----------------

(ICIs)	Immune checkpoint inhibitors
---------------	------------------------------

(MOI)	Multiplicity of Infection
--------------	---------------------------

(MRI)	Magnetic resonance imaging
--------------	----------------------------

(MV)	Microvesicles
-------------	---------------

(MVBs)	Multivesicular bodies
---------------	-----------------------

(NTA)	Nanoparticle tracking analysis
--------------	--------------------------------

(NPC)	Nuclear pore complex
--------------	----------------------

(OV)	Oncolytic viruses
(PBS)	Phosphate Buffered Saline
(PFU)	Particle Forming Units
(RPMI)	Roswell Park Memorial Institute
(RT)	Room temperature
(SSC)	Side scatter
(SEC)	Size-exclusion chromatography
(TEM)	Transmission electron microscopy
(TNBS)	Triple negative breast cancer
(TSG101)	Tumour susceptibility gene 101 protein
(TME)	Tumour microenvironment
(UF)	Ultrafiltration
(VSV)	Vesicular stomatitis virus

List of Figures

FIGURE 1.1: AN ILLUSTRATION OF THE PARTICLE STRUCTURE OF THE HERPES SIMPLEX VIRUS.	17
FIGURE 1.2: BREAST CANCER TUMOUR MICROENVIRONMENT.	20
FIGURE 1.3: EXTRACELLULAR VESICLES: EXOSOMES, MICROVESICLES AND APOPTOTIC BODIES.	22
FIGURE 1.4: EXTRACELLULAR VESICLES FACILITATE CELL-TO-CELL COMMUNICATION BY TRANSPORTING BIOACTIVE SUBSTANCES ACROSS THE CELL MEMBRANE (PROTEINS, LIPIDS AND NUCLEIC ACIDS)..	29
FIGURE 2.1: PCR BASED MYCOPLASMA DETECTION RESULTS.	40
FIGURE 2.2: FBS PARTICLE CONCENTRATION IN UNPROCESSED SERUM, IN-HOUSE DEPLETED SERUM	42
FIGURE 2.3: A DIAGRAM OF AN ULTRACENTRIFUGATION PROCEDURE.....	43
FIGURE 2.4: SERIAL DILUTION OF HSV-1716 STOCK..	45
FIGURE 2.5: BCA STANDARD CURVE EXAMPLE..	50
FIGURE 2.6: ISOLATION OF LABELLED EVs FROM BLOOD SERUM COLLECTED FROM TREATED MICE..	56
FIGURE 3.1: EVs PURIFIED FROM MDA-MB-231 USING dUC EXPRESS TYPICAL EV MARKERS AND CARRY VIRAL CARGO..	74
FIGURE 3.2: MCF-7 DERIVED EV AND EV-OV INDUCED CYTOTOXICITY ON MCF-7 CELLS..	75
FIGURE 3.3: MDA-MB-231 DERIVED EV AND EV-OV INDUCED CYTOTOXICITY ON MDA-MB-231 CELLS.	76
FIGURE 3.4: EV-OV INDUCE MCF-7 CELL UPTAKE.	78
FIGURE 3.5: EV-OV INDUCE MDA-MB-231 CELL UPTAKE.	79
FIGURE 3.6: EV-OV CONTAIN VIRAL CARGO AS EVIDENCED BY STAINING OF MCF-7 CELLS.	81
FIGURE 3.7: EV-OV CONTAIN VIRAL CARGO AS EVIDENCED BY STAINING OF MDA-MB-231 CELLS.	82
FIGURE 3.8: MDA-MB-231 DERIVED EV-OV INHIBIT CELL MIGRATION IN MDA-MB-231 CELLS.	83
FIGURE 4.1: HISTOGRAM OF LFQ INTENSITY COLUMNS FOR REPLICATES OF MDA-MB-231 DERIVED EV AND EV-OV.	92
FIGURE 4.2: VOLCANO PLOT SHOWING EV PROTEINS DIFFERENTIALLY REGULATED FOLLOWING INFECTION WITH OV.	96
FIGURE 4.3 : GENE ONTOLOGY ENRICHMENT ANALYSIS OF EXTRACELLULAR VESICLES COMPARED TO THE HUMAN GENOME.....	98
FIGURE 4.4 : AN EXAMPLE OF SUBSTANTIALLY ENRICHED PROTEINS CLASSIFIED INTO DIFFERENT PATHWAYS.	99
FIGURE 4.5: MASS SPECTROMETRY VALIDATION OF DIFFERENTIALLY EXPRESSED PROTEINS USING WESTERN BLOTTING.	101
FIGURE 5.1: TREATMENT SCHEME IN C57BL/6 FEMALE MICE WITH MAMMARY CARCINOMA.	110
FIGURE 5.2: EO771 BREAST CANCER DERIVED EVs PREFERENTIALLY ACCUMULATE IN MAMMARY TUMOURS FOLLOWING SYSTEMIC DELIVERY.	112
FIGURE 5.3: EV-OV SHRINKS PRIMARY MAMMARY TUMOURS.....	114
FIGURE 5.4: REPRESENTATIVE DOT PLOT OF CYTOKINE STANDARDS.	117
FIGURE 5.5: EFFECT OF EV-OV CYTOKINES ANALYSIS IN PRO-INFLAMMATORY OR ANTI-INFLAMMATORY CYTOKINES ON MURINE MICE SERUM.	118
FIGURE 5.6: EV-OV INCREASES TUMOUR NECROSIS.....	120
FIGURE 5.7: DETECTION OF THE FLUORESCENT LABELLED EVs WITH ALEXAFLUOR 488 DERIVED FROM IN C57BL/6 MOUSE SERUM AT 24H POST INFECTION.	122
FIGURE 5.8: TUMOUR INFILTRATING IMMUNE CELLS ARE UPREGULATED BY EV-OV.	123
FIGURE 5.9: EVOV UP REGULATED THE EXPRESSION OF A RANGE OF IMMUNE PATHWAY GENES SIMILAR TO OV TREATMENT.....	125

List of Tables

TABLE 1.1: ONCOLYTIC VIRUS IN CLINICAL STUDIES.....	18
TABLE 2.1: CHEMICALS AND REAGENTS USED IN THIS STUDY.....	34
TABLE 2.2: EQUIPMENT AND AAPPARATUS AND USED IN THIS STUDY.	35
TABLE 2.3: PRIMARY ANTIBODIES USED IN THIS STUDY.	36
TABLE 2.4: SECONDARY ANTIBODIES USED IN THIS STUDY.	37
TABLE 2.5: SOFTWARE USED IN THIS STUDY.	37
TABLE 2.6: CELL LINES AND CHARACTERISATION OF THE CELLS	39
TABLE 2.7: BSA PREPARATION.....	50
TABLE 4.1: CORRELATION VALUES OF MDA-MB-231 DERIVED EV AND EV-OV REPLICATES DATASETS..	92
TABLE 5.1:THE EFFECT OF EV-OV ON THE LEVELS OF PRO-INFLAMMATORY OR ANTI-INFLAMMATORY CYTOKINES IN MURINE MICE SERUM.....	116
TABLE 5.2: TOP 10 GENES DIFFERENTIALLY REGULATED IN EV-OV TREATED TUMOURS.	126

Abstract

Background: Breast cancer is the major kind of cancer among women in the United Kingdom. To treat radio-/chemo-resistant cancer as well as advanced illness, novel medicines are necessary. Oncolytic viruses (OV) are naturally cytotoxic and infect and kill tumour cells whilst sparing healthy tissues. The full mechanism by which this occurs remains to be elucidated, but it may in part be mediated by extracellular vesicles (EVs). EVs are nanosized, membrane-enclosed vesicles that contain molecular cargo. EVs can be taken up by cells, for instance immune cells, at local or distant sites, causing phenotypic changes in the recipient cells. We hypothesise that infection of breast cancer cells with an oncolytic virus causes release of EVs carrying viral and immunogenic cargo that leads to activation of anti-tumour immunity.

Methods: To determine this, we infected breast cancer cells lines MCF-7 and MDA-MB-231 with the herpes simplex virus (HSV1716). EVs were isolated from the OV conditioned medium of infected cells and control cells by differential ultra-centrifugation (dUC). Characterization of these EVs' physical properties in order to determine the size ranges and rates of EV generation in breast cell lines and investigation on the oncolytic potential of EV-OV was carried out using Nanoparticle tracking analysis (NTA), Transmission electron microscopy (TEM) and mass spectroscopy. The antitumour efficacy of purified EVs was tested in an immunocompetent mouse model of mammary cancer using the luciferase labelled triple negative breast cancer cell line E0771.

Results: EVs were isolated from MCF-7 and MDA-MB-231 cells after infection with OV, these are typically exosome-like with a diameter of ~150 nm. The purified EVs expressed exosome markers including CD9, CD63, TSG101 and carried viral and immune cargo. These EVs were internalised by breast cancer cells and inhibited tumour cell migration *in vitro*. Furthermore, systemic delivery of EVs derived from OV (EV-OV) infected breast cancer cells was able to inhibit primary tumour growth and pulmonary metastasis *in vivo*, more effectively than OV given alone.

Conclusion: This indicates that EVs generated from cells that have been infected with OV may have antitumour characteristics. The use of EV-OV as a treatment with other cancer medications, such as immune checkpoint inhibitors, which may attract and activate T cells, changing a "cold" tumour into a "hot," tumor might lead to the creation of a new therapeutic approach for treating breast cancer.

Chapter 1: Introduction and literature review

1.1 Breast cancer

Breast cancer is the most often diagnosed disease in women worldwide, with around 2.3 million new cases expected in 2020. (Łukasiewicz et al., 2021). As the name suggests, breast cancer refers to the abnormal growth of breast cells, leading to a lump or tumour with unique cellular and molecular roots. It is classified into two broad categories: invasive ductal carcinoma (originating from milk-producing ducts' cells) and invasive lobular carcinoma from lobules or other epithelial tissues or cells in the breast (Łukasiewicz et al., 2021).

Regarding breast cancer diagnosis, magnetic resonance imaging (MRI) and mammography are the most commonly used methods for detecting breast cancers. The combination of these technologies has a sensitivity of between 92% and 100% and a specificity of between 51% and 71%, according to the study (Berg et al., 2012, Shao et al., 2013). However, when compared to mammography, breast MRI has emerged as a more sensitive technique for identifying ductal carcinoma in situ (DCIS) (Pinker, 2020). According to Waks and Winer most breast cancers are diagnosed when an abnormal lump or mass is discovered in a woman's breast. Although nipple and breast skin changes can also be an early indicator of breast cancer, such cases are considered rare (Waks and Winer, 2019). Breast cancer cells can be detected in the axillary lymph nodes, breast tissues, or other distant body parts during diagnosis. The information of where these cancer cells are located helps classify the disease into stages, from stage I to IV, with IV being the most advanced stage (metastatic breast cancer). When cancer has progressed to stage IV, it has moved beyond the breast and into other vital organs such as the lungs, bone, liver, and brain, and the disease is now considered incurable. (Sun et al., 2017).

1.1.1 Subtypes of breast cancer

Breast cancer is classified into four subtypes: hormone receptor-positive, ERBB2-positive (previously called HER2-positive), hormone receptor-negative, and triple-negative (McDermott et al., 2020). This classification is determined by the presence or lack of a number of different proteins in breast cancer cells. For instance, hormone-receptor-positive cancer is recognised from other types of cancer by the presence of oestrogen receptor (ER) or progesterone receptor (PR) protein in the cancer cells. It accounts for about 80% of all invasive breast cancer cases and is associated with a better prognosis and more favourable clinicopathologic features than other subtypes (Dauphine et al., 2020). Treatment for this breast cancer subtype usually involves hormone therapy, whereby drugs are used to block the hormones from supporting the growth and functioning of breast cells or reduce estrogen or

progesterone levels. Their tendency to grow slower than hormone receptor-negative means that those with this type of breast cancer have a better short-term outlook than their counterparts. However, Dauphine and colleagues note that hormone receptor-positive breast cancers can reoccur many years after treatment. As their name suggests, ERBB2-positive/ HER2-positive cancers are distinguished by the presence of the protein human epidermal growth factor receptor 2 (HER2), which encourages the growth of cancer cells in the breast. Research indicates that this subtype accounts for about 15% to 20% of invasive breast cancer cases (Prat et al., 2020, Waks and Winer, 2019). Its tendency to grow and spread faster than HER2-negative means significant clinical concern due to its aggressiveness and poor prognosis. However, they have been found to respond well to medications that target the HER2 protein and anti- ERBB2 therapy. For instance, studies have demonstrated that Lapatinib is primarily effective at inhibiting cancer cells that overexpress ERBB2 tyrosine kinases, thus preventing the activation of cellular signals that enhance the survival and multiplication of cancer cells (Waks and Winer, 2019).

The hormone receptor-negative subtype is characterised by the absence of estrogen and progesterone receptors in the cancer cells (Prat et al., 2020). This characteristic means that hormone therapy is ineffective for such cancers. Research also indicates that this subtype of breast cancer progresses faster than the hormone receptor-positive one and is more common in women who are yet to reach menopause (Waks and Winer, 2019). The final breast cancer subtype (triple-negative) is characterised by the lack of estrogen and progesterone receptors and the ERBB2 protein in the cancer cells. It is usually invasive and often starts in the breast ducts. Research indicates that it accounts for about 15% of all breast cancer cases (Perrier et al., 2018, Waks and Winer, 2019). Like the hormone receptor-negative subtype, TNBC, or triple-negative breast cancer, is a kind of breast cancer that cannot be cured using hormone therapy or drugs that inhibit HER2/ ERBB2 protein because they do not contain the two hormone receptors. However, other alternatives such as radiation therapy and chemotherapy can be used (Perrier et al., 2018, Kwan et al., 2021b).

1.1.2 Current treatment strategies for breast cancer

The treatment strategy or plan for breast cancer is influenced by the biology and the behaviours of the tumour because some tumours are small but progress rapidly. In contrast, others are large and move slowly. According to Łukasiewicz et al treatment strategies are personalised and heavily dependent on the following factors: breast cancer subtype, stage, genomic markers, the

presence, or absence of known mutations in inherited breast cancer genes, such as BReast CAncer gene 1 (BRCA1) or BReast CAncer gene 2 (BRCA2), and the patient's history, including age, overall health, preferences, and menopausal status (Łukasiewicz et al., 2021). Although breast cancer treatment is personalised, some general steps are followed when dealing with early-stage and locally advanced breast cancer. For instance, surgery is frequently advised for ductal carcinoma in situ (DCIS) and early-stage invasive breast cancer to remove the tumour (Minami et al., 2020, Sonnenschein and Soto, 2016). The purpose of surgery is to remove of surgery is to remove all the visible tumours in the breast, but microscopic cells can be left unattended, increasing the probability of reoccurrence. To this end, systemic treatment using drugs are recommended after surgery (Łukasiewicz et al., 2021, Sonnenschein and Soto, 2016).

After surgery, the next step involves lowering the recurrence risk by getting rid of any remaining cancer cells in the body (Sonnenschein and Soto, 2016). These cells cannot be detected using the current approaches, but they are strongly linked with recurrence because they grow over time. Therefore, adjuvant therapy, which includes radiotherapy, targeted therapy, chemotherapy, and hormonal therapy, is recommended after surgery. Other treatment options such as radiotherapy, chemotherapy, targeted therapy, and hormonal therapy are recommended to manage the disease when breast cancer is inoperable. Recurrent cancers are treated based on the initial treatment and the subtype involved (Waks and Winer, 2019). Besides the conventional strategies described above, immunotherapy is a novel approach to treating cancer, particularly those with a high genetic burden (Zhang and Plitas, 2021). The rationale for using immunotherapy to treat breast cancer is based on several factors, including the fact that treatments such as chemotherapy are costly to the patient because they require growth factor usage. Chemotherapy is also toxic and associated with adverse effects on many organs and side effects such as hair loss, vomiting, neuropathy, myeloid cell suppression, and others. Another factor is that hormone therapy, a non-targeted treatment option like chemotherapy and radiotherapy, is linked with a high risk of serious negative effects (Simonian et al., 2021). These limitations have increased the demand for targeted therapies to improve the sustainability of breast cancer treatment. As observed by Simonian et al targeted treatments such as immunotherapy are currently the best option for fighting cancer. Immunotherapy works by targeting specific proteins, which stimulates the body's immune system, allowing it to detect and eradicate malignant cells (Simonian et al., 2021).

1.2 Overview of oncolytic virotherapy

Oncolytic viruses, or OV, have been considered as a promising novel immunotherapy for the treatment of cancer in recent years. Oncolytic viruses are naturally occurring, or genetically modified viruses designed to destroy cancer cells by discerningly replicating within them without harming the normal cells (Uche et al., 2021). The idea of using these viruses for cancer treatment was conceived in the 1950s when oncolytic virus preparations were used to treat hundreds of cancer patients using almost every possible route. Although the patients' immune systems usually halted the viruses, some tumours regressed, especially those immunosuppressed (Li et al., 2020a). Further, OVs can be modified to stimulate anti-tumour immune responses within the host to increase tumour cell death (Achard et al., 2018).

One of the fundamental features of OVs is their ability to infect different cell types, which has been established by several OVs that have natural specificity for tumour cells (Howells et al., 2017). The properties of tumour cells make them attractive to OVs as they avoid detection and elimination by the immune system and resist apoptosis and translational suppression, all of which prevent viral infection and spread (Russell et al., 2012).

Herpes simplex virus type 1 (HSV-1) is the most often employed OV in clinical settings, followed by adenovirus and vesicular stomatitis virus (VSV). Although a significant number of genetically and naturally occurring oncolytic viruses have been developed, most of them are still in their clinical research stages as cancer therapies such as T-VEC (GM-CSF) in combination with Ipilimumab and Nivolumab and T-VEC (GM-CSF) in combination with Pembrolizumab (Chaurasiya et al., 2021). The first OV approved by the FDA was Amgen's T-VEC (an oncolytic HSV-1 expressing granulocyte macrophage colony stimulating factor) in melanoma (Almstätter et al., 2015, Li et al., 2020a). Likewise, in China, the H101 adenovirus has been authorised for the treatment of head and neck cancer. (Garber, 2006, Yuan et al., 2003). Both viruses are given to patients via direct tumour injection, this is because delivery of OV systemically is challenging due to rapid clearance of the virus by the immune system. Our research group and many others are investigating ways to overcome this so virotherapy can be used to treat all cancer types particularly those in inaccessible sites (Nutter Howard et al., 2022).

1.2.1 The mechanism of action of HSV on tumour cells

Herpes simplex viruses are members of the Herpesviridae viral family's Alphaherpesvirinae subfamily. Many HSVs are used in cancer therapy, including HSV1716, G207, G47, and T-Vec, which is a deliberately replicating oncolytic HSV type I virus that replicates in rapidly proliferating cells but not in terminally differentiated cells. The virus has a 150 kbp linear double stranded DNA (dsDNA) genome that encodes at least 84 polypeptides and causes genital warts and cold sores. (Liu and Zhou, 2007, Whitley and Roizman, 2001, Piret and Boivin, 2011, Simmons, 2002). This PhD focuses on herpes simplex virus (HSV-1) as shown in **Figure (1.1)**. Genetically modified HSV that may trigger immune-mediated elimination of tumour cells (Kaur et al., 2012). Research shows that this virus replicates in tumour cells that are rapidly dividing, including melanoma, human embryonal carcinoma and non-small cell lung carcinoma in vivo and in vitro studies (Mace et al., 2008). ICP-34.5 protein from HSV1716 has been deleted. ICP-34.5 allows the virus to destroy healthy cells. Therefore, deleting such a gene ensures that the virus can no longer multiply in normal tissues. (Benencia et al., 2008). HSV replication in breast cancer starts after the viral genome has been deposited in an environment where the production of viral genes and viral genome replication is supported (Oku et al., 2021, Rode et al., 2011). In most cases, this process involves the introduction of viral DNA into the host cell's nucleus. The viral genome is separated from the cellular environment with a capsid (Rode et al., 2011). However, the ability to discharge the genome from its protective location must be retained at the appropriate time they received into the nucleus. The mechanism under which a virus enters the nucleus differs from one virus to another, with most of them applying the stepwise disassembly of protective layers (Jean Beltran et al., 2018, Oku et al., 2021).

HSV is also one of the viruses that apply stepwise disassembly. The interaction between the viral envelope and the cell membrane usually causes the envelope to come out of the capsid. Much of its tegument also disconnects from the capsid after the entry and during the movement to the nucleus. The tegument disconnects from the capsid called loosely associated tegument, while the one that remains in the capsid is referred to as tightly associated tegument. Once it reaches the nucleus, HSV capsids are attached to the nuclear pore complex (NPC) through interaction with Nup358. This attachment causes a protease to cut the tightly associated tegument, leading to a change that produces the viral DNA (Jean Beltran et al., 2018, Copeland et al., 2009).

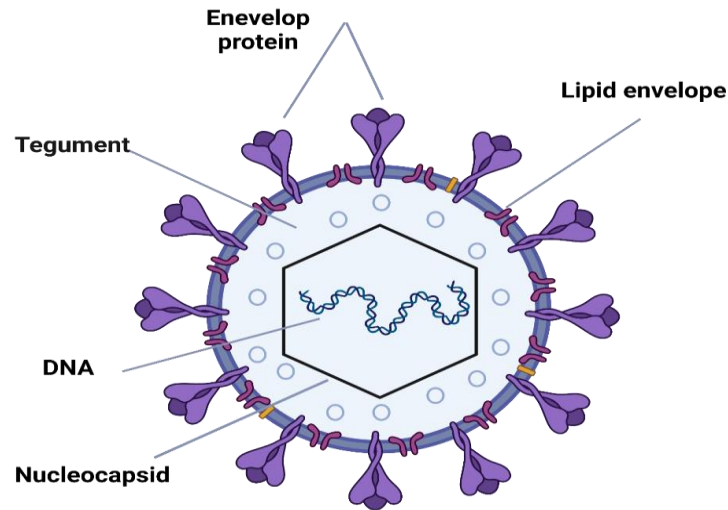


Figure 1.1: An illustration of the particle structure of the Herpes simplex virus. (Biorender).

1.2.2 Development of oncolytic HSV in clinical trials

Liu et al provide a comprehensive review of clinical trial results with oncolytic virotherapy. The review summarizes and interprets data from clinical reports over the past century, including safety, efficacy, and biological endpoints (viral and immunological). Systemic safety and efficacy were demonstrated for some virotherapeutics (Liu and Kirn, 2007). One of the most important points was that oncolytic viruses, unlike other therapeutics, are not cross-resistant; their response to virotherapy is species and tumor-specific. Moreover, preclinical and clinical trials of HSV HF10's genomic signature as a cancer therapy, for example, are still in the early stages of development, but there are limited directions for future research focusing on HF10 (Eissa et al., 2017). A recent study by (Kwan et al., 2021b) examined the treatment of breast cancer with oncolytic virotherapy based on barriers and current progress. It reported that there have been numerous preclinical attempts to explore the use of oncolytic virotherapy in breast cancer, but these have not resulted in meaningful clinical trials. The review assessed the potential and barriers to the use of OV in breast cancer, among which the limitations of monotherapy and the potential of combination therapy, improving viral delivery, and the challenges faced by the breast cancer population (Kwan et al., 2021b). Clinical trials for oncolytic HSV have been greatly advanced. For example, 50 patients with advanced malignant

melanoma received intratumorally injected T-VEC is an engineered HSV that expresses granulocyte-macrophage colony-stimulating factor (GM-CSF) (Eissa et al., 2018). This is likely to result in immediate tumour oncolysis, with GM-CSF expression increasing tumour vascular closure and anti-tumour immunity. **Table 1.1** provides a list of the main HSVs that have been completed as well as those that are currently being studied in clinical studies. Only two projects out of the six presented in the table are completed. The relevance of these works for the present study lies in the fact that they highlight recent developments in the field. Based on these previous studies, many of which are still ongoing, as well as some others reported earlier, the present study analysed the major research questions. In addition, the present study, therefore, established the need for continued research to address pertinent issues.

Table 1.1: Oncolytic virus in clinical studies

Name	Virus	References	Status
H101	Adenovirus	(Liang, 2018)	H101, a genetically altered adenovirus serotype 5, was approved in China 2006 for the treatment of nasopharyngeal cancers
T-VEC	HSV1	(Andtbacka et al., 2015)	in 2015, T-Vec, a modified HSV, was approved in the United States for the treatment of advanced melanoma
Teserpaturev /G47Δ	HSV1	(Frampton, 2022)	It has been authorised in Japan for the treatment of malignant glioma and is now in clinical research for the treatment of prostate cancer (phase II), malignant pleural mesothelioma (phase I), and recurrent olfactory neuroblastoma (phase I).
Adenovirus		(Haller et al., 2020)	AdV-tk + Valacyclovir Treatment in Combination with Pancreas Cancer Surgery and Chemoradiation

1.2.3 The role of HSV in tumour microenvironment (TME)

Besides from cancer cells, the tumour mass is made up of a variety of cellular and subcellular components. These comprise immune cells, cancer-associated fibroblasts (CAFs), extracellular matrix (ECM) proteins as well as resident stromal cells including fibroblast and endothelial cells, together known as the tumour microenvironment (TME) (Belli et al., 2018). Tumour formation, progression and metastasis are greatly influenced by the immunosuppressive

network formed by interactions between cancer cells and TEM components (Hanahan and Coussens, 2012). Crucially, immunosuppression in the TEM may lead to a suboptimal therapeutic response and treatment resistance. Due to the obvious important role played by the tumour microenvironment (TME) in cancer, much effort has been devoted to the development of medicines that target components of the TME. One significant example is the therapeutic effectiveness of immune checkpoint inhibitors (ICIs), which drug that work to restore anti-tumour T-cell activity (Martins et al., 2019). The use of Oncolytic viruses (OV) to destroy cancer cells is a novel approach of immunotherapy that is being explored (De Vries et al., 2015). OV have the ability to change immunologically cold tumour to make it immunogenically 'hot'. This can provide an opportunity to activate the tumour microenvironment and make the tumour more responsive to immunotherapies like the checkpoint inhibitors described above. Bourgeois-Daigneault et al. showed the cytopathic activity of the combined treatment involving Rhabdovirus Maraba-MG1 and Paclitaxel in the EMT6, 4T1 and E0771 murine breast cancer models (Bourgeois-Daigneault et al., 2016). They reported the prolonged survival by controlling the tumour growth. Another study conducted by Tan et al. showed the effect of combination therapy of oncolytic herpes simplex virus HF10 and bevacizumab against a human breast carcinoma xenograft (Tan et al., 2015). They revealed that bevacizumab increased the viral growth and distribution of HF10 virus, expanded the tumour hypoxia and apoptotic cell population in the target tissues, thereby showing the great promise of the OV based combined therapy in treating the breast cancer. Of note, as this was a xenograft model it was not possible to assess antitumour immunity.

The dysfunctional interferon pathway is the hallmark of the tumour microenvironment, due to which, OV can easily infect cancer cells to perform their biological function that is to kill tumour cells and activate a suppressed immune system. Under normal growth conditions, tumour cells develop ability to escape from the immune system by causing mutations in antigens expressed by tumour cells (immuno-editing) (Guo et al., 2017). The immunogenic action of OV is stimulated due to viral mediated immunogenic cell death, which involves the activation of T lymphocytes and dendritic cells. In fact, OV cause destruction of cancer cells, thereby releasing antigens into the micro-environment which are recognized by the immune system, generating immune responses thus disrupting the immuno-editing process. Infection of tumour cells with OV stimulates release of cytokines and subsequent activation of immune responses which turn the "cold" tumour micro-environment into a "hot" tumour micro-environment (Sivanandam et al., 2019).

The cold tumour micro-environment is characterised by a silenced immune system and release of mutated antigens which are unrecognisable by the immune cells, while the hot tumour microenvironment is characterised by a release of specific antigens from the tumour cells which are identifiable by the immune system (de Gruijl et al., 2015, Ferguson et al., 2012). This can lead to creation of long-lasting anti-tumour immunological memory with protective effects against relapse. The basic principle behind the efficacy of OV infection as an anti-tumour therapy is the conversion of the ‘cold tumour microenvironment into ‘hot’ which would be ideal in breast cancer as shown in **Figure (1.2)** (Kwan et al., 2021b). However, one of the major challenges with OV is delivery of the virus to the target tissue due to development of immune response against viral infection (Ferguson et al., 2012).

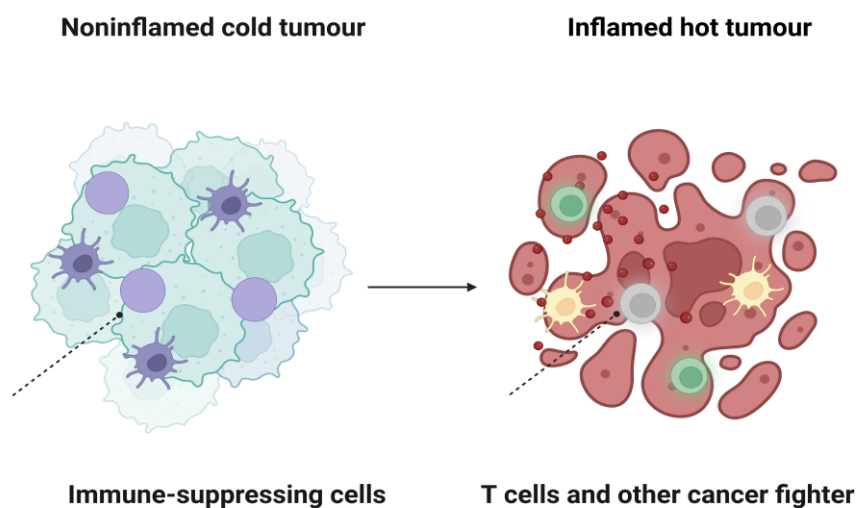


Figure 1.2: Breast cancer tumour microenvironment. This illustration describes the effect of HSV on the microenvironment on the development of cancer. (<https://www.criver.com/eureka/about-us>) (Biorender)

As mentioned earlier so far, clinical studies with OV have mainly relied on direct injection into the tumour. Nevertheless, this is not possible for tumours that are located deep in the body and are therefore not easily accessible (Chaurasiya et al., 2018). The ideal route of administration would be via the circulation so that inaccessible tumours or metastatic tumours can be reached. However, this can provoke the immune system to attack the virus limiting viral efficacy and proliferation in the target oncogenic tissues (O`Bryan and Mathis, 2018). The delivery of OVs

along with chemotherapeutic agents through naturally occurring biological cargo transporters can circumvent some of these limitations (Russell and Bell, 2012). Extracellular vesicles (EVs) have the ability to transfer biological molecules to tissues located in various parts of the body. The lipid membranes of EVs are hydrophobic in nature and can prevent the degradation of biological materials packed in EVs (Fukuhara et al., 2016). This PhD investigates the effects of delivering OV materials through EV. Below is a description of EV biogenesis, cancer and their potential applications.

1.3 Extracellular vesicles

EVs play a fundamental role in short range and long-range communication in intercellular communication (Bebelmann et al., 2018). Whilst the role of EVs is still poorly understood in normal physiological conditions, they are well characterised in the pathological state of cells (Kalra et al., 2016). Based on the main classification of biogenesis, EVs are subdivided into three main classes: exosomes, microvesicles and apoptotic bodies (**Figure 1.3**). In this review of the literature, a detailed discussion of EVs' their biogenesis, secretion mechanisms, isolation methods and techniques for characterization are described. This review also aims to shed light on the role of EVs in cancer with an emphasis on breast cancer and the transfer of cancer cargo. Ultimately, this PhD project will further investigate if EVs are important in the transfer of OV cargo for immune activation on breast cancer.

Extracellular Vesicles (EV)

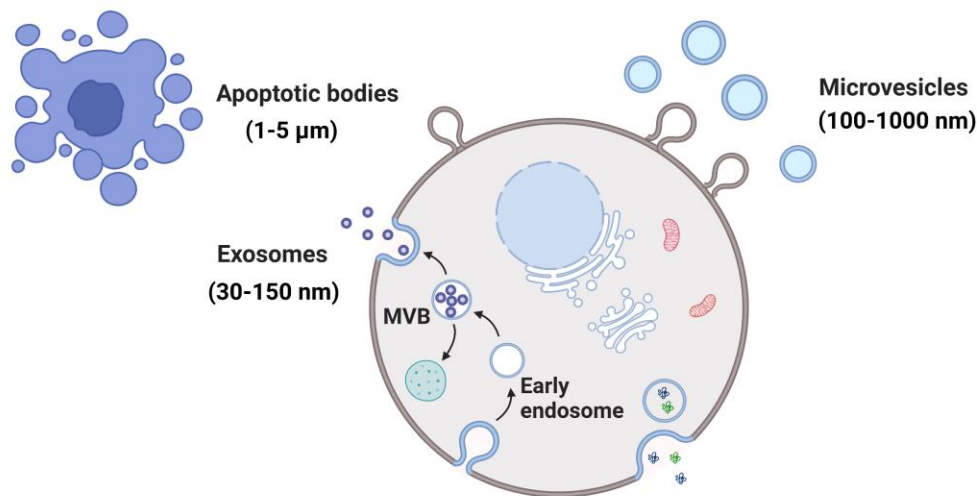


Figure 1.3: Extracellular vesicles: Exosomes, microvesicles and apoptotic bodies. Exosomes originate from intracellular endosomes and are around 30-150 nm. Microvesicles and are approximately 100-1000 nm are released from the cell surface during apoptosis in all eukaryotic cells. Apoptotic bodies with size of 1-5 μm are released from the cell surface at the late stage of the apoptosis. (Medeiros et al., 2020). (Biorender).

1.3.1 Biogenesis of the extracellular vesicles

1.3.1.1 Exosomes

Exosomes are formed as a result of inward budding of early endosomes, which leads to production of intraluminal vesicles (ILVs) and the generation of multivesicular bodies (MVB). MVB undergo fusion with the plasma membrane during the late stages of endosome maturation, which results in the release of exosomes into the extracellular space. Tumour exosomes are thought to play a critical role in the progression of cancer, so it is important to understand the mechanism of biogenesis, so that this insight can be utilised to develop therapeutic strategies (Bebelmann et al., 2018).

It has been suggested that multiple mechanisms are involved in the biogenesis of multivesicular bodies (MVBs). Three important mechanisms are commonly reported in the literature involving lipid-raft based mechanism, ubiquitination-dependent mechanism and the non-ubiquitination mechanism (de Gassart et al., 2004). In the lipid-raft based mechanism, neutral sphingomyelinase 2 (nSMase2), hydrolyses the sphingomyelin into ceramide which initiates the budding into the MVB, thereby generating ILVs (Record et al., 2014). The ubiquitination dependent formation of MVBs uses the ESCRT complex (this includes ESCRT-0, ESCRT-I, ESCRT-II, ESCRT-III), which is responsible for recognition and recruitment of ubiquitinated proteins into the ILVs at the late stage of endosomal maturation. ESCRT-I and ESCRT-II are implicated in generating invagination in the MVB membrane, while ESCRT-III is involved in restriction of the budding neck of the MVB membrane with the help of ATPase VPS4. As explained previously, MVBs may fuse with either lysosomes or the plasma membrane to degrade their contents or release EVs (Van Niel et al., 2018, Kalluri and LeBleu, 2020). However, it is not clear whether the MVBs produced as a result of the ubiquitination mechanism are destined for lysosomal degradation or fusion to the plasma membrane for exosomal release. TSG101 is a member of the ESCRT and is a common EV exosome/marker and plays a critical role in endosomal sorting. This suggests that MVB produced by the ESCRT mechanism release exosomes (Schöneberg et al., 2016, Cesselli et al., 2018).

The non-ubiquitination mechanism involves the interaction between syndecan (heparan sulphate proteoglycan), and ALIX protein associated with ESCRT-III through an adaptor protein, syntenin, thereby giving rise to a syndecan-syntenin-ALIX complex. The syndecan-syntenin-ALIX complex is implicated in trimming of chains of heparan sulphate, sorting of components into ILVs and production of exosomes (Roucourt et al., 2015, Thompson et al., 2016). Taken together, the above suggests that different mechanisms of biogenesis might be involved in sorting specific cargo into EVs or generating subpopulations of vesicles carrying specific cargo. A further ESCRT-independent mechanism that tetraspanins may be able to activate without the involvement of ubiquitination, ESCRT, or ceramides is possible (van Niel et al., 2011, van Niel et al., 2015). In this process, the tetraspanin CD63 is necessary for ILV synthesis and subsequent EV release (van Niel et al., 2011, Hurwitz et al., 2016). While ESCRT or ceramide deficiency has no effect on EV secretion or cargo sorting (van Niel et al., 2015).

1.3.1.1.1 Release of exosomes

After the development of MVB, they might be either directed towards the lysosome or autophagosome for degradation or travel to the plasma membrane for release of exosomes. The ISGylation of ESCRT-I signals the fusion of the MVB to the lysosome, which suggest that post-translational modification of protein cargo in ILVs determines the fate of MVB for lysosomal fusion. ISGylation is the process of expression of interferon stimulated gene 15 (ISG15) and its conjugation to targets such as ESCRT-1 protein and protein kinases R. Exosome secretion defects caused by ISGylation are reversed by inhibiting lysosomal activity or autophagy. However, if the cell undergoes starvation, this leads to fusion of MVB to the autophagosome (Villarroya-Beltri et al., 2016).

In the absence of starvation or ISGylation signals, the MVBs are destined to fuse with the plasma membrane and the subsequent release of exosomes into the extracellular space. The movement of MVB towards the plasma membrane is facilitated across the microtubule network by the Kinesin motor coupled with RAB7 and Arl8 protein complexes. RAB27 or RAB35 are responsible for docking of MVBs on the inner surface of the plasma membrane. The exocytosis of exosomes is mediated by the N-ethylmaleimide-sensitive factor attachment protein receptor (SNARE) protein complex (SNAP23, Syntaxin-4 and VAMP7) from the donor cells (Wei et al., 2017, Verweij et al., 2018). The SNARE complex was previously reported to be implicated in tumour cell invasion by increasing cell membrane permeability and growth (Willms et al., 2016). Raja et al. showed that SNARE caused overexpression of *STX1A* and *VAMP2* (*SYB2*) in bladder cancer derived from patients, which might be involved in increasing the membrane permeability and cell growth (Raja et al., 2019). Hence, it can be argued that processes involved in cancer invasion are also involved in exosomal release (Verweij et al., 2018, Edgar et al., 2016).

1.3.1.2 Microvesicles

Microvesicles, also known as MVs, are another kind of extracellular vesicle (EV). MVs are released from the plasma membrane, but instead of having internal membranes, they contain cytosolic material. (Meckes Jr and Raab-Traub, 2011). According to some studies, they are larger and more heterogeneous in size than exosomes, ranging from 100 to 1000 nm (Sims et al., 1988, Hind et al., 2010, György et al., 2011, Grant et al., 2011). As they have different sizes, it has been postulated that various mechanisms are involved in producing MV. They either pinch off or bud directly from the plasma membrane. The nano-sized microvesicles

containing cell surface proteins can be produced through the ESCRT machinery similarly to exosomal production (Wang and Lu, 2017). Likewise, ceramide containing microvesicles are generated through the action of acid sphingomyelinase (aSMase), which is similar to nSMase2 involved in ILV development, which suggests a role for sphingomyelinase in the development of MVBs and plasma-membrane derived EVs (Bianco et al., 2009). Another mechanism for microvesicles biogenesis is the constant blebbing of non-apoptotic cellular membranes, often observed in aggressive tumour cells, including Walker carcinoma and melanoma (Keller and Bebie, 1996, Cunningham et al., 2013). These membrane blebs are released as microvesicles into the extracellular membrane through the action of cytoskeletal rearrangements which causes restriction of the budding neck of vesicles (Schlienger et al., 2013, Sedgwick et al., 2015).

1.3.1.2.1 Release of microvesicles

Several factors are involved in the release of microvesicles into the extracellular space. Phospholipase D is activated by ADP-ribosylation factor-6 (ARF-6), followed by recruitment of extracellular signal-regulated kinase on the surface of plasma membrane, leading to the activation of myosin light chain kinases which in return results in the release of microvesicles. Another mechanism that can cause the release of microvesicles is the complex of ESCRT-1 and arrestin-1 domain containing protein (tetrapeptide protein) (Nguyen et al., 2017, Nabhan et al., 2012, Abels and Breakefield, 2016).

1.3.1.3 Apoptotic Bodies

Apoptotic bodies are produced as a result of membrane blebbing mediated by contraction and relaxation of cellular membrane. The actin-myosin driven process of membrane blebbing is considered central for production of apoptotic bodies (Taylor et al., 2008, Cotter et al., 1992). Apoptotic bodies are blebs of membrane bound vesicles that are pinched off from cells undergoing programmed cell death as separate vesicles, similar to macrovesicle biogenesis. (Cotter et al., 1992). Moss and co-workers described the active role of concentration in microtubules in the late phase of apoptotic bodies to give rise to stable vesicles (Moss, 2006). They reported that if the microtubule cytoskeleton is disrupted, then the process of apoptotic body development is prevented, suggesting the key role of microtubule skeleton in formation of active bodies (Moss, 2006).

1.3.1.3.1 Release of apoptotic bodies

Apoptotic bodies range in size 1-5 μm and are released by dying cells, facilitating their breakdown into subcellular components (Ihara et al., 1998). Apoptotic bodies are phagocytosed after being released in extracellular space by macrophages, parenchymal cells, or neoplastic cells. Tingible body macrophages are macrophages that engulf and digest apoptotic cells. Tiny bodies are pieces of nuclear debris produced by apoptotic cells (Blander, 2017, Jiang and Poon, 2019).

1.4 Isolation of EVs

The main subtypes of EVs (microvesicles, exosomes, and apoptotic bodies) share overlapping physical characteristics (e.g. size and density) making their separation highly challenging (Liangsupree et al., 2021). EVs are usually fractionated from complex biological fluids and some components, such as lipoproteins, viruses, and chylomicrons, have similar densities and sizes to EVs, hence making density- and size-based isolation complicated (Liangsupree et al., 2021). Since EVs have potential for biomarker discovery crucial for diagnosing different health conditions, a high level of isolation is required as well as high purity isolates for therapeutic purposes such as immunotherapy and drug delivery. This makes EV isolation and separation critical in the diagnosis and treatment of various diseases. Isolation and characterisation of EVs helps to discover the effects of cell origins or states on the composition of EVs. This knowledge is crucial, especially in understanding tumour progression, because carcinogenic materials are shuttled by EVs, which makes them more attractive as biomarkers for cancer prognosis and diagnosis (Liangsupree et al., 2021, Konoshenko et al., 2018). Different techniques are used in the isolation and separation of EVs, which are broadly classified according to the three isolation principles, affinity, charge, and size-based techniques. Some of the popular EV isolation techniques include differential Ultracentrifugation (dUC), density gradient (DG), ultrafiltration (UF), size-exclusion chromatography (SEC) (Liangsupree et al., 2021, Gandham et al., 2020) and precipitation (Ryu et al., 2020). While each of these techniques has its own advantages in isolation, research recommends a combination of different techniques for more robust isolation (Liangsupree et al., 2021, Gandham et al., 2020).

Differential ultracentrifugation (dUC) and density gradient (DG) ultracentrifugation are the most widely used and well-known technique for EV isolation. Successive centrifugation at high centrifugal speeds enables the removal of dead cells and cellular debris, followed by EV

population enrichment. Théry, one of the pioneers in this area, published a thorough strategy for isolating EV populations (Théry et al., 2006). In summary, large EVs (e.g., APOs) are pelleted at 2,000 x g, MVs at 10,000 x g, and exosomes at 100,000 x g. Washing of pelleted EVs is accomplished through resuspension and a subsequent second round of pelleting. dUC has been used successfully to isolate various EV populations (Menck et al., 2013, Crescitelli et al., 2013). Numerous groups have reported minor modifications to this approach throughout the years, such as centrifugation force and time. Interestingly, such modifications have been shown to significantly modify the sedimentation patterns and efficiency of EVs produced from various cell lines (Jeppesen et al., 2014). Furthermore, it has been demonstrated that the quantity and purity of dUC-isolated EVs are strongly impacted by the rotor type and centrifugation period (Cvjetkovic et al., 2014). Differences in isolation procedures used and a lack of standardisation may have an effect on the composition and functionality of EVs reported. Additionally, dUC does not permit complete segregation of EV populations, as some smaller EVs pellet at lower centrifugal forces and vice versa. As a result, variability within isolated populations occurs, making it extremely difficult to analyse EV subtypes using dUC solely. As a result, density gradient flotation (DG) has been used in the EV area to improve the purity of isolated EVs by removing copurified non-EV material or EV fragments that may occur during dUC. DG allows EVs to float in a gradient of decreasing dilutions of viscous liquids such as sucrose or iodixanol. EVs move to their (equilibrium) density upon centrifugation. The rate of migration or float is dependent on the EV's size, shape, and density.

UF uses membranes with known molecular weight cut-off (MWCO) that ranges from 10 to 100 kDa in isolation of EVs from diluted samples, including cell cultures and blood (Liangsupree et al., 2021). The devices used in UF isolation contain a membrane placed in a vessel while filtration is conducted using centrifugal force. A major advantage of UF is that it is a simple, faster, and easy-to-use technique; however, it experiences protein contamination and loss in EVs. Another related UF technique is Tangential flow filtration (TFF), in which, streams of fluids with EV are allowed to flow peripherally by passing through the UF membrane (though not directly across); in this process, molecules that are smaller than MWCO cross and get discarded while those with larger than the threshold level (for example EVs) are left behind (McNamara et al., 2018). Unlike the conventional filtration techniques, TFF does not experience clogging in the pores due to cake formation. Besides, TFF is appropriate for large scale EV isolation from diluted samples because, unlike SEC, it concentrates EVs (McNamara et al., 2018).

In SEC, biomolecules are separated based on their hydrodynamic radius using porous media. The solution is filtrated through a column of porous beads with smaller radii than the EV of interest (Wei et al., 2020, Liangsupree et al., 2021). A major weakness/challenge with SEC is that there is the likelihood of sample contamination by other molecules with similar size eluting at the same rate (Wei et al., 2020). Besides, the overlap in size between EV categories makes it difficult to completely isolate EV samples based on their category. Furthermore, limitations in sample volume, the requirement for specialised equipment and column, and the general complexity of the technique are also major challenges currently facing SEC (Liangsupree et al., 2021).

1.5 Uptake of Extracellular vesicles and signalling

EVs may interact with recipient cells in a variety of ways following their release. For example, endocytosis, phagocytosis, direct membrane fusion, and receptor/ligand binding are some of these (**Figure 1.4**) (Mulcahy et al., 2014, Van Niel et al., 2018). Specific receptors on the surface of cells facilitate the uptake of EVs and triggers intracellular signalling cascades (Van Niel et al., 2018). A heterogeneity in EV and membrane composition may facilitate this process (Mulcahy et al., 2014). It has been demonstrated that integrins on the surface of EVs facilitate uptake by interacting with adhesion molecules on the surface of dendritic cells (Morelli et al., 2004, Van Niel et al., 2018). In addition, vesicles can fuse directly with the plasma membrane, resulting in luminal cargo being delivered to the cytoplasm (Parolini et al., 2009). Alternatively, the EVs may undergo "back-fusion" with the endosomal membrane after endocytosis (Van Niel et al., 2018). The mechanisms are mediated by clathrin pits or caveolae on the surface of the cell, or through more general mechanisms including macropinocytosis and phagocytosis. When EVs are internalised within endosomes, they may fuse back with the membrane, allowing luminal cargo to be delivered cytoplasmically. Additionally, the endosome may undergo lysosomal degradation, resulting in breakdown of the internalised EVs.

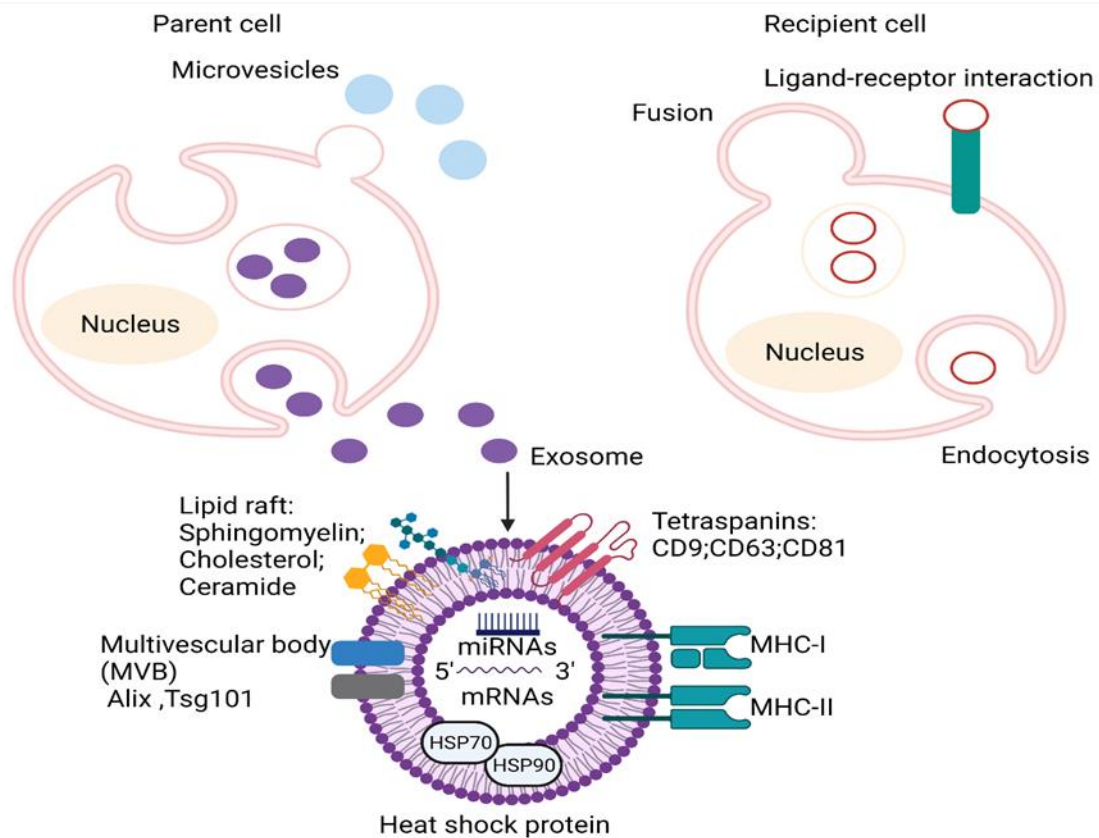


Figure 1.4: Extracellular vesicles facilitate cell-to-cell communication by transporting bioactive substances across the cell membrane (proteins, lipids and nucleic acids). MVs and Exo released from secreting cells may be taken up by the target cell through fusion, endocytosis, or they can interact with the ligand receptors of the target cell. (Yoon et al., 2014). (Biorender).

1.5 Role of EVs in Cancer and Health

EVs contain ribonucleic acid (RNA), deoxyribonucleic acid (DNA), proteins, lipids, metabolites, and glycans from the cell of origin (Luo et al., 2018, Williams et al., 2019). This content makes EVs serve critical functions, which include maintenance of homeostasis, cell-to-cell communication, and different pathological conditions, including cancer. When discharged into the biological fluids or extracellular space, EVs are bound to the recipient cells and transfer their functional nucleic acid and protein contents to change the phenotype of the recipient cell (Salmond and Williams, 2021). Through this communication, EVs play a critical role in various physiological processes, which include immune response coordination, angiogenesis, and coagulation (Zomer et al., 2015, Wortzel et al., 2019, Hoshino et al., 2015).

They also play significant roles in various cardiovascular, neurodegenerative, and inflammatory conditions (Howitt and Hill, 2016, Ibrahim and Marbán, 2016, Chan et al., 2019). Ibrahim and Marbán et al placed much emphasis on cardiovascular physiology and pathophysiology in their study, which sheds light on what is currently known about exosome biogenesis and its content (Ibrahim and Marbán, 2016). The authors stressed that several questions about the diagnostic and therapeutic potential of these extracellular membrane vesicles are currently being investigated. While this study focused on cardiovascular physiology in relation to EVs, it is pertinent to remember that breast cancer and heart diseases share many of the same risk factors (Catalano and O'Driscoll, 2020).

EVs are capable of passing through numerous barriers in an organism, such as the central nervous system's (CNS) blood-brain barrier. Due to their ease of mobility, EVs play a vital role in ferrying genetic information to cells in health and ailment states. They can affect the functioning of a cell located far away from production site (Sjöstrand et al., 2007). EVs help in repairing of tissues, developing, and regenerating organ systems (Longa et al., 2017, Vogel et al., 2018). On the other hand, EVs can transfer miRNAs or pathogenic proteins, hence spreading and exacerbating diseases (Upadhyya and Shetty, 2021). Progenitor/stem cell derived EVs ferry therapeutic proteins and miRNAs cargoes, which offer protection to cells, reduce inflammation and oxidative stress, enhance mood and cognitive functions, and improve neurogenesis (Upadhyya and Shetty, 2021, Kim et al., 2016). They, therefore, help in repairing and regenerating tissues after disease or injuries. Specifically, the microRNAs have been identified as important players in breast cancer angiogenesis and therapeutic targets (Hussen et al., 2021)

The role of EVs in cancer biology is an area that is increasingly attracting the attention of researchers. Numerous studies have been conducted to understand the functional roles of EV in cancer from as early as the 1980s (Trams et al., 1981). For instance, Galland and Stamenkovic successfully separated tumour with antigen-presenting exosomes from tumour antigen-pulsed dendritic cells. This study showed that the immunostimulatory effect of EVs helped reduce the growth of tumours and, in some instances, complete eradication of tumours (Galland and Stamenkovic, 2020). Similar findings were also made in a study by Arkhypov et al which established that EVs taken from tumours shuttled tumour antigens to dendritic cells and provoked antitumour effects. These discoveries demonstrated the potential of EVs in the therapeutic capacity of cancer treatment (Arkhypov et al., 2020). The findings of these previous

studies contribute to the ever-increasing need for breast cancer research by laying a strong foundation for further study.

EVs derived from cancer cells have also been found to promote the ferrying of protein and nucleic acid contents between neoplastic cells to enhance tumorigenic phenotypes. A study by Skog et al demonstrated that EVs taken from cancer cells can transfer the mutant Epidermal Growth Factor Receptor (EGFR) protein and enhance tumorigenic phenotype in recipient cells (Skog et al., 2008). Also, Sabbagh et al observed that glioblastoma cell-derived EVs transferred RNA and protein cargo to recipient cells, promoting tumourigenesis and angiogenesis (Sabbagh et al., 2020). Also, it has been established that EVs derived from melanoma not only train bone marrow progenitor cells but also enhance leaking of vasculature at pre-metastatic sites, hence contributing to the creation of the pre-metastatic niche (Peinado et al., 2012). Also, EVs taken from pancreatic cancer cells are said to promote the formation of the fibrotic pre-metastatic environment in the liver via the recruitment of macrophages and education of kupffer cells (Costa-Silva et al., 2015). These studies suggest a role for EV in promoting cancer development and metastasis. Xavier et al who explained the role of EVs in the hallmarks of cancer and drug resistance emphasised that EVs mediate intercellular signalling and communication, allowing the intercellular exchange of proteins, lipids, and genetic materials. They emphasised that EVs play an important role in maintaining physiological balance (Xavier et al., 2020). However, their study placed a focus on the most recent data supporting the notion that EVs play a role in increasing cell proliferation and escape from apoptosis, maintaining angiogenesis, and modifying the tumour microenvironment. Of particular importance, was their special emphasis on the role of EVs in the transfer of drug-resistant traits and to the EV cargo responsible for this transfer, both between cancer cells or between the microenvironment and tumour cells. However, one of the major concerns is the lack of a thorough understanding of the role of tumour EVs in the genesis, progression, metastasis, and treatment resistance, which is crucial for the creation of novel EV-based therapeutic strategies for cancer. Thus, applied medicine has benefited from the understanding that extracellular vesicles are crucial for cell signaling and can easily penetrate biological barriers. A more in-depth study will be necessary, however, based on the preliminary findings. This strengthens the need for further research to assess the implication of breast cancer extracellular vesicles transfer viral cargo following oncolytic virotherapy (Kakiuchi et al., 2021).

1.6 Hypothesis and Aims

Oncolytic viruses (OV) are naturally cytotoxic and infect tumour cells whilst sparing healthy tissues. More importantly, OV induce anti-tumour immunity most likely via the exposure of tumour antigens. The full mechanism by which this occurs remains to be elucidated, but it may in part be mediated by extracellular vesicles (EVs). EVs can be taken up by cells, for instance immune cells, at local or distant sites, causing phenotypic changes in the recipient cell. Here, we propose to investigate if EVs are responsible for shuttling immunogenic cargo in response to oncolytic virotherapy. Our hypothesis is that infection of breast cancer cells with an oncolytic virus causes increased release of EVs carrying immunogenic cargo that leads to activation of anti-tumour immunity.

Chapter 2: Materials and Methods

2.1 Materials and methods

2.1.1 Chemicals and Reagents

Table 2.1: Chemicals and reagents used in this study

Reagent	Company
(50 to 100 I.U./mL penicillin and 50 to 100 (µg/mL) streptomycin.)	Lonzo BioWhittaker Ltd
10% v/v Foetal Bovine Serum (FBS)	Lonzo BioWhittaker Ltd
Paraformaldehyde	Sigma Aldrich
Dimethyl Sulfoxide (DMSO)	Sigma Aldrich
DMEM-E12	Lonzo BioWhittaker Ltd
(2 mM L -glutamine)	Lonzo BioWhittaker Ltd
4',6-Diamidino-2-Phenylindole,Dihydrochloride (DAPI)	Invitrogen
Phosphate Buffered Saline	Lonzo BioWhittaker Ltd
Roswell Park Memorial Institute (RPMI) Medium	Lonzo BioWhittaker Ltd
TO-PRO-3	Thermo Fisher
Trypan blue	Sigma-Aldrich
TWEEN 20	Thermo Fisher Scientific
Trypsin/EDTA	Sigma-Aldrich
RIPA buffer	Merk Millipore, Massachusetts, USA
iblot gel transfers kit - nitrocellulose	Bio-Rad

Protease inhibitor	Roche, Burgess Hill, UK
Universal nuclease	Thermo Fisher Scientific
mitomycin C	Sigma
Total exosome isolation (from serum)	Invitrogen

2.1.2 Equipment and Apparatus

Table 2.2: Equipment and apparatus and used in this study.

Equipment and apparatus	Company
LSR II Flow cytometer	BD Bioscience
Incubator	SANYO
light microscope	Olympus
Bench centrifuge	SANYO
Laminar airflow hood	Heraeus
Automated Cell Counter	BIO-RAD
Micropipette	Eppendorf
Plate reader	Thermo Scientific
Water bath	Grant
Coverslips	Scientific Laboratory Supplies
Tissue culture flasks 75cm ² ; 175cm ²	Thermo Fisher Scientific
Mr. Frosty™ Freezing Container	Thermo Scientific
Cryovials	Sigma-Aldrich
Polycarbonate (ultra- Centrifuge bottles)	Beckman Coulter
0.22 µm syringe filter	Millex-GP

Exosome spin columns (MW 3000)	Invitrogen
μ -Slide 8 well glass bottom	(ibidi)
(Amicon Ultra-15 Centrifugal Filter Unit)	Millipore

2.1.3 List of Antibodies

Table 2.3: Primary antibodies used in this study.

Antibody	Clone	Supplier	Dilution	Expected weight (kDa)
Rabbit anti-CD63	EPR5702	Abcam Cambridge, UK)	(1 :1000)	26-65
Rabbit anti-CD9	EPR2949	Abcam (Cambridge, UK)	(1 :2000)	24
Anti-PPP6C/Ppv	EPR8764	Abcam	(1 :1000)	35
Anti-Pentraxin 3/PTX3	EPR6699	Abcam	(1 :1000)	42
Anti-HSV1716 mAb	sheep	Virtuu Biologics Ltd	(1:10,000)	-
Anti-Vimentin antibody [EPR3776] Cytoskeleton Marker ab92547	EPR3776	Abcam	(1 :1000)	54
GM130 Rabbit Antibody	Recombinant Monoclonal ARC0589	Invitrogen	(1:500)	130

Purified mouse Anti-51/TSG101 TSG101	BD Biosciences (1:500)	44
New Jersey, USA)		
HSV-1/2 Gb (10B7)	Sc-56987 SANTA CRUZ	(1 :1000) 130
B2M	EP2978Y Abcam	(1 :1000) 14

Table 2.4: Secondary antibodies used in this study.

Antibody	Supplier	Dilution
Anti-rabbit IgG, HRP-linked antibody	Cell signaling	(1:2000)
Rabbit-antimouse IgG antibody (HRP)	Gene Tex	(1:5000)
Donkey Anti-goat IgG H&L (HRP)	Abcam	(1:1000)
m-IgG Fc BP-HRP	SANTA CRUZ	(1:1000)

2.1.4 List of software

Table 2.5: Software used in this study.

Software	Supplier
Fiji	https://imagej.net/Fiji
Flow Jo	TreeStar Inc
GraphPad Prism 7.04	Graph Pad Inc.
Panther gene list analysais	http://pantherdb.org/
Image Scope x64	https://aperio-imagescope-x64.software.informer.com/12.4/

2.1.5 Culturing of breast cancer cells

Breast cancer cell lines (MCF-7 and MDA-MB-231) were obtained from the ECACC. Adenocarcinoma cell line MDA-MB-231 was obtained from a 51-year-old Caucasian metastatic breast cancer patient's pleural effusion. MDA-MB-231 is a triple-negative breast cancer (TNBC) cell line without HER2 receptors for the human epidermal growth factor, progesterone, and oestrogen. Oestrogen receptor-positive MCF7 cells were derived from Caucasian breast adenocarcinoma patients (**Table 2.6**). T75 flasks (Fisher Scientific®) were used to culture MCF-7 and MDA-MB-231 cells, and 70-80% confluent cells were sub-cultured in RPMI 1640 medium with 2mM L-glutamine and 10% (v/v) Foetal Bovine Serum (FBS). Cultured cells were incubated at 37 °C and 5% v/v CO₂ in an incubator. A standard aseptic procedure was adopted in sterile class II laminar flow hood to culture the cells. To allow proper air circulation, the laminar airflow cabinet was switched on 30 min before use. The equipment and laminar airflow cabinet were sterilized with industrial methylated spirit (IMS). T75 or T175 flasks were used to maintain the cell lines in complete cell growth medium at 37 °C and 5% v/v CO₂. The cells were daily monitored to ensure contamination-free growth. The complete growth medium was added every 48 h until the cells had 70-80% confluence for sub-culturing.

2.1.6 Passaging of mammalian cells

Cells at 70% confluency were twice washed with 10 ml magnesium and calcium-free DPBS to remove residual serum from the cells that could later interfere with the trypsin activity. The trypsinization of the cells was carried out with 0.05% (v/v) trypsin-EDTA solution. Trypsinized cells were detached from the flask surface by incubating for about 2-5 min at 37 °C and 5% v/v CO₂. Magnesium and calcium were removed from the cell surface by adding a mixture of trypsin and EDTA. The trypsin hydrolyses the specific peptide bonds to detach the cells from the flask surface. The cell culturing flasks were examined under the microscope and sharply knocked to release the cells. Prolonged trypsin exposure results in cell death, which can be differentiated by abnormal morphology. In order to inactivate the trypsin, 7.5ml of complete medium with 10% (v/v) FBS serum and a protease inhibitor were added to the cell culture. The solution was thoroughly mixed with a pipette and centrifuged for 5 min at 1000 x g. The supernatant was discarded, and the cell pellet was resuspended in complete medium (5 ml). This process facilitated the production of 70% confluent cells at specific dates.

Table 2.6: Cell lines and characterisation of the cells

Cell line	Category	Cell type	Tissue	Disease	Stage	Culture medium
MCF-7	Human	Epithelial	Breast; Mammary gland	Adenocarcinoma	ER ⁺ , PR ⁺ HER2 ⁻	RPMI-1640
MDA-MB-231	Human	Epithelial	Breast; Mammary gland	Adenocarcinoma	ER ⁻ , PR ⁻ HER2 ⁻	RPMI-1640
Vero	Animal African green monkey	Epithelial	kidney	Normal	-	DMEM-F12
E0771	Animal (C57BL/6 mice)	Epithelial-like	Breast; Mammary gland	Carcinoma; Breast	ER α -, ER β +and PR +	IMDM

2.1.7 Cryopreservation and retrieval of cells

The cells were cryopreserved in liquid nitrogen until they were utilised. To avoid the development of ice crystals during the freezing procedure, the cells (1×10^6 cells/ml) were resuspended in a mixture containing 10% DMSO and 90% FBS. Cryovials containing 1 ml cells were put in cell freezing containers (Mr. Frosty) and gently frozen at -80 °C for 24 h before being transferred to liquid nitrogen. To recover the cells from liquid nitrogen, the cryovials were immediately defrosted in a 37 °C water bath. To remove DMSO from the medium, the defrosted cells were centrifuged for 5 mins at $1000 \times g$ for 5 mins. In a T25 flask, the cells were resuspended in pre-warmed 37 °C and 5 ml growth media. The flask was incubated at 37 °C and 5% v/v CO₂. After 24 h, new growth media was introduced, and cell growth was observed until confluency before further passaging.

2.1.8 Mycoplasma testing of cell-lines.

A regular mycoplasma test was carried out by Ms. Svetlana Solovieva at the department of Oncology and Metabolism University of Sheffield shortly after the arrival of cell lines in the laboratory. The cells were regularly tested for mycoplasma every six months, especially after retrieving the frozen cells. The conditioned medium (5ml) of samples was collected and placed in a universal container for testing. Mycoplasma contamination was examined by using EZ PCR Mycoplasma Detection Kit. The PCR results of mycoplasma testing are shown in **Figure 2.1**.

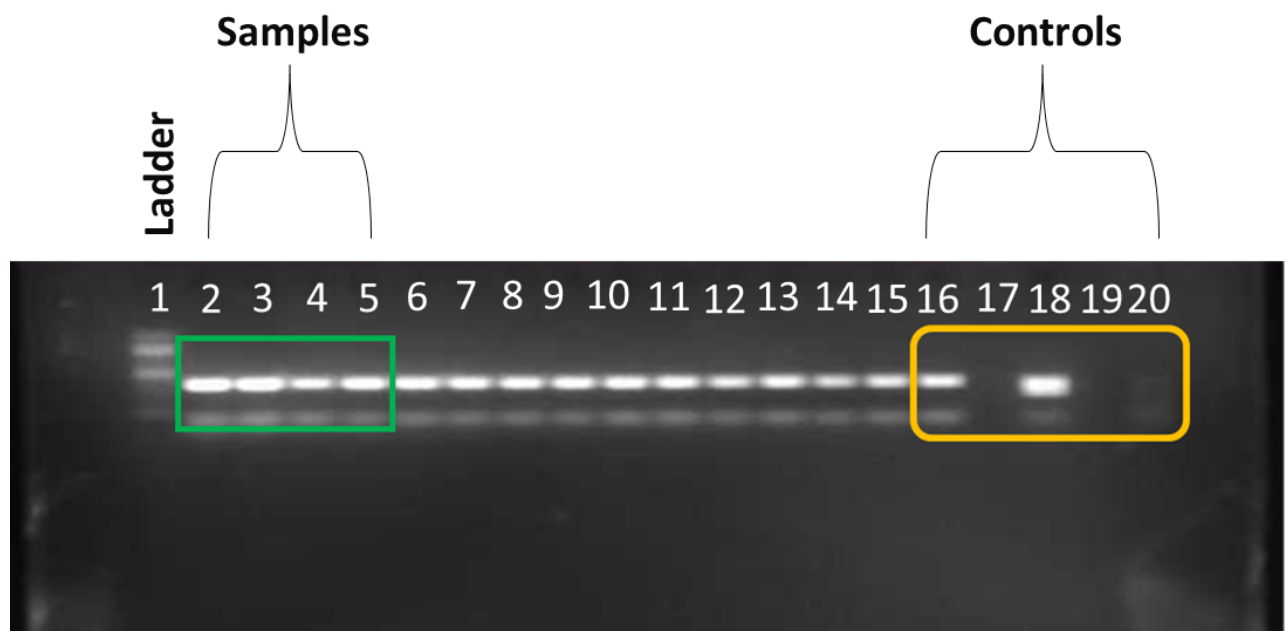


Figure 2.1: PCR based mycoplasma detection results. Lane 1 = 100 bp ladder , samples from lane 2 to 15, from lane 6 to lane 15 unrelated samples,, Lane 2= MCF-7, Lane 3= MDA-MB-231, Lane 4= EO771, Lane 5= Vero cells. Lane 16= negative control (sterile endotoxin-free water), Lane 17= gap, Lane 18= Kit positive control, Lane 19= gap and Lane 20= In house positive control for mycoplasma test (inconclusive)

2.1.9 Cell counting

A TC20™ automated cell counter was used in order to achieve an accurate counting of the total number of cells. After mixing the 10 µl of resuspended cells with 0.4 % (v/v) trypan blue at a ratio of 1:1, 10 µl of the resulting mixture was then placed onto a counting slide. The automatic cell counter determined the overall number of cells as well as the number of viable

cells present in the sample. Trypan blue can only be absorbed to a limited extent by live cells because their cell membranes are neither disrupted nor dissolved, which allows trypan blue to enter the cell. Trypan blue cell exclusion assay is widely used with an automated cell counter as it is an accurate, reliable, and rapid technique. However, the occasional fusion of dye with viable cells is a potential weakness of this technique (Avelar-Freitas et al., 2014).

2.1.10 Depletion of bovine EVs from FBS

Prior to EV separation, it is vital to guarantee that no vesicles from other sources are present that might contaminate the completed product. It has previously been shown that foetal bovine serum (FBS) is a probable source of these contaminated vesicles (Gardiner et al., 2016). This is a problem since cells must be grown in either serum-free or EV-depleted media. Amicon Ultra-15 Centrifugal Filter Unit was used to separate EVs from FBS purchased from Gibco and centrifuged at 3000 g for 1 h before being filter with a 0.22 m filter and used to supplement RPMI-1640 culture medium with the same additives. Nanoparticle tracking analysis was conducted to compare the results of EV depletion methods. RPMI-1640 supplemented with 10% v/v FBS, 10% v/v EV- depleted FBS and EV-depleted medium by adding 10% v/v EV-depleted FBS depicted a decrease in particle count from $4.30\text{E}+10$ to $4.69\text{E}+07$ particle/ml and zero, respectively (**Figure 2.2**).

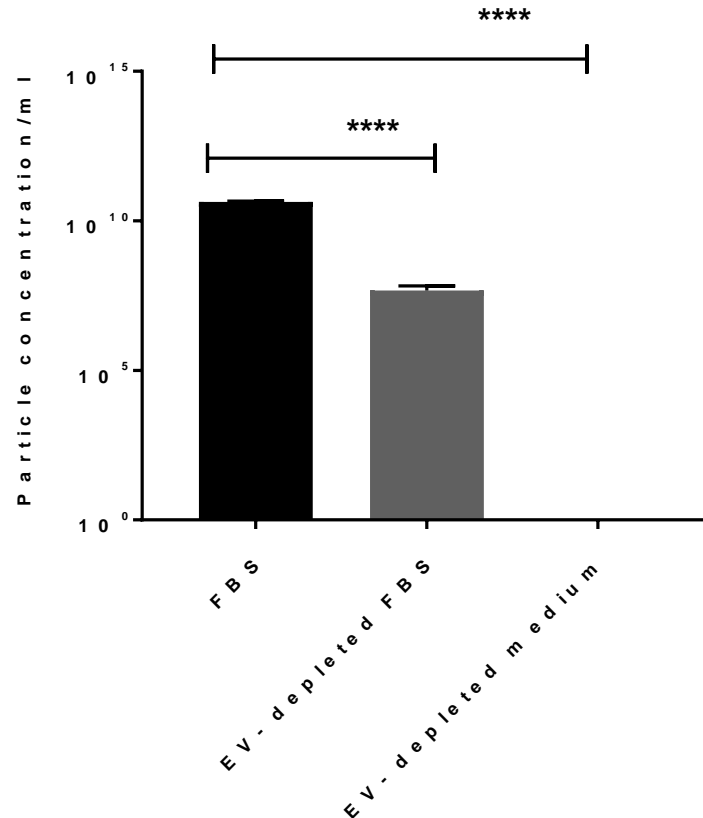


Figure 2.2: FBS particle concentration in unprocessed serum, in-house depleted Serum (centrifugation for 1 h at 3000 g), and EV-depleted medium. The serum was diluted to a final concentration of 1 in 50 and filtered through a 0.22 μm centrifugal filter unit. Samples were analysed by NTA. One-way ANOVA with Dunnett's multiple comparisons test correction revealed fewer particles in in-house serum. N=6 technical replicates; error bars= SEM.

2.1.11 Viral infection

Herpes Simplex Virus 1716 (HSV 1716) (Virtu Biologics, Glasgow) was suspended in Dulbecco's Modified Eagle's Medium to make the stock solution. The stocks were supplied in PBS at a concentration of 108 plaque forming units/ml and kept at -80°C .

MDA-MB-231 and MCF-7 cells were seeded at a density of 10×10^6 cells in a T175 flask and incubated at 37°C for 24 h. Following that, cells were placed in RPMI-1640 media containing free serum and infected with HSV 1716 at MOI 1. Before removing the culture media, the infected cells were cultured for 4 h at 37°C in an incubator with 5% v/v CO_2 . The cells were washed with PBS to remove viral particles that had not entered the cells before being cultured in RPMI-1640 supplemented with 2mM glutamine and 10% v/v EVs-free FBS. Without the addition of HSV 1716, untreated cells behaved similarly. Prior to collecting conditioned media, both control and infected cells were cultured for 48 h.

2.1.12 Extracellular vesicle collection

2.1.12.1 Conditioned medium

MCF-7 and MDA-MB-231 Cells (10×10^6) were seeded in 175 cm culturing flasks containing EVs depleted medium and incubated for 48 h at 37 °C and 5% v/v CO₂. The conditioned medium was collected after 48 h in 50 ml falcon tubes.

2.1.12.2 Differential centrifugation

The EVs were extracted from the MCF-7 and MDA-MB-231 conditioned medium according to Théry et al by centrifuging at 300 x g for 10 min to eliminate cell debris. The supernatant was centrifuged for 10 min at 2,000 x g to remove apoptotic bodies and the microvesicles were removed by centrifugation at 10,000 x g for 30 min (Théry et al., 2006). Further centrifugation was carried out at 100,000 x g for 90 min to pellet exosome as shown in (**Figure 2.3**). Beckman T70 Ti rotor to achieve the pellets of small EVs, which were either resuspended in PBS and kept at -20°C or resuspended in RIPA buffer and stored at - 80 °C for downstream studies.

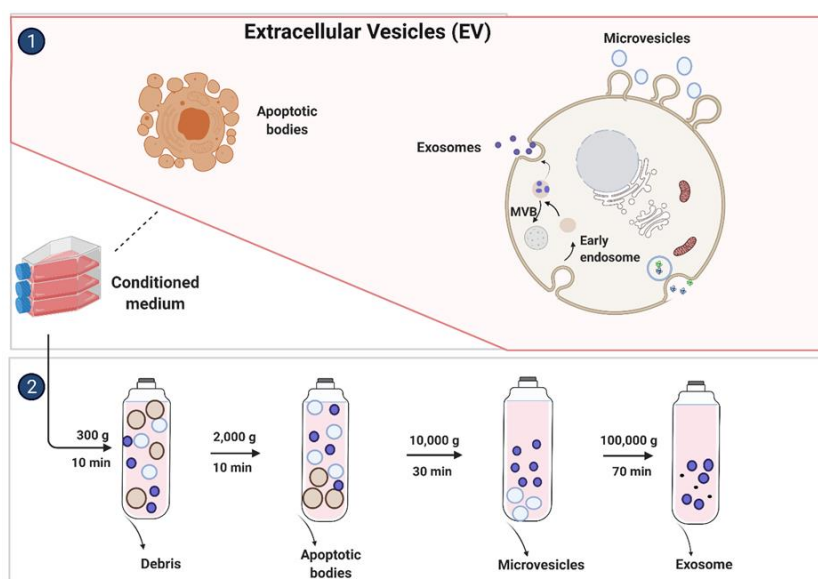


Figure 2.3: A diagram of an ultracentrifugation procedure. To eliminate cell debris, 10 min of centrifugation at 300 x g., the supernatant was centrifuged for 10 min at 2,000 x g to remove apoptotic bodies. Centrifugation at 10,000 x g for 30 min was used to remove microvesicles. A further 90 min centrifugation at 100,000 x g was performed to pellet exosome for further investigation, the pellet is resuspended in phosphate buffered saline (PBS). (**Biorender**)

2.1.13 Transmission Electron Microscopy (TEM)

The Transmission Electron Microscope (TEM) was used by the Department of Biomedical Sciences and was operated at 120kV with an Orius 1000 camera. Studies using the TEM technique were carried out at Sheffield University with the assistance of Chris Hill from the Department of Biomedical Science.

2.1.13.1 Preparation of samples

2.1.13.1.1 Fixation

To prepare samples for electron microscopy, the following approach was used, which was reported by Théry et al. Care was taken at each step to ensure that the grids remained moist on the membrane side while remaining dry on the other side (Théry et al., 2006). After resuspending the EV pellets in 50 µl of 2% paraformaldehyde (PFA) fixative, they were kept on ice. For each sample, three 8 µl droplets of the PFA suspended EVs were deposited onto a square of parafilm on a petri dish. A 200 mesh formvar coated grid was then placed membrane side down on each drop using a pair of forceps. After that, the grids were allowed to sit for twenty mins in a dry atmosphere so that adsorption could take place. After that, the grids were given a single washing in PBS by floating them with the membrane side down in a 100 µl drop that was placed on the parafilm. Following the glutaraldehyde treatment, the grids were washed in distilled water for 2 min each using flotation on drops on parafilm. Following the wash processes, the grids were contrasted and immersed for 5 min in a 50 µl drop of pH 7 uranyl-oxalate solutions, followed by 10 min in a 50 l drop of 9:1 (v/v) 2% methylcellulose: 4 % Uranyl acetate solution on ice. The grids were allowed to air dry prior to being stored, and then any extra liquid was removed from them by gently blotting them with Whatman no. 1 filter paper. The grids were photographed at a voltage of 80 kV using a Tecani Spirit G2 imaging system.

2.1.14 Nanoparticle tracking analysis (NTA)

The concentration and size of the exosomes were measured using Zetaview PMX 120 instrument (Particle Metrix, Malvern Panalytical Ltd., Malvern, UK). The instrument uses the 488 nm laser which detects properties of Brownian motion and light scattering in order to measure the exosomes suspended in the liquid medium. NTA was performed according to the instructions provided by the manufacturer. Briefly, the purified exosomes samples were diluted in PBS were and passed through the sample chamber of the instrument, and 3 movies of 60 seconds each were obtained, which were analysed by NanoSight particle tracking software to generate the sizes and concentrations of the particles in each movie. The experiment was repeated in triplicate, and the afore-mentioned procedure was performed for each experiment. The measurements from three experiments were averaged to order to calculate the sizes of the particles.

2.1.15 Plaque assay

2.1.15.1 Preparation of cells

Vero cells (2×10^5) were seeded in a 12-well plate and recommended growth medium (DMEM-F12) was added. Cells were incubated overnight at 37 °C and 5% v/v CO₂ in a humidified incubator.

2.1.15.2 Dilutions and Infections

Before infection, the cells were washed with Dulbecco's Phosphate-Buffered Saline (DPBS) and the growth media was removed. The diluted virus was added to each well (**Figure 2.4**) by following multiple wells per dilution method. Viral adsorption was carried out by incubating the cells for 2 h with gentle swirling after every 30 mins. The process ensured an even coverage and prevented the drying of the cellular monolayer. Then, the inoculum was removed and washed with a basal medium.

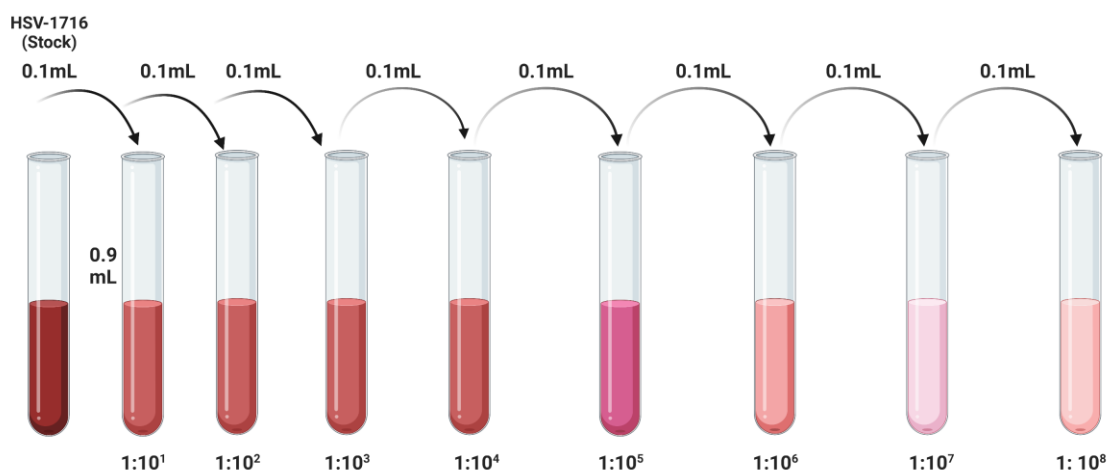


Figure 2.4: Serial dilution of HSV-1716 stock. Initially, the test tubes were filled with 0.9 mL of mixing reagent. Then, 0.1 mL of the original sample was added into the first test tube to make a volume of 1.0 mL. The virus sample was further diluted by 1-10fold. The serial dilution was continued until the original virus sample was diluted to 10⁸. The serial dilution was carried out because the original virus sample was too concentrated. (**Biorender**).

Cell infection was carried out for 2 h. 4% sterile agarose was prepared in dH₂O by autoclaving at 121 °C for 20 mins. An appropriate volume of immobilising medium was directly overlayed to the inoculums in the well at a ratio of 1:10 (1 part of plaque media and 9 parts of immobilising overlay of agarose). The plates were gently rocked to mix the contents and incubated for 72 h.

2.1.15.3 Cell Fixing and Staining

After 72 h, a fixing solution containing 4% formaldehyde was prepared in dH₂O (3 ml of 37% stock formaldehyde mixed with 27 ml of dH₂O). The solution was incubated for 1 h and agarose plugs were removed by using a spatula. Then, the cell monolayer was washed with PBS. To prepare a crystal violet stain, 2.5g Crystal Violet (CV) was mixed in 500 ml dH₂O. The cell staining was carried out by covering the cells for ~15 min with a minimal amount of crystal violet solution. The plates were gently rocked to ensure even coverage. Crystal violet stain was gently washed off with water. Once fixed, stained, and dried, the plaques were stored for future analyses.

2.1.15.4 Determining Viral Titers

The plaques in each well were counted and an average of technical replicates of the same dilution was calculated. For large plate formats, the wells were represented as fewer than five or greater than 100 plaques. Plaque size and morphology were carefully noted. The negative control with a uniform monolayer was used as a reference control. The viral titer of the stock sample was determined according to the following formula:

$$\text{Number of Plaques} / (D \times V) = \text{pfu/ml}$$

Where D is the dilution factor and V is the Volume of diluted virus/well.

2.1.16 Assessment of cell proliferation and survival

Two methods were adopted to determine the cell proliferation including the counting of viable cells, and the AlamarBlue assay for measuring the cellular metabolic activity.

2.1.16.1 Cell counting in response to EVs treatment.

The impact of EVs on MDA-MB-231 cell proliferation and growth was assessed by seeding 1×10^5 cells in 12-well plates. Different EVs concentrations (10^7 , 10^6 , 10^5 , 10^4 particles/ml) were simultaneously added in the medium containing depleted EVs 10% serum. The cells were incubated at 37 °C and cell proliferation was determined after 24, 48, and 72-h through trypsinization, and cells were counted.

2.1.16.2 AlamarBlue Cell proliferation/ viability

AlamarBlue® Cell Viability Assay Reagent (Thermo Fisher, DAL 1025) quantifies cellular metabolic activity and viable cell concentration in each sample. It can also quantitatively measure the proliferation of fungi, bacteria, and mammalian cell lines. The REDOX (oxidation-

reduction) indicator in the dye fluoresces and changes the color after chemical reduction due to cell growth. The high stability and nontoxic nature of AlamarBlue facilitate continuous cell culture monitoring at different intervals. The oxidized form of AlamarBlue is non-fluorescent and blue. Cell growth-based chemical reduction turns AlamarBlue dye from non-fluorescent blue to fluorescent red. The steady growth of viable cells continuously maintains a reducing environment (fluorescent, red) whereas the cell growth inhibition maintains an oxidizing environment (non-fluorescent, blue). These conditions are detected through a fluorescence or absorbance detector. Cells in the log phase of growth were harvested and counted, which revealed an optimal cell count of 5×10^3 cells/ml (cell density). The test compounds were added in 96 well-plate with a final volume of 100 μ l in each well. The plates were incubated at 37 °C for 4 h in an incubator to estimate the exposure effect of each test compound. After incubation, the assay plates were gently shaken to mix the compounds, and 10 μ l of AlamarBlue Reagent was aseptically added to each well. The positive control wells contained 10 μ l of ultrapure sterile water. Cell cultures with AlamarBlue Reagent were incubated at 37 °C for 4h. After incubation, the plates were taken out, and fluorescence was measured at an Excitation wavelength of 530-560nm and Emission wavelength of 590nm.

2.1.17 Scratch (wound healing) assay

The scratch test was used to evaluate cell migration ability because it may imitate the behaviour of tumour cells during *in vivo* migration. This is a simple, cost-effective, and convenient method for *in vitro* cell migration analysis. However, certain limitations are associated with this method as it can only be performed at the confluent cell level and wounding a confluent cell monolayer surface can damage the extracellular matrix components (Liang et al. 2007). The measuring of gap closure at different intervals quantifies cell proliferation and migration. To ensure only the measurement of cell migration, the cell proliferation was reduced by using 2 μ g/ml mitomycin C. A 24-well plate was used to seed all the cell lines (1×10^5 cells/well) in a final medium volume of 500 μ l. A confluent monolayer was achieved by incubating the plate for a total of 48 h. Then, the medium was replaced with serum-free medium, and cells were starved for a further 48 h. Mitomycin C was added to the medium about one h before making a straight-line scratch with a pipette tip (p200). To remove floating cells and cell debris, the cells were washed once with DPBS (500 μ l) and 500 μ l medium was added and plates were incubated 30 min to equilibrate the stressed cells. Then, the serum-free medium was replaced with fresh medium (500 μ l) containing 1% serum. Microscopic images (10x magnification) of each plate well were captured before and after scratching. The plates were incubated at 37 °C

in a tissue culture incubator, and microscopic images were captured at different intervals (0, 6, and 24 h). The gap closure and remaining clear areas at each interval (0, 6, and 24 h) were assessed by using ImageJ software and compared with the control (0 h). The same procedure was repeated for each cell line. The experiments of each cell line were carried out in triplicate with three wells per cell line per repeat. The wound closure percentage was calculated according to the following equation:

$$\text{Wound closure (\%)} = \frac{\text{width of initial scratch} - \text{width of scratch at 0, 6 \& 24h}}{\text{width of the initial scratch}} \times 100$$

2.1.18 Cell death and uptake of EVs

HSV1716 or HSV1716-GFP OVs were defrosted on ice for around 15 min. MDA-MB-231 and MCF-7 cells were grown in 500 μ l serum-free RPMI after being seeded into 6-Well Plates (Section 2.1.6) 24 h earlier. Following that, OVs or EVs-OV complexes produced as described in Section 2.1.11 were added to the wells at MOI 1 (1×10^8 pfu/ml) and incubated for 4 h at 37° C preceding the addition of 2.5 ml of complete medium to each well. OVs and cells were treated for 24, 48, and 72h respectively. Following the completion of the culture, the cells were detached for flow cytometry using trypsin/EDTA and then washed with 2 ml of PBS as described in section 2.1.6.

All samples were placed into 400 μ l flow cytometry tubes. Prior to analysis on the FACS Calibur, 5 μ l of the viability dye TOPRO-3 was added to each sample to measure cell death (BD biosciences). The findings were analysed using FlowJo® software, and cell death was determined by creating dot plots based on a change in fluorescence against FL-4-H. The uptake of HSV1716 GFP and EVs by cells was evaluated using variations in forward scatter (FL-1-H) and side scatter (SSC-H). GFP expression in the FL1-H channel was used to measure viral infection of cells in research employing the HSV1716 GFP.

2.1.19 Western blot analysis

The expression of target proteins of different cell lines, used in this study, was examined through Western blot analysis. Proteins were isolated from cell lines and culture media. Western blot analysis used SDS-PAGE to separate proteins based on molecular weight. These proteins were transported to a membrane, and particular antibodies were used to identify target proteins. The primary antibody was confirmed by a secondary antibody. The reaction was

detected through a band producing chemiluminescent light in the presence of a soluble enzyme-substrate (Mahmood and Yang, 2012).

2.1.19.1 Sample preparation and extraction

80-90% confluent cells were twice washed with cold DPBS (10 ml). Proteins were extracted by adding 1 ml of RIPA lysis buffer (0.1% SDS, 25 mM Tris-HCl pH 7.6, 1% NP-40, 1% sodium deoxycholate, 150 mM NaCl) mixed with 10 μ l protease phosphatase cocktail inhibitor (leupeptin, targeting serine, and cysteine proteases) to the cell extracts. These inhibitors inactivate or block endogenous phosphorolytic and proteolytic enzymes, released during cell lysis, to avoid protein degradation. Then, the cells were incubated with lysis buffer for 5 min and continuously shaken on ice to avoid protein degradation. Later, the cells were scraped and collected in Eppendorf tubes. Lysed cells were further incubated on ice for 30 mins for complete lysis. This step was followed by centrifugation for 15 min at 13000 \times g and 4 °C to remove the cell debris. The protein was extracted from supernatants, and just a little amount was used in the protein quantification assay. The remaining protein samples were stored at -80 °C.

2.1.19.2 Measurement of protein concentration

A BCA (bicinchoninic acid) protein assay kit was used to measure the protein content of samples (Thermo-Fisher Scientific). As stated in Table 2.7, known concentrations of bovine serum albumin (BSA) standards (0 to 250 g/ml) were produced in the same buffer as samples. Each sample and standard were examined in triplicate, with 10 μ l of each placed to a microplate. Each well received 200 μ l of test reagent (a 50:1 mixture of A and B solutions). The plate was covered with a plastic film cover and incubated at 37° C for 30 min. The absorbance was measured at 562 nm using a Multimode plate reader EnSight™ after incubation. A standard curve was constructed by graphing absorbance values against BSA concentrations, and a polynomial equation was used to calculate sample concentration (**Figure 2.5**).

Table 2.7: BSA preparation

No.	Diluent volume (µl)	BSA volume and source (µl)	Final BSA concentration (µg/ml)
A	700	100 of stock	250
B	400	400 of vial A dilution	125
C	450	300 of vial B dilution	50
D	400	400 of vial C dilution	25
E	400	100 of vial D dilution	5
F	400	0	0= Blank

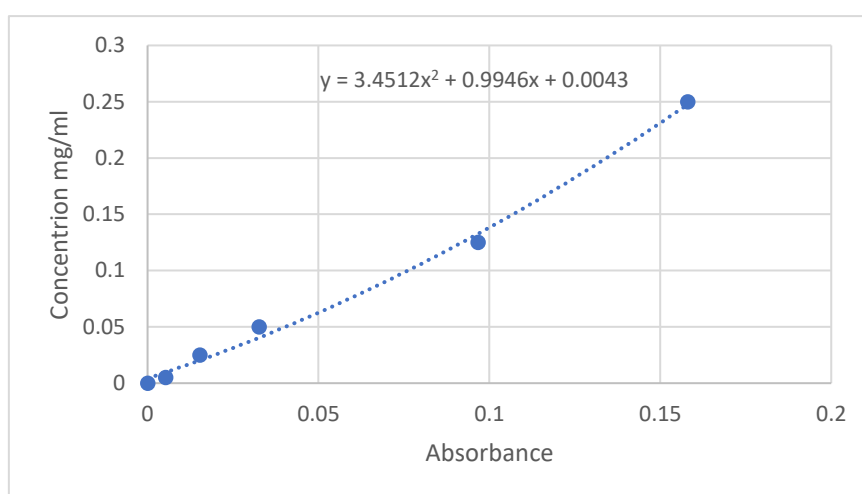


Figure 2.5: BCA standard curve example. The absorbance readings were plotted against BSA concentrations, and a polynomial equation was used to estimate the sample concentrations. This established a standard curve, which was then used to determine sample concentrations.

2.1.19.3 Sample preparation and loading

1x cell lysate volume was diluted to a final concentration of 2 µg protein in dH₂O. The solution was incubated for 10 min at 95 °C with 1x volume of 2X Laemmli. Laemmli buffer contains 4% (w/v)(SDS-PAGE) is an electrophoretic method that is used in the field of biotechnology to separate proteins according to their molecular weight. In general, proteins are amphoteric molecules, which means that they have both positive and negative charges contained inside the same molecule, 20% (v/v) Glycerol to increase sample density, 1% (v/v) Bromophenol blue tracking dye, 10% 2-mercaptoethanol to reduce disulphide bonds, 0.125 M Tris-HCl (pH 6.8), and dH₂O.

2.1.19.4 Electrophoresis and protein transfer

To determine the molecular weight of each band, the first lane was loaded with 5 µl of precision

plus protein dual-color standards (MW range: 10-250 kDa). To generate an electric connection between electrodes and gel, prepared cell lysates were loaded onto 12% Mini-PROTEAN TGX precast gels (BIO-RAD) in a tank containing 1X TGS running buffer (190 mM glycine, 25 mM Tris, and 0.01% (w/v) SDS). After 30 min at 120v, the voltage was raised until the blue dye flowed off the gel bottom. The gel was then put on top of the iblot cathode's nitrocellulose membrane and topped with filter paper pre-soaked in transfer paper. After carefully removing the air bubbles, a sponge and anode were added to the stack. Proteins were transferred for 6 min at 23 V using the Thermo Scientific™ iBlot® Blotting System.

2.1.19.5 Blocking and antibody incubation

Pre-stained standards were visually observed to confirm the successful protein transfer to the membrane. 1X TBST (100 ml of 10X TBS and 500 µl of Tween-20 0.05% (v/v) in 900 ml dH₂O) washing buffer was used to wash the membrane. Non-specific binding of antibodies was prevented by incubating the membrane for one h in blocking solution (5% (w/v) non-fat milk in 0.05% TBS-Tween) at room temperature on a shaker. Then, the membrane was incubated with primary Ab (optimum dilution) at 4°C. Each membrane was washed on the following day with TBST (5x) for 5 min and incubated at room temperature for one h with an appropriate dilution of the relevant horseradish peroxidase (HRP) secondary antibody and again washed with TBST (5x) for 5 min. This step was followed by the addition of the WASTER SUPERNOVA Chemiluminescent Substrate Kit to the membrane and left for 2 min to react. Then, the membrane was imaged using ChemiDoc™ MP System (BIO-RAD).

2.1.20 Labelling of extracellular vesicles with Alexa fluor 488

To label EVs, C5-Maleimide-Alexa fluor 488 (2.5 µl) was added to a 30 µl EV aliquot and 17.5 µl PBS was added to make a final volume of 50 µl. The solution was incubated at room temperature for 60 min in the dark (Roberts-Dalton et al., 2017). The Exosome Spin Columns (Invitrogen) were prepared in accordance with the instructions provided by the manufacturer. During this step, the powdered resin was allowed to hydrate at room temperature for 15–30 mins. After inserting the spin columns into the collecting tubes, the 750g of material was centrifuged for two mins in a swing-out rotor. The collection tubes were discarded and labelled EV aliquot was added to the resin. Labelled EVs were collected by centrifuging (750g for 3 min) the spin columns placed in 1.5 ml Eppendorf tubes. The resin retained the non-incorporated excess dye that was confirmed from the controls having dye without EVs. Labelled EVs (EVs 488) were gently mixed in 1000 µl of phenol red-free DMEM and filtered

through 0.22 µm filter (Millex), aliquoted, and stored at –80 °C until required for microscopy analysis.

2.1.20.1 Cell internalization of Alexa488 and labelling of extracellular vesicles in breast cancer cell lines

MCF-7 and MDA-MB-231 cells (5×10^3) were seeded in 8 well glass bottom (ibidi) and cultivated for 24 h to achieve 80–90% confluency. EVs in an imaging media contained 20 mM HEPES and phenol-red free DMEM that included 0.05 % w/v BSA were given to the cells at a concentration of 2µg ml⁻¹ 4h before fixed-cell confocal microscopy was performed. Cells were incubated with the nuclear label DAPI (1: 1000) for 5 min, washed with imaging medium, and microscopic images were captured.

2.1.21 Label-free mass spectrometry

Mass spectrometry of all the samples was carried out by Dr. Caroline Evans at the Chemistry Mass Spectrometry Facility. EV purification from the conditioned medium was carried out by ultracentrifugation at 100,000 x g for 1 h. The pellet was resuspended, and a compatible detergent (Rapigest) was used for the mass spectrometry of the extracted protein. Rapigest detergent generates peptides by reducing, denaturing, digesting, and alkylating the proteins. High-performance liquid chromatography (HPLC) was carried out to further separate the peptide samples into fractions. Briefly, the peptides were eluted in a HPLC loading buffer (0.1 v/v Trifluoroacetic acid, 97% v/v Acetonitrile), and passed through HPLC capillary (0.075 x 500 mm) from buffer A (0.1% v/v Formic Acid, Water) to buffer B (0.1% v/v formic acid, 80% Acetonitrile).

2.1.21.1 Mass spectrometry data analysis

MaxQuant v1.5.3.30 was used to pre-process the initial mass spectrometry data. The samples were compared to a proprietary database of human proteomes. To summarise, group-specific trypsin digestion and label-free analytic settings were used to represent label-free data' Type Standard Multiplicity 1 no labels'. Methylthio was employed as a global measure to analyse the changes in protein structure induced by alkylation and reduction during sample processing. To equalise the overall intensity across samples, intensity measurements were transformed to LFQ intensity values. Data that has been pre-processed was loaded into Perseus v1.5.2.6 for additional analysis. Contaminant proteins were eliminated, and results obtained without labels were transformed to a Log₂x score.

2.1.22 Flow cytometry to assess EVs uptake and cell death in tumour cells MCF-7 and MDA-MB-231

Following an overnight incubation of cells with EVs and HSV1716, flow cytometry was utilised to determine EV uptake and cytotoxicity. To detach the cells, trypsin/EDTA was employed (**Section 2.1.6**), and the cell pellet was washed twice in 5ml PBS. The supernatant was discarded, and the pellet was re-suspended in 500µl PBS. All samples were placed in 400µl flow cytometry tubes. Cell death was determined by adding 2µl TOPRO-3 to each sample shortly before to FACS Calibur analysis (BD Biosciences). 10,000 events per sample (equivalent to 10,000 cells) were recorded, and FlowJo® software was used to analyse cell death by generating fluorescent dot plots based on changes in fluorescence against FL3-H and EVs, as well as HSV 1716 uptake based on changes in forward scatter (FSC-H) and side scatter (SSC-H).

2.1.23 In Vivo

2.1.23.1 Murine model of breast cancer

C57BL/6 female mice were obtained from Envigo when they were 6-8 weeks old and were kept in the University of Sheffield Biological Services Unit, where they were cared for in accordance with the University of Sheffield code of ethics and Home Office rules. Animal study was carried out with the support of Mr Matt Fisher and under Dr Munitta Muthana's Home office project licence (PPL1099883). Mice were given a week to acclimate after arriving from the supplier. The following technique was used to inject 1×10^6 EO771-Luc cells into the nipple of mice. Inhalant isoflurane (IsoFlo) was used to anaesthetise mice. They were then shaved across the whole abdomen region to expose both nipples (inguinal group), and the skin was disinfected with Hibiscrub. Following that, 1×10^6 EO771 cells (taken from flasks during their exponential development phase) were injected into the nipple using an insulin syringe in 20ul PBS containing 50 % matrigel/50 % PBS/. Mice were checked on a regular basis and weighed every three to four days. The volume of the tumour was measured with callipers and recorded every three days using the following equation:

$$\text{Tumour volume (mm}^3\text{)} = \frac{W^2 \times L}{2}$$

For the bioluminescence test, mice were subcutaneously injected for 10 min with 100 L of d-Luciferin. A non-invasive in vivo imaging equipment was then used to scan the mice (IVIS

200 System, Xenogen), while under isoflurane anaesthesia administered through a nasal cone. Each group of mice in this research had n=10 animals per group. A power calculation utilizing the following equation was used to justify the number of animals: When the tumours reached 150-200 mm³, the mice were given the following intravenous treatments (i.v.).

1. Control: Mice were given three injections in total i.v. (13, 15, 17 days) with 100 µl PBS.
2. EV: Mice were given three injections in total i.v. (13, 15, 17 days) with 100µl labelled EV with Alexa flour 488 (30µg).
3. EV-OV: Mice were given three injections in total i.v. (13, 15, 17 days) with 100µl labelled EV-OV with Alexa flour 488 (30µg).
4. HSV-1716 (OV): Mice were given three injections in total i.v. (13, 15, 17 days) with 100µl HSV1716 GFP at 10⁷ pfu/ml. After receiving therapy, 5 mice from each group were culled after 24 h and the remaining mice were culled after 72 h by cervical dislocation, and the organs and tumour were removed and kept in liquid nitrogen for post-mortem examination.

2.1.23.2 Tissue preparation of samples for post-mortem analysis

Tumours were divided into two groups immediately after being removed from the mice. One of them was placed in cryobuffer (90 % FCS with 10 % DMSO) and frozen in liquid nitrogen until it was utilized for flow cytometry, RNA extraction for NanoString technology. Optimal cutting temperature (OCT) was used to embed the remaining half of the tumours, which were then frozen at -80°C in preparation for cryosectioning. Frozen slices (14 microns thick) were cut for Haematoxylin and Eosin staining.

2.1.23.3 Dissociation of EO771 cells tumours

Prior to freezing tumour pieces and washing 3 times with DPBS, ice-cold DPBS containing 2% FCS (FACS buffer) was produced. Tumor chunks were then incubated for 30 min using a rotator in a warm environment with 5ml enzymatic dissociation solution comprising 0.2 mg/ml collagenase, 2 mg/ml dispase, and 1.25ug/ml DNase I in serum-free Iscove's Modified Dulbecco's Medium (IMDM) (37°C). The scattered material was then passed through a 40-70m nylon filter after 10 % FBS was added to neutralise the enzymes in the medium. The cell solution was then filtered and centrifuged at 4500 rpm for 5 min before being washed three times in 500µL DPBS for flow cytometry (see 2.2.20.4).

2.1.23.4 Preparation of tumour cells for flow cytometry

Tumour pieces were dissociated as described in section 2.1.22.3. The cell pellet was resuspended in Zombie UV viability dye (1µL in 100µL) and incubated on ice for 45-60 min. After washing the samples twice with 500µL of FACS buffer (50ml DPBS with 25µL FCS), the cell suspension was centrifuged at 4500 rpm for 5 min in a microcentrifuge. Finally, samples were resuspended in 300µl of FACS buffer (1 %FBS/PBS solution) and transferred to flow cytometry tubes (400µl). The BD LSR II flow cytometer was used to quantify Alexaflour 488 labelled EVs and HSV1716-GFP. FlowJo software was used to further process the data sets.

2.1.23.5 Cytokine Protein Level Expression Analysis with Cytokine Bead Array (CBA)

Mice were infected with OV, EV-OV, and EV alone, in addition to the control group as was detailed in section 2.2.20.1 On day 21, the serum was obtained by separating it from mice blood. After that, CBA was carried out in order to evaluate the levels of expression of a number of different cytokines the following cytokines were purchased from BD Biosciences (IL-2, IL-10, IL-12, IL-4, and MCP-1, TNF, and IFN- γ). Multiplex beads are coated with antibodies to cytokines in this experiment.

Following this, the antibodies bind to and remove the cytokines from the serum of mice. In order to determine the cytokine concentrations in each sample, an Attune Autosampler was used. Two vials of standard were included in the CBA Flex Set, along with one vial of both the Capture Bead and the PE Detection Reagent (reporter). The protein concentration of the standard was 10,000 pg/ml, and it was reconstituted in 4.0 ml of assay diluent. To protect the prepared components from light exposure, they were kept at 4 °C. The fluorescent signal that is produced by the binding complex between the antibody and the cytokine reflects the concentration of the analyte that is present in the test matrix. For the purpose of determining the amount of each analyte present in the sample being tested, standard curves were created. Of note, the samples were kindly run on the Attune by the flow team.

2.1.23.6 Haematoxylin and Eosin staining

Tumours and lung pieces were fixed for 10-20 min in acetone (methanol 50:50 mix (kept in freezer) or methanol alone). After washing twice in PBS, the sections were put in Gill's Haematoxylin solution for 1 min before being rinsed in tap water for 5 min until the water ran

clear. Slides were immersed in 70% ethanol for 3 min, then in 90% ethanol for another 2 min. These parts were then immersed in eosin (2g eosin dissolved in 400ml 95 % ethanol) for 1 min before being rinsed in 100% ethanol for 5 mins. After that, the slides were mounted using DPX mounting media. The slides were scanned using an Aperio ScanScope CS with a 40x objective lens.

2.1.23.7 Isolation of labelled EVs from serum

Following the treatments outlined in the section 2.2.20.1. 24 h after the infection blood samples were obtained from all treated groups of C57BL/6 mice, and the blood was allowed to clot at room temperature for 15-30 min (**Figure 2.6**). After that, the blood was centrifuged at 3000 xg for 10 min, and the top liquid layer, known as serum, was collected. To remove debris from the serum, it was centrifuged at 2000 xg for 30 min at room temperature. After transferring the cleared serum, 200ul of the total exosome isolation solution was added on serum. The samples were mixed and incubated for 30 min at 2-8 ° C. Following incubation, the samples were centrifuged for 10 min at 10,000 x g at room temperature. Supernatant was removed; an exosome pellet was collected from the bottom of the tube and resuspended 50ul in 1x PBS; and the isolated exosomes were stored at -20 ° C for long-term storage.

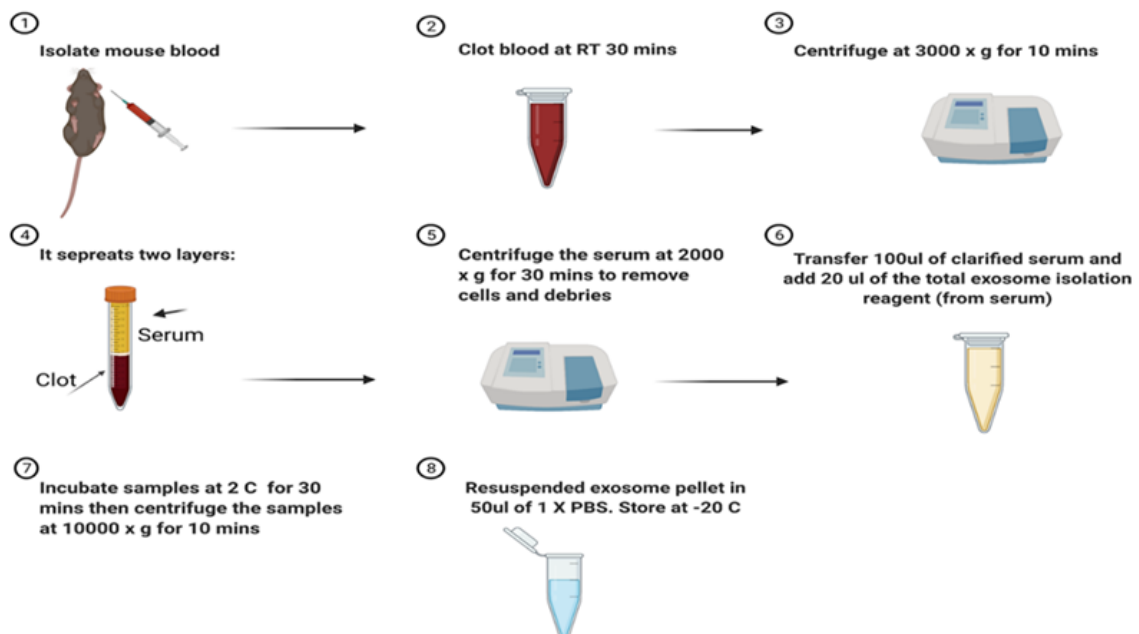


Figure 2.6: Isolation of labelled EVs from blood serum collected from treated mice. (Biorender).

2.1.23.8 Nano-Flow Cytometry (NanoFCM)

For the simultaneous detection of side scatter (SSC) and fluorescence of individual particles, a NanoAnalyzer U30 instrument manufactured by NanoFCM Inc. was utilised. This instrument was equipped with dual 488/640 nm lasers as well as single-photon counting avalanche photodiode detections (SPCM APDs). Bandpass filters enabled the collecting of light in certain channels (SSC = 488/10; FL1 = 525/40; FL2 = 670/30), respectively. A gravity feed was used to provide HPLC-grade water as the sheath-fluid, which resulted in a reduction in the sample core stream diameter $\sim 1.4 \mu\text{m}$. The measurements were obtained at a sample pressure of 1.0kPa, which was maintained by an air-based pressure module for the duration of the one-min measurement period. Every sample was diluted to the point where the particle count was brought down to an acceptable level between 2,000 and 12,000 per min. During the process of sample acquisition, the sample stream is fully illuminated within the central region of the focused laser beam. This results in a detection efficiency of approximately one hundred percent, which in turn leads to accurate particle concentration measurement via single-particle enumeration. In order to calibrate the sample flow rate, the concentration of the samples was calculated by comparing them to silica nanoparticles with a known concentration that were 250 nm in size. EV isolates were measured in accordance with the techniques outlined in the standard operating procedures using a unique 4-modal silica nanosphere cocktail (NanoFCM Inc., S16M-Exo). Using the NanoFCM software (NanoFCM Profession V1.8), a standard curve was generated based on the side scattering intensity of the four different silica particle populations with diameters of 68, 91, 113, and 155 nm respectively. This curve was used to compare the results of the four different silica particle populations. Silica offers a steady and monodisperse standard with a refractive index of around 1.43 to 1.46, which is similar to the range of refractive indices that have been reported in the literature for EVs ($n = 1.37$ to 1.42). The laser was adjusted to a setting of 10 MW with a 10 % SSC decay. The processing of the data was taken care of inside the nFCM Professional Suite v1.8 software, and the statistical data, dot plots, and histograms were all delivered in a single PDF. The programme has gating that enables proportional analysis of subpopulations that have been segregated by fluorescence intensities, with size distribution and concentration data provided for each subpopulation.

2.1.23.9 NanoString gene expression analyses.

A murine pan-cancer immune profiling panel was used to conduct the analysis of the gene expression profile of EO771 cell tumour samples at Nottingham Trent University's John van Geest Cancer Research Centre, which is located in the College of Science and Technology.

Using a Nanodrop 8000, we evaluated the quality of each of the RNA samples, and then we utilised 150ng of total RNA from each sample to set up the NanoString. Raw data were analysed using nSolver Analysis Software (V.4.0), imaging quality control (QC), mRNA positive control QC, and normalisation QC were checked, and all of the samples were in agreement with the quality criteria of NanoString gene expression assays. In order to perform differential expression analysis, route scoring, and cell type scoring, the nSolver advance analysis module version 2.0.115 was used. Prior to the calculation of cell-type signature and pathway expression scores, normalised gene expression intensities were mean-centered. These scores were calculated as the mean average \log_2 expression intensity for all genes in each ontology (annotation), as described in the NanoString document LBL-10094-02 (nCounter Mouse PanCancer Immune Profiling Panel Gene List).

2.1.24 Statistical analysis

GraphPad Prism 7.04 was used throughout each statistical analysis (GraphPad Inc, San Diego, CA, USA). The data are shown with the mean value and the standard error of the mean (SEM). A variety of statistical analyses, including one-way, two-way ANOVA, Tukey's multiple comparisons, and student T tests, have been used.

Chapter 3: Characterisation of Extracellular vesicles and Extracellular vesicles derived from OV infected tumour cells carry viral cargo.

3.1 Introduction

As previously discussed in chapter 1, lipid-bound extracellular vesicles are secreted by cells into extracellular space (Yáñez-Mó et al., 2015, Zaborowski et al., 2015). These vesicles, especially exosomes, efficiently transfer signals and biomolecular cargo to distant cells and nearby tissues (Mir and Goettsch, 2020, Joshi et al., 2020). Diagnostic, therapeutic, and clinical applications of extracellular vesicles are rapidly increasing, and EV based cell-free therapy is considered safer and less toxic (Morris et al., 2022). Researchers have discovered the therapeutic potential of EVs generated by stem/progenitor cells' secretome (conditioned media) as immunomodulatory and anti-inflammatory tools (Kwon et al., 2021). Furthermore, they are being examined in the drug delivery research field because they have the potential to be loaded with therapeutic cargo and altered for targeted treatment delivery (Kwon et al., 2021). The membrane of extracellular vesicles provides an extra shield to the encapsulated cargo (e.g. oncolytic viruses, proteins, drugs, nucleic acids), which increases its shelf life (Bunggulawa et al., 2018). EVs are a heterogeneous group and are classified according to size and biogenesis process. Microvesicles and exosomes are the two primary types. However, the process of effectively sorting EVs into these various populations is hampered by a lack of unique, subset-specific identifiers. As a result, most isolation strategies tend to focus on distinguishing EVs based on physical features, with size being the most often used. However, according to overlapping size profiles, this is insufficient and cannot be relied on to yield homogeneous vesicle preparations. Therefore, the general term "extracellular vesicle" is used to represent this uncertainty. Each isolation process is often focused towards enriching a certain EV subtype. The isolation procedures used in this study (see section **2.1.12.2**) are aimed to enrich for exosomes, although it is crucial to note that a mixed EV population will be created and therefore these are referred to as EVs. EV production rates and size ranges may be quantified using tools like nanoparticle tracking analysis (NTA), and variations in these quantities across different breast cancer cell lines can be readily observed. TEM investigations may be utilised to confirm the size ranges seen using particle counting tools, as well as to detect any significant changes in the morphology of the EVs.

3.1.1 Hypothesis

We hypothesise that EVs purified from breast cancer cells following infection with OV carry viral cargo. Therefore, when EV from cell lines that have been infected with OV are utilised

(referred to as EV-OV) and EV from cell lines that have not been infected with OV are used (referred to as EV), this was only done in a "autologous" manner, meaning that EV-OV from MCF-7 and MDA-MB-231 only went back onto those two cell lines.

3.1.2 Aims

The aim of this chapter was to separate EVs from the culture medium of breast cancer cell lines following infection with OV. EVs were purified using the dUC procedures as described in the previous chapter (2.1.12.2). A combination of NTA and TEM were used to characterise the physical features of these EVs to identify the size ranges and rates of EV formation for the breast cell lines. Protein markers that are transported by the EVs generated and the presence of viral cargo OV from infected breast cancer cells in purified EVs were identified using western blotting. In addition, AlamarBlue was used to determine the toxicity of breast cancer cell derived EVs on breast cancer cell lines. Finally, a scratch wound assay was used to determine tumour cell migration in response to EVs from OV-infected tumour cells.

3.2 Results

3.2.1 OV induced breast cancer cell oncolysis.

In the first instance we wanted to confirm the oncolytic effect of our virus HSV1716 following infection of breast cancer cells and the concentration of virus required to infect breast cancer cells without inducing complete cell death. In brief, MCF-7 and MDA-MB-231 cells were seeded into 96-well plates at 5×10^3 cells/well for 24h and then infected with different concentrations of virus as follows (MOI 0.1, MOI 0.5, MOI 1, and MOI 5). Non-infected cells were used as controls and cells were incubated for 24, 48 and 72 h to estimate the exposure effect of each test compound (Kwan et al., 2021b). After incubation, 10 μ l of AlamarBlue Reagent was aseptically added to each well for 4 h and fluorescence was measured at an excitation wavelength of 530 nm on a spectrophotometer. The results showed that the virus successfully replicated within the cells, resulting in a significant increase in cell death (**Figure 3.1**). MCF-7 cell viability at MOI 0.1 and MOI 0.5 was 74.10%, 80.92% (* $p < 0.05$), respectively compared to the control (untreated cells) at 24h (**Figure 3.1 A & B**). However, at 48h the MCF-7 viability significantly decreased further with (MOI 0.5, MOI 1, and MOI 5) to 45.99%, 33.40%, 33.40% (**** $P < 0.00001$), respectively compared to the control (**Figure 3.1 B, C & D**). Even the lowest MOI of 0.1 induced cell death 42.65% (*** $p < 0.0001$) at 48 h (**Figure 3.1A**). This might be because the virus's life cycle bursts open at this time and kills

the cancer cells. Denes et al demonstrated that the timescale of the replication cycle within a culture varies on cell type and infection multiplicity, although as a rough estimate, maximal progeny virus yields are reached 24 h after infection for most common laboratory cell types infected at a multiplicity sufficient to infect all cells (Denes et al., 2019). At 72h, MOI 0.1 and MOI 5 induced some cytotoxicity at 72.45%, 76.91% (* $p < 0.05$), respectively as compared to the control (**Figure 3.1 A & D**). On the other hand, MOI 0.5 and MOI 1 showed no significant difference on cell viability (**Figure 3.1 B & C**).

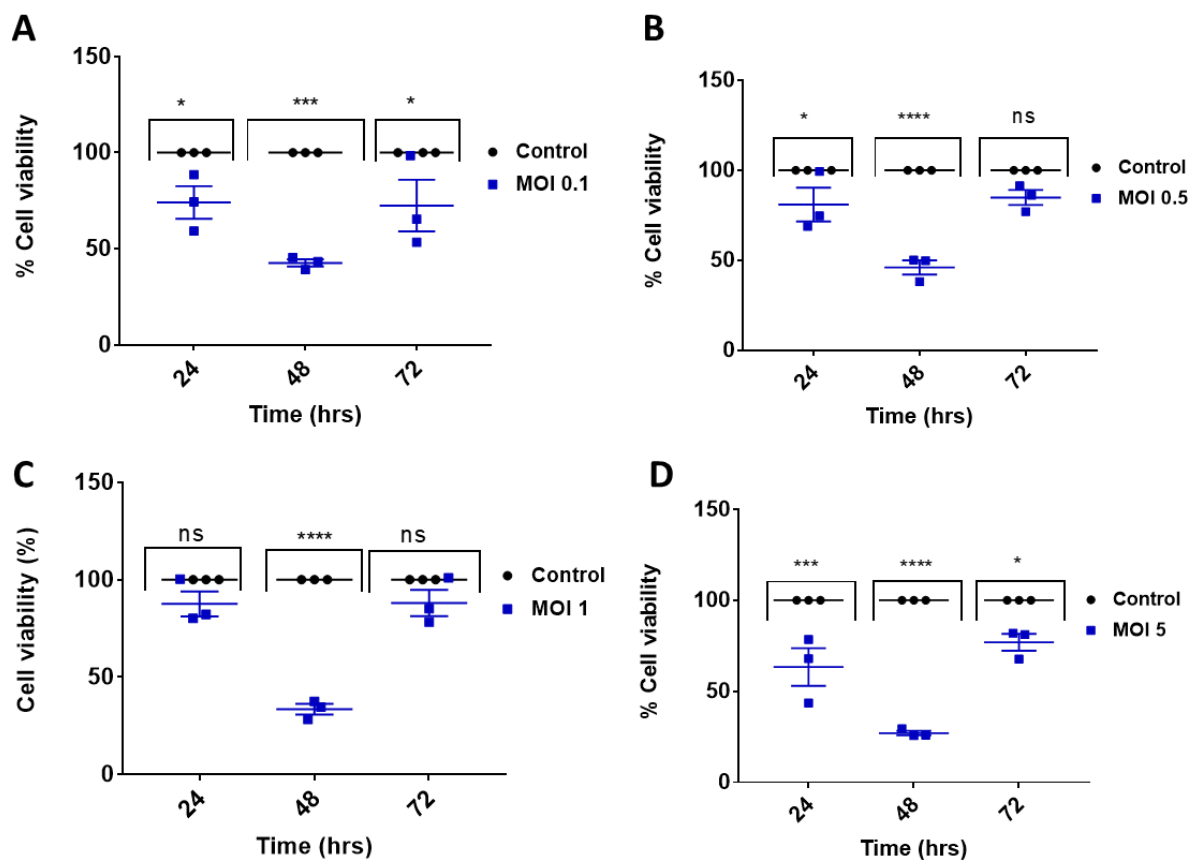


Figure 3. 1: OV infection decreases cell metabolic activity on MCF-7 cells. Cells were seeded at 5×10^3 in 96-well plate and incubated with HSV-1716 at MOIs 0.1,0.5,1 and 5 for 24,48&72 h. Untreated cells were used as a negative control. Alamar blue reagent ($10 \mu\text{l}$) was added and incubated for 4 h before a spectrophotometer measured the absorbance at 530nm. The data represent the \pm mean SEM of $n=3$ independent experiments, and statistical analysis was performed using the two-way Anova test with multiple comparisons. * $p < 0.05$ ** $p < 0.01$ *** $p < 0.001$ **** $p < 0.0001$

Next, we looked at the TNBC cell line MDA-MB-231 at MOI 0.5 and MOI 1 no significant differences were observed on cell viability at 24 h (**Figure 3.2 B & C**). On the other hand, at 24 h the cell viability was reduced significantly at MOI 0.1 and MOI 5 compared to control ($*p < 0.05$) (**Figure 3.2 A & D**). Likewise, for MOI 0.1 no significant differences were showed at 48h (**Figure 3.2 A**). However, at MOI 0.5 and MOI 1 and MOI 5 significantly reduced cell viability 51.71%, 55.90%, 34.81% ($*p < 0.05$), ($****p < 0.0001$), respectively compared to the control at 48h (**Figure 3.2 B, C & D**). In addition, at 72h the results observed that no significant differences were obtained at MOI 0.1 (**Figure 3.2 A**). However, MOI 0.5, MOI 1 and MOI 5 significantly reduced cell viability 47.32%, 51.56%, 34.23% ($**P < 0.001$), ($****p < 0.0001$), respectively compared to the control. (**Figure 3.2 B, C & D**). Together this data shows that both cell lines are sensitive to HSV1716, with MDA-MB-231 being more sensitive at all MOIs. For our studies it was essential to choose MOI of virus that had an impact but did not destroy all cells. so that we could collect vesicles without contamination of apoptotic and necrotic bodies. Therefore, MOI of 1 for MDA-MB-231 and MOI 0.5 for MCF-7 were chosen for future studies in terms of the dose of drug required to cause at least 50% cell death.

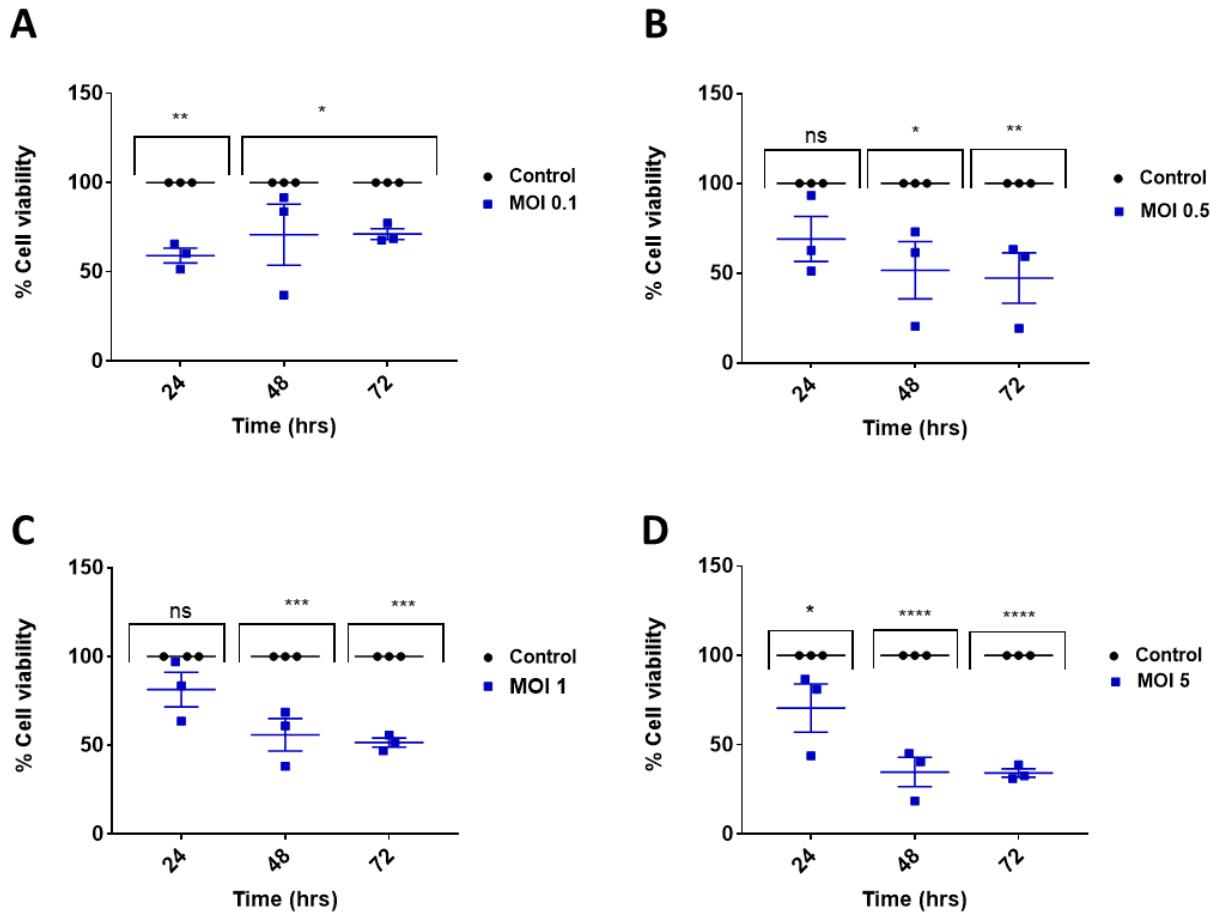


Figure 3. 2: OV infection decreases cell metabolic activity on MDA-MB-231 cells. Cells were seeded at 5×10^3 in 96-well plate and incubated with HSV-1716 at MOIs 0.1, 0.5, 1 and 5 for 24, 48 & 72 h. Untreated cells were used as a negative control. Alamar blue reagent ($10 \mu\text{l}$) was added and incubated for 4 h before a spectrophotometer measured the absorbance at 530nm. The data represent the \pm mean SEM of $n=3$ independent experiments, and statistical analysis was performed using the two-way Anova test with multiple comparisons. * $p < 0.05$ ** $p < 0.01$ *** $p < 0.001$ **** $p < 0.0001$

3.2.2 Characterisation of EVs released from MCF-7 and MDA-MB-231 cells after ultracentrifugation by nanoparticle tracking analysis (NTA)

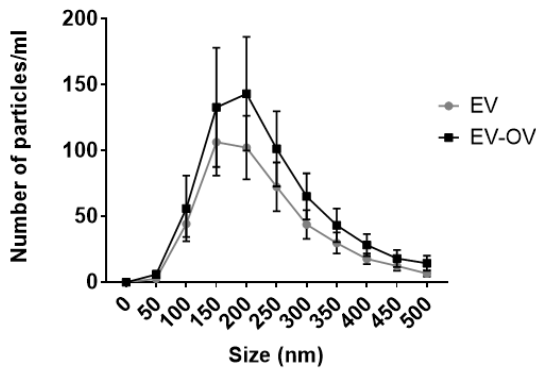
Next, we investigated the size and concentration of the EVs secreted from MCF-7 and MDA-MB-231 control and infected cells with HSV1716 at MOI 0.5 and MOI 1, respectively. Medium from cells was replaced with FBS-depleted medium when cells were 90% confluent and supernatant was collected after 48 hrs, for isolation of EVs by differential centrifugation (Théry et al., 2006). Supernatants were centrifuged at 300 x g to remove debris, 2000 x g to remove apoptotic bodies, 10,000 x g to remove microvesicles and then 100,000 x g to collect exosomes. The resulting supernatant was then analysed by NTA. This nanoparticle tracking analysis (Zetaview), is an instrument that can be used for measuring particle concentration and

size ranges, based on the characteristic movement of nanoparticles in solution as for the Brownian motion. There is a camera that can be used to document the particles' path in a specific volume through using a laser to capture the scattered light upon illumination of the particles (Defante et al., 2018). The EVs released from MCF-7 showed a particle size ranging from 50 to 500 nm in diameter and the mean diameter 50 nm (**Figure 3.3A**). The concentration of MCF-7 derived EVs was $2.88E+8$ /ml and whilst EV-OV was greater at $3.59E+8$ /ml, this was not statistically significant (**Figure 3.3B**).

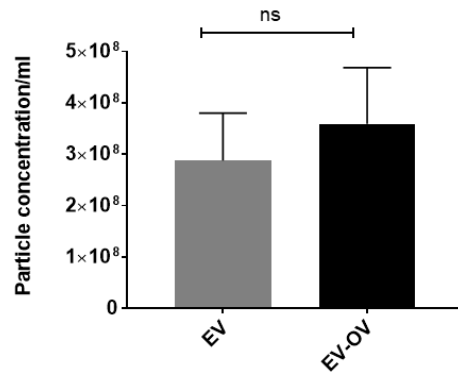
Moreover, the EVs released from MDA-MB-231 showed that a particle size ranging from 50 to 500 nm in diameter and the mean diameter 50nm (**Figure 3.3 C**). The concentration levels of MDA-MB-231 derived EV-OV $4.71E+10$ /ml were significantly increased compared to MDA-MB-231 derived EV $6.9E+9$ /ml (**Figure 3.3D**). Interestingly MDA-MB-231s produced more vesicles than the MCF7 cells ($\sim 3.59E+8$ /ml vs. $4.71E+10$ /ml for EVs from treated cells, respectively). Garcia et al support our finding, the results of NTA of conditioned media demonstrate that treatment of MDA-MB-231 cells with Linoleic acid (LA) results in an increase in the secretion of EVs (Garcia-Hernandez et al., 2021). Moreover, our findings are similar with the findings of Silva et al who proved that according to NTA study, MDA-MB-231 cells released the greatest number of extracellular vesicles, followed by the less aggressive MCF-7 cells (Silva et al., 2016). NTA data may contain probable contaminants (e.g., particulate matter, EV aggregates) and thus exaggerate the number of particles present in a sample (**Figure 3.3 A and C**). The graph shows that the average size of MCF-7 and MDA-MB-231 derived EVs were close to 150 and 200 nm, indicating that we have successfully enriched for a population of small nanosized vesicles, most likely exosomes.

MCF-7

A

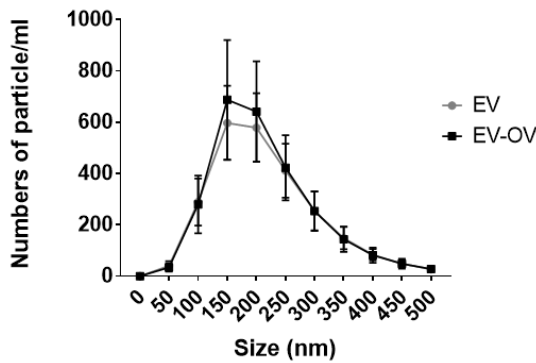


B



MDA-MB-231

C



D

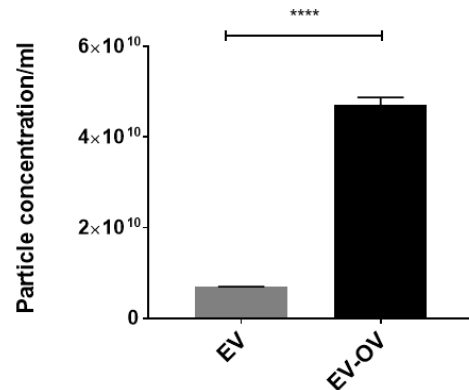


Figure 3.3: Analysis of EVs purified from MCF-7 and MDA-MB-231 cells by differential centrifugation by NTA. EVs were isolated by differential ultracentrifugation (dUC). A) NTA was then performed to determine particle number of MCF-7 derived EV and EV-OV. B) Particle concentration of MCF-7 derived EV and EV-OV. C) NTA was then performed to determine particles number of MDA-MB-231 derived EV and EV-OV. D) Particle concentration of MDA-MB-231 derived EV and EV-OV. The data represent the mean SEM of n=4 independent experiments, with statistical analysis performed using the unpaired Student's t-test.

3.2.3 Characterization of MCF-7 and MDA-MB-231 derived EVs using transmission electron microscopy (TEM)

Transmission electron microscopy (TEM) was used to confirm the size of the EVs secreted from MCF-7 and MDA-MB-231 control and cells treated with OV. dUC was used for purification of the EVs released from MCF-7 and MDA-MB-231 cells treated with OV and from the control cells. The EVs were processed for TEM by fixation in 3% glutaraldehyde, then adsorbed on to formvar coated EM grids, and were negatively stained using uranyl acetate and uranyl oxalate before imaging with a Tecani Spirit G2 microscope. The released EVs either from OV MCF-7 and MDA-MB-231 treated cells or from the control cells bore the artefactual cup-shaped morphology associated with membrane bound vesicles. These vesicles had a diameter range of 30-160 nm (**Figure 3.4 A & B**) which broadly agrees with NTA data.

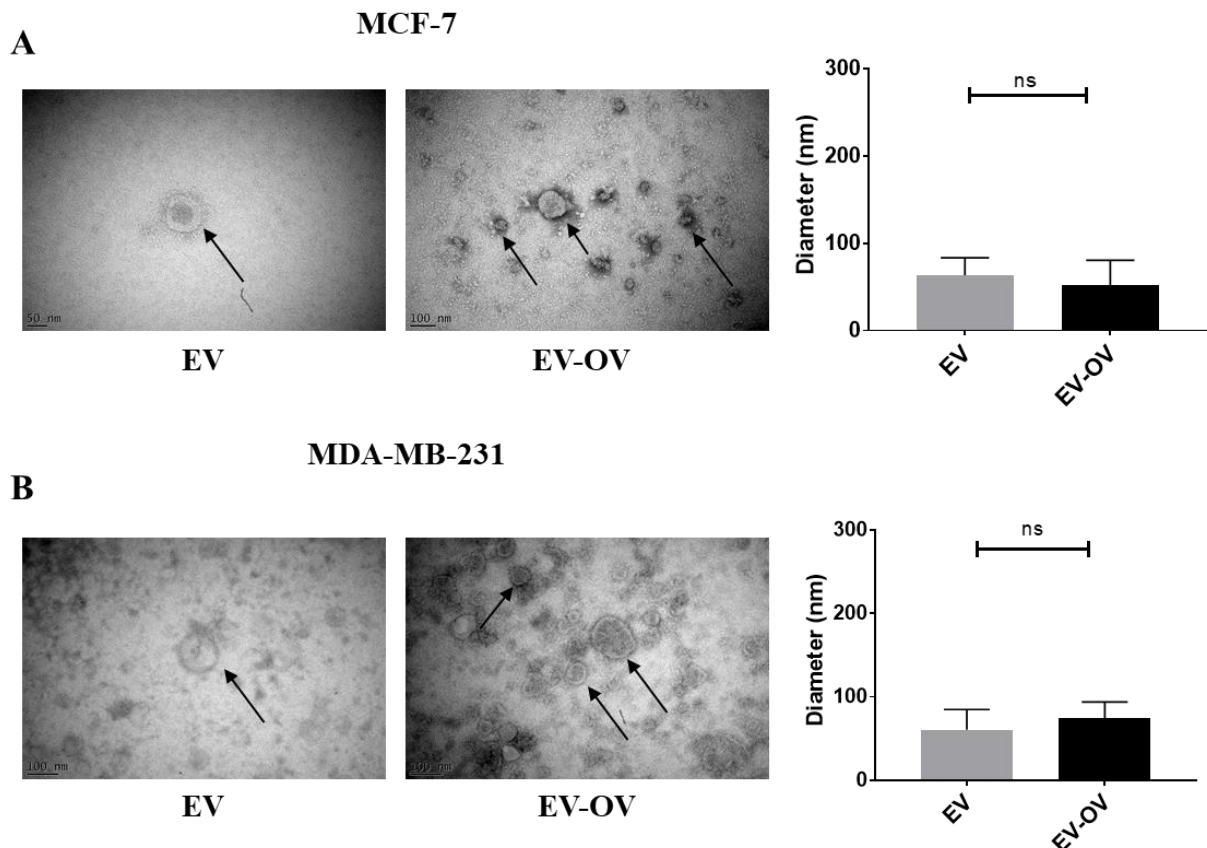


Figure 3.3: Transmission electron microscopy of MCF-7 and MDA-MB-231 derived EV and EV-OV. EVs were extracted from the culture medium of confluent MCF-7 and MDA-MB-231 cells using dUC and resuspended in PBS. The final suspension was frozen at -20°C . After being fixed in 3% paraformaldehyde, both were adsorbed on formvar coated EM grids and negatively stained with uranyl acetate and uranyl oxalate before being imaged with a Tecani Spirit G2 microscope. EVs were visible with intact membrane structures (see arrows) and were typically between the range of 30-150 nm A.

MCF-7 derived EV and EV-OV B. MDA-MB-231 derived EV and EV-OV. A student's T-test was carried out on n=12 biological replicates where data is the Mean and SEM.

3.2.4 MCF-7 and MDA-MB-231 derived EV-OV do not contain contaminating free virus.

Next, we wanted to determine if our purified EVs contained any contaminating free virus that could be responsible for observed biological effects in our future experiments. The gold standard procedure in virology for measuring the concentration of viruses in a sample is the plaque assay (Baer and Kehn-Hall, 2014). This determines the quantity of infectious virus in a sample. Vero cells were seeded into 12-well plates (2×10^5 cells/well) with DMEM-F12 growth medium and allowed to adhere for at least 24 h. Cells were then treated with the following:

HSV1716 virus (10^8 pfu/ml). The viral stock was serially diluted in PBS at concentrations ranging from 10^1 to 10^8 pfu/ml. MCF-7 and MDA-MB-231 derived EVs or EV-OV at 1×10^7 /ml and control untreated cells were used as a negative control. Viral adsorption was carried out by incubating the cells for 2 h followed by the addition of 4% sterile agarose in growth medium (DMEM-F12) and this was incubated for 72 h. To visualise the plaques, cells were stained with Crystal violet. This allows for naked-eye visibility. For MCF-7 results, plaque assays showed that only HSV1716 resulted in plaque formation with 2×10^7 pfu/ml. (**Figure 3.5 A**). Moreover, for MDA-MB-231 results, plaque assays showed that only HSV1716 resulted in plaque formation with 1.7×10^7 pfu/ml. (**Figure 3.5 B**). In terms of MCF-7 and MDA-MB-231 derived EVs there were no plaques detected in any of the other groups. Therefore, these results confirmed that the MCF-7 and MDA-MB-231 derived EV-OV samples do not contain contaminating free virus (**Figure 3.5 A and B**).

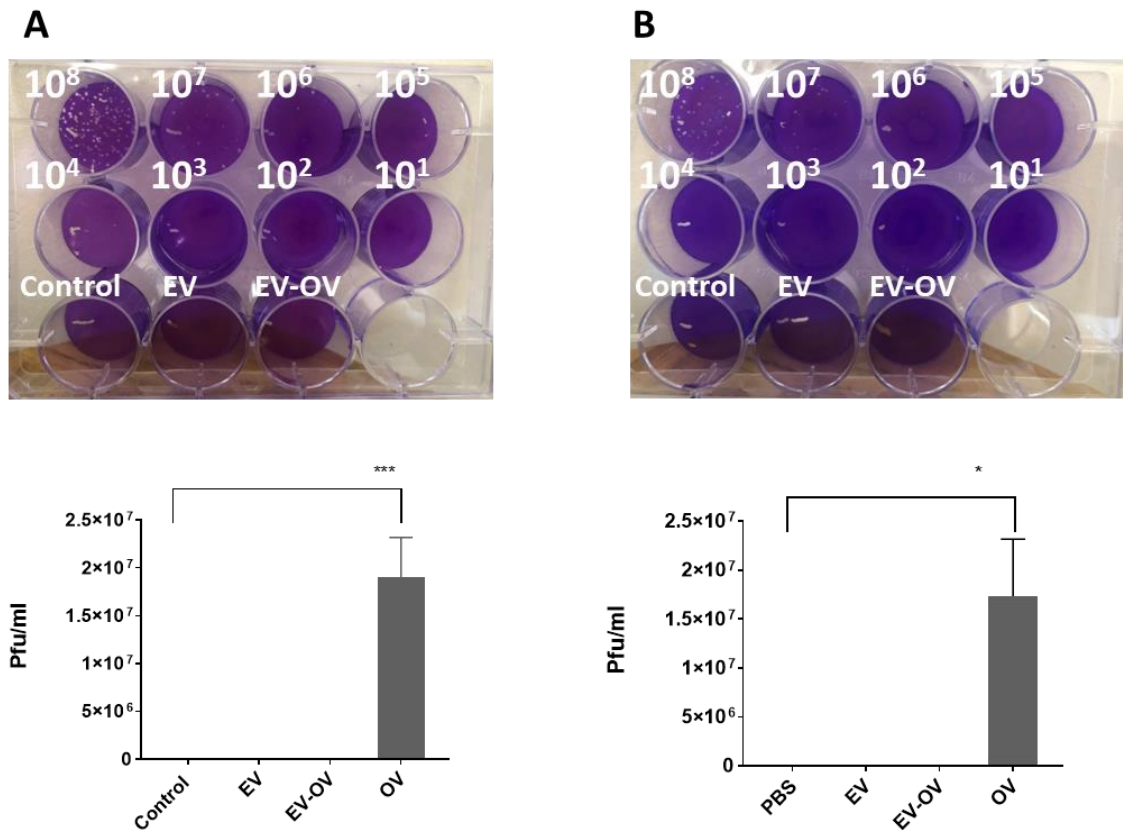


Figure 3. 4: Breast cancer cells derived EV-OV do not contain contaminating free virus. Vero cells 2×10^5 grown in 12-well plates are inoculated with 100 μ l of HSV-1716 (10^8 pfu/ml). The virus stock was serially diluted in PBS at concentrations ranging from 10^1 to 10^8 . **A)** MCF-7 derived EV or EV-OV at 1×10^7 /ml and control cells used as a negative control. **B)** MDA-MB-231 derived EV or EV-OV at 1×10^7 /ml and control cells used as a negative control. Plaques can only be seen in naked-eye and are characterised by HSV1716 forming plaques. The data represent the mean SEM of $n=3$ independent experiments, and statistical analysis was performed using the two-way Anova test with multiple comparisons *** $P < 0.000$

3.2.5 Characterisation of breast cancer derived extracellular EVs

Specific protein markers are frequently used to identify EVs in addition to determining their origin inside the cell, which may be either the plasma membrane or MVBs, and then to define which vesicle subclass they belong to. Small EVs have been shown to be abundant in many important indicators. CD9 and CD63 are two tetraspanins that are substantially abundant in EVs because the microdomains they generate, tetraspanin-enriched microdomains (TEMs), communicate with several signalling proteins and are crucial in EV formation (Andreu and Yáñez-Mó, 2014). Because tetraspanins are a fundamental component of the plasma membrane and are therefore expected to be present in different vesicle subpopulations (Andreu and Yáñez-Mó, 2014), additional markers must be included. TSG101 is another often utilised EV marker since it is a component of the ESCRT-I complex, which regulates vesicular trafficking (Matsuo et al., 2004, Baietti et al., 2012). Western blot analysis was performed to detect EV protein markers in cell lysates and in the purified EVs from MCF-7 and densitometry measurements of the bands was also performed to quantitate proteins within the linear dynamic range (**Figure 3.6**). The presence of the negative control marker GM130, a Golgi body marker, in cell lysate samples indicates that the EV protein is devoid of contamination by intracellular components (**Figure 3.6A**). Western blot analysis of the tetraspanin proteins CD9 and CD63 and TSG101 were substantially enriched in all the MCF-7 cell lysates and their derived EVs (EV and EV-OV) preparations (**Figure 3.6 B, C and D**). In addition, to confirm if EVs derived from MCF-7 and infected cells contain viral cargo we used an established anti-HSV1716 antibody (MacLean et al., 1991) to detect the Herpes simplex virus (HSV) released antigens on MCF-7 infected cell lysate and EVs derived from infected cells. Interestingly, the western blot data confirmed that infected cells contain viral proteins but EVs purified from these cells also carry viral cargo (**Figure 3.6 E**). Among the HSV-1716's most prominent antigens was enveloped viral glycoproteins B proteins with a MW of 130 KDa. MCF-7 infected cells and derived EV-OV had gB, which was observed in our study (**Figure 3.6 F**).

MCF-7

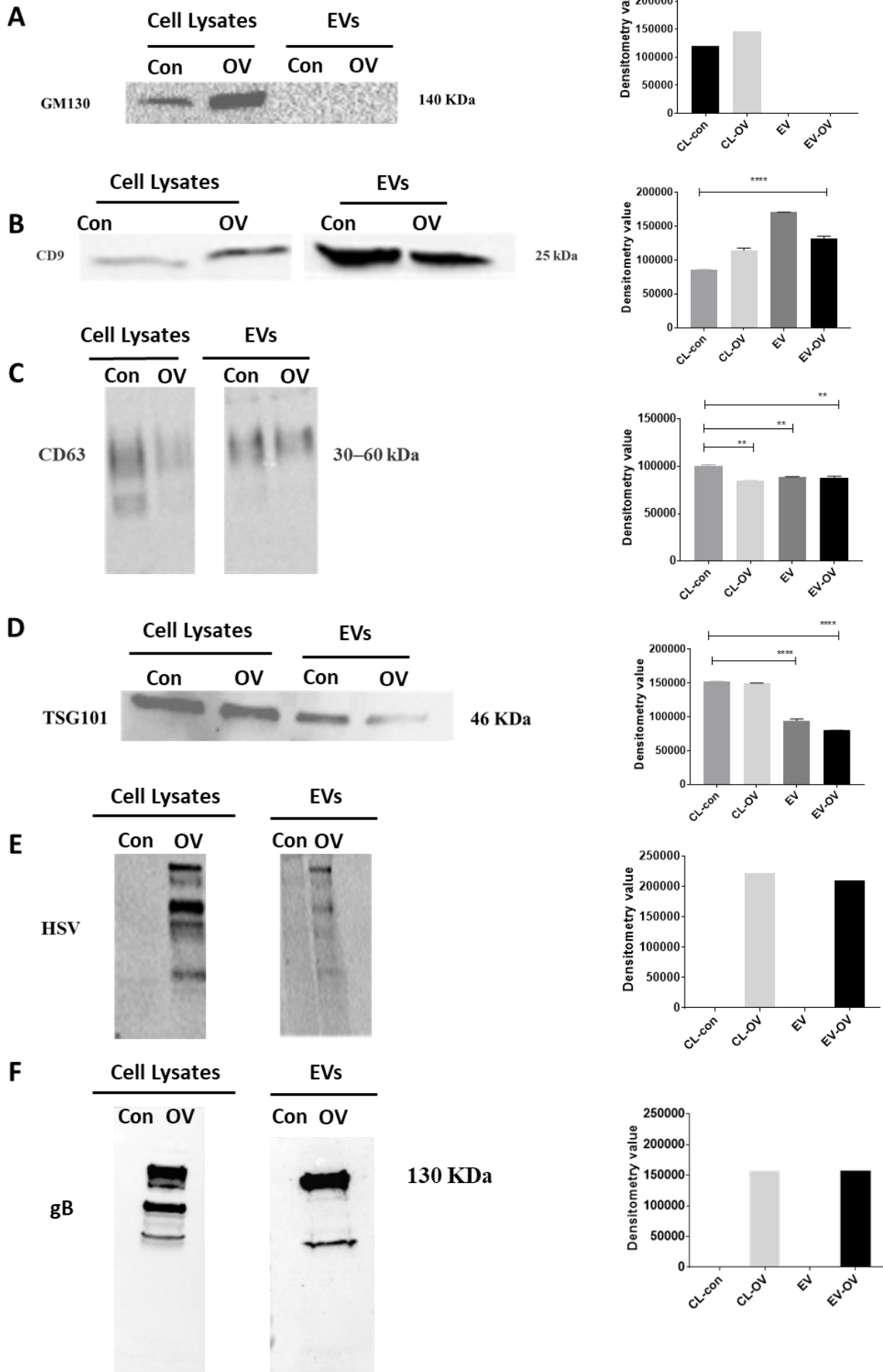


Figure 3. 5: EVs purified from MCF-7 using dUC express typical EV markers and carry viral cargo. A Western blot was carried out using whole-cell lysates in addition to EVs. 20µl of each with equal protein amount (2µg) were mixed with 5µl of 4x LDS Sample Buffer. The mixtures were incubated at 90°C for 10 min, and 20µl were loaded to each well of 12% acrylamide gel. After transferring to a nitrocellulose membrane. They were blocked with 5% milk for 1h at RT, then incubated overnight with appropriate primary antibody diluted in 10 mL milk at 4°C. This included A) GM130 B) CD9 C) CD63 D) TSG101 E) HSV F) gB. On the next day, the membranes were washed and incubated with appropriate secondary antibody for 1hr at RT, then washed three times for 5 min each in PBST. WA WESTAR® Supernova HRP Detection Substrate Kit was added to the membrane then imaged using ChemiDoc™ MP System (BIO-RAD).

Moreover, western blot analysis was performed to detect EV protein markers in cell lysates and in the purified EVs from MDA-MB-231 and densitometry measurements of the bands was also performed to quantitate proteins within the linear dynamic range (**Figure 3.7**). The negative control marker GM130, a Golgi body marker was apparent in cell lysate samples indicating that the EV protein is free from contamination by intracellular components (**Figure 3.7G**). Western blot analysis of the tetraspanin proteins CD9 and CD63 and TSG 101 tumour susceptibility gene were substantially enriched in all the MDA-MB-231 cell lysates and their derived EVs (EV and EV-OV) preparations (**Figure 3.7 H, I and J**). In addition, to confirm if EVs derived from MDA-MB-231 and infected cells contain viral cargo we used an established sheep anti-HSV1716 antibody (MacLean et al., 1991) to detect the Herpes simplex virus (HSV) released antigens on MDA-MB-231 infected cell lysate and EVs derived from infected cells. Interestingly, the western blot data confirmed that infected cells contain viral proteins but EVs purified from these cells also carry viral cargo (**Figure 3.7 K**). Among the HSV-1716's most prominent antigens was enveloped viral glycoproteins B proteins with a MW of 130 KDa. MDA-MB-231 infected cells and derived EV-OV had gB, which was observed in our study (**Figure 3.7 L**).

MDA-MB-231

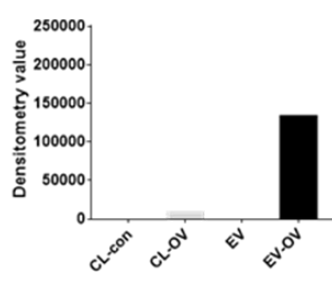
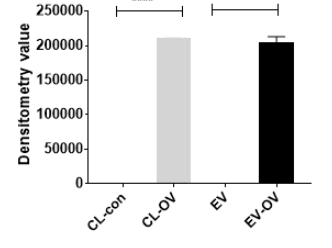
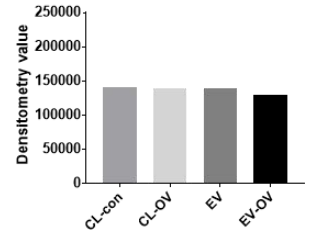
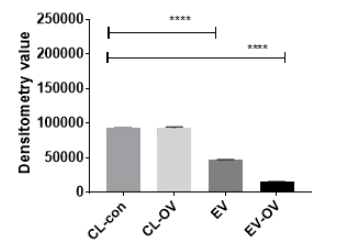
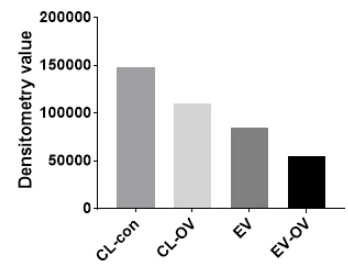
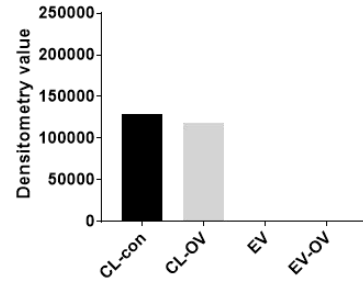
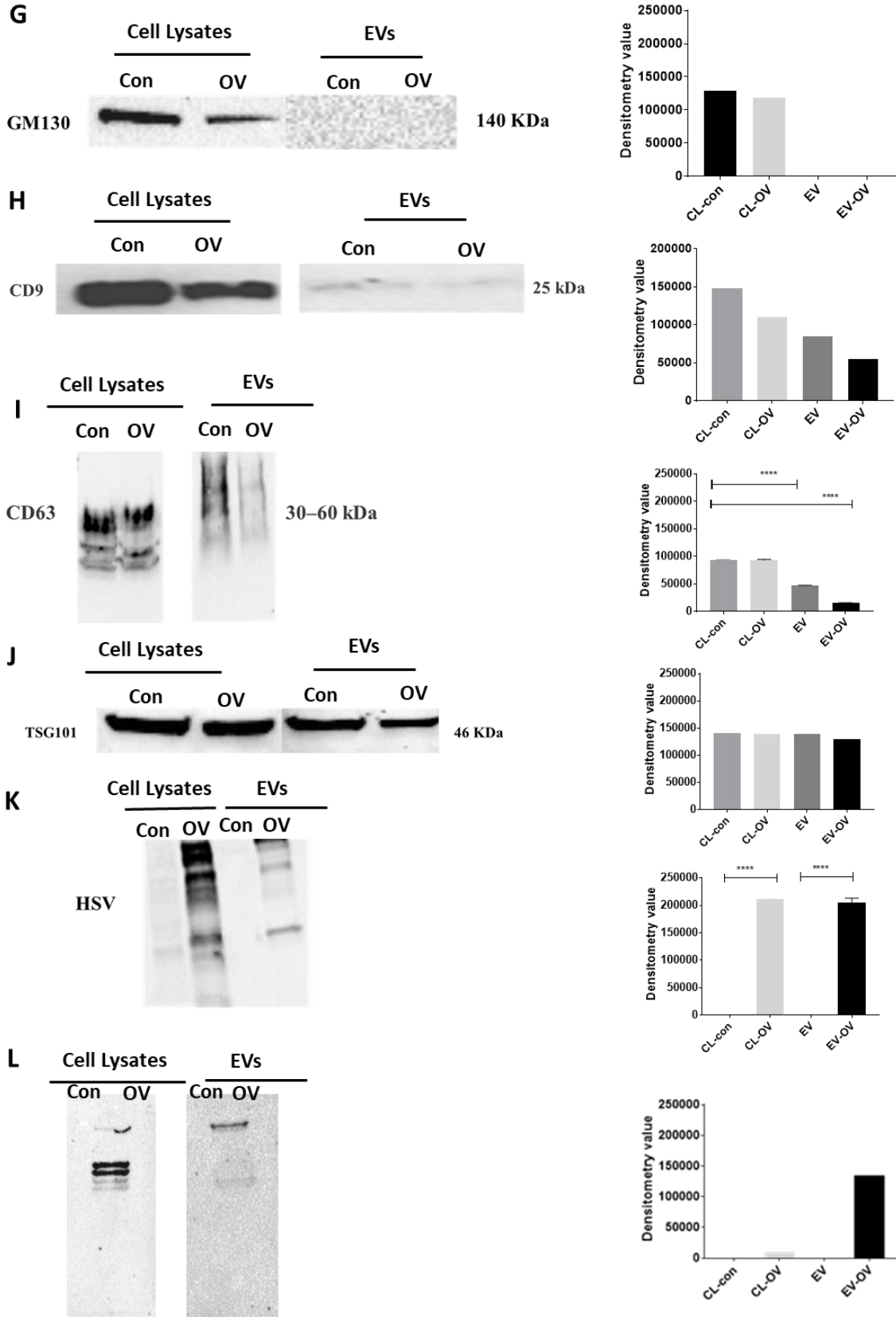
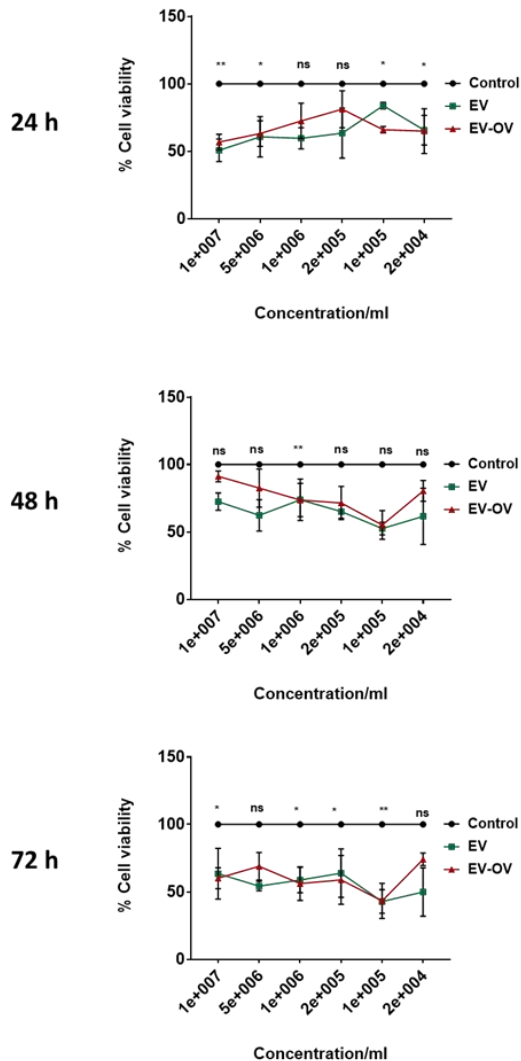


Figure 3.1: EVs purified from MDA-MB-231 using dUC express typical EV markers and carry viral cargo. A Western blot was carried out using whole-cell lysates in addition to EVs. 20µl of each with equal protein amount (2µg) were mixed with 5µl of 4x LDS Sample Buffer. The mixtures were incubated at 90°C for 10 min, and 20µl were loaded to each well of 12% acrylamide gel. After transferring to a nitrocellulose membrane. They were blocked with 5% milk for 1h at RT, then incubated overnight with appropriate primary antibody diluted in 10 mL milk at 4°C. This included G) GM130 H) CD9 I) CD63 J) TSG101 K) HSV L) gB. On the next day, the membranes were washed and incubated with appropriate secondary antibody for 1hr at RT, then washed three times for 5 min each in PBST. WA WESTAR® Supernova HRP Detection Substrate Kit was added to the membrane then imaged using ChemiDoc™ MP System (BIO-RAD).

3.2.6 Culture of purified EVs with breast cancer cells induces cell death

To assess the vitality of breast cancer cells in longer-term of the EV cultures. Alamar blue assays were performed. It is considered that this is preferable to other cell viability tests, such as the MTT test, since it is non-toxic to cells and does not necessitate their death during the procedure of the assay. While Alamar blue decreases exclusively in metabolically active cells, the amount of activity is a measure of cell viability. To test the cytotoxic effects, MCF-7 was incubated with various concentrations ($1e+007$, $5e+006$, $1e+006$, $2e+005$, $1e+005$ and $2e+004$) of EV and EV-OV derived from MCF-7, respectively for 24, 48, and 72 h. Untreated cells served as negative controls displaying 100% viability. Following that, Alamar blue reagent was added to each well, followed by a 4 h incubation period. Cell viability was measured spectrophotometrically at 570 nm. The results showed that both MCF-7 derived EV and EV-OV at all concentrations mentioned above induced toxicity to MCF7 cells, respectively as compared to control at 24, 48 and 72 h (**Figure 3.7A and B**). Together this data shows that EVs purified from MCF-7 breast cancer cells induce cell death at all the concentration of particles. We have selected $1e+007$ concentration of EVs to conduct further downstream analysis. Other studies where EVs were collected from the liver HepG2 cancer cell line showed that a concentration of $1e+007$ HepG2 EVs resulted in significant effects on cell viability compared with the extract black bean with no carrier as a negative control (p-value <0.0001) (Donoso-Quezada et al., 2019).



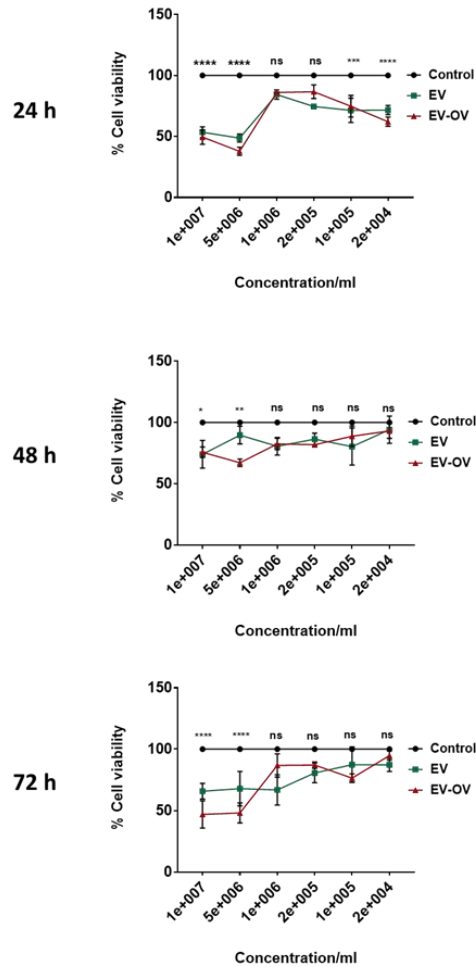
Concentration/ml	MCF-7 derived EV	MCF-7 derived EV-OV
1e+007	50.79%	56.86%
5e+006	60.71%	63.14%
1e+006	59.64%	72.52%
2e+005	63.50%	81.17%
1e+005	83.81%	65.97%
2e+004	65.68%	65.01%

Concentration/ml	MCF-7 derived EV	MCF-7 derived EV-OV
1e+007	72.52%	91.28%
5e+006	62.34%	82.52%
1e+006	73.90%	73.70%
2e+005	65.14%	71.49%
1e+005	52.58%	55.21%
2e+004	61.60%	80.45%

Concentration/ml	MCF-7 derived EV	MCF-7 derived EV-OV
1e+007	63.51%	60.15%
5e+006	54.34%	68.95%
1e+006	58.81%	56.19%
2e+005	63.93%	58.88%
1e+005	42.93%	43.36%
2e+004	49.92%	74.17%

Figure 3.2: MCF-7 derived EV and EV-OV induced cytotoxicity on MCF-7 cells. MCF-7 were seeded at 5×10^3 in 96-well plate and incubated with EV and EV-OV at $1e+007$, $5e+006$, $1e+006$, $2e+005$, $1e+005$ and $2e+004$ particle/ml for 24, 48 and 72 h. Control cells were untreated. Alamar blue reagent ($10 \mu\text{l}$) was added and incubated for 4 hrs before a spectrophotometer measured the absorbance at 570nm. The data shows the mean SEM of $n=3$ independent experiments, and statistical analysis was performed using the two-way Anova test with multiple comparisons. A mean difference was considered significant when $**P<0.001$, $***P<0.0001$ and $****P<0.00001$.

Moreover, MDA-MB-231 were treated with EVs as above. The results showed that both MDA-MB-231 derived EV and EV-OV at all concentrations mentioned above induced toxicity to MDA-MB-231 cells, respectively as compared to control at 24, 48 and 72 h (**Figure 3.7A and B**). Together this data shows that EVs purified from MDA-MB-231 breast cancer cells induce cell death at all the concentration of particles.



Concentration/ml	MDA-MB-231 derived EV	MDA-MB-231 derived EV-OV
1e+007	53.50%	49.52%
5e+006	48.68%	37.82%
1e+006	84.34%	86.09%
2e+005	74.57%	86.68%
1e+005	71.39%	74.78%
2e+004	71.64%	62.12%

Concentration/ml	MDA-MB-231 derived EV	MDA-MB-231 derived EV-OV
1e+007	74.05%	75.67%
5e+006	89.64%	67.08%
1e+006	80.57%	82.41%
2e+005	86.38%	81.82%
1e+005	80.30%	88.75%
2e+004	94.05%	93.11%

Concentration/ml	MDA-MB-231 derived EV	MDA-MB-231 derived EV-OV
1e+007	65.78%	46.94%
5e+006	67.87%	48.12%
1e+006	66.86%	86.80%
2e+005	80.62%	87.09%
1e+005	87.35%	76.52%
2e+004	87.24%	94.79%

Figure 3.3: MDA-MB-231 derived EV and EV-OV induced cytotoxicity on MDA-MB-231 cells. MDA-MB-231 were seeded at 5×10^3 in 96-well plate and incubated with EV and EV-OV at 1e+007, 5e+006, 1e+006, 2e+005, 1e+005 and 2e+004 particle/ml for 24, 48 and 72 h. Control cells were untreated. Alamar blue reagent (10 μ l) was added and incubated for 4 hrs before a spectrophotometer measured the absorbance at 570nm. The data shows the mean SEM of n=3 independent experiments, and statistical analysis was performed using the two-way Anova test with multiple comparisons. A mean difference was considered significant when **P<0.001, ***P<0.0001 and ****P<0.00001.

3.2.7 EV uptake by breast cancer cells: Flow cytometry

MCF-7 and MDA-MB-231 cells were seeded into 6-well plates (3×10^5 cells/well) and after 24 h, cells were incubated with EV, EV-OV at 1e+007 particle/ml fluorescently labelled with the membrane dye C5-Maleimide-Alexa flour 488. The fluorescent label was used to study the uptake of MCF-7 and MDA-MB-231 derived EV, EV-OV and OV alone at MOI 0.5 (MCF-7 and MOI 1 (MDA-MB-231), these MOIs were selected based on earlier results (**Figure 3.1 and Figure 3.2**) with non-infected cells as controls for 24h. For these studies we used the reporter virus HSV1716-GFP so that the GFP could be used to confirm viral infection. After 24 h of culture with the virus and EVs, flow cytometry was utilised to evaluate the cells after

the plates were harvested. The proportion of GFP (+) cells was used to determine the amount of viral infection. Similarly, TOPRO3 was utilised as a viability dye where dead/dying cells take up the dye while live cells exclude it. This dye was used to assess the extent of cell death caused by EVs at 24, 48 and 72 h . TOPRO3 was immediately added to all samples prior to flow cytometric analysis using the FL3-H laser (wavelength 642 nm). For the MCF-7 cells this result showed that virus HSV1716-GFP (OV) was able to infect the tumour cells as demonstrated by the significant increase in GFP expression (**Figure 3.10 A and B**). As expected, OV induced significant tumour cell death compared to all the treatment groups (**Figure 3.10 C**). In addition, EV and EV-OV demonstrated significant uptake at 24h of culture in all the treatments groups compared to the control (**Figure 3.10 A and B**). No significant difference in uptake between EV and EV-OV.

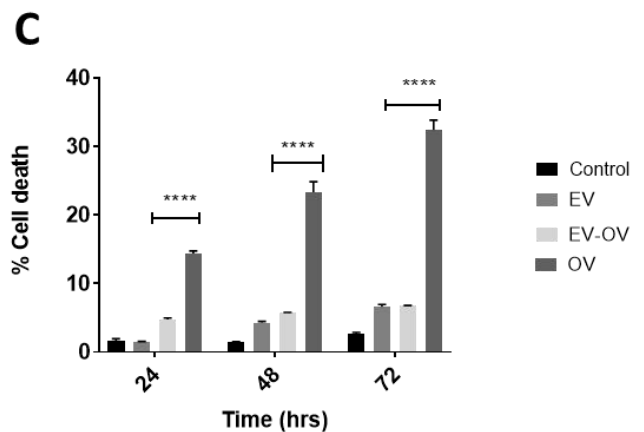
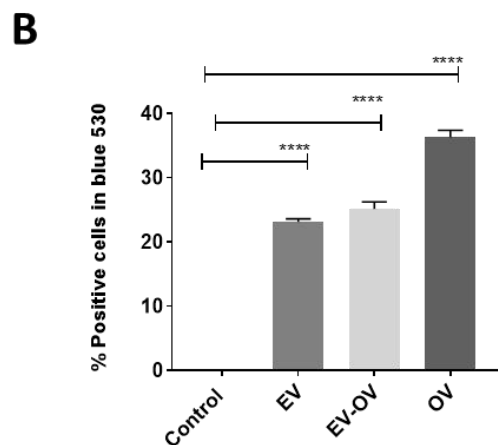
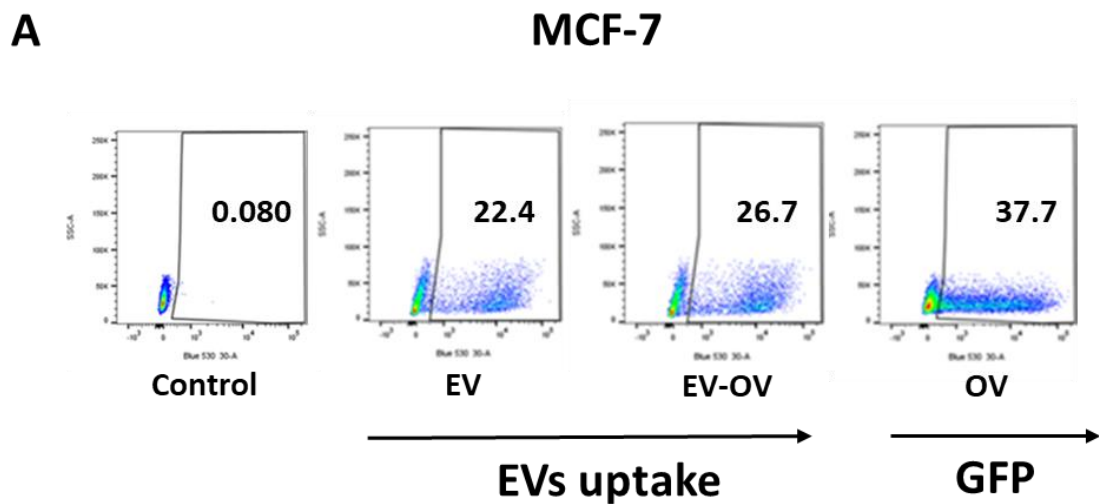


Figure 3.4: EV-OV induce MCF-7 cell uptake. A. Representative dot plots of cell uptake GFP and 488 expressions following 24h incubation of MCF-7 cells with EV and EV-OV at 1×10^7 , OV at MOI 0.5, and untreated cells as a negative control cell. B. A significant increase in percentage uptake of EVs was observed in the EV and EV-OV group compared to all other groups after 24h. Similarly, infection with OV showed infection and high GFP expression. C. In comparison to the control and EVs group at all time points, OV caused statistically significant cell death. Of note, the data represent the mean SEM of $n=3$ independent experiments, and statistical analysis has been performed using the two-way Anova test with multiple comparisons. When a mean difference was considered significant, $**P<0.001$, $***P<0.0001$ and $****P<0.00001$.

For the MDA-MB-231 cells this result showed that virus HSV1716-GFP (OV) was able to infect the tumour cells as demonstrated by the significant increase in GFP expression (**Figure 3.11 A and B**). As expected, OV induced significant tumour cell death compared to all the treatment groups (**Figure 3.11 C**). In addition, EV and EV-OV demonstrated significant uptake at 24h of culture in all the treatments groups compared to the control (**Figure 3.11 A and B**). Together this suggests that the EVs were not toxic to the cancer cells compared to cells treated with HSV1716 (OV).

MDA-MB-231

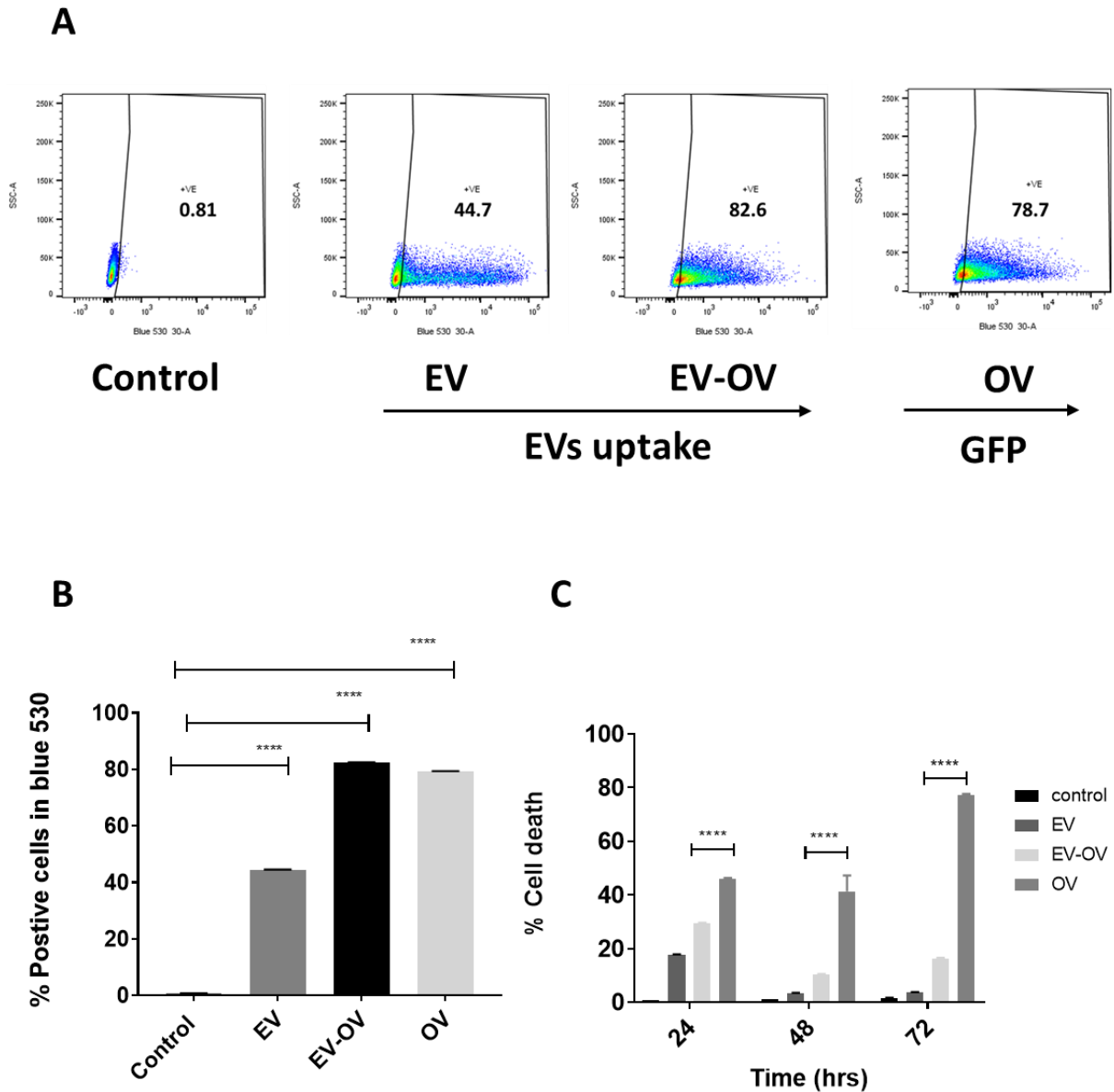


Figure 3.5: EV-OV induce MDA-MB-231 cell uptake. **A.** Representative dot plots of cell uptake GFP and 488 expressions following 24h incubation of MDA-MB-231 cells with EV and EV-OV at $1e+007$, OV at MOI 0.5, and untreated cells as a negative control cell. **B.** A significant increase in percentage uptake was observed in HSV1716-GFP, EV and EV-OV compared to all other groups after 24h. **C.** In comparison to the control and EVs group at all time points, OV caused statistically significant cell death. Of note, the data represent the mean SEM of $n=3$ independent experiments, and statistical analysis has been performed using the two-way Anova test with multiple comparisons. When a mean difference was considered significant, $**P<0.001$, $***P<0.0001$ and $****P<0.00001$.

3.2.8 EV uptake by breast cancer cells: Immunofluorescence

MCF-7 and MDA-MB-231 cells (5×10^3) were grown on 8 well glass bottom slides and incubated with either EV, EV-OV at 1×10^7 particle/ml fluorescently labelled with the membrane dye C5-Maleimide-Alexa fluor 488 for 24 hr. Following that, the cells were fixed and stained with a sheep antibody to identify HSV1716 (Conner et al., 2005). In addition, a 50ng/ml DAPI solution was added for 2 min to identify the nucleus. Coverslips placed on microscope slides and images were taken using a Nikon A1 confocal microscope . For MCF-7 cells uptake by EV was shown by the presence of the C5-Maleimide-Alexa fluor 488 (green) for both EV and EV-OV (**Figure 3.12 A**) was also detected (red) suggesting that the vesicles contained viral cargo (**Figure 3.12 A**). The presence of OV infected MCF-7 cells was greater than the virus (**Figure 3.12 B**). Virus was detected within the cytoplasm of most cells as shown in (**Figure 3.12A**).

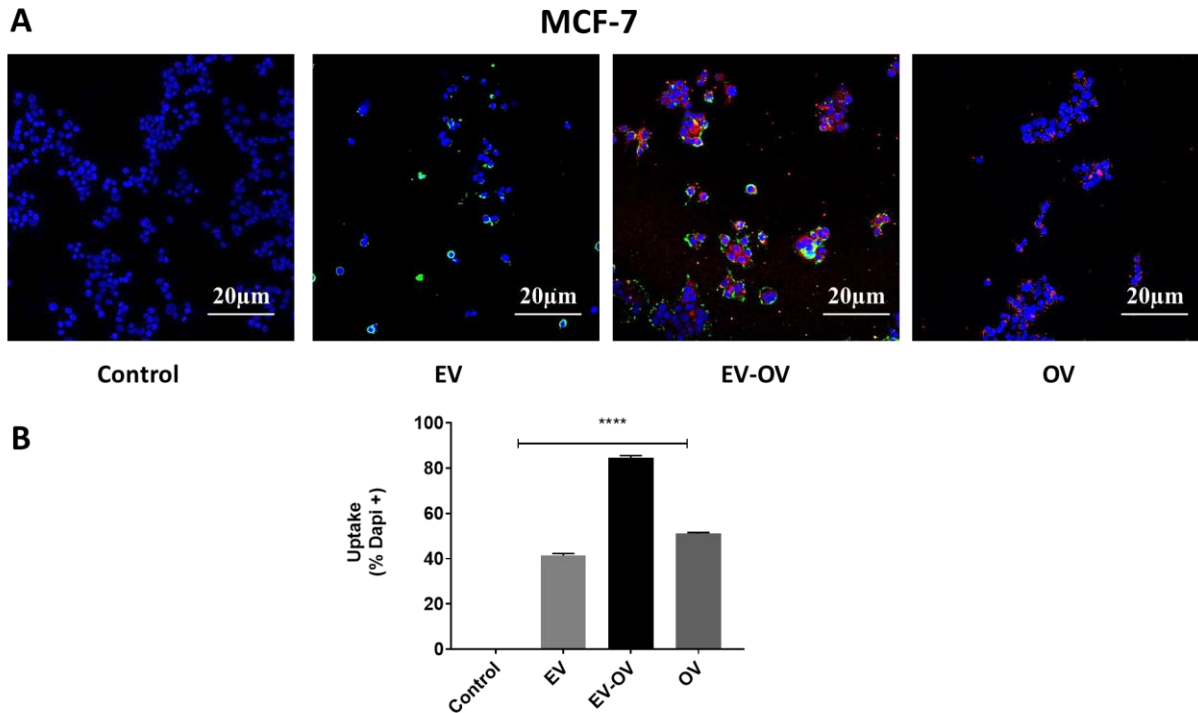


Figure 3.6: EV-OV contain viral cargo as evidenced by staining of MCF-7 cells. **A.** MCF-7 cells were seeded at 5×10^3 in μ -slide 8 well glass bottom for 24 h. Next day, cells were incubated with either EV, EV-OV at $1e+007$ particle/ml fluorescently labelled with the membrane dye C5-Maleimide-Alexa fluor 488 (green). Cells were also infected with OV (MOI 0.5) for 4 h and confocal laser-scanning microscope was used to analyse cells after they had been treated and stained with sheep antibody to recognise HSV1716 (red) and (4',6-diamidino-2-phenylindole) (DAPI: blue). All data are from a single experiment that was repeated $N=3$. **B.** The density of EV, EV-OV and OV were calculated by dividing the total number of OV, EV, and EV-OV positive cells by the number of DAPI+ events in each specified region and multiplying by 100. Data are presented as Mean \pm SEM ($n=3$), and statistical analysis was performed using the one-way Anova test with multiple comparisons (**** $P < 0.00001$).

In addition, for MDA-MB-231 cells uptake by EV was shown by the presence of the C5-Maleimide-Alexa fluor 488 (green) for both EV and EV-OV (**Figure 3.13 A**) was also detected (red) suggesting that the vesicles contained viral cargo (**Figure 3.13 A**). Similarly, MDA-MB-231 cells showed the same pattern of staining of OV infected MDA-MB-231 and the virus (**Figure 3.13 B**). Virus was detected within the cytoplasm of most cells as shown in (**Figure 3.13A**). These data suggest that viral cargo can be transferred by EV.

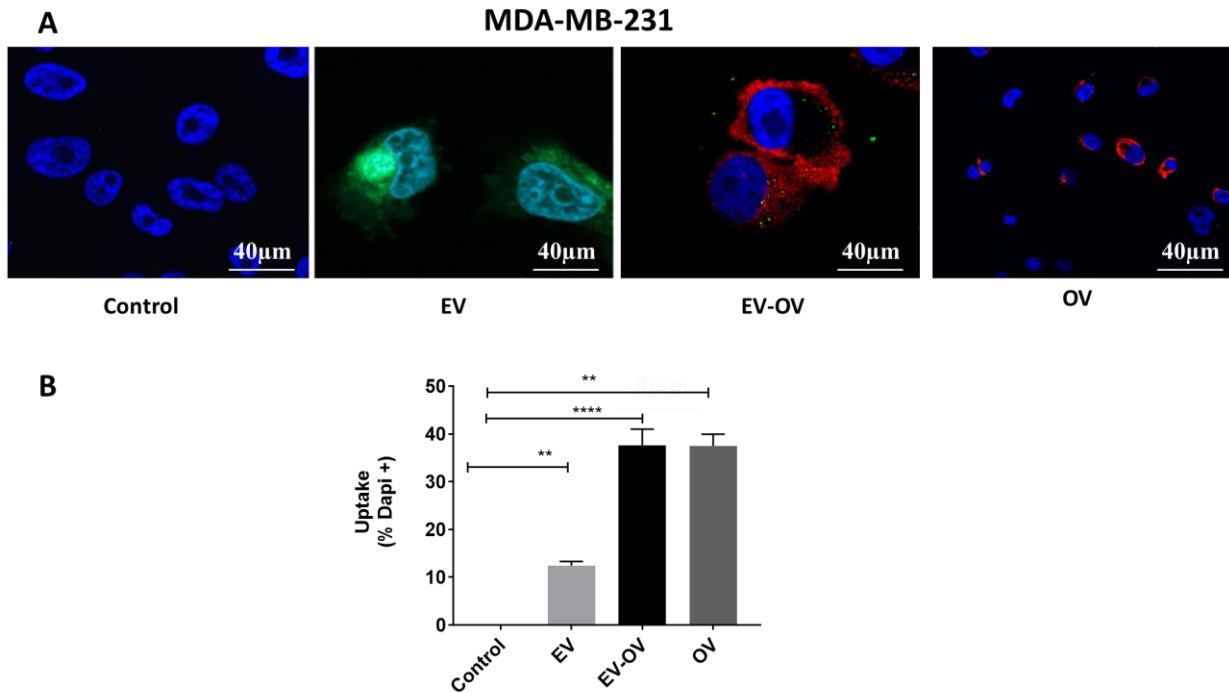


Figure 3.7: EV-OV contain viral cargo as evidenced by staining of MDA-MB-231 cells. **A.** MDA-MB-231 cells were seeded at 5×10^3 in μ -slide 8 well glass bottom for 24 h. Next day, cells were incubated with either EV, EV-OV at $1e+007$ particle/ml fluorescently labelled with the membrane dye C5-Maleimide-Alexa fluor 488 (green). Cells were also infected with OV (MOI 1) for 4 h and confocal laser-scanning microscope was used to analyse cells after they had been treated and stained with sheep antibody to recognise HSV1716 (red) and (4',6-diamidino-2-phenylindole) (DAPI: blue). All data are from a single experiment that was repeated N=3. **B.** The density of EV, EV-OV and OV were calculated by dividing the total number of OV, EV, and EV-OV positive cells by the number of DAPI+ events in each specified region and multiplying by 100. Data are presented as Mean \pm SEM (n=3), and statistical analysis was performed using the one-way Anova test with multiple comparisons. **P<0.001 (****P<0.00001).

3.2.9 EV-OV suppress migration of MDA-MB-231

Next, we looked at the impact of EVs on cell migration. Cell migration assays were performed using the scratch-wound assays with MDA-MB-231 cells treated with $1e+007$ /ml EV and EV-OV at 0, 6 and 24h. The results indicated that EV-OV secreted from infected breast cancer cell inhibit cell migration compared with untreated MDA-MB-231 and MDA-MB-231 cells treated with EV, for the latter the rate for closing the wound was comparable to control at 24 h (**Figure 3.14**) (****P<0.0001).

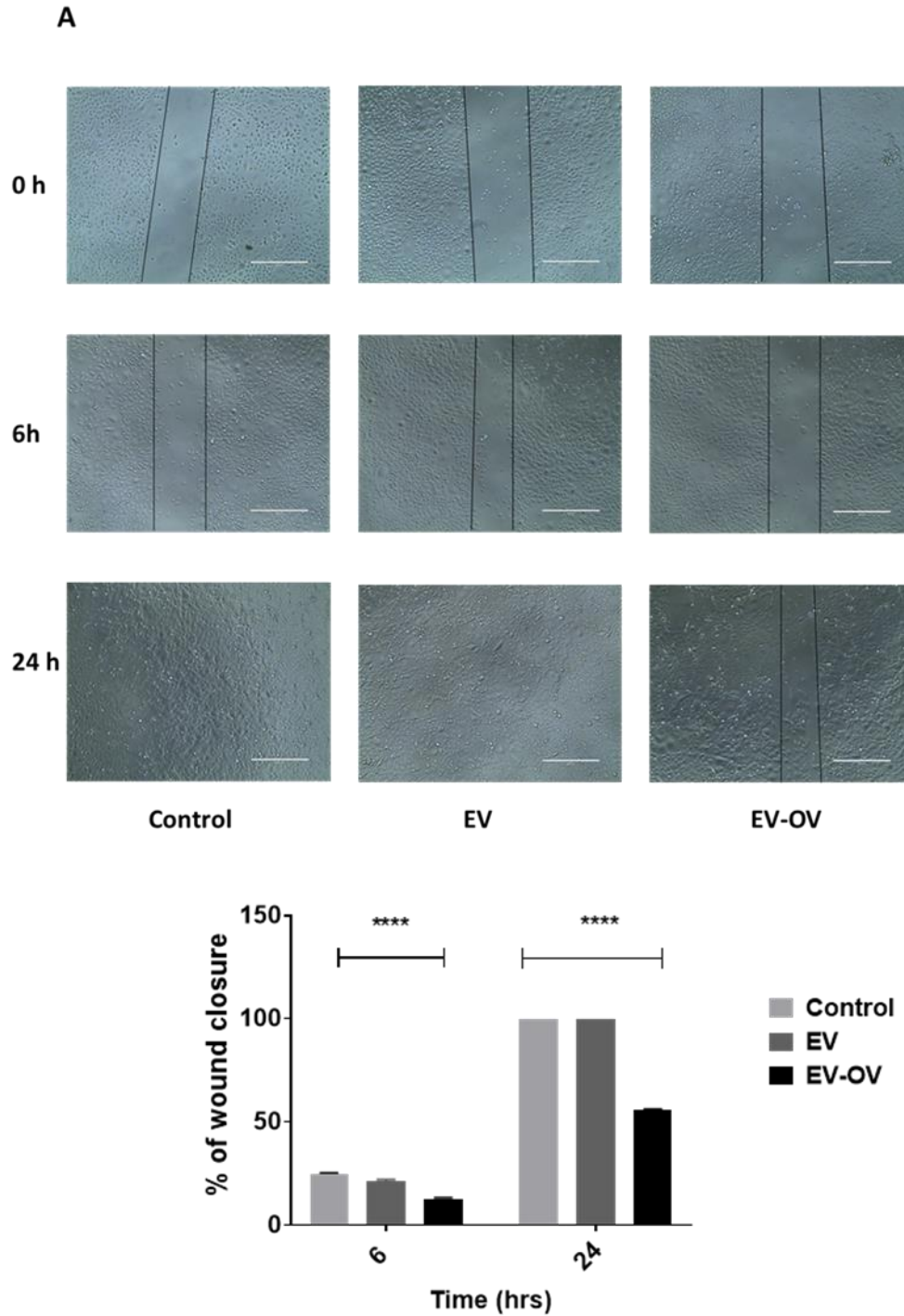


Figure 3.8: MDA-MB-231 derived EV-OV inhibit cell migration in MDA-MB-231 cells. A scratch was introduced on confluent MDA-MB-231 cells and treated for 0, 6 and 24 h with 1×10^7 /ml EV and EV-OV. **A.** Representative images of cell migration captured at 0, 6, and 24 hrs on the EVOS® Cell Imaging System. Scale bar = 400 μ m. **B.** Percentage of wound closure at all time points. The data represent the mean \pm SEM of $n=3$ independent experiments, and statistical analysis was performed using the two-way Anova test with multiple comparisons. **** $P < 0.0001$.

3.3 Discussion

3.3.1 OV induced oncolysis of breast cancer cells

OV are a novel class of cancer therapies that are being used in the clinic and are being tested in clinical trials (Sprague et al., 2018). In this study, first we determined the optimum MOI required to successfully infect breast cancer cell lines without completely inducing cell death. HSV1716 was equally efficient in infecting MCF-7 and MDA-MB-231 cells after 24 h of culture (**Figure 3.1 and 3.2**). Prior studies have shown that HF10, a spontaneous mutant clone produced from the HSV-1 strain, caused 50 % and 20 % cell death at MOI 1 in the TNBC MDA-MB-231 cell line after 24 and 48 h following infection, respectively (Tan et al., 2015). Other studies have also confirmed the effects of HSV-1 strain 17⁺ a mutant strain on the growth of MCF-7 and MDA-MB-231 cells. They observed that the virus significantly reduced the growth of both cells, which was further reduced in the presence of a caspase inhibitor (Wood and Shillitoe, 2011). Chen et al explored the oHSV-1 based lysis of breast cancer cells (MDA-MB-231 and MCF-7). They noted a dose-dependent reduction of MDA-MB-231 and MCF-7 viability after 48 h of co-culturing (Chen et al., 2016). These results are in line with our study, we demonstrated cell death at MOI 1 on MDA-MB-231 and MOI 0.5 on MCF-7. These MOIs were selected because were required to reduce the cell viability to 50 % without completely killing the cells so that EV could still be collected but with cell death contaminants such as apoptotic bodies. The main reason to not kill all the cells was so that viable cells were present to release EVs.

3.3.2 NTA assessment of tumour cell derived EVs size and concentration

After we showed that OV was able to infect breast cancer cells. We then characterised MCF-7 and MDA-MB-231 breast cancer cells derived EVs from untreated and OV infected cells by NTA. EVs are considered to mediate regeneration and repairing of tissues and induction of immune response that favours their applications in various therapies (Lamichhane et al., 2015, Bobrie et al., 2011). During the last decade, EVs have emerged as crucial tools for intercellular communications by transferring lipids, proteins, and nucleic acids. This function helps EVs to affect the pathological and physiological functions of parent and recipient cells (Yáñez-Mó et al., 2015). EVs are formed at the end of the endocytic recycling pathway by the fusion of MVBs and plasma membranes (Raposo and Stoorvogel, 2013a). However, EV variability because of different isolation techniques and structural complexity requires the characterization

NTA allows for the assessment of relative concentration and size distribution of microvesicles such as exosomes in the supernatants of biological fluids and cell cultures (Soo et al., 2012). NTA analysis revealed that the MCF-7 and MDA-MB-231 derived EV and EV-OV possessed a size range of 50 to 500 nm in diameter and an average size of 150 and 200 nm diameter (**Figure 3.3A and C**) suggesting a successful enrichment of nanosized vesicles most likely exosomes. The findings of this study are in line with multiple studies, which have reported approximately similar sizes of EVs ranging between 30-100nm (Jansen et al., 2014, Lázaro-Ibáñez et al., 2014). Based on the size, density, composition, and origin, several terms are used to describe EVs including exosomes (30-100 nm), microvesicles (100-1000 nm) and apoptotic bodies (50-5000 nm) (Barrachina et al., 2019, Andreu and Yáñez-Mó, 2014, György et al., 2011). We demonstrated that OV infection of cells increased the concentration of MDA-MB-231 derived EV-OV (**Figure 3.3 D**). This is in keeping with previous studies where HSV-1 infection resulted in an increase in the concentration of EVs derived from human epithelial infected cells compared to uninfected cells with approximately 1×10^{10} /ml and 2×10^{10} /ml respectively (Deschamps and Kalamvoki, 2018). Therefore, it can be assumed that the methodology adopted during this study successfully enriched the population of nanosized vesicles, most likely comprising exosomes. However, there is a probability of contamination as NTA data might contain particulate matter and EV aggregates that could exaggerate the number of particles present in a sample. To help address this we performed TEM analysis. MCF-7 and MDA-MB-231 derived EV and EV-OV presented a spherical shape with a diameter of about 100 nm as shown in **Figure 3.4 A and B**. This is in keeping with previous studies which showed that the round or spherical shape of EVs and further elaborated that the cup shape of EVs under TEM could be attributed to the fixation process (Raposo and Stoorvogel, 2013b).

3.3.3 EVs purified from OV infected breast cancer cells express exosome markers and carry viral cargo

Next, during this study, EV protein markers in the protein lysates from both MCF-7 and MDA-MB-231 producing cell and their EVs (EV and EV-OV) were detected through western blot analysis. First, the tetraspanin proteins CD9 and CD63, and TSG101 were substantially enriched in all the MCF-7 and MDA-MB-231 derived EVs preparations. On the other hand, CD63 and CD9 were less abundant in MDA-MB-231 derived EV-OV (**Figure 3.6 and 3.7**). This is consistent with prior research, which found that HSV-1 infection resulted in a reduction in intracellular CD63 (Dogrammatzis et al., 2019). They found that HSV-1- causes the release

of CD63-positive EVs derived from human embryonic lung infected cells but has no effect on TSG101 exocytosis, it indicates that the infection causes EV release through ESCRT-independent pathways while not altering ESCRT-dependent pathways in which TSG101 play a role (Dogrammatzis et al., 2019). Another major explanation for the loss of intracellular CD63 could be exocytosis, rather than protein breakdown and a lack of accumulation owing to decreasing levels of its transcripts. The CD63 tetraspanin protein is found on the plasma membrane, and it travels to late endosomes through clathrin- and perhaps caveola-dependent endocytosis. CD63 transports its cargo from late endosomes to lysosomes for breakdown or to intraluminal vesicles (ILVs), which are released as exosomes following MVB fusion to the plasma membrane; hence, CD63 is regarded as an EV marker (Pols and Klumperman, 2009, Yáñez-Mó et al., 2009). The expression of CD63, tumour marker and an integrin binding partner, inversely correlates with cancer metastasis (Kwon et al., 2007, Chirco et al., 2006). Whereas TSG101, initially defined as tumour susceptibility gene, is a subunit of endosomal sorting complex that is needed for ESCRT-1 (Odorizzi, 2006). Kowal et al have elaborated that these are common exosome markers but can also appear in other EV subtypes to some extent such as apoptotic bodies and ectosomes (Kowal et al., 2016). These markers could efficiently separate the particles isolated by ultracentrifugation for their role in cargo sorting and biogenesis regulation (Hurwitz et al., 2017, Nishida-Aoki et al., 2017). Importantly, our western blot data confirmed the presence of viral cargo on the MCF-7 and MDA-MB-231 derived EV-OV and infected cell lysates (**Figure 3.6 and 3.7**). Among the HSV-1716's most prominent antigens were enveloped viral glycoproteins B proteins with a MW of 130 KDa. Both MCF-7 and MDA-MB-231 infected cells and derived EV-OV had level of gB, which was observed in our study (**Figure 3.6 and 3.7**). Our findings are consistent with earlier research and demonstrated that the envelope protein was shown to be the most prevalent viral protein via western blot and mass spectrometry (Birzer et al., 2020). They found that L-particles that were released by mDCs that had HSV-1 infection had a significant abundance of gB and gD as key envelope proteins (Birzer et al., 2020). Other studies demonstrated that exosomes carry pathogen signatures from human hepatoma (Huh7.5) infected cells with HCV, as well as host cellular components, as has been found to contain HCV RNA (Ramakrishnaiah et al., 2013). Another study discovered that exosomes generated from EBV-infected lymphoblasts (LCL) contain both Epstein–Barr virus viral proteins and viral RNAs (Pegtel et al., 2010). In general, our findings are consistent with those of previous studies, despite differences in virus strains

and cell lines used to produce the virions packed into particles. However, this is the first study that has shown the EVs can carry OV viral cargo, and this may have therapeutic implications.

3.3.4 EV-OV are taken up by tumour cells and inhibit tumour cell migration

Finally, we wanted to determine if MCF-7 and MDA-MB-231 derived EVs could be taken up by breast cancer cells. It was found that EV and EV-OV were successfully internalised and this was demonstrated using two main approaches flow cytometry and confocal microscopy. After 24h of culture, these complexes were seen inside MCF-7 and MDA-MB-231 cells, displaying highly comparable viral GFP expression to the OV alone group (**Figure 3.12 and 3.13**). We showed that EV and EV-OV derived from MCF-7 and MDA-MB-231 cells demonstrated significant uptake at 24h of culture in all the treatments groups compared to the control, respectively (**Figure 3.10 A and B**) and (**Figure 3.11 A and B**). Previous studies showed that observed CD63-green fluorescent protein (GFP) EVs were detectable on A431 cells, and the highest uptake was observed at 24h by using nano-flow cytometry (Choi et al., 2019). Lee et al used confocal microscopy to reveal the presence of ADIBO-Cy3 labelled EVs signals inside MCF-7 recipient cells (Lee et al., 2018). Therefore, it can be assumed that the confocal microscopy conducted during our study accurately assessed the EV and EV-OV uptake by MCF-7 and MDA-MB-231 cells. In addition, our result showed that virus HSV1716-GFP (OV) was able to infect the MCF-7 and MDA-MB-231 tumour cells as demonstrated by the significant increase in GFP expression (**Figure 3.10 A and B**) and (**Figure 3.11 A and B**). Furthermore, using an anti-HSV antibody we showed that the vesicles EV-OV derived from MCF-7 and MDA-MB-231 contained viral cargo (**Figure 3.12 A and Figure 3.13 A**). These exciting data suggest that viral cargo can be transferred by EV. OV induced significant tumour cell death on MCF-7 and MDA-MB-231 compared to all the treatment groups (**Figure 3.10 C and Figure 3.11 C**). Our result is consistent with an *in vitro* study on MCF-7 and MDA-MB-231 breast cancer cells that revealed that the cells were susceptible to HSV1716 infection and virus-mediated death (Kwan et al., 2021a). Cockle et al used scratch assay to determine the impact of HSV1716 on the migration of two Pediatric high-grade glioma (pHGG) cells lines such as SF188 and KNS42. This suggests that HSV1716 has the ability to suppress tumour cell migration and may play a role to their therapeutic promise for invasive cancers with a dismal prognosis. At 24 h after infection, HSV1716 at 1 or 10 (PFU)/cell substantially inhibited the migration of SF188 cells compared with untreated cells. Moreover, KNS42 cell migration was considerably inhibited by HSV1716 at a concentration of 10 PFU/ cell 24 h after infection. (Cockle et al., 2017). This study is in the line with our study, EV-OV derived from infected

breast cancer cell inhibit cell migration compared with untreated MDA-MB-231 and MDA-MB-231 cells treated with EV at 24h (**Figure 3.14**). In the future, the migration experiment for MCF-7 cells should be repeated, and it would be interesting to include additional kinds of breast cancer subtypes. Moreover, for the MCF-7 and MDA-MB-231 cells, an invasion test is required to conduct and examine the chemoattractant gradient-related characteristics of each cell line. However, owing to the COVID 19 pandemic and the delay in reagent supply, such as for the invasion assay kit and mitomycin C for the migration test, these experiments were not carried out.

This chapter shows that EVs, can be purified from two types of breast cancer cell lines and that following infection with OV the purified EVs carry viral cargo. These EVs can be internalised and transfer viral cargo to the cancer cells resulting in inhibition of cell migration. This suggests that EVs from virally infected cells may have antitumour properties and this will be investigated in the following chapters.

Chapter 4: Mass spectroscopy analysis of Extracellular Vesicles derived from HSV1716 infected breast cancer cells

4.1 Introduction

Proteins are a key element of EVs, and they are often reported to be transported as functional signalling molecules and to be involved in interactions between the membrane surface and related ligands (Ratajczak et al., 2006). Furthermore, the EV proteins that are most prevalent, such as the tetraspanins CD63, CD9, and CD81, are the most common used for detecting EVs. However, one must consider protein patterns of EVs are often affected by disease states of cells, partially reflecting changes in the secretory cell. while also affecting biological characteristics of EVs and the roles they play when interacting with neighbouring cells (Pegtel et al., 2014). As more extensive fundamental research is completed, EV proteomic studies may lead to therapeutic advancements in the future.

One limitation of EV proteome research is the extensive purification required to make EV proteins more visible than contaminating proteins found in conjunction with EVs (Greening et al., 2017). Modern EV isolation approaches that use various methodologies have enabled more robust proteomic studies, but other difficulties remain visible and challenging to avoid. Attempts to reduce the use of contaminated serum proteins in culture, for example, may have an effect on the quantity and content of EV proteomes. (Li et al., 2015). EV proteomics is still an exciting field with tremendous potential for discovery.

The field of proteomics has achieved significant advancements, particularly in the area of mass spectrometry-based proteomic technologies, which have made it possible to identify and quantify proteins. Several vesicular protein databases have been developed, such as the ExoCarta (Mathivanan and Simpson, 2009), a collection of data from various studies focusing on EV proteomics from a variety of cell types, body fluids, and disease states. These findings allow for better pathway analysis and corroboration of research data, which drives the development of EV-based diagnostics and therapeutic protein targets.

This chapter aimed to analyse the protein content of EVs derived from TNBC cells and investigate how this content changes following infection of these cells with OV (i.e. do these EVs from infected cells carry inflammatory immune cargo?). We used mass spectrometry and extensive bioinformatics methods to detect changes in vesicle content. The subcellular origin and pathway to which the discovered proteins belonged were determined using GO analysis methods. This knowledge could provide an understanding of the possible biological effects of EVs on recipient cells, enabling further experiments to be planned. Western blotting was used to confirm the validity of mass spectrometry results by analysing differentially expressed

proteins identified by mass spectrometry. In these validation procedures, whole-cell lysates and EV lysates were used to compare the relative abundance of proteins in EVs and their parental cells.

4.2 Results

4.2.1 Label-free mass spectrometry

EVs generated from MDA-MB-231 were purified by ultracentrifugation and solubilized in Rapigest. Label-free mass spectrometry was used to analyse them at the University of Sheffield's Chemical and Biological Engineering Department, with assistance from Dr Caroline Evans. Reverse-phase HPLC-MS was used to analyse samples in technical duplicate. In summary, materials were reduced, alkylated, and digested with trypsin. Maxquant software was used to analyse and quantify peptide data collected by the Orbitrap Velos instrument, detecting relative abundances of proteins based on peptide hits. As the best estimate proxy for absolute protein abundance, a profile of label-free quantitation (LFQ) intensities was constructed for each protein. The Perseus programme was used to compare profile similarities and differences across duplicate samples.

4.2.2 Proteome profiling of MDA-MB-231 derived EV versus MDA-MB-231 derived EV-OV

Following the post-processing carried out by the Perseus software, a total of 1482 distinct proteins were identified. It is a well-known software for processing quantitative proteomics data downstream in bioinformatics (Tyanova et al., 2016), Such as the removal of contaminants. Intensity histograms for MDA-MB-231 derived EVs were displayed to indicate that the data was regularly distributed (**Figure 4.1 A&B**). To further support the data's quality, the correlation study of repetitions of MDA-MB-231 derived EV, and EV-OV proteins showed a strong correlation between 3 replicates within groups. Together this data gives confidence that our technique was robust and reproducible (**Table 4.1**).

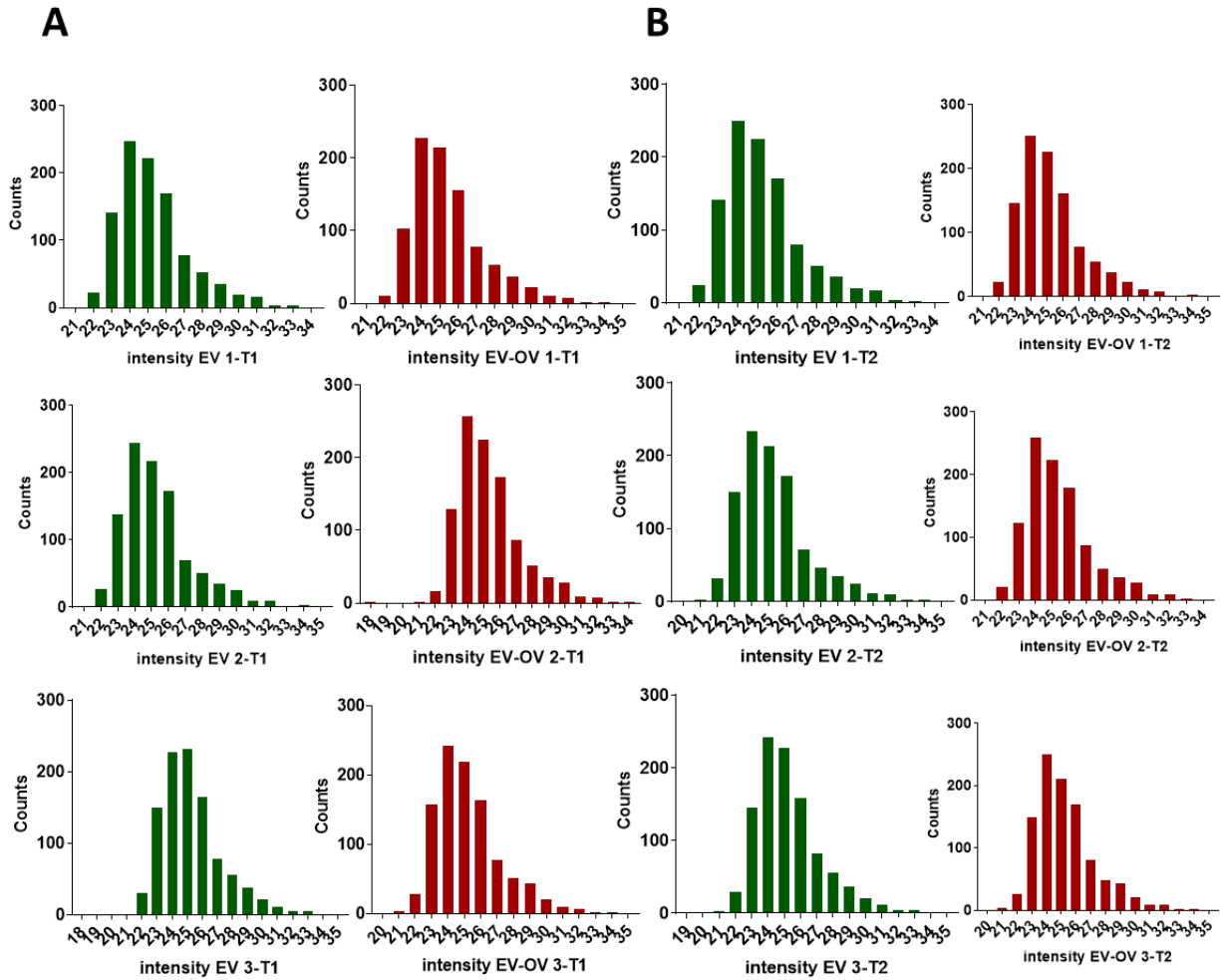


Figure 4.1: Histogram of LFQ intensity columns for replicates of MDA-MB-231 derived EV and EV-OV. A) Showing a normally distributed intensity. B) With normalised and imputed intensity values for statistical analysis.

LFQ intensity EV_1-T1	LFQ intensity EV_1-T2	LFQ intensity EV_2-T1	LFQ intensity EV_2-T2	LFQ intensity EV_3-T1	LFQ intensity EV_3-T2	LFQ intensity EV-OV_1-T1	LFQ intensity EV-OV_1-T2	LFQ intensity EV-OV_2-T1	LFQ intensity EV-OV_2-T2	LFQ intensity EV-OV_3-T1	LFQ intensity EV-OV_3-T2	
NaN	1.00	0.96	0.96	0.96	0.96	0.95	0.95	0.96	0.96	0.96	0.96	LFQ intensity EV_1-T1
1.00	NaN	0.96	0.96	0.96	0.96	0.95	0.95	0.96	0.96	0.96	0.96	LFQ intensity EV_1-T2
0.96	0.96	NaN	0.99	0.95	0.95	0.94	0.94	0.95	0.95	0.94	0.93	LFQ intensity EV_2-T1
0.96	0.96	0.99	NaN	0.95	0.95	0.94	0.93	0.94	0.95	0.93	0.93	LFQ intensity EV_2-T2
0.96	0.96	0.95	0.95	NaN	1.00	0.96	0.96	0.96	0.96	0.96	0.96	LFQ intensity EV_3-T1
0.96	0.96	0.95	0.95	1.00	NaN	0.96	0.96	0.96	0.96	0.96	0.96	LFQ intensity EV_3-T2
0.95	0.95	0.94	0.94	0.96	0.96	NaN	0.99	0.97	0.97	0.97	0.97	LFQ intensity EV-OV_1-T1
0.95	0.95	0.94	0.93	0.96	0.96	0.99	NaN	0.98	0.98	0.98	0.98	LFQ intensity EV-OV_1-T2
0.96	0.96	0.95	0.94	0.96	0.96	0.97	0.98	NaN	1.00	0.96	0.96	LFQ intensity EV-OV_2-T1
0.96	0.96	0.95	0.95	0.96	0.96	0.97	0.98	1.00	NaN	0.96	0.96	LFQ intensity EV-OV_2-T2
0.96	0.96	0.94	0.93	0.96	0.96	0.97	0.98	0.96	0.96	NaN	1.00	LFQ intensity EV-OV_3-T1
0.96	0.96	0.93	0.93	0.96	0.96	0.97	0.98	0.96	0.96	1.00	NaN	LFQ intensity EV-OV_3-T2

Table 4.1: Correlation values of MDA-MB-231 derived EV and EV-OV replicates datasets. The table represents the correlation of the biological replicates high (green), middle (yellow), low (red). Correlation in the same group was highest at 0.99; in between groups, the lowest was 0.93. These show that biological replicates inside the same groups were reproducible.

4.2.3 Differential expression of proteins

A quantitative comparison of protein levels between MDA-MB-231 derived EV, and EV-OV was performed using Perseus (Tyanova et al., 2016). Data were filtered proteins that were only identified by sites in at least three replicates of each group, contaminants were removed, statistical t-test were performed with FDR 5% (Tyanova et al., 2016). A total of 30 proteins achieved the <0.05 FDR criteria (Benjamini-Hochberg) (**Table 4.2**). They were identified as differentially expressed between the two groups by student t-test and are marked in colour on the volcano plot (**Figure 4.2**). The volcano plot shows that 24 of the proteins identified by dots were primarily upregulated in the MDA-MB-231 derived EV-OV falling to the left of the volcano plot such as protein phosphatase 6 catalytic subunit (PPP6C), Beta-2 microglobulin (B2M), Vimentin (VIM). To begin, (PPP6C) is a part of the serine/threonine protein phosphatase family, which is found in all eukaryotes. The PPP6C complex is extensively presented in a variety of tissue types and has been linked in a variety of activities including, inflammatory response, cell cycle and lymphocyte differentiation (Hammond et al., 2013, Ogoh et al., 2016). Second, B2M is a small protein and an important part of major histocompatibility complex (MHC) class I which performs fundamental physiologic effects in tumorigenesis and immune regulation (Wang et al., 2021). It was identified as a cancer diagnostic marker and therapeutic target (Min et al., 2002). Third, (VIM) is a cytoskeletal protein of type III intermediate filaments that is mostly expressed in mesenchymal cells. As a result, it is identified in fibroblasts, endothelial cells, immune cells, ovarian and prostate cancer cells (Gan et al., 2016, Duarte et al., 2019). Extracellular vimentin receptors have a role in the immune response to viral infections. However, six proteins were downregulated in the MDA-MB-231 derived EV as dots falling to the right of the volcano plot such as Pentraxin-related protein (PTX3) and Charged multivesicular body protein 2a (CHMP2A). PTX3 is a member of the pentraxin superfamily, which functions as an immune system pattern recognition molecule (PRM). This molecule has the ability to identify cellular debris, to stimulate phagocytosis (opsonization), to trigger the complement system, and to control the inflammatory response in a variety of situations (Garlanda et al., 2018). In the endosomal sorting complexes needed for transport III (ESCRT-III), CHMP2A is a component that participates in the development of multivesicular bodies and EV biogenesis (Teis et al., 2008). Despite this, the mass spectrometry study did not find any OV-derived proteins, even after comparing the peptide data to the database of relevant viral proteins.

Table 4.2 List of proteins in MDA-MB-231 derived EV-OV

Gene name	Log2-fold change	Protein name
Upregulated genes		
TPP2	3.79	Tripeptidyl-peptidase 2
COL12A1	2.97	Collagen alpha-1(XII) chain
LCP1	2.88	Plastin-2
TGFBI	2.85	Transforming growth factor-beta-induced protein ig-h3
SF3B3	2.76	Splicing factor 3B subunit 3
TIMP2	2.76	Metalloproteinase inhibitor 2
TXNDC5	2.72	Thioredoxin domain-containing protein 5
ATP5A	2.53	ATP synthase subunit alpha, mitochondrial
B2M	2.45	Beta-2-microglobulin; Beta-2-microglobulin
EIF2AK	2.45	Interferon-induced, double-stranded RNA-activated protein kinase
VIM	2.32	Vimentin
EFEMP1	2.28	EGF-containing fibulin-like extracellular matrix protein 1
PPP6C	1.83	Serine/threonine-protein phosphatase 6 catalytic subunit
PSMB2	1.65	Proteasome subunit beta type-2
PLOD3	1.64	Procollagen-lysine,2-oxoglutarate 5-dioxygenase 3
EML4	1.56	Echinoderm microtubule-associated protein-like 4
ATP5B	1.48	ATP synthase subunit beta, mitochondrial
ACTA1	1.45	Actin, alpha skeletal muscle
CALR	1.44	Calreticulin
EXOSC4	1.44	Exosome complex component RRP41
PSMA7	1.44	Proteasome subunit alpha type 7
GLUD1	1.41	Glutamate dehydrogenase 1
TALDO1	1.41	Transaldolase
U2AF2	1.38	Splicing factor U2AF 65 kDa subunit

Gene name	Log fold change	Protein name
Downregulated genes		
PTX3	1.44	Pentraxin-related protein PTX3
CHMP2A	2.18	Charged multivesicular body protein 2a
FARSB	1.31	Phenylalanine--tRNA ligase beta subunit
EFNB1	2.28	Ephrin-B1
NDFIP1	1.44	NEDD4 family-interacting protein 1
A0A6I8PLG0	2.33	Pentraxin-related protein PTX3

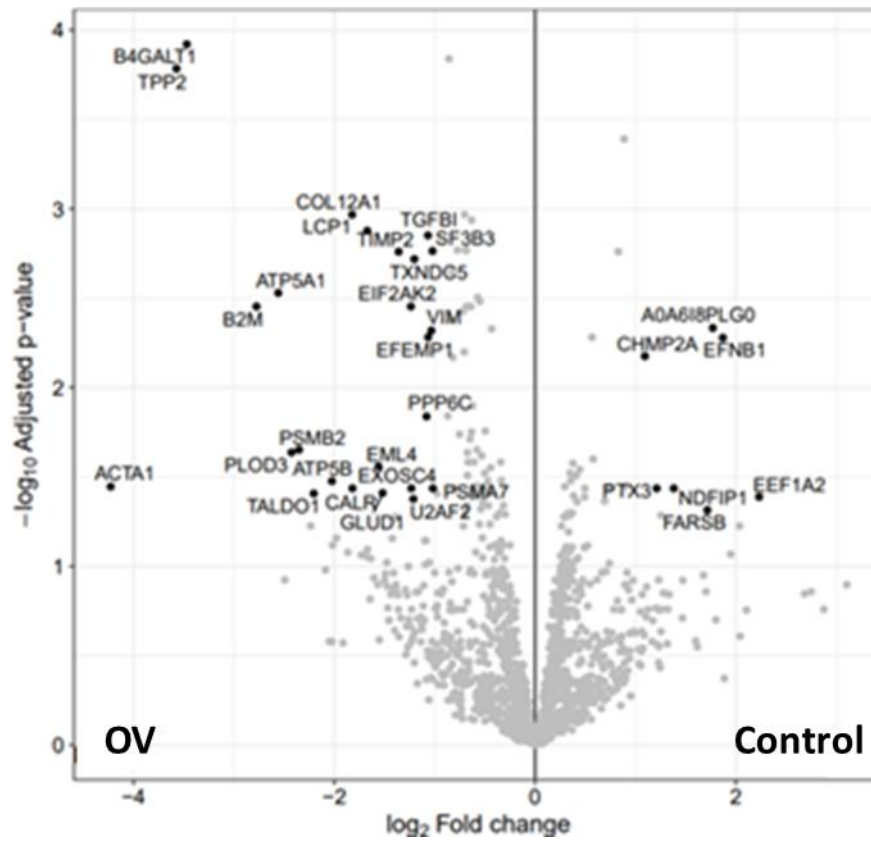


Figure 4.2: Volcano plot showing EV proteins differentially regulated following infection with OV. Differential expression of immune related genes (a). Data expressed as \log_2 fold change in the gene expression of EV-OV versus EV control groups, where each data point represents one gene. Increase in gene expression $p < 0.05$ represented by datapoints falling to the left of the volcano plot. Decrease in gene expression $p < 0.05$ represented by datapoints falling to the right of the volcano plot. $n = 3$ technical replicates.

4.2.4 Functional Characterisation of Identified Proteins

In order to have a better understanding of the isolated proteome, we carried out an analysis of gene abundance on the list of proteins that were discovered. The Panther database was used to conduct the gene ontology (GO) study. GO is an ontology of specified concepts that reflect the features of protein gene products and describe how they function in a biological setting. Firstly, the cellular component (CC) implies crucial activity location for a proportion of the proteins. Secondly, molecular functions (MF) describe individual gene products' molecular activities. Finally, Biological processes (BP) are operations or collections of molecular events that comprise but do not entirely constitute a biological pathway. This analysis was performed to identify enriched terms compared to the significant human genome at FDR < 0.05. In cellular component, we found an enrichment of six proteins such as COL12A1, TGFBI, TIMP2, EFEMP1, CALR and PLOD3 in localisation in the collagen-containing extracellular matrix and five proteins such as COL12A1, TXNDC5, B2M, PLOD3 and CALR were localised in endoplasmic reticulum, but the highest enrichment of three proteins such as B2M, PTX3 and TIMP2 were in the Tertiary granule lumen and specific granule lumen (**Figure 4.3 A**). In the molecular function, we demonstrated that the highest enrichment of proteins CALR and PTX3 were localised in complement component C1q binding significantly enriched the identified proteins (**Figure 4.3 B**). In the biological process, we demonstrated the highest enrichment proteins B4GALT1, COL12A1, LCP1, TGFBI, TIMP2, PLOD3 and PTX3 contributed to extracellular matrix organisation and extracellular structure organisation (**Figure 4.3 C**).

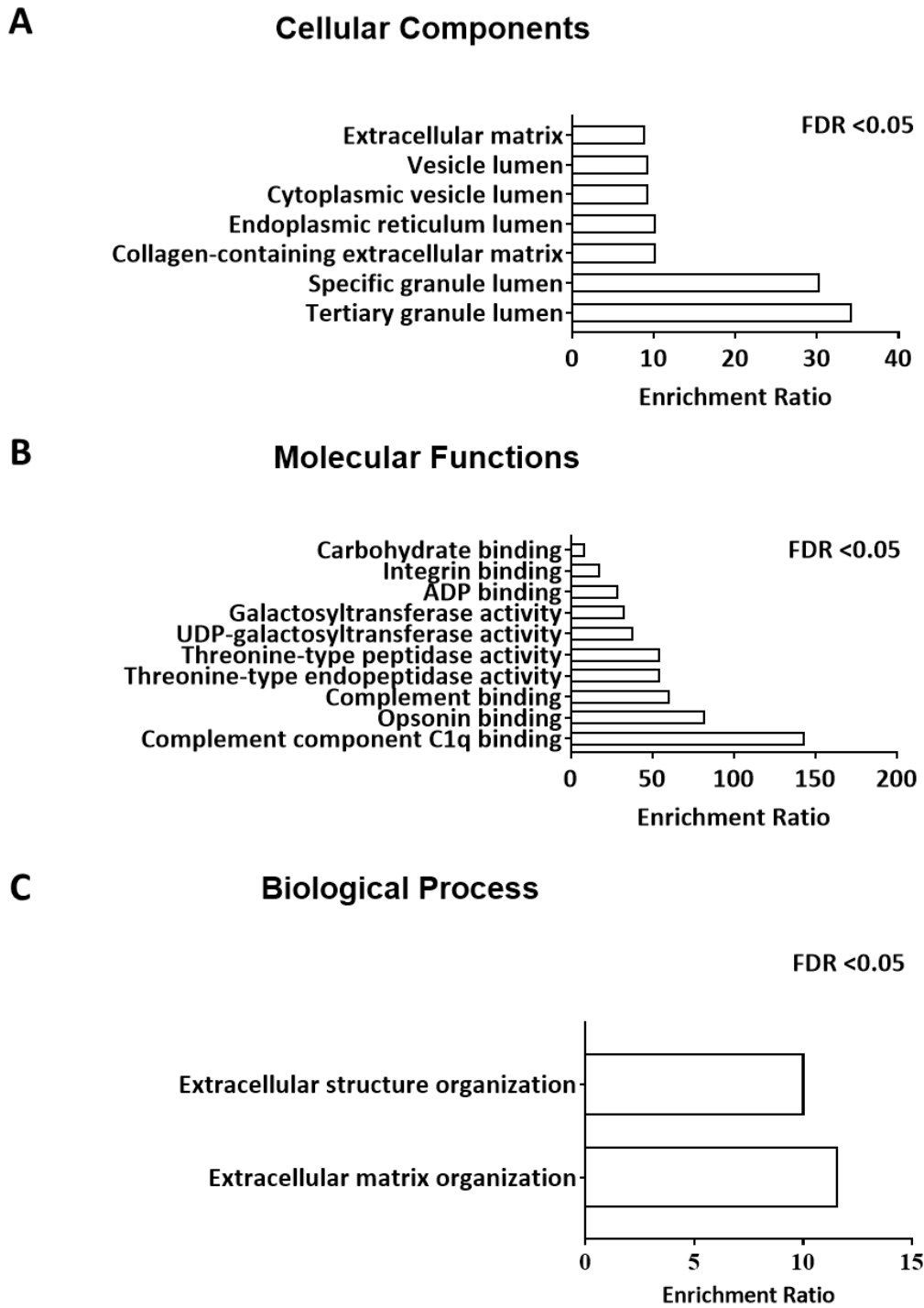


Figure 4.3 : Gene ontology enrichment analysis of extracellular vesicles compared to the human genome. Gene ontology enrichment analysis of extracellular vesicles compared to the human genome. 30 statistically significant proteins found in extracellular vesicles purified from the conditioned media of confluent flasks of the MDA-MB-231 control and infected cells. Panther Gene Ontology databases were used to search for statistically significant enriched proteins. The above graphs detail the distribution of cellular region, molecular roles and biological processes for the proteins detected. N =3 technical replicates.

In order to determine which pathways MDA-MB-231 derived EV-OV proteins are engaged in, a pathway analysis must be performed. The Panther GO database was used to match the enriched proteins to the pathways that they belong to (**Figure 4.4**). The findings revealed that two proteins produced from EV-OV, COL12A1 and ACTA1, were associated in the top two pathways, integrin signalling system and inflammation mediated by chemokine and cytokine signalling pathway. In addition, B2M protein was implicated in T cell activation pathway. Furthermore, PPP6C protein derived from EV-OV was shown to be involved in the EGF receptor and FGF signalling pathways. Work from our laboratory has shown that the same virus used in this study (HSV1716) leads to the recruitment of tumour infiltrating T cells in mice with mammary carcinoma following administration into circulation (Kwan et al., 2021b)

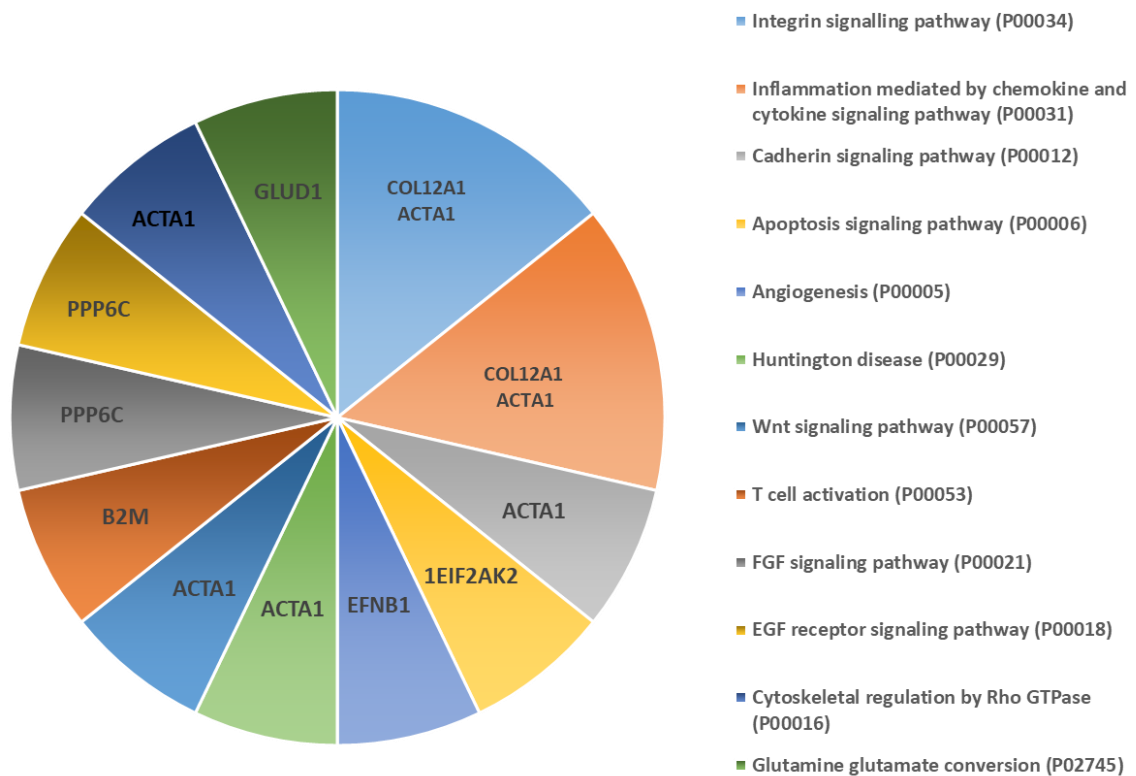


Figure 4.4 : An example of substantially enriched proteins classified into different pathways.

Panther enrichment study of the substantially upregulated and downregulated proteins in MDA-MB-231 derived EV and EV-OV. The top pathways are the integrin signalling pathway and Inflammation mediated by chemokine and cytokine signalling pathway.

4.2.5 Label-free mass-spectrometry validation

4.2.5.1 Western blotting

To verify these findings, proteins were chosen as candidates for western blotting in both cell and EVs protein lysates. Four candidates were chosen that were enriched in individual pathways. The first protein chosen for validation was Protein phosphatase 6 catalytic subunit (PPP6C), which was abundant in cell lysates (CL) derived from MDA-MB-231 and OV infected MDA-MB-231. Interestingly, PPP6C was highly enriched in EV-OV derived from infected MDA-MB-231 but was not detected in EV only (**Figure 4.5 A**). Our validation confirmed that PPP6C was upregulated in MDA-MB-231 derived EV-OV, as shown in our mass spectrometry analysis above (**Figure 4.2**). Moreover, PPP6C is involved in the EGF receptor signalling pathway and FGF signalling pathway further linking this protein to the pathway analysis in **Figure 4.4**. It is positively associated with CD8 + T cell, macrophage and neutrophil infiltration (Xie et al., 2022). Together this points to a role for PPP6C in immune activation and further studies investigating this are warranted. The second protein to validate was Beta-2-microglobulin (B2M), which was more abundant in the cell lysates derived from control and infected MDA-MB-231 cells. However, a faint band was detected in MDA-MB-231 derived EV-OV. (**Figure 4.5 B**). B2M is involved in the T cell activation pathway (**Figure 4.4**). The most notable function of B2M is its association with the tertiary structure of the MHC-I α -chain. As a result, antigenic peptides are therefore presented to cytotoxic T cells and will rapidly bind and disintegrate the cancer cells presented by the antigen during the process of identifying the foreign peptide antigen on the cell surface (Christianson et al., 1997, Höglund et al., 1998). Next, we looked at vimentin, a type III intermediate filament protein of the cytoskeleton that is mostly expressed in mesenchymal origin cells (Gan et al., 2016). Vimentin (VIM) was upregulated in MDA-MB-231 derived EV-OV, as shown in volcano plot (**Figure 4.1**) and was abundant in both cell lysates and was enriched in MDA-MB-231 derived EV-OV. However, none were detected in MDA-MB-231 derived EV (**Figure 4.5 C**). The last validation marker was Pentraxin3 (PTX3), the most important enriched protein involved in extracellular matrix organisation in biological processes at cellular levels (Figure 4.3) and was found to be downregulated in our mass spectrometry analysis above (**Figure 4.2**). PTX3 was detected in both cell lysate samples. In contrast, findings from western blots demonstrate that PTX3 was only detected in EV-OV samples obtained from the MDA-MB-231 cell line, but absent in MDA-MB-231 derived EV (**Figure 4.5 D**).

MDA-MB-231

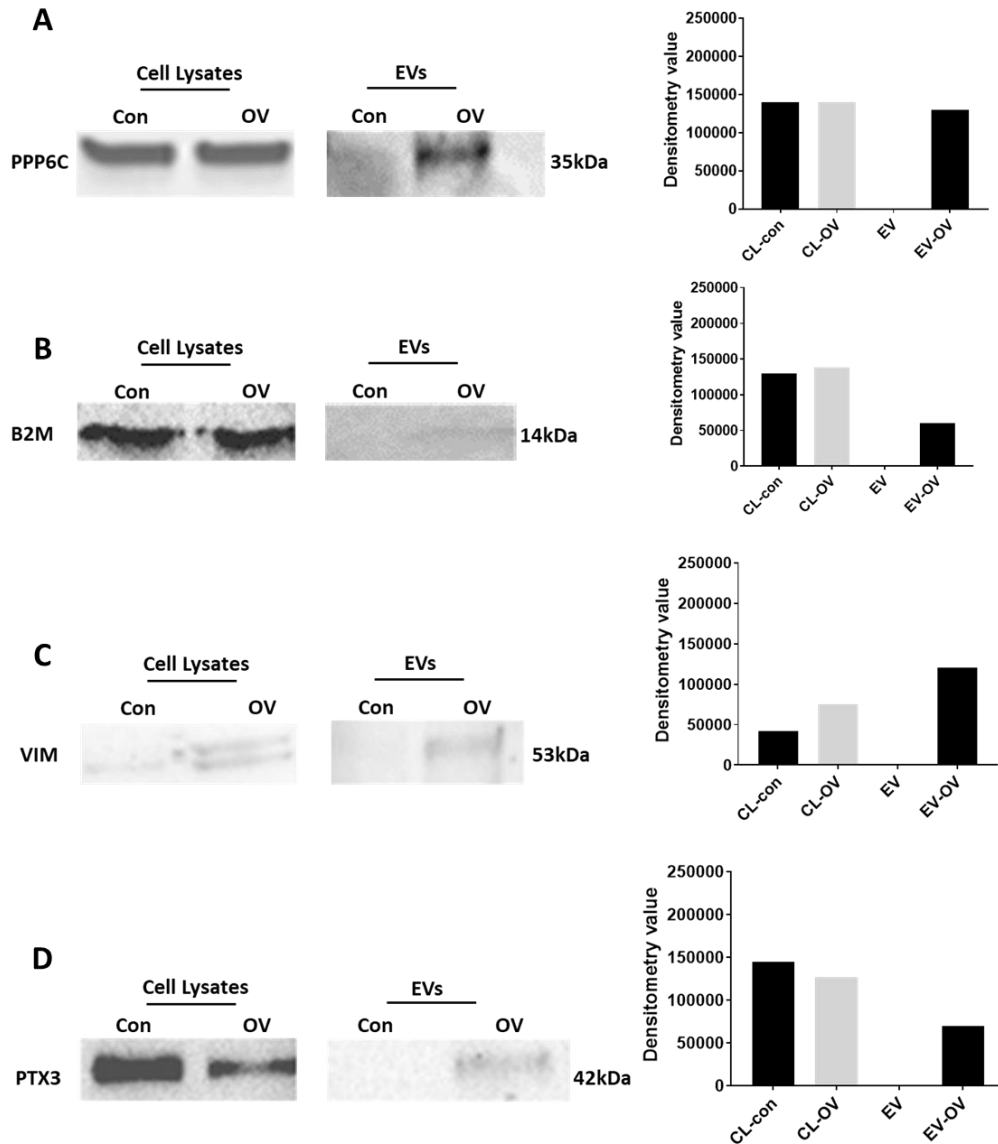


Figure 4.5: Mass spectrometry validation of differentially expressed proteins using western blotting. Immunoblotting of proteins were upregulated in the MDA-MB-231 derived EV-OV and down-regulated in the MDA-MB-231 derived EV. Western blot was carried out using whole-cell lysates in addition to EVs. 20 μ l of each with equal protein amount (2 μ g) were mixed with 5 μ l of NuPAGE LDS Sample Buffer (4X). The mixtures were incubated at 90 $^{\circ}$ C for 10 min, and 20 μ l were loaded to each well of 12% acrylamide gel. After transferring to a nitrocellulose membrane. They were blocked with 5% milk for 1h at RT, then incubated overnight with appropriate primary antibody diluted in 10 mL milk at 4 $^{\circ}$ C. This included **A**) PPP6C **B**) B2M **C**) VIM and **D**) PTX3. On the following day, the membranes were washed and incubated with appropriate secondary antibody for 1hr at RT, then washed three times for 5 min each in PBST. WASTER[®] SUPERNOVA HRP Detection Substrate was added to the membrane then imaged using ChemiDoc[™] MP System (BIO-RAD). N=1.

4.3 Discussion

Extracellular vesicles (EVs) are responsible for the transfer of proteins, lipids, and nucleic acids from one cell to another, and they are essential in cell-to-cell communication (Yáñez-Mó et al., 2015). Proteomic analyses of these biological tools could provide in-depth insights. The experimental data of MDA-MB-231 derived EV, and EV-OV proteomic analysis revealed interesting results. EV proteins were studied using GO analysis, which provided more insight into the proteins found in the EVs. During this study, we performed proteomic analysis to reveal what cargo might be carried by EVs purified from infected breast cancer cells. We successfully identified 1482 distinct proteins by Perseus software. 30 proteins were significantly expressed in MDA-MB-231 derived EVs. 24 proteins were upregulated in MDA-MB-231 derived EV-OV such as PPP6C and B2M as shown in **(Figure 4.2)** and six proteins were downregulated in MDA-MB-231 derived EV such as PTX3 as shown in **(Figure 4.2)**. Our study demonstrated that Protein phosphatase 6 catalytic subunit (PPP6C) was found in both cell lysates and was highly enriched and upregulated in MDA-MB-231 derived EV-OV **(Figure 4.5)**. The results also revealed the involvement of PPP6C in the EGF and FGF receptor signaling pathways as shown in **(Figure 4.4)**. In different malignancies, it has been shown that the PPPCs family of proteins play a critical role in the formation and progression of tumours. However, the expression patterns and functional roles of the PPPCs family in breast cancer remain unknown currently. As a result, researchers sought to examine the clinical relevance and biological roles of the PPP6C family to understand better their potential importance in the diagnostics and therapy of breast cancer (Xie et al., 2022). Xie et al have established a positive association of PPP6C with macrophages, CD8 + T cell, and neutrophil infiltration in tumours (Xie et al., 2022). TIMER (<https://cistrome.shinyapps.io/timer/>) is a database that has been developed to study immune cell infiltration in a variety of malignancies including breast cancer (Li et al., 2020b). For estimating tumour immune infiltration by macrophages, neutrophils, B cells, dendritic cells, and CD4/CD8 T cells, the database employs statistical approaches that have been verified by pathological investigation of tumours. Xie et al utilised this information to investigate the association between the PPPCs family and the amount to which distinct immune cell subpopulations were infiltrated by the PPPCs (Xie et al., 2022). The findings of their study revealed that numerous members of the PPPCs family such as PPP1CA and PPP4C were significantly connected with breast cancer prognosis and that blocking the expression of these genes may have the potential to improve the survival of breast cancer patients. Therefore, It was discovered that inhibiting PPP1CA and PPP4C expression

substantially impacted breast cancer growth and migration (Xie et al., 2022). As a result, the combination of chemotherapy or surgery with certain PPP6C-targeted medications may enhance the treatment prognosis of breast cancer patients. Also discovered was that abnormal expression of the PPPCs family members such as PPP1CA and PPP4C can suppress the infiltration of immune cells in breast cancer. As a result, increasing the efficacy of immune checkpoint inhibitors in breast cancer treatment may be enhanced by utilising drugs that target PPPCs specifically (Esteva et al., 2019, Xie et al., 2022). Therefore, OV upregulation of PPP6C during the current study could be attributed to the activation of anti-tumour immunity against breast cancer, this begs the question of a potential therapeutic application of our EVs derived from HSV1716 infected cells and will be investigated in the following chapter.

In addition, we found that B2M was upregulated in MDA-MB-231 derived EV-OV in volcano plot (**Figure 4.2**). Also, expressed in MDA-MB-231 derived EV-OV in our validation by western blot (**Figure 4.5**). In addition, B2M was localised in endoplasmic reticulum in cellular component as described in (**Figure 4.3A**). Moreover, B2M protein was implicated in T cell activation pathway (**Figure 4.5**). Beta-2 microglobulin (B2M) has been shown to be expressed in almost all nucleated cells, including immune cells, and is highly expressed in stromal cells surrounding tumour cells (Pereira et al., 2017). B2M play a critical role in T cell activation pathway and is a key component of the MHC class I complex that plays a critical role in carcinogenesis and immune response (Rosano et al., 2005). To enter the endoplasmic reticulum, B2M proteins in the cytoplasm of tumour cells must first be digested by the proteasome and then transported there by a transporter linked with antigen presentation. T cell receptors (TCRs) recognise tumour antigens when they are released and displayed on the tumour cell surface, and this activation results in the activation of antigen-specific cytolytic T lymphocytes (CTLs), which are critical in the elimination of tumour cells in the course of an adaptive immune response (Halle et al., 2017). Some studies indicated that B2M deficiency allows tumour cells to escape the host's immune control. Therefore, the absence of B2M protein results in the failure of surface MHC class I expression (Germano et al., 2021). Furthermore, researchers discovered that melanoma cells lacking a copy of the B2M gene were unable to express MHC class I (Hicklin et al., 1998). In the absence of B2M, the heavy chain of MHC class I aggregates in the endoplasmic reticulum and is destroyed in the cytosol (Hughes et al., 1997). MHC class I depletion is one of the primary mechanisms of tumour resistance to cytolytic activity of T lymphocytes (Schreiber et al., 2011). Other studies elevated that tumour B2M deficiency has previously been linked to immune escape in non-small-cell

lung cancer (NSCLC) and melanoma (Sucker et al., 2014, Datar et al., 2021). There were less infiltrating CD4+, CD8+, and FOXP3+ T cells in NSCLCs with downregulated B2M expression in tumour cells (Datar et al., 2021). OV induces inflammation within tumours, leading to the recruitment of T cells necessary for eliminating tumour cells, which induces antitumour immunity (Kwan et al., 2021a). This is carried out by exposing the tumour-associated antigens (TAA) to the circulatory system that activates the anti-tumour response of the body's immune system by generating tumour-specific T cells (Ito et al., 2007). T cell activation provides longer immunity against re-occurring tumours (Oliva et al., 2017). Therefore, some of these proteins could be further explored for their diagnostic or therapeutic applications in breast cancer patients. On the other hand, PTX3 is protein downregulated in MDA-MB-231 derived EV in mass spectrometry analysis above (**Figure 4.2**) and was upregulated in MDA-MB-231 derived EV-OV in western blot analysis (**Figure 4.5 D**). Our results demonstrated that PTX3 highly enriched in complement component C1q (**Figure 4.3 B**). PTX3 works as a pattern recognition molecule (PRM) in the immune system, and it belongs to the pentraxin superfamily of opsonin (Garlanda et al., 2018). Bonavita et al when PTX3 interacts with C1q, it has been shown that it may influence complement activation leading to the recruitment of leukocytes, generation of proinflammatory cytokines, and angiogenesis in the tumour microenvironment (Bonavita et al., 2015). Although, the fact that PTX3's involvement in tumour inflammation is well understood (Hamad et al., 2012, Suliman et al., 2008). Giacomini et al discovered that the expression of PTX3 is elevated by about 2-fold in Doxorubicin (DXR)-EVs produced from the highly metastatic MDA-MB-231 cell line, compared to the DXR-EVs generated from the MCF-7 and MDA-MB-468 cell lines with little metastatic potential. Taken together, DXR therapy increases both the production of primary breast tumour small EVs (sEVs) and the quantity of PTX3 sEV cargo (Bandari et al., 2018). However, PTX3 also plays a vital role in tumour development (Giacomini et al., 2018) and it has been linked to an increased risk of tumour spread (Chi et al., 2015). However, the involvement of PTX3 in the formation of metastatic microenvironments remains uncertain(Giacomini et al., 2018). In order to understand the role of EV-OV in breast cancer more study is required. Additionally, it is vital to investigate if PTX3 may be a potential therapeutic agent.

In addition, our results showed that proteins from MDA-MB-231 derived EV-OV were involved in the top pathway cytokines and chemokines pathways are important for intercellular channels of communication in tumours (Anderson and Simon, 2020). Some cytokines such as type I and III IFNs , (IL-1b), IL-12, IL-6 tumour necrosis factor-alpha (TNF-a) and granulocyte

macrophage colony-stimulating factor (GM-CSF) are recognised for its potential to induce the maturation of antigen-presenting cells (APCs) and enhance functional properties of natural killer (NK) and T cells and can make the tumour cells susceptible to the oncolytic virus by damaging the signaling pathway. (Gujar et al., 2018, Puzanov et al., 2016). Chemokines such as CCL2 (also known as MCP-1) and CCL5 (also known as RANTES are well known for mediating the migration of immune cells between tissues. They also facilitate cell interaction and positioning within tissues. They mediate the movement of leukocytes into tumour lesions to influence host response against cancer (Pol et al., 2020).

Taken together these data suggest that the potential of these EV-OV could transfer antitumour immunity. Therefore, the next chapter will study whether EV-OV can transfer viral immunity in a mouse model of breast cancer.

**Chapter 5: Antitumour activity of extracellular vesicles
derived from infection breast cancer cells**

5.1 Introduction

Oncolytic viruses are genetically engineered viruses that are targeted to eliminate cancer cells by selectively duplicating while causing no damage to normal cells (Uche et al., 2021). The immunogenic activity of OV is increased by viral-mediated immunogenic cell death, which includes the activation of T lymphocytes and dendritic cells. In fact, OV trigger cancer cell death, releasing antigens into the microenvironment that are recognised by the immune system, eliciting immunological responses, and compromising the immuno-editing process. One of the most challenging aspects of OV is the transport of the virus to the target area, which is complicated by the establishment of an immune response to viral infection (Ferguson et al., 2012). Clinical trials have mostly relied on direct injection into tumours. However, this is not practicable for tumours that are positioned deep the body and so are not readily accessible (Chaurasiya et al., 2018). The optimal route of delivery would be via the circulation, allowing inaccessible or metastatic tumours to be treated. However, this may activate the immune system, reducing viral efficiency and multiplication in the target oncogenic tissues (O`Bryan and Mathis, 2018).

Some of these limitations may be overcome by delivering OVs and chemotherapeutic drugs through naturally existing biological cargo transporters (such as EVs) (Russell and Bell, 2012). EVs have the potential to transport biological substances to tissues throughout the body. EV lipid membranes are hydrophobic in nature and may protect biological components contained within from degrading (Fukuhara et al., 2016).

The application of EVs from DCs and tumour cells is one of the anti-tumour immunotherapeutic techniques. All eukaryotic cells generate nano-sized vesicles capable of transporting nucleic acids, lipids and proteins to other cells and participating in cell-to-cell communication, resulting in paracrine control (Gurunathan et al., 2019). It has been shown that EVs can play a role in the regulation of the immune system, the remodelling of the matrix, the pathways that transmit signals, the interchange of oncoproteins and oncogenes between cells, the stimulation of angiogenesis, and the formation of a pre-metastatic niche (Lee et al., 2011). It has been demonstrated that EVs produced from tumour cells could stimulate the immune system on anti-tumour DCs (André et al., 2002, Liu et al., 2018). Immunotherapeutic vaccines made from tumour cell derived EVs have the potential to transform cancer treatment. The advantages of EVs involved that vaccines that are based on EV may be kept for long periods of time without a reduction in their immunotherapeutic effectiveness (Jeyaram and Jay, 2017). Moreover, there is more efficient absorption of EVs from antigen-presenting cells rather than

soluble substances (Zeelenberg et al., 2008). In chapters 3 we have shown that EV purified from cancer cells by ultracentrifugation are in the exosome size range and following infection with an oncolytic virus (HSV-1716) these EVs contain viral cargo, suggesting that EVs from virally infected cells may have antitumour properties.

In chapter 4 we also show that these EV-OV could potentially transfer antitumour immunity.

In this chapter will study whether EV-OV can transfer viral immunity in a mouse model of breast cancer.

In this chapter the antitumor activity of isolated EVs is investigated in this chapter in an immunocompetent mouse model of breast cancer. C57/BL6 mice were injected with the luciferase-labeled breast cancer cell line EO771-Luc into the nipple. This cell line is produced from C57BL/6 mice and represents a spontaneously growing medullary breast cancer (Sugiura and Stock, 1952). This cell line is also a triple negative breast cancer (TNBC) cell line for the progesterone, oestrogen and human epidermal growth factor HER2 receptors, making it challenging to target therapeutically (Johnstone et al., 2015). Furthermore, in C57BL/6 mice, this tumour type readily spreads to the lungs (Johnstone et al., 2015). Bioluminescence imaging with the IVIS was utilised to monitor tumour development and metastasis since the cell line has luciferase labelled.

The specific objective of the study was to evaluate the targeting of OV in vivo using EVs:

- 1- Determine the biodistribution of EV-OV in the E0771 mammary carcinoma model.
- 2- Assess induction of antitumour immunity following treatment with EV-OV.
- 3- Measure immune activation by expression of pro and anti-inflammatory markers by cytokine bead array (CBA).
- 4- Perform NanoString Immune profiling analysis of tumours following treatment with EV-OV.

5.2 Results

5.2.1 The antitumour efficacy of EV-OV in the E0771 mammary carcinoma model

5.2.1.1 *In vivo study design*

Female C57BL/6 mice were obtained from Envigo at 6-8 weeks of age and kept in the University of Sheffield Biological Services Unit, where they were cared for in accordance with

the University of Sheffield code of ethics and Home Office rules. With the assistance of Mr Matthew Fisher, all work was completed under Dr. Munitta Muthana's Home office project licence (PPL1099883). Mice were injected with 1×10^6 EO771-Luc cells into the nipple and weighed every three days. Every three days, the tumour volume was measured with callipers and documented (Figure 5.1). When the tumours reached 150-200 mm³, mice were given the following intravenous (i.v.) treatments:

1. Control: Mice were given three injections in total i.v. (13, 15, 17 days) with 100µl PBS.
2. EV: Mice were given three injections in total i.v. (13, 15, 17 days) with 30µg, 100 µl EV derived from EO771 cells and labelled with Alexa fluor 488.
3. EV-OV: Mice were given three injections in total i.v. (13, 15, 17 days) with 30µg, 100 µl EV-OV derived from EO771 infected with OV (MOI 5) and labelled with Alexa fluor 488.
4. HSV-1716 (OV): Mice were given three injections in total i.v. (13, 15, 17 days) with 100 µl HSV1716 GFP at 10^7 pfu/ml. After receiving therapy, 5 mice from each group were culled after 24 h and the remaining mice were culled after 72 h by cervical dislocation, and the organs and tumour were removed and kept in liquid nitrogen for post-mortem examination.

Each treatment group consisted of n=10 mice/group. EVs were isolated by dUC from EO771 untreated and HSV1716 infected cells with MOI 5 (Kwan et al., 2021a).

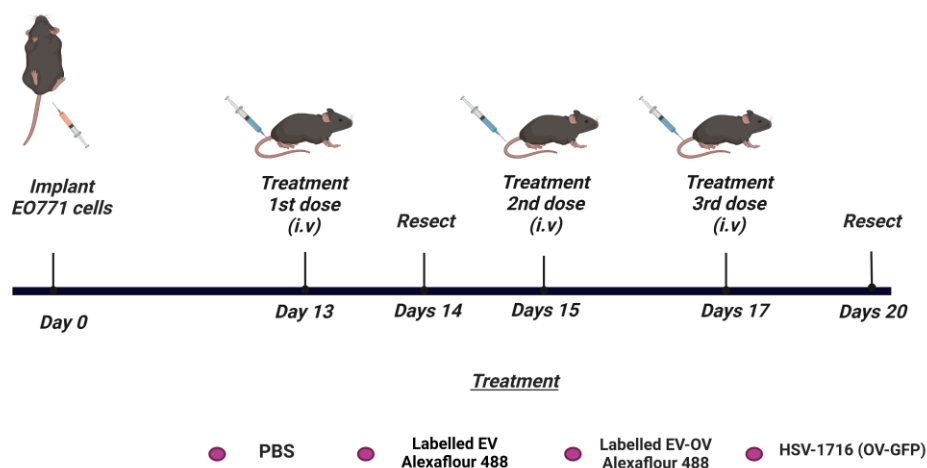


Figure 5.1: Treatment scheme in C57BL/6 female mice with mammary carcinoma. Mice were injected into the nipple with 1×10^6 EO771- luciferase cells. Once the tumours reached ~ 150 - 200 mm^3 mice were injected three times i.v. (13, 15, 17 days) with 100ul of PBS, 30 ug EV from control EO771 cells, 30 ug EV-OV from HSV1716 infected EO771 cells and 10^7 pfu HSV-1716 (OV-GFP). On days 14 half of the mice were culled after 24 hrs treatment, the organs and tumours were removed and stored in liquid nitrogen for post-mortem analysis. Each treatment group included in this study consisted of $n=10$ mice/group.

5.2.2 Biodistribution of EV-OV in mice of the harvested tumour and organs

To efficiently target cancer directly with EVs, the EVs need localise to tumour tissue *in vivo*. We developed the following proof-of-principle experiment to examine whether systemically administered EVs may home into tumour tissue. to visualize the biodistribution of EO771 derived EV in tumour bearing mice. C57BL/6 mice were injected with EO771-Luc cells at a concentration of (1×10^6) into the nipple of each mouse. At 24 h post injection, the mice were sacrificed, tumour and organs (lung and spleen) collected, digested, and subjected to flow cytometry. Generally, as shown in **Figure 5.2 A**, Flow cytometry revealed no significant differences in the fluorescent signals obtained in mice treated with Alexaflour 488 labelled EV-OV (96.9%) compared to tumours treated with labelled EV from control cells (95.9%) and OV (using HSV-1716GFP) (83.1%), respectively. To investigate the biodistribution of labelled EV, EV-OV, and OV in organs 24 h after injection, lung and spleen tissues were digested and analysed using a flow cytometer. As demonstrated in **Figure 5.2 B**, relatively low levels of labelled EV accumulated in the lungs from untreated EO771 cells (1.79%), EV-OV (3.74%), and OV (3.60% OV), with no substantial differences as compared to PBS. In digested spleens,

there was no notable change in EV, EV-OV, and OV (2.12%, 2.94%, and 3.77%, respectively) compared to PBS (**Figure 5.2 C**). This shows that EVs preferentially aggregate in tumours and, as a result, have tumour targeting potential when delivered via the circulation.

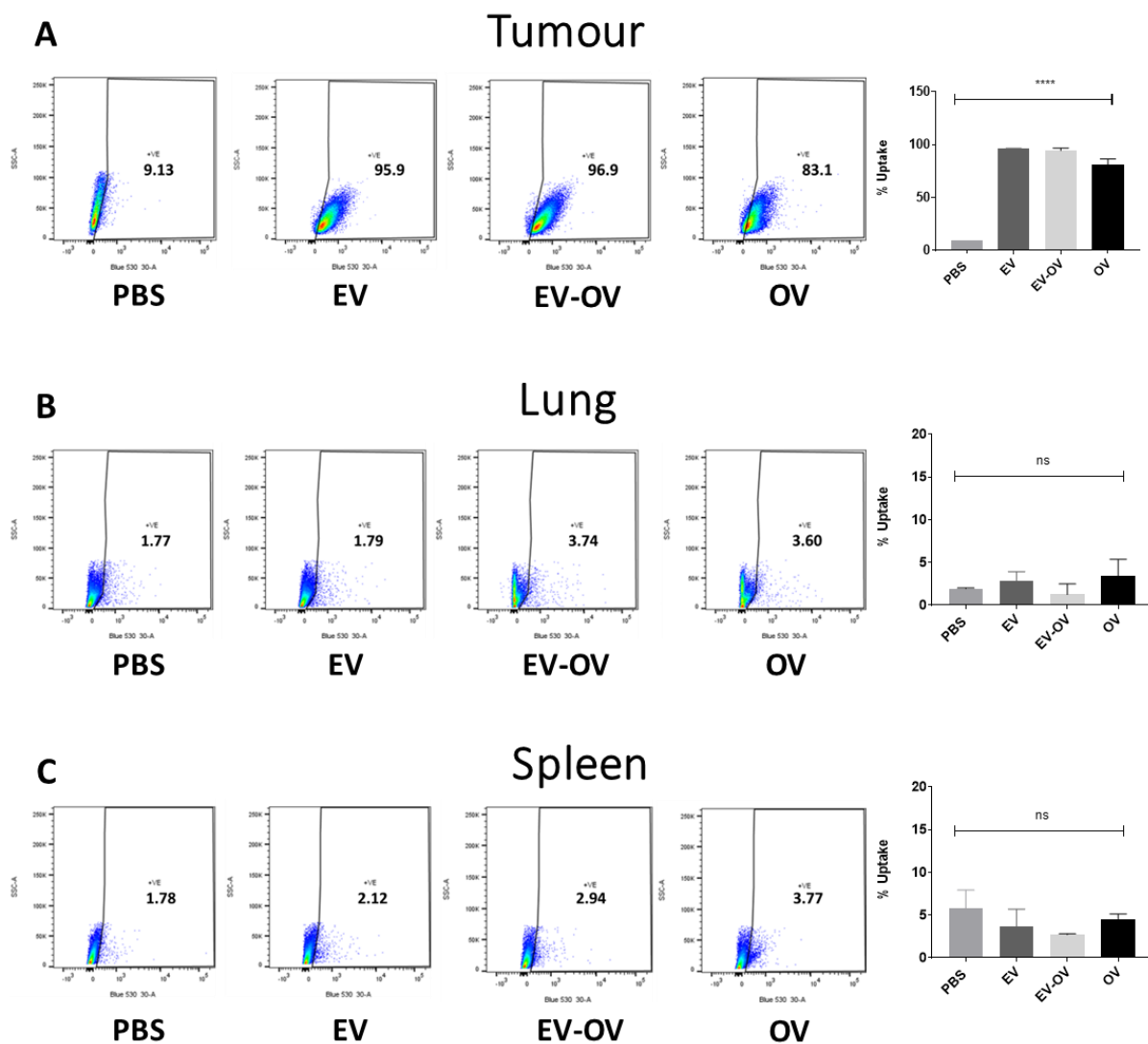


Figure 5.2: EO771 breast cancer derived EVs preferentially accumulate in mammary tumours following systemic delivery. Here the biodistribution of EO771 breast cancer derived EVs was investigated following systemic administration in mammary tumour bearing mice. C57BL/6 mice Envigo at 6-8 weeks old were given intravenous injections of 30 μ g fluorescently Alexa fluor 488 labelled EO771 -derived EV, Alexa fluor 488 labelled EO771 -derived EV -OV and 10⁷pfuOV (HSV1716: GFP) and PBS as a control. Tumour and Organs (Lung and Spleen) were harvested 24 h after intravenous injection and digested into single cell suspensions, and fluorescence was quantified using flow cytometry. **A.** Representative flow cytometric plots and quantification of fluorescent Alexa fluor 488 EO771 derived EV, Alexa fluor 488 EO771 derived EV-OV and 10⁷pfu OV (HSV1716:GFP) and PBS as a control at tumour site after 24h. **B.** Representative flow cytometric plots and quantification of fluorescently labelled EO771 derived EV, labelled EO771 -derived EV-OV and 10⁷pfuOV (HSV1716:GFP) and PBS as a control at Lung tissues after 24h. **C.** Representative flow cytometric plots and quantification of fluorescently labelled EO771 derived EV, labelled EO771 -derived EV-OV and 10⁷pfu OV (GFP) and PBS as a control in Spleen after 24h. Of note, results are presented as mean \pm SEM (n=3) and analysed by two-way ANOVA *p<0.05 **p<0.01 ***p<0.001 ****p<0.0001.

5.2.3 EV-OV shrinks primary mammary tumours.

In this experiment, we determined the effect of delivering EO771 derived EVs via the circulation in mice with primary mammary tumours. The concentration levels of EO771 derived EV-OV $7.40E+08/ml$ whilst EV was greater at $1.35E+09/ml$, this was not statistically significant, as determined by NTA (**Figure 3.5A**) or $30 \mu g$ protein, as measured by the Bradford method. Mice were intravenously treated (via the tail vein) with three doses of $30 \mu g$ of EV, EV-OV, OV and PBS as a control and monitored over time. When compared to the PBS-treated mice, there was no difference in body weight between any of the treatment groups after two weeks of treatment. (**Figure 5.3B**). This suggest that the treatments were not toxic or causing any adverse effects on mouse weight. Tumour progression was particularly rapid in PBS treated mice and although treatments initially retarded tumour growth between days 13-16, following cessation of treatment tumours continued to grow. On day 20 after treatment, however, a statistically significant reduction in the volume of the average tumour was observed in mice who were given EV-OV as opposed to mice that were given PBS ($P < 0.0001$). In addition, a statistically significant reduction in the volume of the average tumour was seen on days 16 and 20 after treatment in mice given OV and EV in comparison to animals that were given PBS ($P < 0.0001$). (**Figure 5.3C**). Although overall tumour growth was not affected, this indicates that EV-OV may have anti-tumour properties. Interestingly this was even more effective than the intravenous administration of the OV alone, while the injection of HSV1716 slowed tumour growth the tumours began to regrow at a fast rate compared to EV-OV once the treatment was discontinued. Of note, the use of HSV1716 either alone (OV) or via EV-OV does not eliminate tumour completely after treatment is stopped. This suggests that the therapy is ineffective on its own and may benefit from combination with other cancer therapies, or that the virus must be administered on a continual basis. Furthermore, combining our EVs with another cancer therapy might be exciting and should be considered in future work. Furthermore, for bioluminescence imaging (BLI), d-Luciferin was administered subcutaneously into mice in a volume of $100 \mu l$ for 10 min. The mice were then imaged using a non-invasive in vivo imaging equipment (IVIS 200 System, Xenogen). Based on the detection and quantification of photons generated by luciferin oxidation by luciferase enzymes. Bioluminescence imaging of mice receiving EV-OV were in agreement with the calliper measurements on day 20 of treatment and showed as marked reduction in the size of the primary tumours as shown in (**Figure 5.3D**). Interestingly, this data suggests that EV-OV are more effective that OV alone. This could be due to the vesicles protecting the viral cargo from immune recognition or clearance.

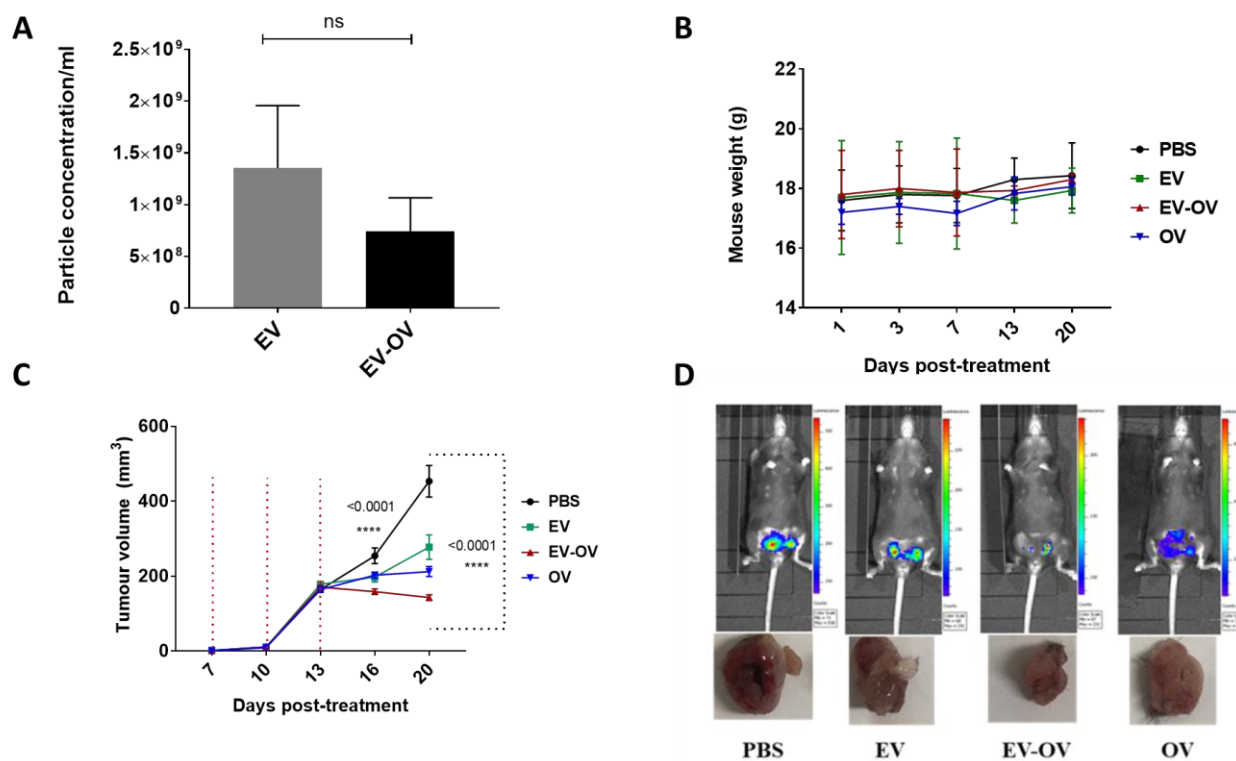


Figure 5.3: EV-OV shrinks primary mammary tumours. EO771 tumour-bearing mice were measured daily using callipers and weighed every three days. **A.** Particle concentration of E0771 derived EV and EV-OV **B.** For the first two weeks after treatment, there was no difference in body weight between treated and untreated mice. **C.** On day 20 following treatment, there was a significant difference in average tumour volume between mice given EV-OV (red line: EV-OV) and mice given PBS (blue line: PBS). **D.** Representative bioluminescence photos of mice injected subcutaneously with 100µl of d-Luciferin for 10 min, as well as photographs of tumours from each treatment group on day 20. The IVIS 200 was used to capture images of mice. Based on the detection and quantification of photons generated by luciferin oxidation by luciferase enzymes. On day 20 of treatment, BLI of mice undergoing EV-OV therapy revealed a significant decrease in the main tumour. Data are provided as mean ± SEM (n=10), and statistical analysis was done using a one-way ANOVA test with multiple comparisons for tumour volume ****p<0.0001

5.2.4 EV-OV does not induce changes in pro-inflammatory cytokines and anti-inflammatory cytokines

As previously stated, OV are known to induce inflammatory responses and we have shown this following HSV1716 treatment in breast cancer models (Kwan et al., 2021b, Nutter Howard et al., 2022). Here we investigated if EV-OV were able to elicit similar responses to OV using a panel of proinflammatory and anti-inflammatory markers and whether cancer cell death in

response to our treatments had an impact on the tumour microenvironment. The expression of cytokines such as pro-inflammatory cytokines (TNF and INF) as well as anti-inflammatory cytokines (IL-2, IL-10, IL-12, IL-4, IL-7A, and MCP-1) at the protein level was determined using a cytokine bead array (CBA), as described in chapter 2 section (2.1.22.5). Total serum was obtained from all treated groups of C57BL/6 mice, and the blood was allowed to clot at room temperature for 15-30 min. After that, the blood was centrifuged at 3000 xg for 10 min, and the top liquid layer, known as serum, was collected. To remove debris from the serum, it was centrifuged at 2000 xg for 30 min at room temperature. The CBA's performance for all eight cytokines was previously assessed according to the kit's instructions. Prior to the tests, representative dot plots of the standards and standard curves were produced (**Figure 5.4**). The concentrations in pg/ml of cytokines in mouse serum by cytokine bead array assays (**Table 5.1**). Moreover, cleared serums were read using an Attune Autosampler which depicts the cytokine levels that were measured (**Figure 5.5**). Only IL-7A was only shown to be significantly downregulated in the both the EV treatment and OV groups compared to control (**Figure 5.5**). IL-7 is a cytokine that plays a critical role in the adaptive immune system and is essential for maintaining homeostasis in T cells as well as driving lymphopenia-driven proliferation (Surh and Sprent, 2008) . Apart from IL-7 no other cytokines were significantly altered in these samples. This may be because the cytokine analysis was done at the end of the experiment rather than at earlier time points so we may have missed in any changes.

Table 5.1: The effect of EV-OV on the levels of pro-inflammatory or anti-inflammatory cytokines in murine mice serum. PBS samples from tubes 1-3, EV samples from tubes 4-6, EV-OV samples from tubes 7-9, and OV samples from tubes 10-12.

Tube	IL-10	IL-2	IL-12	MCP-1	IL-4	TNF	IL-7A	INF-Y
1	0.80	0.59	0.89	1.83	39.92	1.97	0.45	-1.48
2	0.65	0.32	0.92	1.69	37.83	0.75	0.51	-1.09
3	0.55	0.59	0.24	3.31	31.80	1.93	0.19	-1.30
4	-0.78	0.19	-0.40	4.38	41.52	2.02	-0.48	-1.29
5	0.35	0.25	0.15	4.04	59.11	2.43	0.01	-1.40
6	-0.16	0.39	0.76	3.53	61.05	2.06	-0.38	-1.43
7	1.33	0.39	1.08	2.60	46.48	1.50	-0.14	-1.16
8	1.11	0.38	1.12	1.69	62.37	1.79	-0.56	-1.42
9	0.24	0.41	0.85	2.19	40.45	1.57	-0.12	-0.90
10	0.85	0.23	0.21	4.60	40.99	2.39	0.01	-1.36
11	0.48	0.45	0.57	4.69	42.06	2.12	-0.35	-1.34
12	0.57	0.50	0.94	2.94	13.97	2.08	-0.13	-1.47

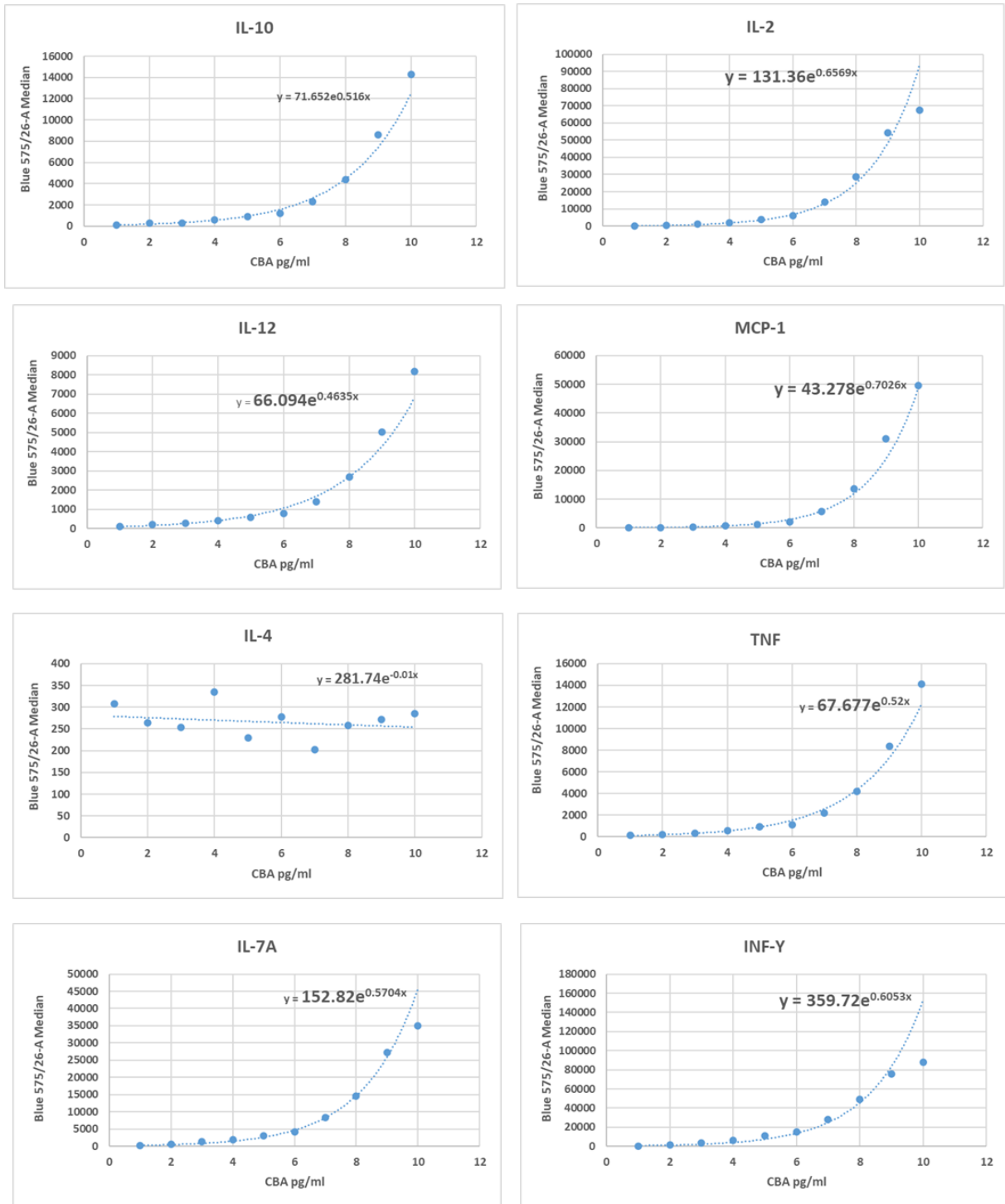


Figure 5.4: Representative dot plot of cytokine standards. Cytokines were measured in twelve samples. The performance of the CBA for all eight cytokines was previously evaluated as per the instructions given in the kit. The representative dot plots of the standards and the standard curves were obtained before the experiments were carried out

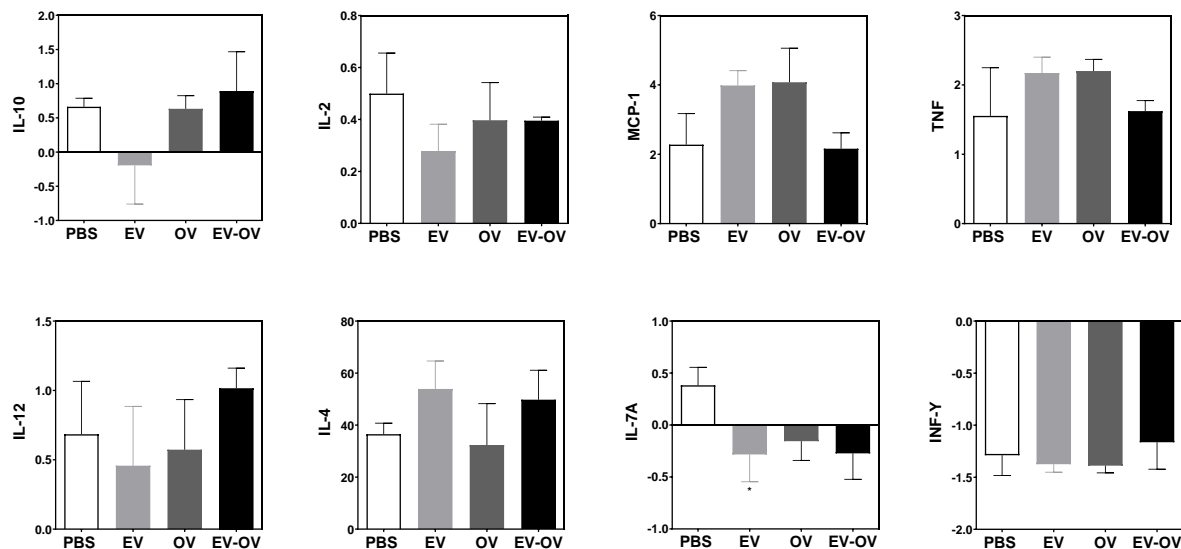


Figure 5.5: Effect of EV-OV cytokines analysis in pro-inflammatory or anti-inflammatory cytokines on murine mice serum. The protein levels of pro-inflammatory and anti-inflammatory cytokines were measured using a cytokine bead array after 24 h of tumour bearing mice C57BL/6 mice infection with the OV, EV-OV, and EV alone (CBA). IL-7A protein levels were significantly lower in treated groups compared to controls. Additional than IL-7, no other cytokines were identified. The data are the mean \pm SEM of $n=3$ independent experiments, and the statistical analysis was carried out using the one-way Anova test with Tukey's multiple comparisons test.

5.2.5 EV-OV possess anti-tumour properties

The anti-tumour activity of EV-OV was assessed within the tumour microenvironment, including tumour necrosis and pulmonary metastasis. Using OVs to target tumour vasculature is an exciting approach in cancer treatment. OV, like vaccinia and vesicular stomatitis virus, may naturally attack tumour vasculature, producing vessel destruction. (Toro Bejarano and Merchan, 2015). Research from our lab has shown that HSV1716 alters the tumour microenvironment (TME) in order to induce necrosis and antitumour immunity (Kwan et al., 2021b).

Necrosis is a form of cell death that can be triggered by external sources such as viruses or bacterial infection (Mohammadinejad et al., 2019). The extent of necrosis was determined by estimating the proportion of necrotic regions in the entire tumour section after staining with Haematoxylin and Eosin. EV-OV-treated tumours tended to be more necrotic than PBS-treated tumours (EV-OV $14\pm 3.2\%$ vs PBS $5.87\pm 3\%$) (**Figure 5.6A&C**). While tumours treated with OV alone or EV showed no significant difference when compared to those treated with PBS (OV 8.6% and EV 7.6 % vs. PBS 5.87%).

Additionally, EO771 cells injected into mammary fat pads metastasise to the lungs in C57BL/6 mice (Johnstone et al., 2015) with many lung metastases identified in PBS-injected mice at the end of the study (9.3 ± 1.5). EV, EV-OV, and OV treatments reduced the number of pulmonary metastases but only EV-OV was able to provide significant protection compared to PBS-treated animals ($p<0.05$) (**Figure 5.6B**). Microscopy showed metastases clusters per lung, which appeared as tumour nodules bigger than 10 mm (**Figure 5.6C**) (Kaseda et al., 2016).

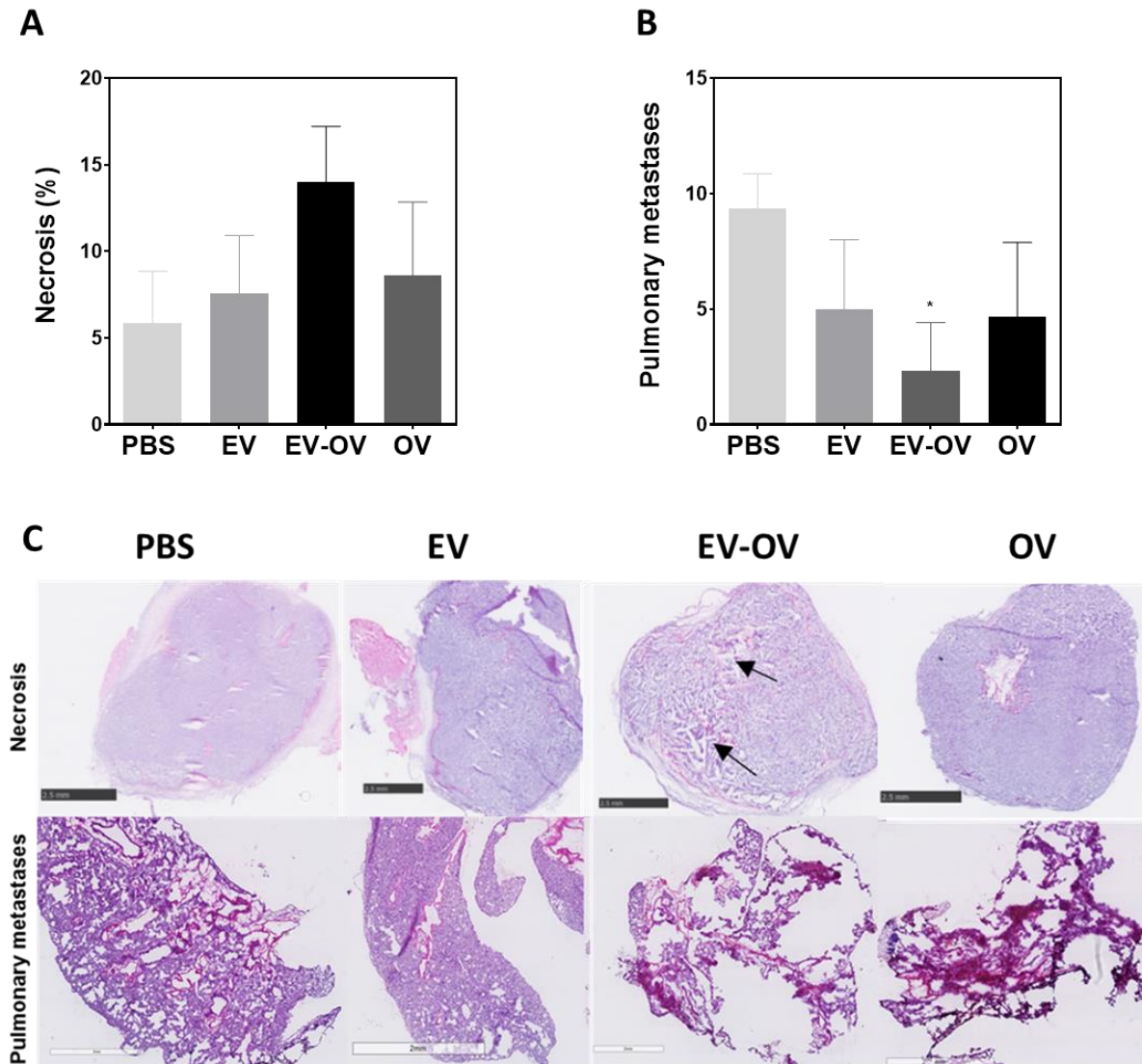


Figure 5.6: EV-OV increases tumour necrosis **A.** The haematoxylin and eosin staining (scale bar = 2.5mm) revealed that tumours treated with EV-OV were substantially more necrotic than those treated with PBS (See arrow in A). **B.** Mice that were given EV-OV had a much lower frequency of lung metastases than mice who were given PBS (scale bar = 2.5mm). Data are mean \pm SEM (n=3 mice per treatment), and statistical analysis was performed using the one-way Anova test with multiple comparisons. *p<0.01.

5.2.6 Successful fluorescent EVs isolation from mice serum

The ability to identify EVs in mouse serum with high sensitivity and specificity in the pre-clinical stage using invasive techniques is critical for a more effective approach and enhanced therapeutic outcomes (Danielson et al., 2016). Nanoscale flow cytometry (or nanoFCM) is a novel approach that can detect particles ~100 nm in sized (Danielson et al., 2016). To assess that the labelled EVs from mouse serum 24 h after infection with OV were truly EVs, and to

compare EV concentration, size, and fluorescence we used a NanoAnalyzer U30 instrument (NanoFCM Co. Ltd., Nottingham, UK). This work was performed with the support of Dr Ben Peacock at NanoFCM. Using 488/640 nm lasers and single-photon counting avalanche photodiode detections (SPCM APDs), this machine could detect side scatter (SSC) as well as fluorescence from individual particles similar to a flow cytometer but with the capacity to detect much smaller particles. To achieve this, the concentration of our EV samples was evaluated by comparing them to 250 nm silica nanoparticles of known concentration, which were used to calibrate the flow rate of the sample solution. A customised 4-modal silica nanosphere cocktail was used to size EV isolates according to conventional operating protocols utilising a proprietary silica nanosphere cocktail (NanoFCM Inc., S16M-Exo). The following treatments were administered intravenously (i.v.) to C57BL/6 mice: 30 µg of Alexa fluor 488 labelled EO771 derived EV, 30µg of Alexa fluor 488 labelled EO771 derived EV-OV, OV (GFP) at 10^7 pfu/ml. At 24 h post treatment mice were sacrificed, and blood samples were obtained, and the blood was allowed to clot at room temperature. After that, the blood was centrifuged at 3000 xg for 10 min, and the top liquid layer (serum) was collected. To this 200µl of the total exosome isolation solution (Invitrogen) was added then samples were centrifuged for 10 min at 10,000 xg at room temperature. Supernatant was removed and the exosome pellet was collected resuspended in 50µl of 1x PBS. Samples were shipped to NanoFCM for analysis. The NanoFCM analysis revealed no significant changes in particle concentrations between serum -derived EV-OV ($2.06E+09$ /ml) and serum-derived EV ($9.77E+08$ /ml) (**Figure 5.7A**). Furthermore, the size of both EV and EV-OV particles recovered from the serum of these mice confirmed to the normal exosome size range, with a mean median size of (80-85) nm (**Figure 5.7 B**). In general, no variations in particle concentration or size range were detected. Furthermore, we demonstrated that the total Exosome Isolation Reagent (from serum) was suitable for EV isolation from mouse blood serum. Interestingly using this approach, we could still detect the fluorescent serum derived EV that we administered to the mice. For the control serum derived EV this was 1% and for the serum derived EV-OV this was (4%) (**Figure 5.7 C**).

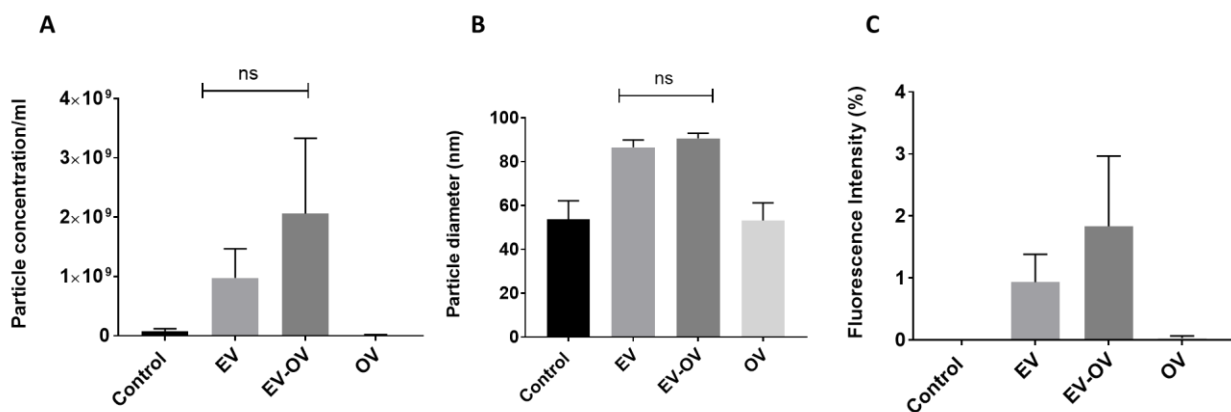


Figure 5.7: Detection of the fluorescent labelled EVs with Alexafluor 488 derived from in C57BL/6 mouse serum at 24h post infection. Exosome precipitation method was used to isolate fluorescent labelled EVs from C57BL/6 mice blood serum. **A.** The particle concentrations of the serum derived EVs. **B.** Size distribution of the serum derived EVs determined by NanoFCM. Mean median size of (80-85) nm. **C.** Representative scatter plots of NanoFCM analysis, in this case, data processing was carried out via the nFCM Professional Suite v1.8 software. The software's gating enables proportional analysis of subpopulations segregated by fluorescent intensities, with size distribution and concentration accessible for each subpopulation. Data are shown as mean with SEM, where n=3 and analysed with one way ANOVA. No statistical significance was apparent.

5.2.7 EV-OV treated tumours induce anti-tumour immunity: NanoString analysis

Previous research has shown that when oncolytic virotherapy is administered, cellular immune responses collaborate with virally induced mechanisms to promote tumour destruction (Nutter Howard et al., 2022, Kwan et al., 2021b).

Therefore, to determine the impact that EV-OV has on the immune pathways, RNA was extracted from treated mouse tumours (Section 2.2.20.8). RNA samples at concentrations of 150 ng were checked for purity on the Nanodrop 8000 (Absorbance at 260nm) and sent for NanoString analysis on dry ice. Mr. Jayakumar Vadakekolathu performed this research at Nottingham Trent University's John van Geest Cancer Research Centre, College of Science and Technology, using the NanoString murine pan-cancer immune profiling panel. We

examined the various immune cells that infiltrated the tumour. Cell-type and pathway profiling analysis across treatment groups were performed in R v4.2.0. Normalised gene expression intensities were mean-centred before calculating cell-type signature and pathway expression scores as the mean average \log_2 expression intensity for all genes in each ontology (annotation) detailed in the NanoString document LBL-10094-02 (nCounter Mouse PanCancer Immune Profiling Panel Gene List). Interestingly in the EV-OV-treated tumours, the majority of the immune-related cell types in the panel showed a trend towards elevation to similar levels as mice treated with virus HSV1716 alone (OV) (**Figure 5.8**). However, NK cells (CD56dim), T cells (cytotoxic CD8), neutrophils, and total TILs increased significantly more in EV-OV-treated tumours than in PBS-treated tumours.

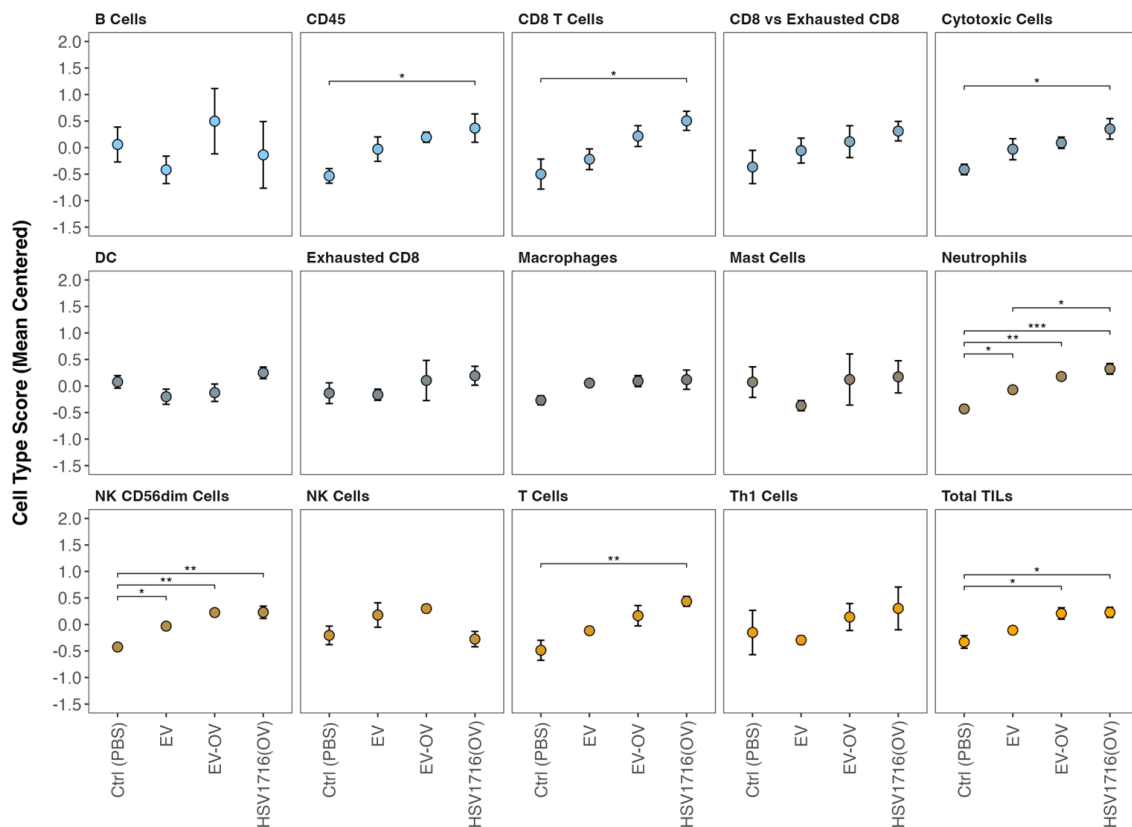


Figure 5.8: Tumour infiltrating immune cells are upregulated by EV-OV. The R v4.2.0 was used to score cell types to demonstrate the presence of tumour-infiltrating immune cells in PBS, EV, EV-OV, or OV-treated tumours. The bulk of the immune-related genes in the panel showed an upregulation when the tumours were treated with EV-OV. Notably, group means were compared using Tukey's post-hoc comparison following ANOVA; all groups are compared to all groups. Graphical plotting was carried out using ggplot2 v3.3.6. Data are expressed as the mean average centred signature score \pm SEM for $n = 3$ mice/treatment. * $p < 0.05$ ** $p < 0.01$ *** $p < 0.001$

In addition, we looked at the immunological pathways of the genes in the PBS, EV, EV-OV, and OV-treated tumours. We found a substantial increase in the expression of immune-pathway genes in EV-OV-treated tumours compared to PBS-treated tumours (**Figure 5.9 and Table 5.2**). Many of these pathways have previously been associated with immunological activation by OVs (Thomas and Fraser, 2003, Miller and Fraser, 2000). In the EV-OV treated tumours, significant upregulation of the following genes related to adhesion (Thy1-mRNA, Itgal-mRNA, Cdh5-mRNA), dendritic cell function (Ccr1-mRNA, Ccr5-mRNA, Ccr2-mRNA), B cell function (Cd81-mRNA, Cd40-mRNA, Cd83-mRNA), antigen processing (Relb-mRNA, Cd74-mRNA, H2-Aa-mRNA), MHC (Cd74-mRNA, H2-Aa-mRNA), leukocyte function (Ccr1-mRNA, Itgal-mRNA, Tlr2-mRNA), macrophage function pathway (Ccr5-mRNA, Csf1r-mRNA, Msr1-mRNA) microglial function (Cx3cr1-mRNA, Casp1-mRNA, Nod2-mRNA), T-cell function (Cd3d-mRNA, Cd74-mRNA, H2-Aa-mRNA), and TLR (Tlr9-mRNA, Tlr2-mRNA, Tlr8-mRNA) were seen. The top 10 genes differentially regulated genes for the EV-OV treatment group and the PBS treatment group are summarised in **Table 5.2**. Together the NanoString analysis demonstrates that EV-OV have potential to induce immune pathways in a similar manner to OV treatment that could be responsible for the antitumour properties we see earlier. This also supports the use of EVs as an alternative source of OV for cancer treatment.

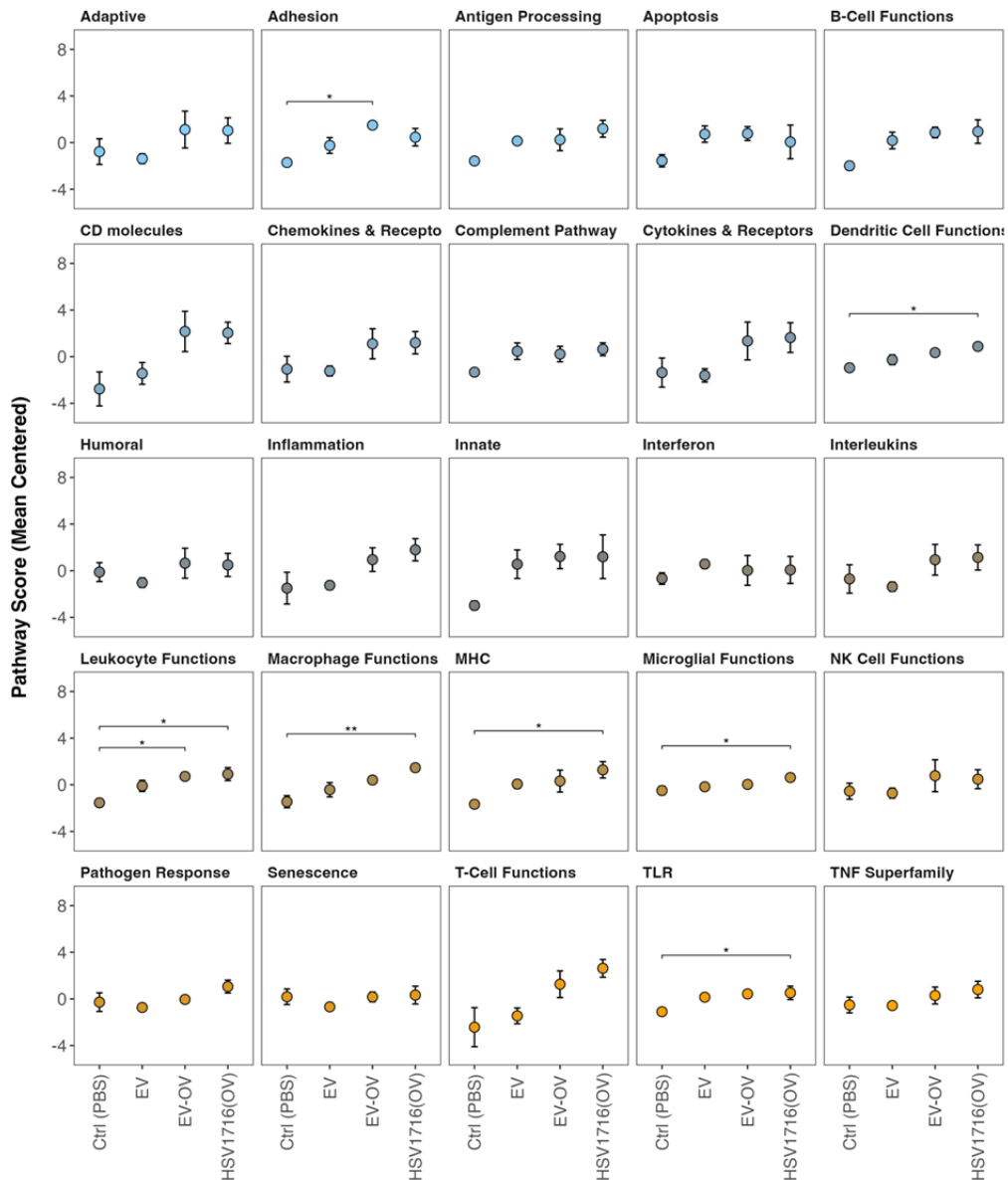


Figure 5.9: EVOV up regulated the expression of a range of immune pathway genes similar to OV treatment. A significant increase in the expression of a variety of genes associated to immune pathways was observed in EV-OV treated tumours than those treated with PBS, including adhesion, dendritic cell function, B cell function, antigen processing, MHC, leukocyte function, macrophage function pathway, microglial function, T-cell function, and TLR. Of note, Groups means were compared using Tukey's post-hoc comparison following ANOVA; all groups are compared to all groups. Graphical plotting was carried out using ggplot2 v3.3.6. Data are expressed as the mean average centred signature score \pm (SEM) for n=3 mice/treatment group. *p<0.05 **p<0.01 ***p<0.001.

Table 5.2: Top 10 genes differentially regulated in EV-OV treated tumours. Genes related to adhesion (Thy1-mRNA, Itgal-mRNA, Cdh5-mRNA) , dendritic cell function (Ccr1-mRNA, Ccr5-mRNA,Ccr2-mRNA), B cell function (Cd81-mRNA, Cd40-mRNA, Cd83-mRNA) , antigen processing (Relb-mRNA, Cd74-mRNA, H2-Aa-mRNA), MHC (Cd74-mRNA, H2-Aa-mRNA), leukocyte function (Ccr1-mRNA, Itgal-mRNA, Tlr2-mRNA),macrophage function pathway(Ccr5-mRNA, Csf1r-mRNA, Msr1-mRNA) microglial function (Cx3cr1-mRNA, Casp1-mRNA, Nod2-mRNA), T-cell function (Cd3d-mRNA, Cd74-mRNA, H2-Aa-mRNA), and TLR (Tlr9-mRNA, Tlr2-mRNA, Tlr8-mRNA) are indicated (n=3) with fold change in expression over the control (PBS) and the pathways or gene sets. Data was processed and analysed using nSolver Analysis Software, using the Advanced Analysis module.

Gene	Log2 fold change	Gene Sets
H2-Aa-mRNA	1.1	Antigen Processing, Interferon, MHC, T-Cell Functions
Ccr5-mRNA	0.642	Adaptive, CD molecules, Chemokines & Receptors, Cytokines & Receptors, Dendritic Cell Functions, Macrophage Functions, T-Cell Functions, Transporter Functions
Ccr1-mRNA	0.532	CD molecules, Chemokines & Receptors, Adaptive, Cytokines & Receptors, Inflammation, Innate, Leukocyte Functions, Transporter Functions, Dendritic Cell Functions
Ccr5-mRNA	0.642	Adaptive, CD molecules, Chemokines & Receptors, Cytokines & Receptors, Dendritic Cell Functions, Macrophage Functions, T-Cell Functions, Transporter Functions
Tlr9-mRNA	0.903	CD molecules, Chemokines & Receptors, Inflammation, Innate, Interleukins, TLR, Transporter Functions
Cx3cr1-mRNA	0.456	Chemokines & Receptors, Cytokines & Receptors, Macrophage Functions, Microglial Functions
Cd81-mRNA	0.783	B-Cell Functions, CD molecules
Thy1-mRNA	0.48	Adhesion, CD molecules, T-Cell Functions
Cd74-mRNA	0.945	B-Cell Functions, CD molecules, Antigen Processing, Innate, MHC, T-Cell Functions
Cd3d-mRNA	0.669	CD molecules, T-Cell Functions

5.3 Discussion

In this chapter the effect of purified EVs were investigated for their antitumour efficacy in a mouse model of mammary carcinoma.

5.3.1 Biodistribution of EVs to the tumour

The most prevalent cause of cancer-related mortality is metastatic dissemination of tumour cells to distant places (Gupta and Massagué, 2006). Compared to healthy blood vessels, tumour vessels exhibit leakier vasculature and reduced lymphatic drainage (Bae and Park, 2011, Walker et al., 2019), which is thought to facilitate the transit of nanoparticles into the interstitial space and produce excessive retention inside tumour tissue. In view of the fact that EV are as small as nanoparticles, it is plausible that accumulation of EV in tumours may adopt the same approach (Wiklander et al., 2015). In this study, ex vivo fluorescence characterization was used to assess the biodistribution of EO771-derived EVs after tail vein injection into mice. Indeed, a considerable accumulation of EO771-derived EV-OV in the tumour (96.9%) was noted compared to the spleen and lungs 24 h after IV injection. In fact, this was higher than delivering virus on its own suggesting that using EVs as a delivery vehicle is superior to OV delivery (83.1%). Other studies have also reported that small-EVs tagged with Cy5.5 can be successfully delivered into tumours after 24h following intravenous injection in SKOV3 xenograft mice (Kim et al., 2017). In other studies that looked specifically at the biodistribution of EVs in mice with tumours, following IV delivery, no small-EVs were found in the tumour during the first h (Jung et al., 2018). Moderate quantities of EVs were observed in tumours between 2–12 h and 24 h (Abello et al., 2019, Gao et al., 2018, Goh et al., 2017, Kim et al., 2017, Kooijmans et al., 2016, Lee et al., 2018, Li et al., 2018, Smyth et al., 2015). Finally, after 24 h, there was a relatively small detection in the tumour (Abello et al., 2019). For this reason, we chose to use the 24-h time point for further analysis.

5.3.2 Extracellular vesicles derived from OV infected cells shrink primary mammary tumours.

Extracellular vesicles derived from HSV1716 infected breast cancer cells have a significant impact on tumour volume and pulmonary metastasis reduction compared to the other treatment groups (**Figure 5.3**). Interestingly this was even more effective than the intravenous administration of the OV alone, while the injection of HSV1716 slowed tumour growth the tumours began to regrow at a fast rate compared to EV-OV once the treatment was

discontinued. Of note, the use of HSV1716 either alone (OV) or via EV-OV does not eliminate tumour completely after treatment is stopped. This suggests that the therapy is ineffective on its own and may benefit from combination with other cancer therapies, or that the virus must be administered on a continual basis. Furthermore, combining our EVs with another cancer therapy might be exciting and should be considered in future work. Prior research has created a technique for encapsulating anti-cancer medicines in EVs, such as oncolytic virus (Ad5D24-CpG) with one of the most often used chemotherapeutics Paclitaxel (PTX). The IV administration of the A549-derived EV-Virus-PTX formulation to nude mice resulted in considerably lower tumour development when compared to naked virus and Virus + Abraxane (Garofalo et al., 2019). A disadvantage to this study is they were unable to investigate the immune effects as this was performed in immune compromised mice.

5.3.3 EV-OV induces anti-tumour properties.

Necrosis is a form of cell death that is triggered by outside stimuli such as infection and toxins. Many strategies, including necrosis, are used by OVs to cause cell death (Wang et al., 2014).

Our group demonstrated that mice with prostate tumours injected with HSV1716-carrying macrophages (MDM + OV) had considerably more necrotic tumours than those who received OV without macrophages (MDM) (Muthana et al., 2015). Moreover, Kwan et al revealed that C57BL/6 mice were given an intravenous injection of HSV1716, and the results revealed a suppression of the development of primary mammary tumours, as well as a decrease in pulmonary metastasis and an enhancement in tumour necrosis (Kwan et al., 2021a). These finding was also consistent with our in vivo investigations in this chapter, which showed that necrosis increases in mice treated with EV-OV (**Figure 5.5A**). However, pulmonary metastasis decreases in mice treated with EV-OV (**Figure 5.5B**). No significant change was observed in the production of proinflammatory cytokines such as tumour necrosis factor (TNF) (Fadok et al., 2001). However, these cytokines were measured at the end of the experiment (day17) so these changes may have been missed. It would have been interesting to look at cytokine profiles at earlier timepoints.

5.3.4 Successful detection of fluorescent EVs isolation from mice serum after infection with OV

EVs have been identified as novel biomarkers and cell-to-cell communicators that might be used as a significant diagnostic, prognostic, and therapeutic tool. Previous research has employed the NanoFCM method to identify EVs in plasma from healthy blood donors. In order to collect plasma, the blood was centrifuged for 5 min at 500 x g, then for 15 min at 5,000 x g and for 15 min at 12,000 x g, all at room temperature (Danielson et al., 2016). Danielson et al demonstrated that NanoFCM can be used to visualise the distribution of EVs in the 100–500 nm size range, and that EVs can be detected in the range of 100 nm. Another study have employed fluorescence-based thresholding to identify tagged beads or immune cell-derived EVs in the 100–200 nm range (van der Vlist et al., 2012). In addition to this, our results demonstrate the labelled EVs with Alexaflour 488 populations isolated from small samples of mouse serum by commercial exosome isolation reagent, the EVs were mostly composed of vesicles with sizes (80-85) nm in the range of exosomes (**Figure 5.7 B**). Our result detected that the fluorescent serum derived EV that we administered to the mice even after 24 h (**Figure 5.7 C**). This is exciting as they were not all cleared even after 24 h so could have longer antitumour activity. Li et al demonstrated that the variability that may be seen in the biogenesis of various MSC-EVs. Throughout the cell culture process, distinct MSC-EVs were collected at certain time periods, including 3 h, 6 h, 12 h, 24 h, and 48 h. This was done so that the pattern of MSC-EV secretion could be better understood. A comparison of the secretion curves of MSCEVs reveals that they are distinct from one another, 12 to 24 h after cell seeding was when the concentration of MSC-EVs reached its highest point (Li et al., 2023).

5.3.5 EV-OV treated tumours induce expression of immune-related genes

EV-OV triggered a variety of immune-related pathways, according to NanoString analysis. Genes related to adhesion (Thy1-mRNA, Itgal-mRNA, Cdh5-mRNA), dendritic cell function (Ccr1-mRNA, Ccr5-mRNA, Ccr2-mRNA), B cell function (Cd81-mRNA, Cd40-mRNA, Cd83-mRNA), antigen processing (Relb-mRNA, Cd74-mRNA, H2-Aa-mRNA), MHC (Cd74-mRNA, H2-Aa-mRNA), leukocyte function (Ccr1-mRNA, Itgal-mRNA, Tlr2-mRNA), macrophage function pathway (Ccr5-mRNA, Csf1r-mRNA, Msr1-mRNA), microglial function (Cx3cr1-mRNA, Casp1-mRNA, Nod2-mRNA), T-cell function (Cd3d-mRNA, Cd74-mRNA, H2-Aa-mRNA), and TLR (Tlr9-mRNA, Tlr2-mRNA, Tlr8-mRNA) were

increased following EV-OV therapy. This shows that EV-OV therapy might increase the expression of the vast majority of immune-related genes in the NanoString immune profiling panel. OVs are well-known for their ability to stimulate the immune system. A study by Zhang et al. explored the therapeutic impact of oncolytic type 2 oHSV2 in mice with colon cancer. In both unilateral and bilateral colon cancer models, oHSV2 demonstrated anticancer effects in vivo. The amount of positive immune cells (natural killer [NK], CD8+ T, and dendritic cells [DCs]) was elevated in the spleen as a result of oHSV2 therapy.

In contrast, the content of inhibitory immune cells (myeloid-derived suppressor cells [MDSCs] and regulatory T cells [Tregs]) decreased (Zhang et al., 2020). A group of researchers has modified OV to be more immunogenic. It produces genes that enhance the activity of immune cells. For instance, it has been proven that expressing HSV and vaccinia virus may attract antigen-presenting cells (APCs) through the production of granulocyte-macrophage colony-stimulating factor (GM-CSF)(Andtbacka et al., 2015, Breitbach et al., 2011). According to our findings, EV-OV stimulates tumour necrosis and activates antitumour immunity by T cell antitumoral activity. Chen et al. elevated that cancer therapies cause the death of tumour cells and the release of tumour antigens. After that, dendritic cells display these antigens in the lymph nodes that are drained by the tumour in order to regulate and boost the immune response. Tumour-specific T lymphocytes then enter the bloodstream, allowing them to penetrate the tumour bulk. T cell-mediated cancer cell lysis results in the release of additional tumour antigens that contribute to the perpetuation of the cycle (Chen and Mellman, 2013).

Our findings confirm that OV may be delivered to mouse mammary tumours through EV, inhibiting tumour development while boosting tumorigenesis and triggering anti-tumour immunity. Together this data suggests that EVs can deliver viral cargo.

Chapter 6: Summary of key findings and general conclusion

6.1 Summary of main outcomes and general conclusion

EVs offer expeditiously multidimensional roles in the safe delivery of encapsulated cargo. EV-based cell-free therapy has emerged as a comparatively safe strategy in clinical treatments (Bunggulawa et al., 2018). EVs are considered important vehicles for regulating the phenotype and function of EV recipient cells, and they are capable of transporting therapeutic agents from one cell to another (Gangadaran et al., 2017). Oncolytic viruses render a novel class of cancer therapies and are being extensively examined in clinical trials (Sprague et al., 2018). The current study investigates the capacity of EVs to carry viral cargo from OV-infected breast cancer cells. Chapter 3 specifically deals with the characterization of EVs through multiple techniques. Initially, the concentration of HSV1716 required to kill 50% of MCF-7 and MDA-MB-231 was calculated. MDA-MB-231 cells were found to be more sensitive to HSV1716 than MCF-7 cells. Based on the data, MOI 0.5 for MCF-7 cells and MOI 1 for MDA-MB-231 cells (causing 50 % cell mortality) were selected for further studies (**Figures 3.1 and 3.2**). This is in line with published work from our laboratory which has demonstrated that MOI 5 was effective at killing between 50-70% these tumour cells (Kwan et al., 2021a). In this study, virus titrations at lower MOIs showed similar effects. As well as these findings, Tan et al reported that MDA-MB-231 cells were 50% viable after 48 h of treatment with a mutant HSV-1 strain (Tan et al., 2015). As a next step, we assessed the physical characteristics of the EVs purified from the tumour cell lines with and without HSV1716 infection. NTA and TEM analysis revealed that the MCF-7 and MDA-MB-231 derived EV (no viral infection of cells) and EV-OV (after infection with OV) had a diameter of approximately 50 to 500 nm with an average size of 150 and 200 nm (**Figure 3.3 A and C & Figure 3.4 A, B**). This size range depicts that the EV population mainly consisted of small nanosized vesicles, most likely exosomes. Raposo and Stoorvogel have also noticed the round or spherical shape of EVs under TEM and the associated cup-shaped EVs with the fixation process (Raposo and Stoorvogel, 2013a). Interestingly, MDA-MB-231 cells were noted to produce more EVs than MCF7 cells (**Figure 3.3 D**). This may be due to the more aggressive nature of this TNBC cell line and its ability to divide rapidly in culture (Oh et al., 2018). A previous study also showed HSV-1 infection enhanced the concentration of human epithelial cells derived EVs (Deschamps and Kalamvoki, 2018). Garcia-Hernandez et al also demonstrated an increase in EV secretion by MDA-MB-231 cells after Linoleic acid (LA) treatment (Garcia-Hernandez et al., 2021). Indeed, increased production of EVs by cells in response to an insult or injury has been reported previously (Dias et al., 2018). Additionally, a study by (Lu et al., 2023) evaluated the varying oncolytic effects

of conditionally replicating adenoviruses (CRAd) on different cancer cells, including breast cancer. The study found that CRAds killed different types of cancer cells but were safe for normal human cells as well. The multiplicity of infections or duration of treatment was found to correlate positively with antitumour activity. The sensitivity of cancer cells to CRAds varies depending on their type. Oesophageal cancer cells EC109 and breast cancer cells MCF-7 demonstrated the most efficient oncolytic effects. The survival rate of BJ-1 cells was 85.43 + 3.56% at MOI 10, showing that CRAAd was safe for human normal cells.

It was important to confirm that the EVs we were purifying were not contaminated with free OV particles that hadn't been taken up by cells or released from the cells following viral replication, particularly as HSV1716 is similar in size to EVs. A typical HSV1716 virus is 70-100 nm in diameter (Howard et al., 2022). This was achieved by utilising the purified EVs in a plaque assay. This confirmed the absence of free contaminating virus in MCF-7 and MDA-MB-231 derived EV-OV as no viral replication was detected compared to when adding the virus directly to the Vero cells (**Figure 3.5 A and B**).

Satisfied that our EVs were free from contaminating OV, next we performed western blot analysis using typical marker proteins for EVs including CD9, CD63, and TSG101. The data revealed the enrichment of these proteins in MCF-7 and MDA-MB-231 cell lysates as well as their derived EVs (EV and EV-OV) (**Figure 3.6 B, C, and D**), (**Figure 3.7 H, I, and J**). As discussed earlier in chapter 3, these protein markers have been frequently used to characterize EVs in various studies (Dogrammatzis et al., 2019). To develop robust high-throughput screening methodologies for the identification of exosome inhibitors in breast cancer models, a rapid, convergent approach was developed recently to modulate exosome biogenesis or release in various tumour types to speed drug repurposing against metastasis progression (Andreu et al., 2023). Specifically, the study stated that CD9 and CD63 tetraspanins represent a reliable means of isolating exosomes from other vesicular populations (Andreu et al., 2023). Importantly, in this study, we wanted to determine if any viral cargo was found in our purified EVs. By western blotting with sheep anti-HSV1716 antibody, we detected viral proteins in infected MCF-7 and MDA-MB-231 cell lysates and enveloped viral gB proteins were the most prominent proteins in the EVs from OV-infected cells (**Figure 3.6 F**), (**Figure 3.7 L**). Birzer et al., have also reported the envelope protein as the most prevalent viral protein (Birzer et al., 2020), which is an essential part of the fusion mechanism for viral entry and cell-cell fusion (Krawczyk et al., 2011). This suggests that EVs can transfer viral cargo between cells and

therefore have the potential to induce viral responses. Therefore, we investigated the potential anti-tumour activities of adding our EVs to naïve breast cancer cells.

First, we looked at the uptake of EVs. Membrane dye C5-Maleimide-Alexa flour 488 was used to label the EVs before culturing with cells and using fluorescence imaging, uptake of EV and EV-OV was evident in both MCF-7 and MDA-MB-231 cells. Using an antibody to HSV1716 we could also detect viral proteins within cells that have been exposed to either OV only or EV-OV. Virus-only infected cells demonstrated the presence of the virus in the cytoplasm of the cells whereas the EV-OV virus proteins were also detected in the nuclei (**Figure 3.12 A and B**), (**Figure 3.13 A and B**). This is exciting as it demonstrates that EV-OV can transfer viral cargo within the cells. Current discussion centres on the role of EVs in viral transport and pathogenesis and the relationships between EVs, viruses, and the immune system. The role of EVs in virus-associated diseases is now considered a promising approach for combining viruses and EVs as therapeutics, with a particular focus on cancer-related therapies (Sheta et al., 2023).

Next, our research focused on determining the impact of the EV-OV on cell migration. The data of the scratch-wound assay indicated that EV-OV inhibited cell migration compared to untreated MDA-MB-231 cells and EV-treated MDA-MB-231 cells. This suggests that the EVs derived from OV infected breast cancer cells may have anti-tumour properties and could lead to developing better clinical methods for the application of OV. A limitation of this study is that only OV was used, not in comparison with other approaches in this study. However, it should be noted that OV is an emerging promising class of anticancer immunotherapies (Shalhout et al., 2023). Many OVs exhibit profiles and up-to-date clinical trials have shown encouraging results however, challenges remain regarding optimising appropriate clinical endpoints, regulatory pathways, and clinical logistics (Shalhout et al., 2023).

In chapter 4, label-free mass spectrometry was carried out to determine the protein content of the EVs. The peptide data analysis identified the relative protein abundances and label-free quantitation (LFQ) intensities of each protein were calculated. Perseus software identified 1482 unique proteins (Tyanova et al., 2016). Three replicates of MDA-MB-231 derived EV, and EV-OV proteins within a group exhibited a strong correlation thus confirming the reliability of the adopted methodology (**Table 4.1**). MDA-MB-231 derived EVs intensity histogram depicted regular distribution of the data (**Figure 4.1**). Thirty proteins were significantly

expressed in MDA-MB-231 derived EVs. The volcano plot presents 24 up-regulated proteins of MDA-MB-231 derived EV-OV in red dots, which mainly included (PPP6C), (B2M), and (VIM) (**Figure 4.2**). PPP6C complex participates in an inflammatory response, lymphocyte, and cell differentiation and is also associated with macrophages, CD8 + T cells, and neutrophil infiltration in tumours (Xie et al., 2022). B2M is a cancer diagnostic marker protein that produces physiologic effects in tumorigenesis and immune regulation (Wang et al., 2021). Pathway analysis was also performed in the Panther GO database to better understand which pathways these differentially expressed proteins are involved in. OV induces inflammation within tumours that recruit T cells for inducing anti tumour immunity through exposing tumour-associated antigens (TAA) to produce tumour-specific T cells (Ito et al., 2007). The results of this study revealed the involvement of MDA-MB-231 derived EV-OV proteins in various important pathways including T cell activation, cytokines and chemokines, EGF receptor, and FGF signalling pathways which are important for intercellular channels of communication in tumours (Anderson and Simon, 2020). In a related study, it was observed that the TGF β and EGF signalling can facilitates the AP-1- and p63 transcriptional regulation of breast cancer spread (Sundqvist et al., 2020). Based on the study, treating individuals with breast cancer that has an active EGFR-RAS-RAF pathway is essential. We performed additional western blotting to validate the enrichment of PPP6C, B2M in MDA-MB-231 derived EV-OV. Time permitting more of these markers would have been validated. In short, the data demonstrates that the EV-OV cargo has the potential of initiating antitumour immunity. Therefore, the role of these proteins becomes crucial in the diagnostics or therapeutics of breast cancer. On the other hand, OV were not detected in EV released by infected MDA-MB-231 cells when mass spectrometry was done. This might be due to the fact that the complex structure of herpesviruses, which includes both viral and host proteins, makes MS analysis challenging. (Knipe and Howley, 2013). Effective therapy requires a prompt and accurate identification of a viral cargo. In addition, the brief duration of the study is essential, since the timing of antiviral medicine administration is crucial. Various identification techniques are currently available; serological typing (e.g., by identifying antibodies in the serum) and reverse transcription polymerase chain reaction (RT-PCR) are target directed, which means that they may miss unselected or emerging pathogenic viruses (Binnicker et al., 2013).

Genetically engineered oncolytic viruses induce cancer cell mortality, evoke immune responses, and release antigens in the cancer microenvironment (Uche et al., 2021). Generally, direct injection into cancer is carried out, however, this is not feasible for deeply located

tumours (Chaurasiya et al., 2018). From above, it is evident that EVs purified from OV-infected cancer carry viral cargo and have antitumour properties. In this regard, EVs constituting lipid membranes could be handy to protect and efficiently deliver biological components such as OVs (Fukuhara et al., 2016, Russell et al., 2012). In chapter 5, a study was conducted to confirm the antitumour effects of EV-OV. An immunocompetent mouse mammary carcinoma model (C57/BL6) was used with EO771-Luc cells. This is a TNBC cell line that metastasises to mouse lungs (Johnstone et al., 2015). First the bio-distribution of EO771-derived EVs in tumour-bearing mice was investigated following intravenous injection. Here the EVs were labelled with Alexa flour 488 for easy tracking. Flow cytometry of dissected tumours and organs (24 h post-injection) revealed the highest fluorescence signals (~71.5%) were in tumours treated with Alexaflour 488 labelled EV-OV as compared to other treatments (**Figure 5.2 A**). This suggests that EVs derived from the virus (EV-OV) infected cells have tumour targeting properties. Additionally, EO771-derived EV-OV preferentially accumulated in the tumour (71.5 %) compared to the spleen and lungs 24 h after IV administration. In fact, this was greater than virus delivery on its own, indicating that employing EVs as a transport vehicle is better than OV delivery (45 %). Other research has supported the use of EVs as potential delivery vehicles, For example, Kim et al demonstrated that small-EVs tagged with Cy5.5 are effectively transported into tumours 24 h after intravenous injection in SKOV3 xenograft mice (Kim et al., 2017). In other investigations that looked particularly at the biodistribution of EVs in mice with tumours, after IV infusions, no small-EVs were discovered in the tumour within the first hour of the study (Jung et al., 2018). However, in the periods of 2–12 hrs. and 24 hrs., moderate amounts of EVs were seen in tumours. Abello et al investigated the biodistribution of Gdl or DiR-labeled MSC exosomes delivered into tumor-bearing mice after intravenous injection accumulate in the tumour during a 24-48 h period. The accumulation of DiR labelled exosomes inside tumour resulted in about twice the fluorescence in tumour compared to labelled liposomes used as controls at the 48h observation point; similarly, around 18% of the GdL was identified within the tumour 24 h after injection. Since DiR-labeled liposomes did not accumulate inside the tumour after 3 hours, this discrepancy shows that exosomes continue to exit the vasculature and reach the tumour, where they are sequestered for up to 48 hours. Finally, DiR tagged exosomes have a biodistribution that is strikingly comparable to that of other DiR labelled nanoparticles, including exosomes produced from different tissues following intravenous injection (Abello et al., 2019). As a result of this, we decided to perform our biodistribution at the 24-h time point. The timepoint should be noted for future studies because it has a substantial impact, particularly on the biodistribution of EVs in mice with

tumours. This is true even though the determination of the biodistribution timepoint depends on the source of EV, administration route, a dose of EV, recipient animal, and organs being studied (Kang et al., 2021).

We also determined the presence of our fluorescently labelled EVs in the circulation after IV administration using Nanoscale flow cytometry. This allowed us to assess the EV particle size in mouse blood samples. In general, the purified EV and EV-OV particles recovered from mouse serum were in the exosome size range (80-85 nm) (**Figure 5.6 A**). The fluorescent percentage of our administered serum-derived EV and EV-OV was noted as 1% and 4%, respectively (**Figure 5.6 B**). Danielson et al., have also established Nanoscale flow cytometry as a reliable method for detecting particles of 100nm size (Danielson et al., 2016). If more time was permitted, it would have been useful to further characterise the EVs purified from mouse serum. NanoFCM is an innovative technique that can detect particles with sizes less than 100 nm (Danielson et al., 2016). As imaging flow cytometry has become increasingly capable of morphologically characterizing EVs, recent studies suggest that imaging flow cytometry could also detect EVs cell types and distinguish between different EV subpopulations using antibody labelling approaches because the technique uses high resolution from 20 nm to 1 μ m (Pirisinu et al., 2022).

The average tumour volume was considerably smaller in the EV-OV-treated group than in the OV group (**Figure 5.3B**). Given viral cargo was successfully transported to the tumour via EVs, this suggests that EV-OV has antitumour activity. Interestingly, despite IV HSV1716 inhibiting tumour development, the tumour resumed to recur at a faster pace than EV-OV after the therapy was terminated. It is important to highlight that the use of HSV1716 either on its own (OV) or via EV-OV does not eradicate the tumour after the therapy has been discontinued. This would imply that the treatment is inefficient on its own with limited doses but may work better in conjunction with other cancer medicines, or that the virus would need to be given continuously. Although this may lead to resistance in the long term. In addition, combining our EVs with another cancer treatment is an interesting prospect, and this idea needs to be taken into consideration for future research. EV-OV treatments in combination with other cancer therapies such as immune checkpoint inhibitors (ICIs) that can recruit and activate T cells thus transforming a "cold" tumour into a "hot" one may eventually result in the development of a novel therapeutic strategy for treating breast cancer. For example, (ICIs) are cancer

immunotherapies that work by targeting immunologic receptors on the surface of T-lymphocytes (Robert, 2020). ICIs serve critical roles in cancer immunotherapy, and the large therapeutic benefits produced by ICI have considerably improved the prognosis of many advanced malignancies. Despite the efficacy of ICI, resistance to these drugs limits the formation of immune responses. The mechanisms of ICI resistance are diverse and include a lack of sufficient T cell infiltration and a tumour immunosuppressive microenvironment (Bagchi et al., 2021). Anti-ICI resistance therapy is essential to boost the possible response rates. Repolarizing tumour associated macrophages (TAMs) is one of the potential ways for improving ICI resistance by increasing T-cell antitumor immunity and alleviating tumour immunosuppression (Jones et al., 2018, Wu et al., 2019). For immunotherapy to be successful, immunosuppressive cells need to have their wiring rewired so that they can produce anti-cancer immunity. Based on recent developments, it has been reported that engineered EVs are gradually being used as combination therapies instead of monotherapies to combat diverse cancerous cells and intricate tumor microenvironment (Chen et al., 2022). As previously stated, synthetic EVs are powerful weapons for reverting M2 macrophages in the tumour microenvironment (TME), like TAMs to the M1 macrophages are known to prevent tumour growth (DeNardo and Ruffell, 2019). In the Choo et al. study, exosome-mimetic nanovesicles produced from M1 macrophages (M1NVs) were employed to reset M2 TAMs to M1 macrophages, demonstrating the potential anti-cancer effectiveness of ICI (Choo et al., 2018). Moreover, OV have already been combined with many cancer therapies and even in the clinical studies. The current clinical result of ICIs has indicated that they have a beneficial effect in melanoma prognosis (Zhang et al., 2019). In this study, OV and ICI therapies for advanced melanoma result in long-term antitumor responses in patients. Nonetheless, each has grave flaws (Harrington et al., 2019). In terms of OV, the activation and recruitment of immune cells during OV-mediated oncolysis eventually activate immunological checkpoints for limiting antitumor response and inflammation.

More and more trials using OV, either alone or in conjunction with ICIs, have recently begun. The clinical result suggests that these approaches may have a significant therapeutic advantage in advanced melanoma patients (Bommareddy et al., 2018). Nevertheless, the clinical response rate and severe irAEs induced by single OV treatment and combination OV/ICI therapy have not been comprehensively studied. Based on those treatments, Zou et al did a detailed review of single OV treatment and combination OV/ICI therapy for advanced melanoma. According to their findings, a single OV therapy may result in a 25% objective response rate (ORR),

whereas 12% of patients have severe immune-related adverse events. (irAEs). The combination of OV and ICIs may increase ORR to 48%, suggesting that combined treatment was a more realistic and efficient method for advanced melanoma care (Zou et al., 2020). As a result, with the approval of ipilimumab (Ledford, 2011) in 2011, ICIs were deemed a revolutionary therapy approach, transforming cancer treatment. In certain cases, these drugs enabled long-term benefits with a decreased toxicity profile (Johnson et al., 2022). In contrast to established treatment techniques, ICIs kill tumour cells by reinvigorating the host immune system (Cai et al., 2021). In homeostatic circumstances, immune checkpoints maintain a balance of pro-inflammatory and anti-inflammatory signals.

On inspecting the tumours in more detail, we found that EV-OV-treated tumours exhibited substantially higher anti-tumour necrosis (14 %) than other treatments and controls (**Figure 5.5 A**). Kwan et al., have reported that HSV1716 could alter the tumour microenvironment (TME) to initiate necrosis and antitumour immunity (Kwan et al., 2021a). Here we show that EV-OV treatment could be just as effective in promoting tissue necrosis and cell death. Collectively, these findings point to possible new treatment targets that may be explored. As a consequence, these methodologies can be further expanded to evaluate their therapeutic impact on breast cancer in humans based on the evidence presented here. This is due to the fact that breast cancer in its advanced stages is notably difficult to cure, and the development of novel medicines is a pressing medical priority. The administration of OV via EVs offers the possibility of systemic administration, which helps to circumvent the difficulties associated with injecting virus into circulation. This makes it possible to target tumours that are located deep inside the body.

The EV-OV impact on the immune pathways was assessed by extracting treated mouse tumour RNA and analyzing it through the NanoString murine pan-cancer immune profiling panel. The results demonstrated that various immune-related cells such as T cells (cytotoxic CD8), NK cells (CD56dim), neutrophils, and total TILs considerably increased in EV-OV-treated tumours as compared to PBS-treated tumours. Contrarily, EV-OV-treated tumours possessed lower levels of DC cells than PBS-treated tumours (**Figure 5.8**). Our group has also reported enhanced tumour destruction following HSV1716 treatment via the collaboration of cellular immune responses and virally induced mechanisms (Nutter Howard et al., 2022, Kwan et al., 2021b).

Moreover, the expression of immune-pathway genes significantly increased in EV-OV-treated tumours than in PBS-treated tumour (**Figure 5.9 and Table 5.2**). Specifically, the genes related to adhesion, dendritic cell function, B cell function, antigen processing, MHC, leukocyte function, macrophage function pathway, microglial function, T-cell function, and TLR were found in EV-OV treated tumours. Similar alterations in gene expression after OV-based therapies have been reported in previous studies (Zhang et al., 2020, Thomas and Fraser, 2003). In short, the NanoString data establishes EV-OV-based stimulation of tumour necrosis and antitumour immunity. If more time was available, it would have been interesting to validate some of these gene expression changes at the protein level. This would have been done using immunofluorescence staining of our frozen tumour sections. Immunofluorescent staining will also be used in order to assess the levels of CD3 (T cells), CD8 (Cytotoxic T cells), CD4 (T helper cells), F4/80 and NK1.1 (Natural killer cells) expression that are present inside the tumours. Before freezing the tumours, they will first be imbedded in optimum cutting temperature (OCT), then sectioned using a cryostat (with a thickness of 14 micrometres), fixed with ice cold acetone for ten minutes at room temperature, and then rehydrated with PBST for one minute. After that, the sections will be stained with anti-CD3, CD4, F4/80, CD8, NK1.1, and (4',6-diamidino-2 phenylindole) (DAPI), and then analyses using a confocal laser-scanning microscope. Endothelial cell marker 'CD31' will be co-labeled with F4/80. This might indicate that macrophages inside the TME are distributed throughout the tumour, with some clustering near vascular regions in mice treated with the virus (Howard et al., 2022).

This research provides a potential therapeutic method for transporting OV cargo to tumours whilst preserving the virus from inappropriate immune responses. In addition to overcoming the challenge of delivering OVs systemically, it enables the treatment of many cancer types, especially those that are resistant to traditional treatments or the newer promising immunotherapies that have failed in some cancer types (e.g., checkpoint inhibitors owing to a low abundance of immune cells inside the tumour). This is certainly relevant for breast tumours that are considered to be immunologically 'cold' and unresponsive to checkpoint inhibitors. EV-OV had the potential to reprogram the tumour microenvironment to be immunologically 'hot' (having a higher number of activated T cells), which may open up the possibility of treating this cancer type with immunotherapies that ordinarily would not work. The use of OV in conjunction with other immunotherapies is an interesting prospect that will undoubtedly be investigated in the future (Zou et al., 2020).

6.2 Limitation of the study

A major limitation was that it was unable to identify OV in the EV generated by infected MDA-MB-231 cells when mass spectrometry was performed. It's possible that this is because of the tough nature of MS analysis brought on by the intricate structure of herpesviruses, which comprises proteins from both the virus and the host (Knipe and Howley, 2013). For treatment to be effective, it is necessary to quickly and accurately identify the viral cargo. In addition, it is necessary that the length of the research be kept to a minimum since the timing of the administration of antiviral medication is critical. There are currently a variety of techniques for identification that can be utilised. Serological typing (for example, by identifying antibodies in the serum) and reverse transcription polymerase chain reaction (RT-PCR) are both target directed, which means that they have the potential to miss unselected or emerging pathogenic viruses (Binnicker et al., 2013).

Another limitation of this study is that the 100k pellet was obtained by differential ultracentrifugation. Despite being enriched with exosomes-sized particles, NTA showed the presence of some smaller and larger particles, indicating the presence of microvesicles, apoptotic bodies or protein aggregates. This indicated that differential ultracentrifugation could not yield exosomes with 100% purity. Currently, there is no universal method which can be applied to purify exosomes from the samples with 100% exosome yield. Gardiner et al., mentioned some alternatives to differential ultracentrifugation such as density centrifugation, filtration and size-exclusion chromatography, which can yield the exosomal pellet with relatively high purity (Gardiner et al., 2016). Immunoaffinity has the ability to purify 80% of the EVs from the sample and refers to the chemical affinity between the antigen and antibody, which is used as a basis for separation of antigens from biological fluids (Moser and Hage, 2010). However, the application of these techniques depends on their availability.

One more of these constraints to this study is that we did not have time to do the migration assay for MCF-7 cells or the planned in vitro invasion assay for MCF-7 and MDA-MB-231 cells to examine the chemoattractant gradient-related characteristics of each cell line in response to EV-OV. This is owing to the COVID 19 pandemic and the delay in reagent supply, such as for the invasion assay kit and mitomycin C for the migration test, which is why these experiments were not carried out.

In chapter 5 it would have been interesting to look at biodistribution of the EVs in other organs such as the brain and liver. However, there was no time to do this and as mentioned above it would have been useful to perform more in-depth analysis of the tumours to get a more complete picture of the antitumour properties of the EV-OV.

6.3 Future work

In future, it would be useful to identify the role of PPP6C as a tumour suppressor. First this would need to be confirmed by immunohistochemical staining in the tumour tissue followed by some knockdown studies to see if the tumour cells are still responsive to EV-OV after knockdown of PPP6C. First of all, tumor sections were paraffin-embedded and antigen-retrieved before being blocked with goat serum and treated with primary antibodies overnight at 4 °C. DAB staining was used to identify the target after incubation with the HRP-conjugated secondary antibody (Li et al., 2022). This could be done *in vitro* using siRNA. Ambion supplied the reagents for PPP6C siRNA knockdown (PPP6C: Silencer 43527, non-targeting control: Silencer 4390843). Lipofectamine 3000 Transfection Reagent (Thermo Fisher) will be used to transfect the siRNA oligonucleotides for 72 h at a final concentration of 100 pmol (Maskin et al., 2022). As a result, they sought to identify protein phosphatases that control the innate immune response to DNA viruses. In order to accomplish this, they mutated the protein serine/threonine phosphatases in SV40-immortalized murine lung fibroblasts (MLFs) using the CRISPR-Cas9 system which modify the target sequences, double-stranded oligonucleotides corresponding to those sequences and cloned into the lentiCRISPR V2 plasmid, which will then be transfected with packaging plasmids into the cells. They examined the effects on the transcription of the interferon-1 (*Ifnb1*) gene that was induced by the DNA virus herpes simplex virus type 1 (HSV-1). As a result of these studies, PPP6C was discovered to be a candidate for a negative regulator in the HSV-1-induced transcription of the *ifnb1* gene, knocking down PPP6C enhanced HSV-1-induced transcription of *Ifnb1*, *Ifna4*, *Isg56*, and *Cxcl10* genes (Li and Shu, 2020).

Moreover, the EO771 mammary cancer model was the only one that was employed in this research. It might be beneficial to employ our EV-OV in additional model of breast cancer. The use of breast cancer models that are representative of the many subtypes of breast cancer might offer information on how well this treatment works. There are few murine cell breast cancer cell lines that represent the different subtypes of breast cancer. To address this species-

in vivo preclinical experiments employing immunodeficient mice engrafted with human cells or tissues also known as 'humanised' mice or 'human immune system' (HIS) mice could be used. Humanized mice have also been used to evaluate the safety of medications that target immunoreceptors with species-specific functioning (Allen et al., 2019). To provide another example, the cell-derived xenografts (CDX) transplantation models that are appropriate for observing experimental metastasis are referred to as metastatic cell-derived xenografts. In these models, cancer cells such as MDA-MB-231 and SUM149 cells are injected into the tail veins of mice. When considered as a whole, these CDX models make it feasible to verify target genes of interest and ease the process of assessing new anti-cancer medications and treatments for breast cancer. This is because the CDX models are able to predict the effects of a combination of several genes (Borges et al., 2015). Third, primary human breast carcinomas or tumour fragments are transplanted subcutaneously or orthotopically into immunodeficient mice (such as nude, NOD/SCID, or NOD/SCID/IL2-receptor null (NSG) mice) in PDX transplantation models. These mice lack IL-2 receptors, which prevents them from mounting an immune response to the tumour (Whittle et al., 2015). The features of the resulting tumours are identical to those of the original patients' tumours in terms of histology, genetic signature, and heterogeneity, as well as a high predicted therapeutic response (Rosfjord et al., 2014, Cho et al., 2016). These models are utilised to find biomarkers for individualised medication selection as well as to overcome the limitations of CDX transplantation in clinical therapy (Pillai et al., 2018). Although subcutaneous PDX transplantation models have been employed in research to assess initial tumour development, orthotopic PDX transplantation models are more suited for studying metastasis and therapy resistance.

Mass spectrometry was used to determine the content of the EVs but using this approach we were unable to identify viral proteins. There are currently a variety of identification methods available that could be used in the future; such as reverse transcription polymerase chain reaction (RT-PCR) are both target directed viral nucleic acids, which means that they may miss unselected or emerging pathogenic viruses (Yip et al., 2019, Binnicker et al., 2013). Yip et al used the RealStar® alpha Herpesvirus PCR Kit 1.0 (altona Diagnostics GmbH, Germany) for the detection of HSV-1, HSV-2, and VZV DNA. The samples were run according to the manufacturer's instructions. In brief, PCR was carried out using the kit reagents combined with a 5 L sample template and the LightCycler® 480 Instrument II (Roche, Switzerland) with the

following PCR conditions: 95° C for 10 min, followed by 45 cycles of 95° C for 15 s and 58° C for 1 min. They evaluated that PCR are able to distinguish between HSV-1, HSV-2, and VZV(Yip et al., 2019).

References

- ABELLO, J., NGUYEN, T. D. T., MARASINI, R., ARYAL, S. & WEISS, M. L. 2019. Biodistribution of gadolinium- and near infrared-labeled human umbilical cord mesenchymal stromal cell-derived exosomes in tumor bearing mice. *Theranostics*, 9, 2325-2345.
- ABELS, E. R. & BREAKFIELD, X. O. 2016. Introduction to Extracellular Vesicles: Biogenesis, RNA Cargo Selection, Content, Release, and Uptake. *Cellular and Molecular Neurobiology*. 36, 301–312 (2016).
- ACHARD, C., SURENDRAN, A., WEDGE, M.-E., UNGERECHTS, G., BELL, J. & ILKOW, C. S. 2018. Lighting a Fire in the Tumor Microenvironment Using Oncolytic Immunotherapy. *EBioMedicine*, 31, 17-24.
- ALLEN, T. M., BREHM, M. A., BRIDGES, S., FERGUSON, S., KUMAR, P., MIROCHNITCHENKO, O., PALUCKA, K., PELANDA, R., SANDERS-BEER, B., SHULTZ, L. D., SU, L. & PRABHUDAS, M. 2019. Humanized immune system mouse models: progress, challenges and opportunities. *Nat Immunol*, 20, 770-774.
- ALMSTÄTTER, I., MYKHAYLYK, O., SETTLES, M., ALTOMONTE, J., AICHLER, M., WALCH, A., RUMMENY, E. J., EBERT, O., PLANK, C. & BRAREN, R. 2015. Characterization of magnetic viral complexes for targeted delivery in oncology. *Theranostics*, 5, 667-685.
- ANDERSON, N. M. & SIMON, M. C. 2020. The tumor microenvironment. *Curr Biol*, 30, R921-R925.
- ANDREU, Z., MASIÁ, E., CHARBONNIER, D. & VICENT, M. J. 2023. A Rapid, Convergent Approach to the Identification of Exosome Inhibitors in Breast Cancer Models. *Nanotheranostics*, 7, 1-21.
- ANDREU, Z. & YÁÑEZ-MÓ, M. J. F. I. I. 2014. Tetraspanins in extracellular vesicle formation and function. 5, 442.
- ANDRÉ, F., SCHARTZ, N. E. C., CHAPUT, N., FLAMENT, C., RAPOSO, G., AMIGORENA, S., ANGEVIN, E. & ZITVOGEL, L. 2002. Tumor-derived exosomes: a new source of tumor rejection antigens. *Vaccine*, 20, A28-A31.
- ANDTBACKA, R. H. I., KAUFMAN, H. L., COLLICHIO, F., AMATRUDA, T., SENZER, N., CHESNEY, J., DELMAN, K. A., SPITLER, L. E., PUZANOV, I., AGARWALA, S. S., MILHEM, M., CRANMER, L., CURTI, B., LEWIS, K., ROSS, M., GUTHRIE, T., LINETTE, G. P., DANIELS, G. A., HARRINGTON, K., MIDDLETON, M. R., MILLER, W. H., ZAGER, J. S., YE, Y., YAO, B., LI, A., DOLEMAN, S., VAN DER WALDE, A., GANSERT, J. & COFFIN, R. S. 2015. Talimogene laherparepvec improves durable response rate in patients with advanced melanoma. *J Clin Oncol*, 33, 2780-2788.
- ARKHYPOV, I., LASSER, S., PETROVA, V., WEBER, R., GROTH, C., UTIKAL, J., ALTEVOGT, P. & UMANSKY, V. 2020. Myeloid cell modulation by tumor-derived extracellular vesicles. *Int J Mol Sci*, 21, 1-22.
- AVELAR-FREITAS, B. A., ALMEIDA, V. G., PINTO, M. C. X., MOURÃO, F. A. G., MASSENSINI, A. R., MARTINS-FILHO, O. A., ROCHA-VIEIRA, E. & BRITO-MELO, G. E. A. 2014. Trypan blue exclusion assay by flow cytometry. *Braz J Med Biol Res*, 47, 307-315.
- BAE, Y. H. & PARK, K. 2011. Targeted drug delivery to tumors: Myths, reality and possibility. *J Control Release*, 153, 198-205.
- BAER, A. & KEHN-HALL, K. 2014. Viral concentration determination through plaque assays: Using traditional and novel overlay systems. *J Vis Exp*, e52065-e52065.
- BAGCHI, S., YUAN, R. & ENGLEMAN, E. G. 2021. Immune Checkpoint Inhibitors for the Treatment of Cancer: Clinical Impact and Mechanisms of Response and Resistance. *Annu Rev Pathol*, 16, 223-249.
- BAIETTI, M. F., ZHANG, Z., MORTIER, E., MELCHIOR, A., DEGEEST, G., GEERAERTS, A., IVARSSON, Y., DEPOORTERE, F., COOMANS, C., VERMEIREN, E., ZIMMERMANN, P. & DAVID, G. 2012. Syndecan-syntenin-ALIX regulates the biogenesis of exosomes. *Nat Cell Biol*, 14, 677-685.
- BANDARI, S. K., PURUSHOTHAMAN, A., RAMANI, V. C., BRINKLEY, G. J., CHANDRASHEKAR, D. S., VARAMBALLY, S., MOBLEY, J. A., ZHANG, Y., BROWN, E. E., VLODAVSKY, I. & SANDERSON, R.

- D. 2018. Chemotherapy induces secretion of exosomes loaded with heparanase that degrades extracellular matrix and impacts tumor and host cell behavior. *Matrix Biol*, 65, 104-118.
- BARRACHINA, M. N., CALDERÓN-CRUZ, B., FERNANDEZ-ROCCA, L. & GARCÍA, Á. 2019. Application of Extracellular Vesicles Proteomics to Cardiovascular Disease: Guidelines, Data Analysis, and Future Perspectives. *Proteomics*, 19, e1800247-n/a.
- BEBELMAN, M. P., SMIT, M. J., PEGTEL, D. M. & BAGLIO, S. R. 2018. Biogenesis and function of extracellular vesicles in cancer. *Pharmacology and Therapeutics*, 188, 1-11.
- BELLI, C., TRAPANI, D., VIALE, G., D'AMICO, P., DUSO, B. A., DELLA VIGNA, P., ORSI, F. & CURIGLIANO, G. 2018. Targeting the microenvironment in solid tumors. *Cancer Treat Rev*, 65, 22-32.
- BENENCIA, F., COURRÈGES, M. C., FRASER, N. W. & COUKOS, G. 2008. Herpes virus oncolytic therapy reverses tumor immune dysfunction and facilitates tumor antigen presentation. *Cancer Biol Ther*, 7, 1194-1205.
- BERG, W. A., ZHANG, Z., LEHRER, D., JONG, R. A., PISANO, E. D., BARR, R. G., BÖHM-VÉLEZ, M., MAHONEY, M. C., EVANS, W. P., LARSEN, L. H., MORTON, M. J., MENDELSON, E. B., FARRIA, D. M., CORMACK, J. B., MARQUES, H. S., ADAMS, A., YEH, N. M., GABRIELLI, G. & ACRIN INVESTIGATORS, F. T. 2012. Detection of Breast Cancer With Addition of Annual Screening Ultrasound or a Single Screening MRI to Mammography in Women With Elevated Breast Cancer Risk. *JAMA*, 307, 1394-1404.
- BIANCO, F., PERROTTA, C., NOVELLINO, L., FRANCOLINI, M., RIGANTI, L., MENNA, E., SAGLIETTI, L., SCHUCHMAN, E. H., FURLAN, R., CLEMENTI, E., MATTEOLI, M., VERDERIO, C., BIANCO, F., PERROTTA, C., NOVELLINO, L., FRANCOLINI, M., RIGANTI, L., MENNA, E., SAGLIETTI, L., SCHUCHMAN, E. H., FURLAN, R., CLEMENTI, E., MATTEOLI, M. & VERDERIO, C. 2009. Acid sphingomyelinase activity triggers microparticle release from glial cells.[Erratum appears in *EMBO J*. 2009 May 6;28(9):1374]. *EMBO Journal*, 28, 1043-1054.
- BINNICKER, M. J., BADDOUR, L. M., GRYS, T. E., ESPY, M. J., HATA, D. J., WOTTON, J. T. & PATEL, R. 2013. Identification of an influenza A H1N1/2009 virus with mutations in the matrix gene causing a negative result by a commercial molecular assay. *J Clin Microbiol*, 51, 2006-2007.
- BIRZER, A., KRANER, M. E., HEILINGLOH, C. S., MÜHL-ZÜRBE, P., HOFMANN, J., STEINKASSERER, A. & POPELLA, L. 2020. Mass Spectrometric Characterization of HSV-1 L-Particles From Human Dendritic Cells and BHK21 Cells and Analysis of Their Functional Role. *Frontiers in microbiology*, 11, 1997-1997.
- BLANDER, J. M. 2017. The many ways tissue phagocytes respond to dying cells. *Immunol Rev*, 277, 158-173.
- BOBRIE, A., COLOMBO, M., RAPOSO, G. & THÉRY, C. 2011. Exosome Secretion: Molecular Mechanisms and Roles in Immune Responses. *Traffic*, 12, 1659-1668.
- BOMMAREDDY, P. K., SHETTIGAR, M. & KAUFMAN, H. L. 2018. Integrating oncolytic viruses in combination cancer immunotherapy. *Nat Rev Immunol*, 18, 498-513.
- BONAVITA, E., GENTILE, S., RUBINO, M., MAINA, V., PAPAIT, R., KUNDERFRANCO, P., GRECO, C., FERUGLIO, F., MOLGORA, M., LAFACE, I., TARTARI, S., DONI, A., PASQUALINI, F., BARBATI, E., BASSO, G., GALDIERO, MARIA R., NEBULONI, M., RONCALLI, M., COLOMBO, P., LAGHI, L., LAMBRIS, JOHN D., JAILLON, S., GARLANDA, C. & MANTOVANI, A. 2015. PTX3 Is an Extrinsic Oncosuppressor Regulating Complement-Dependent Inflammation in Cancer. *Cell*, 160, 700-714.
- BORGES, S., PEREZ, E. A., THOMPSON, E. A., RADISKY, D. C., GEIGER, X. J. & STORZ, P. 2015. Effective targeting of estrogen receptor-negative breast cancers with the protein kinase D inhibitor CRT0066101. *Mol Cancer Ther*, 14, 1306-1316.
- BOURGEOIS-DAIGNEAULT, M.-C., ST-GERMAIN, L. E., ROY, D. G., PELIN, A., AITKEN, A. S., ARULANANDAM, R., FALLS, T., GARCIA, V., DIALLO, J.-S. & BELL, J. C. J. B. C. R. 2016. Combination of Paclitaxel and MG1 oncolytic virus as a successful strategy for breast cancer treatment. 18, 83.

- BREITBACH, C. J., BURKE, J., JONKER, D., STEPHENSON, J., HAAS, A. R., CHOW, L. Q. M., NIEVA, J., HWANG, T.-H., MOON, A., PATT, R., PELUSIO, A., LE BOEUF, F., BURNS, J., EVGIN, L., DE SILVA, N., CVANCIC, S., ROBERTSON, T., JE, J.-E., LEE, Y.-S., PARATO, K., DIALLO, J.-S., FENSTER, A., DANESHMAND, M., BELL, J. C. & KIRN, D. H. 2011. Intravenous delivery of a multi-mechanistic cancer-targeted oncolytic poxvirus in humans. *Nature*, 477, 99-104.
- BUNGGULAWA, E. J., WANG, W., YIN, T., WANG, N., DURKAN, C., WANG, Y. & WANG, G. 2018. Recent advancements in the use of exosomes as drug delivery systems. *J Nanobiotechnology*, 16, 81-81.
- CAI, X., ZHAN, H., YE, Y., YANG, J., ZHANG, M., LI, J. & ZHUANG, Y. 2021. Current Progress and Future Perspectives of Immune Checkpoint in Cancer and Infectious Diseases. *Front Genet*, 12, 785153-785153.
- CATALANO, M. & O'DRISCOLL, L. 2020. Inhibiting extracellular vesicles formation and release: a review of EV inhibitors. *J Extracell Vesicles*, 9, 1703244-n/a.
- CESSELLI, D., PARISSÉ, P., ALEKSOVA, A., VENEZIANO, C., CERVELLIN, C., ZANELLO, A. & BELTRAMI, A. P. 2018. Extracellular vesicles: How drug and pathology interfere with their biogenesis and function. *Frontiers in Physiology*, 9, 1-15.
- CHAN, B. D., WONG, W. Y., LEE, M. M. L., CHO, W. C. S., YEE, B. K., KWAN, Y. W. & TAI, W. C. S. 2019. Exosomes in Inflammation and Inflammatory Disease. *Proteomics*, 19, e1800149-n/a.
- CHAURASIYA, S., CHEN, N. & WARNER, S. J. C. 2018. Oncolytic virotherapy versus cancer stem cells: A review of approaches and mechanisms. 10, 124.
- CHAURASIYA, S., FONG, Y. & WARNER, S. G. 2021. Oncolytic virotherapy for cancer: Clinical experience. *Biomedicines*, 9, 419.
- CHEN, DANIEL S. & MELLMAN, I. 2013. Oncology Meets Immunology: The Cancer-Immunity Cycle. *Immunity*, 39, 1-10.
- CHEN, J., TAN, Q., YANG, Z. & JIN, Y. 2022. Engineered extracellular vesicles: potentials in cancer combination therapy. *J Nanobiotechnology*, 20, 132.
- CHEN, X., HAN, J., CHU, J., ZHANG, L., ZHANG, J., CHEN, C., CHEN, L., WANG, Y., WANG, H., YI, L., ELDER, J. B., WANG, Q.-E., HE, X., KAUR, B., CHIOCCA, E. A. & YU, J. 2016. A combinational therapy of EGFR-CAR NK cells and oncolytic herpes simplex virus 1 for breast cancer brain metastases. *Oncotarget*, 7, 27764-27777.
- CHI, J.-Y., HSIAO, Y.-W., LI, C.-F., LO, Y.-C., LIN, Z.-Y., HONG, J.-Y., LIU, Y.-M., HAN, X., WANG, S.-M., CHEN, B.-K., TSAI, K. K. & WANG, J.-M. 2015. Targeting chemotherapy-induced PTX3 in tumor stroma to prevent the progression of drug-resistant cancers. *Oncotarget*, 6, 23987-24001.
- CHIRCO, R., LIU, X.-W., JUNG, K.-K. & KIM, H.-R. C. 2006. Novel functions of TIMPs in cell signaling. *Cancer Metastasis Rev*, 25, 99-113.
- CHO, S.-Y., KANG, W., HAN, J. Y., MIN, S., KANG, J., LEE, A., KWON, J. Y., LEE, C. & PARK, H. 2016. An integrative approach to precision cancer medicine using patient-derived xenografts. *Mol Cells*, 39, 77-86.
- CHOI, D., MONTERMINI, L., JEONG, H., SHARMA, S., MEEHAN, B. & RAK, J. 2019. Mapping Subpopulations of Cancer Cell-Derived Extracellular Vesicles and Particles by Nano-Flow Cytometry. *ACS Nano*, 13, 10499-10511.
- CHOO, Y. W., KANG, M., KIM, H. Y., HAN, J., KANG, S., LEE, J.-R., JEONG, G.-J., KWON, S. P., SONG, S. Y., GO, S., JUNG, M., HONG, J. & KIM, B.-S. 2018. M1 Macrophage-Derived Nanovesicles Potentiate the Anticancer Efficacy of Immune Checkpoint Inhibitors. *ACS Nano*, 12, 8977-8993.
- CHRISTIANSON, G. J., BROOKS, W., VEKASI, S., MANOLFI, E. A., NILES, J., ROOPENIAN, S. L., ROTHS, J. B., ROTHLEIN, R. & ROOPENIAN, D. C. 1997. Beta 2-microglobulin-deficient mice are protected from hypergammaglobulinemia and have defective antibody responses because of increased IgG catabolism. *J Immunol*, 159, 4781-4792.
- COCKLE, J. V., BRÜNING-RICHARDSON, A., SCOTT, K. J., THOMPSON, J., KOTTKE, T., MORRISON, E., ISMAIL, A., CARCABOSO, A. M., ROSE, A., SELBY, P., CONNER, J., PICTON, S., SHORT, S., VILE,

- R., MELCHER, A. & ILETT, E. 2017. Oncolytic Herpes Simplex Virus Inhibits Pediatric Brain Tumor Migration and Invasion.
- CONNER, J., RIXON, F. J. & BROWN, S. M. 2005. Herpes Simplex Virus Type 1 Strain HSV1716 Grown in Baby Hamster Kidney Cells Has Altered Tropism for Nonpermissive Chinese Hamster Ovary Cells Compared to HSV1716 Grown in Vero Cells. *J Virol*, 79, 9970-9981.
- COPELAND, A. M., NEWCOMB, W. W. & BROWN, J. C. 2009. Herpes Simplex Virus Replication: Roles of Viral Proteins and Nucleoporins in Capsid-Nucleus Attachment. *J Virol*, 83, 1660-1668.
- COSTA-SILVA, B., AIELLO, N. M., OCEAN, A. J., SINGH, S., ZHANG, H., THAKUR, B. K., BECKER, A., HOSHINO, A., MARK, M. T., MOLINA, H., XIANG, J., ZHANG, T., THEILEN, T. M., GARCÍA-SANTOS, G., WILLIAMS, C., ARARSO, Y., HUANG, Y., RODRIGUES, G., SHEN, T. L., LABORI, K. J., LOTHE, I. M. B., KURE, E. H., HERNANDEZ, J., DOUSSOT, A., EBBESEN, S. H., GRANDGENETT, P. M., HOLLINGSWORTH, M. A., JAIN, M., MALLYA, K., BATRA, S. K., JARNAGIN, W. R., SCHWARTZ, R. E., MATEI, I., PEINADO, H., STANGER, B. Z., BROMBERG, J. & LYDEN, D. 2015. Pancreatic cancer exosomes initiate pre-metastatic niche formation in the liver. *Nature Cell Biology*, 17, 816-826.
- COTTER, T. G., LENNON, S. V., GLYNN, J. M. & GREEN, D. R. 1992. Microfilament-disrupting agents prevent the formation of apoptotic bodies in tumor cells undergoing apoptosis [published erratum appears in *Cancer Res* 1992 Jun 15;52(12):3512]. *Cancer Res*, 52, 997-1005.
- CRESCITELLI, R., LÄSSER, C., SZABÓ, T. G., KITTEL, A., ELDH, M., DIANZANI, I., BUZÁS, E. I. & LÖTVALL, J. 2013. Distinct RNA profiles in subpopulations of extracellular vesicles: Apoptotic bodies, microvesicles and exosomes. *Journal of Extracellular Vesicles*, 2.
- CUNNINGHAM, C. C., GORLIN, J. E. D. B., KWIATKOWSKI, D. J., HARTWIG, J. H., JANMEY, P. A., BYERS, H. R. & STOSSEL, T. P. 2013. Actin-Binding Protein Requirement for Cortical Stability and Efficient Locomotion. 1-4.
- CVJETKOVIC, A., LÖTVALL, J. & LÄSSER, C. 2014. The influence of rotor type and centrifugation time on the yield and purity of extracellular vesicles. *J Extracell Vesicles*, 3, 23111-n/a.
- DANIELSON, K. M., ESTANISLAU, J., TIGGES, J., TOXAVIDIS, V., CAMACHO, V., FELTON, E. J., KHOORY, J., KREIMER, S., IVANOV, A. R., MANTEL, P.-Y., JONES, J., AKUTHOTA, P., DAS, S. & GHIRAN, I. 2016. Diurnal Variations of Circulating Extracellular Vesicles Measured by Nano Flow Cytometry. *PLoS One*, 11, e0144678-e0144678.
- DATAR, I. J., HAUC, S. C., DESAI, S., GIANINO, N., HENICK, B., LIU, Y., SYRIGOS, K., RIMM, D. L., KAVATHAS, P., FERRONE, S. & SCHALPER, K. A. 2021. Spatial analysis and clinical significance of HLA class-I and class-II subunit expression in non-small cell lung cancer. *Clin Cancer Res*, 27, 2837-2847.
- DAUPHINE, C., MOAZZEZ, A., NEAL, J. C., CHLEBOWSKI, R. T. & OZAO-CHOY, J. 2020. Single Hormone Receptor-Positive Breast Cancers Have Distinct Characteristics and Survival. *Ann Surg Oncol*, 27, 4687-4694.
- DE GASSART, A., GEMINARD, C., HOEKSTRA, D. & VIDAL, M. 2004. Exosome secretion: The art of reutilizing nonrecycled proteins? *Traffic*, 5, 896-903.
- DE GRUIJL, T. D., JANSSEN, A. B. & VAN BEUSECHEM, V. W. J. E. O. O. B. T. 2015. Arming oncolytic viruses to leverage antitumor immunity. 15, 959-971.
- DE VRIES, C. R., KAUFMAN, H. L. & LATTIME, E. C. 2015. Oncolytic viruses: Focusing on the tumor microenvironment. *Cancer Gene Ther*, 22, 169-171.
- DEFANTE, A. P., VREELAND, W. N., BENKSTEIN, K. D. & RIPPLE, D. C. 2018. Using Image Attributes to Assure Accurate Particle Size and Count Using Nanoparticle Tracking Analysis. *J Pharm Sci*, 107, 1383-1391.
- DENARDO, D. G. & RUFFELL, B. 2019. Macrophages as regulators of tumour immunity and immunotherapy. *Nat Rev Immunol*, 19, 369-382.
- DENES, C. E., EVERETT, R. D. & DIFENBACH, R. J. 2019. Tour de Herpes: Cycling Through the Life and Biology of HSV-1. *Methods Mol Biol*, 2060, 1-30.

- DESCHAMPS, T. & KALAMVOKI, M. 2018. Extracellular vesicles released by herpes simplex virus 1-infected cells block virus replication in recipient cells in a STING-dependent manner. *J Virol*, 92.
- DIAS, M. V. S., COSTA, C. S. & DA SILVA, L. L. P. 2018. The ambiguous roles of extracellular vesicles in HIV replication and pathogenesis. *Front Microbiol*, 9, 2411-2411.
- DOGRAMMATZIS, C., DESCHAMPS, T. & KALAMVOKI, M. 2019. Biogenesis of Extracellular Vesicles during Herpes Simplex Virus 1 Infection: Role of the CD63 Tetraspanin. *J Virol*, 93.
- DONOSO-QUEZADA, J., GUAJARDO-FLORES, D. & GONZÁLEZ-VALDÉZ, J. 2019. Exosomes as nanocarriers for the delivery of bioactive compounds from black bean extract with antiproliferative activity in cancer cell lines. *Materials today : proceedings*, 13, 362-369.
- DUARTE, S., VIEDMA-POYATOS, Á., NAVARRO-CARRASCO, E., MARTÍNEZ, A. E., PAJARES, M. A. & PÉREZ-SALA, D. 2019. Vimentin filaments interact with the actin cortex in mitosis allowing normal cell division. *Nat Commun*, 10, 4200-4200.
- EDGAR, J. R., MANNA, P. T., NISHIMURA, S., BANTING, G. & ROBINSON, M. S. 2016. Tetherin is an exosomal tether. *eLife*, 5, 1-19.
- EISSA, I. R., BUSTOS-VILLALOBOS, I., ICHINOSE, T., MATSUMURA, S., NAOE, Y., MIYAJIMA, N., MORIMOTO, D., MUKOYAMA, N., ZHIWEN, W., TANAKA, M., HASEGAWA, H., SUMIGAMA, S., ALEKSIC, B., KODERA, Y. & KASUYA, H. 2018. The current status and future prospects of oncolytic viruses in clinical trials against melanoma, glioma, pancreatic, and breast cancers. *Cancers (Basel)*, 10, 356.
- EISSA, I. R., NAOE, Y., BUSTOS-VILLALOBOS, I., ICHINOSE, T., TANAKA, M., ZHIWEN, W., MUKOYAMA, N., MORIMOTO, T., MIYAJIMA, N., HITOKI, H., SUMIGAMA, S., ALEKSIC, B., KODERA, Y. & KASUYA, H. 2017. Genomic Signature of the Natural Oncolytic Herpes Simplex Virus HF10 and Its Therapeutic Role in Preclinical and Clinical Trials. *Frontiers in Oncology*, 7.
- ESTEVA, F. J., HUBBARD-LUCEY, V. M., TANG, J. & PUSZTAI, L. 2019. Immunotherapy and targeted therapy combinations in metastatic breast cancer. *Lancet Oncol*, 20, e175-e186.
- FADOK, V. A., BRATTON, D. L., GUTHRIE, L. & HENSON, P. M. 2001. Differential Effects of Apoptotic Versus Lysed Cells on Macrophage Production of Cytokines: Role of Proteases. *J Immunol*, 166, 6847-6854.
- FERGUSON, M. S., LEMOINE, N. R. & WANG, Y. J. A. I. V. 2012. Systemic delivery of oncolytic viruses: hopes and hurdles. 2012.
- FRAMPTON, J. E. 2022. Teserpaturev/G47Δ: First Approval. *BioDrugs : clinical immunotherapeutics, biopharmaceuticals, and gene therapy*, 36, 667-672.
- FUKUHARA, H., INO, Y. & TODO, T. 2016. Oncolytic virus therapy: A new era of cancer treatment at dawn. *Cancer Science*, 107, 1373-1379.
- GALLAND, S. & STAMENKOVIC, I. 2020. Mesenchymal stromal cells in cancer: a review of their immunomodulatory functions and dual effects on tumor progression. *J Pathol*, 250, 555-572.
- GAN, Z., DING, L., BURCKHARDT, CHRISTOPH J., LOWERY, J., ZARITSKY, A., SITTERLEY, K., MOTA, A., COSTIGLIOLA, N., STARKER, COLBY G., VOYTAS, DANIEL F., TYTELL, J., GOLDMAN, ROBERT D. & DANUSER, G. 2016. Vimentin Intermediate Filaments Template Microtubule Networks to Enhance Persistence in Cell Polarity and Directed Migration. *Cell Syst*, 3, 252-263.e8.
- GANDHAM, S., SU, X., WOOD, J., NOCERA, A. L., ALLI, S. C., MILANE, L., ZIMMERMAN, A., AMIJI, M. & IVANOV, A. R. 2020. Technologies and Standardization in Research on Extracellular Vesicles. *Trends Biotechnol*, 38, 1066-1098.
- GANGADARAN, P., HONG, C. M. & AHN, B.-C. 2017. Current Perspectives on In Vivo Noninvasive Tracking of Extracellular Vesicles with Molecular Imaging. *Biomed Res Int*, 2017, 9158319-11.
- GAO, X., RAN, N., DONG, X., ZUO, B., YANG, R., ZHOU, Q., MOULTON, H. M., SEOW, Y. & YIN, H. 2018. Anchor peptide captures, targets, and loads exosomes of diverse origins for diagnostics and therapy. *Sci Transl Med*, 10.
- GARBER, K. 2006. China Approves World's First Oncolytic Virus Therapy For Cancer Treatment. *JNCI J Natl Cancer Inst*, 98, 298-300.

- GARCIA-HERNANDEZ, A., LEAL-ORTA, E., RAMIREZ-RICARDO, J., CORTES-REYNOSA, P., THOMPSON-BONILLA, R. & SALAZAR, E. P. 2021. Linoleic acid induces secretion of extracellular vesicles from MDA-MB-231 breast cancer cells that mediate cellular processes involved with angiogenesis in HUVECs. *Prostaglandins Other Lipid Mediat*, 153, 106519-106519.
- GARDINER, C., VIZIO, D. D., SAHOO, S., THÉRY, C., WITWER, K. W., WAUBEN, M. & HILL, A. F. 2016. Techniques used for the isolation and characterization of extracellular vesicles: Results of a worldwide survey. *Journal of Extracellular Vesicles*, 5.
- GARLANDA, C., BOTTAZZI, B., MAGRINI, E., INFORZATO, A. & MANTOVANI, A. 2018. PTX3, a Humoral Pattern Recognition Molecule, in Innate Immunity, Tissue Repair, and Cancer. *Physiol Rev*, 98, 623-639.
- GAROFALO, M., VILLA, A., CRESCENTI, D., MARZAGALLI, M., KURYK, L., LIMONTA, P., MAZZAFERRO, V. & CIANA, P. J. T. 2019. Heterologous and cross-species tropism of cancer-derived extracellular vesicles. 9, 5681.
- GERMANO, G., LU, S., ROSPO, G., LAMBA, S., ROUSSEAU, B., FANELLI, S., STENECH, D., LE, D. T., HAYS, J., TOTARO, M. G., AMODIO, V., CHILÀ, R., MONDINO, A., DIAZ, L. A., DI NICOLANTONIO, F. & BARDELLI, A. 2021. Cd4 t cell-dependent rejection of beta-2 microglobulin null mismatch repair-deficient tumors. *Cancer Discov*, 11, 1844-1859.
- GIACOMINI, A., GHEDINI, G. C., PRESTA, M. & RONCA, R. 2018. Long pentraxin 3: A novel multifaceted player in cancer. *Biochim Biophys Acta Rev Cancer*, 1869, 53-63.
- GOH, W. J., ZOU, S., ONG, W. Y., TORTA, F., ALEXANA, A. F., SCHIFFELERS, R. M., STORM, G., WANG, J.-W., CZARNY, B. M. S. & PASTORIN, G. 2017. Bioinspired Cell-Derived Nanovesicles versus Exosomes as Drug Delivery Systems : A Cost-Effective Alternative. *Sci Rep*, 7, 14322-10.
- GRANT, R., ANSA-ADDO, E., STRATTON, D., ANTWI-BAFFOUR, S., JORFI, S., KHOLIA, S., KRIGE, L., LANGE, S. & INAL, J. 2011. A filtration-based protocol to isolate human Plasma Membrane-derived Vesicles and exosomes from blood plasma. *J Immunol Methods*, 371, 143-151.
- GREENING, D. W., XU, R., GOPAL, S. K., RAI, A. & SIMPSON, R. J. 2017. Proteomic insights into extracellular vesicle biology - defining exosomes and shed microvesicles. *Expert Rev Proteomics*, 14, 69-95.
- GUJAR, S., POL, J. G., KIM, Y., LEE, P. W. & KROEMER, G. 2018. Antitumor Benefits of Antiviral Immunity: An Underappreciated Aspect of Oncolytic Virotherapies. *Trends Immunol*, 39, 209-221.
- GUO, Z. S., LIU, Z., KOWALSKY, S., FEIST, M., KALINSKI, P., LU, B., STORKUS, W. J. & BARTLETT, D. L. J. F. I. I. 2017. Oncolytic immunotherapy: conceptual evolution, current strategies, and future perspectives. 8, 555.
- GUPTA, G. P. & MASSAGUÉ, J. 2006. Cancer Metastasis: Building a Framework. *Cell*, 127, 679-695.
- GURUNATHAN, S., KANG, M.-H., JEYARAJ, M., QASIM, M. & KIM, J.-H. 2019. Review of the Isolation, Characterization, Biological Function, and Multifarious Therapeutic Approaches of Exosomes. *Cells*, 8, 307.
- GYÖRGY, B., SZABÓ, T. G., PÁSZTÓI, M., PÁL, Z., MISJÁK, P., ARADI, B., LÁSZLÓ, V., PÁLLINGER, É., PAP, E., KITTEL, Á., NAGY, G., FALUS, A. & BUZÁS, E. I. 2011. Membrane vesicles, current state-of-the-art: emerging role of extracellular vesicles. *Cell Mol Life Sci*, 68, 2667-2688.
- HALLE, S., HALLE, O. & FÖRSTER, R. 2017. Mechanisms and Dynamics of T Cell-Mediated Cytotoxicity In Vivo. *Trends Immunol*, 38, 432-443.
- HALLER, S. D., MONACO, M. L. & ESSANI, K. 2020. The present status of immuno-oncolytic viruses in the treatment of pancreatic cancer. *Viruses*, 12, 1318.
- HAMAD, R. R., ERIKSSON, M. J., BERG, E., LARSSON, A. & BREMME, K. 2012. Impaired endothelial function and elevated levels of pentraxin 3 in early-onset preeclampsia. *Acta Obstet Gynecol Scand*, 91, 50-56.
- HAMMOND, D., ZENG, K., ESPERT, A., BASTOS, R. N., BARON, R. D., GRUNEBERG, U. & BARR, F. A. 2013. Melanoma-associated mutations in protein phosphatase 6 cause chromosome instability and DNA damage owing to dysregulated Aurora-A. *J Cell Sci*, 126, 3429-3440.

- HANAHAH, D. & COUSSENS, LISA M. 2012. Accessories to the Crime: Functions of Cells Recruited to the Tumor Microenvironment. *Cancer Cell*, 21, 309-322.
- HARRINGTON, K., FREEMAN, D. J., KELLY, B., HARPER, J. & SORIA, J.-C. 2019. Optimizing oncolytic virotherapy in cancer treatment. *Nat Rev Drug Discov*, 18, 689-706.
- HICKLIN, D. J., WANG, Z. G., ARIENTI, F., RIVOLTINI, L., PARMIANI, G. & FERRONE, S. 1998. beta 2-microglobulin mutations, HLA class I antigen loss, and tumor progression in melanoma. *The Journal of clinical investigation*, 101, 2720-2729.
- HIND, E., HEUGH, S., ANSA-ADDO, E. A., ANTWI-BAFFOUR, S., LANGE, S. & INAL, J. 2010. Red cell PMVs, plasma membrane-derived vesicles calling out for standards. *Biochem Biophys Res Commun*, 399, 465-469.
- HOSHINO, A., COSTA-SILVA, B., SHEN, T.-L., RODRIGUES, G., HASHIMOTO, A., MARK, M. T., MOLINA, H., KOHSAKA, S., GIANNATALE, A. D., CEDER, S., SINGH, S., WILLIAMS, C., SOPLOP, N., URYU, K., PHARMER, L., KING, T., BOJMAR, L., DAVIES, A. E., ARARSO, Y., ZHANG, T., ZHANG, H., HERNANDEZ, J., WEISS, J. M., DUMONT-COLE, V. D., KRAMER, K. & WEXLER, L. H. 2015. Tumour exosome integrins determine organotropic metastasis. *Nature*, 527, 329-335.
- HOWARD, F. H. N., AL-JANABI, H., PATEL, P., COX, K., SMITH, E., VADAKEKOLATHU, J., POCKLEY, A. G., CONNER, J., NOHL, J. F., ALLWOOD, D. A., COLLADO-ROJAS, C., KENNERLEY, A., STANILAND, S. & MUTHANA, M. 2022. Nanobugs as drugs: bacterial derived nanomagnets enhance tumor targeting and oncolytic activity of HSV-1 virus.
- HOWELLS, A., MARELLI, G., LEMOINE, N. R. & WANG, Y. 2017. Oncolytic viruses-interaction of virus and tumor cells in the battle to eliminate cancer. *Front Oncol*, 7, 195-195.
- HOWITT, J. & HILL, A. F. 2016. Exosomes in the Pathology of Neurodegenerative Diseases. *J Biol Chem*, 291, 26589-26597.
- HUGHES, E. A., HAMMOND, C. & CRESSWELL, P. 1997. Misfolded Major Histocompatibility Complex Class I Heavy Chains are Translocated into the Cytoplasm and Degraded by the Proteasome. *Proc Natl Acad Sci U S A*, 94, 1896-1901.
- HURWITZ, S. N., CONLON, M. M., RIDER, M. A., BROWNSTEIN, N. C. & MECKES, D. G. 2016. Nanoparticle analysis sheds budding insights into genetic drivers of extracellular vesicle biogenesis. *J Extracell Vesicles*, 5, 31295-n/a.
- HURWITZ, S. N., NKOSI, D., CONLON, M. M., YORK, S. B., LIU, X., TREMBLAY, D. C. & MECKES, D. G. 2017. CD63 regulates Epstein-Barr virus LMP1 exosomal packaging, enhancement of vesicle production, and noncanonical NF- κ B signaling. *J Virol*, 91.
- HUSSEN, B. M., ABDULLAH, S. T., RASUL, M. F., SALIHI, A., GHAFOURI-FARD, S., HIDAYAT, H. J. & TAHERI, M. 2021. MicroRNAs: Important Players in Breast Cancer Angiogenesis and Therapeutic Targets. *Frontiers in Molecular Biosciences*, 8.
- HÖGLUND, P., GLAS, R., MÉNARD, C., KÅSE, A., JOHANSSON, M. H., FRANKSSON, L., LEMMONIER, F. & KÄRRE, K. 1998. β 2-Microglobulin-deficient NK cells show increased sensitivity to MHC class I-mediated inhibition, but self tolerance does not depend upon target cell expression of H-2Kb and Db heavy chains. *European journal of immunology*, 28, 370-378.
- IBRAHIM, A. & MARBÁN, E. 2016. Exosomes: Fundamental Biology and Roles in Cardiovascular Physiology. *Annu Rev Physiol*, 78, 67-83.
- IHARA, T., YAMAMOTO, T., SUGAMATA, M., OKUMURA, H. & UENO, Y. 1998. The process of ultrastructural changes from nuclei to apoptotic body. *Virchows Arch*, 433, 443-447.
- ITO, N., DEMARCO, R. A., MAILLIARD, R. B., HAN, J., RABINOWICH, H., KALINSKI, P., STOLZ, D. B., ZEH, H. J. & LOTZE, M. T. 2007. Cytolytic cells induce HMGB1 release from melanoma cell lines. *J Leukoc Biol*, 81, 75-83.
- JANSEN, F., YANG, X., PROEBSTING, S., HOELSCHER, M., PRZYBILLA, D., BAUMANN, K., SCHMITZ, T., DOLF, A., ENDL, E., FRANKLIN, B. S., SINNING, J. M., VASA-NICOTERA, M., NICKENIG, G. & WERNER, N. 2014. MicroRNA Expression in Circulating Microvesicles Predicts Cardiovascular Events in Patients With Coronary Artery Disease. *J Am Heart Assoc*, 3, e001249-n/a.

- JEAN BELTRAN, P. M., COOK, K. C., HASHIMOTO, Y., GALITZINE, C., MURRAY, L. A., VITEK, O. & CRISTEA, I. M. 2018. Infection-Induced Peroxisome Biogenesis Is a Metabolic Strategy for Herpesvirus Replication. *Cell Host Microbe*, 24, 526-541.e7.
- JEPPESEN, D. K., HVAM, M. L., PRIMDAHL-BENGTSON, B., BOYSEN, A. T., WHITEHEAD, B., DYRSKJØT, L., ØRNTØFT, T. F., HOWARD, K. A. & OSTENFELD, M. S. 2014. Comparative analysis of discrete exosome fractions obtained by differential centrifugation. *J Extracell Vesicles*, 3, 25011-n/a.
- JEYARAM, A. & JAY, S. M. 2017. Preservation and Storage Stability of Extracellular Vesicles for Therapeutic Applications. *AAPS J*, 20, 1-1.
- JIANG, L. & POON, I. K. H. 2019. Methods for monitoring the progression of cell death, cell disassembly and cell clearance. *Apoptosis*, 24, 208-220.
- JOHNSON, D. B., NEBHAN, C. A., MOSLEHI, J. J. & BALKO, J. M. 2022. Immune-checkpoint inhibitors: long-term implications of toxicity. *Nat Rev Clin Oncol*, 19, 254-267.
- JOHNSTONE, C. N., SMITH, Y. E., CAO, Y., BURROWS, A. D., CROSS, R. S. N., LING, X., REDVERS, R. P., DOHERTY, J. P., ECKHARDT, B. L., NATOLI, A. L., RESTALL, C. M., LUCAS, E., PEARSON, H. B., DEB, S., BRITT, K. L., RIZZITELLI, A., LI, J., HARMEY, J. H., POULIOT, N. & ANDERSON, R. L. 2015. Functional and molecular characterisation of EO771.LMB tumours, a new C57BL/6-mouse-derived model of spontaneously metastatic mammary cancer. *Dis Model Mech*, 8, 237-251.
- JONES, K. I., TIERSMA, J., YUZHALIN, A. E., GORDON-WEEKS, A. N., BUZZELLI, J., IM, J. H. & MUSCHEL, R. J. 2018. Radiation combined with macrophage depletion promotes adaptive immunity and potentiates checkpoint blockade. *EMBO Mol Med*, 10, n/a.
- JOSHI, B. S., DE BEER, M. A., GIEPMANS, B. N. G. & ZUHORN, I. S. 2020. Endocytosis of Extracellular Vesicles and Release of Their Cargo from Endosomes. *ACS Nano*, 14, 4444-4455.
- JUNG, K. O., JO, H., YU, J. H., GAMBHIR, S. S. & PRATX, G. 2018. Development and MPI tracking of novel hypoxia-targeted theranostic exosomes. *Biomaterials*, 177, 139-148.
- KAKIUCHI, Y., KURODA, S., KANAYA, N., KUMON, K., TSUMURA, T., HASHIMOTO, M., YAGI, C., SUGIMOTO, R., HAMADA, Y., KIKUCHI, S., NISHIZAKI, M., KAGAWA, S., TAZAWA, H., URATA, Y. & FUJIWARA, T. 2021. Local oncolytic adenovirotherapy produces an abscopal effect via tumor-derived extracellular vesicles. *Mol Ther*, 29, 2920-2930.
- KALLURI, R. & LEBLEU, V. S. 2020. The biology, function, and biomedical applications of exosomes. *Science*, 367, 640.
- KALRA, H., DRUMMEN, G. P. C. & MATHIVANAN, S. 2016. Focus on extracellular vesicles: Introducing the next small big thing. *International Journal of Molecular Sciences*, 17.
- KANG, M., JORDAN, V., BLENKIRON, C. & CHAMLEY, L. W. 2021. Biodistribution of extracellular vesicles following administration into animals: A systematic review. *J Extracell Vesicles*, 10, e12085.
- KASEDA, K., WATANABE, K. I., SAKAMAKI, H. & KAZAMA, A. 2016. Solitary pulmonary metastasis from occult papillary thyroid carcinoma. *Thorac Cancer*, 7, 261-263.
- KAUR, B., CHIOCCA, E. A. & CRIFE, T. P. 2012. Oncolytic HSV-1 Virotherapy: Clinical Experience and Opportunities for Progress. *CPB*, 13, 1842-1851.
- KELLER, H. U. & BEBIE, H. 1996. Protrusive activity quantitatively determines the rate and direction of cell locomotion. *Cell Motility and the Cytoskeleton*, 33, 241-251.
- KIM, D.-K., NISHIDA, H., AN, S. Y., SHETTY, A. K., BARTOSH, T. J. & PROCKOP, D. J. 2016. Chromatographically isolated CD63⁺CD81⁺ extracellular vesicles from mesenchymal stromal cells rescue cognitive impairments after TBI. *Proc Natl Acad Sci U S A*, 113, 170-175.
- KIM, S. M., YANG, Y., OH, S. J., HONG, Y., SEO, M. & JANG, M. 2017. Cancer-derived exosomes as a delivery platform of CRISPR/Cas9 confer cancer cell tropism-dependent targeting. *J Control Release*, 266, 8-16.
- KNIPE, D. M. & HOWLEY, P. 2013. Fields virology: Sixth edition. 1.
- KONOSHENKO, M. Y., LEKCHNOV, E. A., VLASSOV, A. V. & LAKTIONOV, P. P. 2018. Isolation of Extracellular Vesicles: General Methodologies and Latest Trends. *Biomed Res Int*, 2018, 8545347-27.

- KOOIJMANS, S. A. A., FLIERVOET, L. A. L., VAN DER MEEL, R., FENS, M. H. A. M., HEIJNEN, H. F. G., VAN BERGEN EN HENEGOUWEN, P. M. P., VADER, P., SCHIFFELERS, R. M., CELBIOLOGIE, SUB G, T. & SUB CELL, B. 2016. PEGylated and targeted extracellular vesicles display enhanced cell specificity and circulation time. *Journal of controlled release*, 224, 77.
- KOWAL, J., ARRAS, G., COLOMBO, M., JOUVE, M., MORATH, J. P., PRIMDAL-BENGTSON, B., DINGLI, F., LOEW, D., TKACH, M. & THÉRY, C. 2016. Proteomic comparison defines novel markers to characterize heterogeneous populations of extracellular vesicle subtypes. *Proc Natl Acad Sci U S A*, 113, E968-E977.
- KRAWCZYK, A., KRAUSS, J., EIS-HUEBINGER, A. M., DAEUMER, M. P., SCHWARZENBACHER, R., DITTMER, U., SCHNEWEIS, K. E., JAEGER, D., ROGGENDORF, M. & ARNDT, M. A. E. 2011. Impact of Valency of a Glycoprotein B-Specific Monoclonal Antibody on Neutralization of Herpes Simplex Virus. *J Virol*, 85, 1793-1803.
- KWAN, A., WINDER, N., ATKINSON, E., AL-JANABI, H., ALLEN, R. J., HUGHES, R., MOAMIN, M., LOUIE, R., EVANS, D., HUTCHINSON, M., CAPPER, D., COX, K., HANDLEY, J., WILSHAW, A., KIM, T., TAZZYMANN, S. J., SRIVASTAVA, S., OTTEWELL, P., VADAKEKOLATHU, J., POCKLEY, G., LEWIS, C. E., BROWN, J. E., DANSON, S. J., CONNER, J. & MUTHANA, M. 2021a. Macrophages mediate the antitumor effects of the oncolytic virus HSV1716 in mammary tumors. *Mol Cancer Ther*, 20, 589-601.
- KWAN, A., WINDER, N. & MUTHANA, M. 2021b. Oncolytic Virotherapy Treatment of Breast Cancer: Barriers and Recent Advances. *Viruses*, 13, 1128.
- KWON, M. S., SHIN, S.-H., YIM, S.-H., LEE, K. Y., KANG, H.-M., KIM, T.-M. & CHUNG, Y.-J. 2007. CD63 as a biomarker for predicting the clinical outcomes in adenocarcinoma of lung. *Lung Cancer*, 57, 46-53.
- KWON, S., SHIN, S., DO, M., OH, B. H., SONG, Y., BUI, V. D., LEE, E. S., JO, D.-G., CHO, Y. W., KIM, D.-H. & PARK, J. H. 2021. Engineering approaches for effective therapeutic applications based on extracellular vesicles. *J Control Release*, 330, 15-30.
- LAMICHHANE, T. N., SOKIC, S., SCHARDT, J. S., RAIKER, R. S., LIN, J. W. & JAY, S. M. 2015. Emerging roles for extracellular vesicles in tissue engineering and regenerative medicine. *Tissue Eng Part B Rev*, 21, 45-54.
- LEDFORD, H. 2011. Melanoma drug wins US approval. *Nature*, 471, 561-561.
- LEE, T. H., D'ASTI, E., MAGNUS, N., AL-NEDAWI, K., MEEHAN, B. & RAK, J. 2011. Microvesicles as mediators of intercellular communication in cancer—the emerging science of cellular ‘debris’. *Semin Immunopathol*, 33, 455-467.
- LEE, T. S., KIM, Y., ZHANG, W., SONG, I. H. & TUNG, C.-H. 2018. Facile metabolic glycan labeling strategy for exosome tracking. *Biochim Biophys Acta Gen Subj*, 1862, 1091-1100.
- LI, G.-N., ZHAO, X.-J., WANG, Z., LUO, M.-S., SHI, S.-N., YAN, D.-M., LI, H.-Y., LIU, J.-H., YANG, Y., TAN, J.-H., ZHANG, Z.-Y., CHEN, R.-Q., LAI, H.-L., HUANG, X.-Y., ZHOU, J.-F., MA, D., FANG, Y. & GAO, Q.-L. 2022. Elaiophyllin triggers paraptosis and preferentially kills ovarian cancer drug-resistant cells by inducing MAPK hyperactivation. *Signal transduction and targeted therapy*, 7, 317-317.
- LI, J., LEE, Y., JOHANSSON, H. J., MÄGER, I., VADER, P., NORDIN, J. Z., WIKLANDER, O. P. B., LEHTIÖ, J., WOOD, M. J. A. & ANDALOUSSI, S. E. L. 2015. Serum-free culture alters the quantity and protein composition of neuroblastoma-derived extracellular vesicles. *J Extracell Vesicles*, 4, 26883-n/a.
- LI, L., LIU, S., HAN, D., TANG, B. & MA, J. 2020a. Delivery and Biosafety of Oncolytic Virotherapy. *Front Oncol*, 10, 475-475.
- LI, M. & SHU, H.-B. 2020. Dephosphorylation of cGAS by PPP6C impairs its substrate binding activity and innate antiviral response. *Protein Cell*, 11, 584-599.
- LI, T., FU, J., ZENG, Z., COHEN, D., LI, J., CHEN, Q., LI, B. & LIU, X. S. 2020b. TIMER2.0 for analysis of tumor-infiltrating immune cells. *Nucleic Acids Res*, 48, W509-W514.
- LI, X., WANG, Y., WANG, Q., LIU, Y., BAO, W. & WU, S. 2018. Exosomes in cancer: Small transporters with big functions. *Cancer Lett*, 435, 55-65.

- LI, Y., CHEN, Y.-H., LIU, B.-Y., NIE, Q., LI, L.-J., DUAN, X., WU, L.-Z. & CHEN, G. 2023. Deciphering the Heterogeneity Landscape of Mesenchymal Stem/Stromal Cell-Derived Extracellular Vesicles for Precise Selection in Translational Medicine. *Adv Healthc Mater*, e2202453-e2202453.
- LIANG, M. 2018. Oncorine, the World First Oncolytic Virus Medicine and its Update in China. *CCDT*, 18, 171-176.
- LIANGSUPREE, T., MULTIA, E. & RIEKKOLA, M.-L. 2021. Modern isolation and separation techniques for extracellular vesicles. *Journal of Chromatography A*, 1636.
- LIU, F. & ZHOU, Z. H. 2007. Comparative virion structures of human herpesviruses. Cambridge University Press.
- LIU, H., CHEN, L., PENG, Y., YU, S., LIU, J., WU, L., ZHANG, L., WU, Q., CHANG, X., YU, X. & LIU, T. 2018. Dendritic cells loaded with tumor derived exosomes for cancer immunotherapy. *Oncotarget*, 9, 2887-2894.
- LIU, T.-C. & KIRN, D. 2007. Systemic efficacy with oncolytic virus therapeutics: Clinical proof-of-concept and future directions. *Cancer Res*, 67, 429-432.
- LONGA, Q., UPADHYA, D., HATTIANGADY, B., KIM, D.-K., AN, S. Y., SHUAI, B., PROCKOP, D. J. & SHETTY, A. K. 2017. Intranasal MSC-derived A1-exosomes ease inflammation, and prevent abnormal neurogenesis and memory dysfunction after status epilepticus. *Proc Natl Acad Sci U S A*, 114, E3536-E3545.
- LU, W., FANG, Y., MENG, X., WANG, X., LIU, W., LIU, M. & ZHANG, P. 2023. Improving the Transduction Efficiency and Antitumor Effect of Conditionally Replicative Adenovirus by Application of 6-cyclohexyl Methyl-β-D-maltoside. *Molecules*, 28, 528.
- LUO, X., AN, M., CUNEO, K. C., LUBMAN, D. M. & LI, L. 2018. High-Performance Chemical Isotope Labeling Liquid Chromatography Mass Spectrometry for Exosome Metabolomics. *Anal. Chem*, 90, 8314-8319.
- LÁZARO-IBÁÑEZ, E., SANZ-GARCIA, A., VISAKORPI, T., ESCOBEDO-LUCEA, C., SILJANDER, P., AYUSO-SACIDO, Á. & YLIPERTTULA, M. 2014. Different gDNA content in the subpopulations of prostate cancer extracellular vesicles: Apoptotic bodies, microvesicles, and exosomes. *Prostate*, 74, 1379-1390.
- MACE, A. T. M., GANLY, I., SOUTAR, D. S. & BROWN, S. M. 2008. Potential for efficacy of the oncolytic Herpes simplex virus 1716 in patients with oral squamous cell carcinoma. *Head Neck*, 30, 1045-1051.
- MACLEAN, A. R., UL-FAREED, M., ROBERTSON, L., HARLAND, J. & BROWN, S. M. 1991. Herpes simplex virus type 1 deletion variants 1714 and 1716 pinpoint neurovirulence-related sequences in Glasgow strain 17+ between immediate early gene 1 and the 'a' sequence. *J Gen Virol*, 72, 631-639.
- MAHMOOD, T. & YANG, P.-C. 2012. Western blot: Technique, theory, and trouble shooting. *N Am J Med Sci*, 4, 429-434.
- MARTINS, F., SOFIYA, L., SYKIOTIS, G. P., LAMINE, F., MAILLARD, M., FRAGA, M., SHABAFROUZ, K., RIBI, C., CAIROLI, A., GUEX-CROSIER, Y., KUNTZER, T., MICHIELIN, O., PETERS, S., COUKOS, G., SPERTINI, F., THOMPSON, J. A. & OBEID, M. 2019. Adverse effects of immune-checkpoint inhibitors: epidemiology, management and surveillance. *Nat Rev Clin Oncol*, 16, 563-580.
- MASKIN, C. R., RAMAN, R. & HOUVRAS, Y. 2022. PPP6C, a serine-threonine phosphatase, regulates melanocyte differentiation and contributes to melanoma tumorigenesis through modulation of MITF activity. *Sci Rep*, 12, 5573-5573.
- MATHIVANAN, S. & SIMPSON, R. J. 2009. ExoCarta: A compendium of exosomal proteins and RNA. *Proteomics*, 9, 4997-5000.
- MATSUO, H., CHEVALLIER, J., MAYRAN, N., LE BLANC, I., FERGUSON, C., FAURÉ, J., BLANC, N. S., MATILE, S., DUBOCHET, J., SADOUL, R., PARTON, R. G., VILBOIS, F. & GRUENBERG, J. 2004. Role of LBPA and Alix in Multivesicular Liposome Formation and Endosome Organization. *Science*, 303, 531-534.

- MCDERMOTT, M. S. J., SHARKO, A. C., MUNIE, J., KASSLER, S., MELENDEZ, T., LIM, C.-U. & BROUDE, E. V. 2020. CDK7 Inhibition is Effective in all the Subtypes of Breast Cancer: Determinants of Response and Synergy with EGFR Inhibition. *Cells*, 9, 638.
- MCNAMARA, R. P., CARO-VEGAS, C. P., COSTANTINI, L. M., LANDIS, J. T., GRIFFITH, J. D., DAMANIA, B. A. & DITTMER, D. P. 2018. Large-scale, cross-flow based isolation of highly pure and endocytosis-competent extracellular vesicles. *J Extracell Vesicles*, 7, 1541396-n/a.
- MECKES JR, D. G. & RAAB-TRAUB, N. 2011. Microvesicles and Viral Infection. *J Virol*, 85, 12844-12854.
- MEDEIROS, T., MYETTE, R. L., ALMEIDA, J. R., SILVA, A. A. & BURGER, D. 2020. Extracellular vesicles: Cell-derived biomarkers of glomerular and tubular injury. *Cell Physiol Biochem*, 54, 88-109.
- MENCK, K., KLEMM, F., GROSS, J. C., PUKROP, T., WENZEL, D. & BINDER, C. 2013. Induction and transport of Wnt 5a during macrophage-induced malignant invasion is mediated by two types of extracellular vesicles. *Oncotarget*, 4, 2057-2066.
- MILLER, C. G. & FRASER, N. W. 2000. Role of the immune response during neuro-attenuated herpes simplex virus-mediated tumor destruction in a murine intracranial melanoma model. *Cancer Res*, 60, 5714-5722.
- MIN, R., LI, Z., EPSTEIN, J., BARLOGIE, B. & YI, Q. 2002. β 2-microglobulin as a negative growth regulator of myeloma cells. *British journal of haematology*, 118, 495-505.
- MINAMI, C. A., KANTOR, O., WEISS, A., NAKHLIS, F., KING, T. A. & MITTENDORF, E. A. 2020. Association Between Time to Operation and Pathologic Stage in Ductal Carcinoma in Situ and Early-Stage Hormone Receptor-Positive Breast Cancer. *J Am Coll Surg*, 231, 434-447.e2.
- MIR, B. & GOETTSCHE, C. 2020. Extracellular Vesicles as Delivery Vehicles of Specific Cellular Cargo. *Cells*, 9, 1601.
- MOHAMMADINEJAD, R., MOOSAVI, M. A., TAVAKOL, S., VARDAR, D. Ö., HOSSEINI, A., RAHMATI, M., DINI, L., HUSSAIN, S., MANDEGARY, A. & KLIONSKY, D. J. 2019. Necrotic, apoptotic and autophagic cell fates triggered by nanoparticles. *Autophagy*, 15, 4-33.
- MORELLI, A. E., LARREGINA, A. T., SHUFESKY, W. J., SULLIVAN, M. L. G., STOLZ, D. B., PAPWORTH, G. D., ZAHORCHAK, A. F., LOGAR, A. J., WANG, Z., WATKINS, S. C., FALO, L. D. & THOMSON, A. W. 2004. Endocytosis, intracellular sorting, and processing of exosomes by dendritic cells. *Blood*, 104, 3257-3266.
- MORRIS, E. C., NEELAPU, S. S., GIAVRIDIS, T. & SADELAIN, M. 2022. Cytokine release syndrome and associated neurotoxicity in cancer immunotherapy. *Nat Rev Immunol*, 22, 85-96.
- MOSER, A. C. & HAGE, D. S. J. B. 2010. Immunoaffinity chromatography: an introduction to applications and recent developments. 2, 769-790.
- MOSS, D. K. 2006. A novel role for microtubules in apoptotic chromatin dynamics and cellular fragmentation. *Journal of Cell Science*, 119, 2362-2374.
- MULCAHY, L. A., PINK, R. C. & CARTER, D. R. F. 2014. Routes and mechanisms of extracellular vesicle uptake. *J Extracell Vesicles*, 3, 24641-n/a.
- MUTHANA, M., KENNERLEY, A. J., HUGHES, R., FAGNANO, E., RICHARDSON, J., PAUL, M., MURDOCH, C., WRIGHT, F., PAYNE, C., LYTHGOE, M. F., FARROW, N., DOBSON, J., CONNER, J., WILD, J. M. & LEWIS, C. 2015. Directing cell therapy to anatomic target sites in vivo with magnetic resonance targeting. *Nat Commun*, 6, 8009.
- NABHAN, J. F., HU, R., OH, R. S., COHEN, S. N. & LU, Q. 2012. Formation and release of arrestin domain-containing protein 1-mediated microvesicles (ARMMs) at plasma membrane by recruitment of TSG101 protein. *Proceedings of the National Academy of Sciences*, 109, 4146-4151.
- NGUYEN, D. B., LY, T. B. T. & BERNHARDT, I. 2017. Microvesicles Released from Human Red Blood Cells: Properties and Potential Applications. *Novel Implications of Exosomes in Diagnosis and Treatment of Cancer and Infectious Diseases*.
- NISHIDA-AOKI, N., TOMINAGA, N., TAKESHITA, F., SONODA, H., YOSHIOKA, Y. & OCHIYA, T. 2017. Disruption of Circulating Extracellular Vesicles as a Novel Therapeutic Strategy against Cancer Metastasis. *Mol Ther*, 25, 181-191.

- NUTTER HOWARD, F. H., ISCARO, A. & MUTHANA, M. 2022. Chapter Eight - Oncolytic viral particle delivery. Elsevier Inc.
- ODORIZZI, G. 2006. The multiple personalities of Alix. *J Cell Sci*, 119, 3025-3032.
- OGO, H., TANUMA, N., MATSUI, Y., HAYAKAWA, N., INAGAKI, A., SUMIYOSHI, M., MOMOI, Y., KISHIMOTO, A., SUZUKI, M., SASAKI, N., OHUCHI, T., NOMURA, M., TERUYA, Y., YASUDA, K., WATANABE, T. & SHIMA, H. 2016. The protein phosphatase 6 catalytic subunit (Ppp6c) is indispensable for proper post-implantation embryogenesis. *Mech Dev*, 139, 1-9.
- OH, E., KIM, Y. J., AN, H., SUNG, D., CHO, T. M., FARRAND, L., JANG, S., SEO, J. H. & KIM, J. Y. 2018. Flubendazole elicits anti-metastatic effects in triple-negative breast cancer via STAT3 inhibition. *Int J Cancer*, 143, 1978-1993.
- OKU, M., ISHINO, R., UCHIDA, S., IMATAKI, O., SUGIMOTO, N., TODO, T. & KADOWAKI, N. 2021. Oncolytic herpes simplex virus type 1 (HSV-1) in combination with lenalidomide for plasma cell neoplasms. *Br J Haematol*, 192, 343-353.
- OLIVA, S., GAMBELLA, M., BOCCADORO, M. & BRINGHEN, S. 2017. Systemic virotherapy for multiple myeloma. *Expert Opin Biol Ther*, 17, 1375-1387.
- O'BRYAN, S. M. & MATHIS, J. M. 2018. Oncolytic Virotherapy for Breast Cancer Treatment. *Current Gene Therapy*, 18, 192-205.
- PAROLINI, I., FEDERICI, C., RAGGI, C., LUGINI, L., PALLESCHI, S., DE MILITO, A., COSCIA, C., IESSI, E., LOGOZZI, M., MOLINARI, A., COLONE, M., TATTI, M., SARGIACOMO, M. & FAIS, S. 2009. Microenvironmental pH Is a Key Factor for Exosome Traffic in Tumor Cells. *J Biol Chem*, 284, 34211-34222.
- PEGTEL, D. M., COSMOPOULOS, K., THORLEY-LAWSON, D. A., VAN EIJDHOVEN, M. A. J., HOPMANS, E. S., LINDENBERG, J. J., DE GRUIJL, T. D., WÜRDINGER, T. & MIDDELDORP, J. M. 2010. Functional delivery of viral miRNAs via exosomes. *Proc Natl Acad Sci U S A*, 107, 6328-6333.
- PEGTEL, D. M., PEFEROEN, L. & AMOR, S. 2014. Extracellular vesicles as modulators of cell-to-cell communication in the healthy and diseased brain. *Phil. Trans. R. Soc. B*, 369, 20130516.
- PEINADO, H., ALEČKOVIĆ, M., LAVOTSHKIN, S., MATEI, I., COSTA-SILVA, B., MORENO-BUENO, G., HERGUETA-REDONDO, M., WILLIAMS, C., GARCÍA-SANTOS, G., GHAJAR, C. M., NITADORI-HOSHINO, A., HOFFMAN, C., BADAL, K., GARCIA, B. A., CALLAHAN, M. K., YUAN, J., MARTINS, V. R., SKOG, J., KAPLAN, R. N., BRADY, M. S., WOLCHOK, J. D., CHAPMAN, P. B., KANG, Y., BROMBERG, J. & LYDEN, D. 2012. Melanoma exosomes educate bone marrow progenitor cells toward a pro-metastatic phenotype through MET. *Nat Med*, 18, 883-891.
- PEREIRA, C., GIMENEZ-XAVIER, P., PROS, E., PAJARES, M. J., MORO, M., GOMEZ, A., NAVARRO, A., CONDOM, E., MORAN, S., GOMEZ-LOPEZ, G., GRAÑA, O., RUBIO-CAMARILLO, M., MARTINEZ-MARTÍ, A., YOKOTA, J., CARRETERO, J., GALBIS, J. M., NADAL, E., PISANO, D., SOZZI, G., FELIP, E., MONTUENGA, L. M., ROZ, L., VILLANUEVA, A. & SANCHEZ-CESPEDES, M. 2017. Genomic profiling of patient-derived xenografts for lung cancer identifies B2M inactivation impairing immunorecognition. *Clin Cancer Res*, 23, 3203-3213.
- PERRIER, A., GLIGOROV, J., LEFÈVRE, G. & BOISSAN, M. 2018. The extracellular domain of Her2 in serum as a biomarker of breast cancer. *Lab Invest*, 98, 696-707.
- PILLAI, S. G., LI, S., SIDDAPPA, C. M., ELLIS, M. J., WATSON, M. A. & AFT, R. 2018. Identifying biomarkers of breast cancer micrometastatic disease in bone marrow using a patient-derived xenograft mouse model. *Breast Cancer Res*, 20, 2-2.
- PINKER, K. 2020. Preoperative MRI improves surgical planning and outcomes for ductal carcinoma in situ. *Radiology*, 295, 304-306.
- PIRET, J. & BOIVIN, G. 2011. Resistance of Herpes Simplex Viruses to Nucleoside Analogues: Mechanisms, Prevalence, and Management. *Antimicrob Agents Chemother*, 55, 459-472.
- PIRISINU, M., PHAM, T. C., ZHANG, D. X., HONG, T. N., NGUYEN, L. T. & LE, M. T. N. 2022. Extracellular vesicles as natural therapeutic agents and innate drug delivery systems for cancer treatment: Recent advances, current obstacles, and challenges for clinical translation. *Seminars in Cancer Biology*, 80, 340-355.

- POL, J. G., WORKENHE, S. T., KONDA, P., GUJAR, S. & KROEMER, G. 2020. Cytokines in oncolytic virotherapy. *Cytokine & growth factor reviews*, 56, 4-27.
- POLS, M. S. & KLUMPERMAN, J. 2009. Trafficking and function of the tetraspanin CD63. *Exp Cell Res*, 315, 1584-1592.
- PRAT, A., PASCUAL, T., DE ANGELIS, C., GUTIERREZ, C., LLOMBART-CUSSAC, A., WANG, T., CORTÉS, J., REXER, B., PARÉ, L., FORERO, A., WOLFF, A. C., MORALES, S., ADAMO, B., BRASÓ-MARISTANY, F., VIDAL, M., VEERARAGHAVAN, J., KROP, I., GALVÁN, P., PAVLICK, A. C., BERMEJO, B., IZQUIERDO, M., RODRIK-OUTMEZGUINE, V., REIS-FILHO, J. S., HILSENBECK, S. G., OLIVEIRA, M., DIECI, M. V., GRIGUOLO, G., FASANI, R., NUCIFORO, P., PARKER, J. S., CONTE, P., SCHIFF, R., GUARNERI, V., OSBORNE, C. K. & RIMAWI, M. F. 2020. HER2-Enriched Subtype and ERBB2 Expression in HER2-Positive Breast Cancer Treated with Dual HER2 Blockade. *J Natl Cancer Inst*, 112, 46-54.
- PUZANOV, I., MILHEM, M. M., MINOR, D., HAMID, O., LI, A., CHEN, L., CHASTAIN, M., GORSKI, K. S., ANDERSON, A., CHOU, J., KAUFMAN, H. L. & ANDTBACKA, R. H. I. 2016. Talimogene laherparepvec in combination with ipilimumab in previously untreated, unresectable stage IIIB-IV melanoma. *J Clin Oncol*, 34, 2619-2626.
- RAJA, S. A., ABBAS, S., SHAH, S. T. A., TARIQ, A., BIBI, N., YOUSUF, A., KHAWAJA, A., NAWAZ, M., MEHMOOD, A., KHAN, M. J. J. G. & BIOLOGY, M. 2019. Increased expression levels of Syntaxin 1A and Synaptobrevin 2/Vesicle-Associated Membrane Protein-2 are associated with the progression of bladder cancer. 42, 40-47.
- RAMAKRISHNAIAH, V., THUMANN, C., FOFANA, I., HABERSETZER, F., PAN, Q., RUITER, P., WILLEMSSEN, R., DEMMERS, J., RAJ, S., JENSTER, G., KWEKKEBOOM, J., TILANUS, H., HAAGMANS, B., BAUMERT, T. & LAAN, L. 2013. Exosome-mediated transmission of hepatitis C virus between human hepatoma Huh7.5 cells. *Proc Natl Acad Sci U S A*, 110, 13109-13113.
- RAPOSO, G. & STOORVOGEL, W. 2013a. Extracellular vesicles: Exosomes, microvesicles, and friends. *J Cell Biol*, 200, 373-383.
- RAPOSO, G. & STOORVOGEL, W. 2013b. Extracellular vesicles: Exosomes, microvesicles, and friends. *Journal of Cell Biology*, 200, 373-383.
- RATAJCZAK, J., WYSOCZYNSKI, M., HAYEK, F., JANOWSKA-WIECZOREK, A. & RATAJCZAK, M. Z. 2006. Membrane-derived microvesicles: important and underappreciated mediators of cell-to-cell communication. *Leukemia*, 20, 1487-1495.
- RECORD, M., CARAYON, K., POIROT, M. & SILVENTE-POIROT, S. 2014. Exosomes as new vesicular lipid transporters involved in cell-cell communication and various pathophysiological processes. *Biochimica et biophysica acta. Molecular and cell biology of lipids*, 1841, 108-120.
- ROBERT, C. 2020. A decade of immune-checkpoint inhibitors in cancer therapy. *Nature communications*, 11, 3801-3801.
- ROBERTS-DALTON, H. D., COCKS, A., FALCON-PEREZ, J. M., SAYERS, E. J., WEBBER, J. P., WATSON, P., CLAYTON, A. & JONES, A. T. 2017. Fluorescence labelling of extracellular vesicles using a novel thiol-based strategy for quantitative analysis of cellular delivery and intracellular traffic. *Nanoscale*, 9, 13693-13706.
- RODE, K., DÖHNER, K., BINZ, A., GLASS, M., STRIVE, T., BAUERFEIND, R. & SODEIK, B. 2011. Uncoupling Uncoating of Herpes Simplex Virus Genomes from Their Nuclear Import and Gene Expression. *J Virol*, 85, 4271-4283.
- ROSANO, C., ZUCCOTTI, S. & BOLOGNESI, M. 2005. The three-dimensional structure of $\beta 2$ microglobulin: Results from X-ray crystallography. *Biochimica et biophysica acta. Proteins and proteomics*, 1753, 85-91.
- ROSFJORD, E., LUCAS, J., LI, G. & GERBER, H.-P. 2014. Advances in patient-derived tumor xenografts: From target identification to predicting clinical response rates in oncology. *Biochem Pharmacol*, 91, 135-143.
- ROUCOURT, B., MEEUSSEN, S., BAO, J., ZIMMERMANN, P. & DAVID, G. 2015. Heparanase activates the syndecan-syntenin-ALIX exosome pathway. *Cell Research*, 25, 412-428.

- RUSSELL, S. J., PENG, K.-W. & BELL, J. C. 2012. Oncolytic virotherapy. *Nat Biotechnol*, 30, 658-670.
- RUSSELL, S. J. P. K. W. & BELL, J. C. 2012. Oncolytic virotherapy. *Nature biotechnology. anatureresearch journal*, 30(7), 658.-30(7), 658.
- RYU, K. J., LEE, J. Y., PARK, C., CHO, D. & KIM, S. J. 2020. Isolation of Small Extracellular Vesicles From Human Serum Using a Combination of Ultracentrifugation With Polymer-Based Precipitation. *Ann Lab Med*, 40, 253-258.
- SABBAGH, Q., ANDRE-GREGOIRE, G., GUEVEL, L. & GAVARD, J. 2020. Vesiclemia: counting on extracellular vesicles for glioblastoma patients. *Oncogene*, 39, 6043-6052.
- SALMOND, N. & WILLIAMS, K. C. 2021. Isolation and characterization of extracellular vesicles for clinical applications in cancer - time for standardization? *Nanoscale advances*, 3, 183-1852.
- SCHLIENGER, S., CAMPBELL, S. & CLAING, A. 2013. ARF1 regulates the Rho/MLC pathway to control EGF-dependent breast cancer cell invasion. *Molecular Biology of the Cell*, 25, 17-29.
- SCHREIBER, R. D., OLD, L. J. & SMYTH, M. J. 2011. Cancer Immunoediting: Integrating Immunity's Roles in Cancer Suppression and Promotion. *Science*, 331, 1565-1570.
- SCHÖNEBERG, J., LEE, I. H., IWASA, J. H. & HURLEY, J. H. 2016. Reverse-topology membrane scission by the ESCRT proteins. *Nature Reviews Molecular Cell Biology*, 18, 5-17.
- SEDGWICK, A. E., CLANCY, J. W., OLIVIA BALMERT, M. & D'SOUZA-SCHOREY, C. 2015. Extracellular microvesicles and invadopodia mediate non-overlapping modes of tumor cell invasion. *Scientific Reports*, 5, 1-14.
- SHALHOUT, S. Z., MILLER, D. M., EMERICK, K. S. & KAUFMAN, H. L. 2023. Therapy with oncolytic viruses: progress and challenges. *Nature Reviews Clinical Oncology*.
- SHAO, H., LI, B., ZHANG, X., XIONG, Z., LIU, Y. & TANG, G. 2013. Comparison of the diagnostic efficiency for breast cancer in Chinese women using mammography, ultrasound, MRI, and different combinations of these imaging modalities. *J Xray Sci Technol*, 21, 283-292.
- SHETA, M., TAHA, E. A., LU, Y. & EGUCHI, T. 2023. Extracellular Vesicles: New Classification and Tumor Immunosuppression. *Biology*, 12, 110.
- SILVA, T. A., SMUCZEK, B., VALADÃO, I. C., DZIK, L. M., IGLESIA, R. P., CRUZ, M. C., ZELANIS, A., DE SIQUEIRA, A. S., SERRANO, S. M. T., GOLDBERG, G. S., JAEGER, R. G. & FREITAS, V. M. 2016. AHNAK enables mammary carcinoma cells to produce extracellular vesicles that increase neighboring fibroblast cell motility. *Oncotarget*, 7, 49998-50016.
- SIMMONS, A. 2002. Clinical Manifestations and Treatment Considerations of Herpes Simplex Virus Infection. *The Journal of Infectious Diseases*, 186, S71-S77.
- SIMONIAN, M., GHAFFARI, M. H. & NEGAHDARI, B. 2021. Immunotherapy for breast cancer treatment. *Iranian biomedical journal*, 25, 140-156.
- SIMS, P. J., FAIONI, E. M., WIEDMER, T. & SHATTIL, S. J. 1988. Complement proteins C5b-9 cause release of membrane vesicles from the platelet surface that are enriched in the membrane receptor for coagulation factor Va and express prothrombinase activity. *J Biol Chem*, 263, 18205-18212.
- SIVANANDAM, V., LAROCCA, C. J., CHEN, N. G., FONG, Y. & WARNER, S. G. J. M. T. O. 2019. Oncolytic Viruses and Immune Checkpoint Inhibition: The Best of Both Worlds. 13, 93.
- SJÖSTRAND, M., EKSTRÖM, K., LEE, J. J., VALADI, H., BOSSIOS, A. & LÖTVALL, J. O. 2007. Exosome-mediated transfer of mRNAs and microRNAs is a novel mechanism of genetic exchange between cells. *Nat Cell Biol*, 9, 654-659.
- SKOG, J., WÜRDINGER, T., VAN RIJN, S., MEIJER, D. H., GAINCHE, L., SENA-ESTEVEZ, M., CURRY, W. T., CARTER, B. S., KRICHEVSKY, A. M. & BREAKEFIELD, X. O. 2008. Glioblastoma microvesicles transport RNA and proteins that promote tumour growth and provide diagnostic biomarkers. *Nat Cell Biol*, 10, 1470-1479.
- SMYTH, T., KULLBERG, M., MALIK, N., SMITH-JONES, P., GRANER, M. W. & ANCHORDOQUY, T. J. 2015. Biodistribution and delivery efficiency of unmodified tumor-derived exosomes. *J Control Release*, 199, 145-155.

- SONNENSCHNEIN, C. & SOTO, A. M. 2016. Carcinogenesis explained within the context of a theory of organisms. *Prog Biophys Mol Biol*, 122, 70-76.
- SOO, C. Y., SONG, Y., ZHENG, Y., CAMPBELL, E. C., RICHES, A. C., GUNN-MOORE, F. & POWIS, S. J. 2012. Nanoparticle tracking analysis monitors microvesicle and exosome secretion from immune cells. *Immunology*, 136, 192-197.
- SPRAGUE, L., LEE, J. M., HUTZEN, B. J., WANG, P.-Y., CHEN, C.-Y., CONNER, J., BRAIDWOOD, L., CASSADY, K. A. & CRIPE, T. P. 2018. High mobility group box 1 influences HSV1716 spread and acts as an adjuvant to chemotherapy. *Viruses*, 10, 132.
- SUCKER, A., ZHAO, F., REAL, B., HEEKE, C., BIELEFELD, N., MAßEN, S., HORN, S., MOLL, I., MALTANER, R., HORN, P. A., SCHILLING, B., SABBATINO, F., LENNERZ, V., KLOOR, M., FERRONE, S., SCHADENDORF, D., FALK, C. S., GRIEWANK, K. & PASCHEN, A. 2014. Genetic evolution of T-cell resistance in the course of melanoma progression. *Clin Cancer Res*, 20, 6593-6604.
- SUGIURA, K. & STOCK, C. C. 1952. Studies in a tumor spectrum. I. Comparison of the action of methylbis (2-chloroethyl)amine and 3-bis(2-chloroethyl)aminomethyl-4-methoxymethyl -5-hydroxy-6-methylpyridine on the growth of a variety of mouse and rat tumors. *Cancer*, 5, 382-402.
- SULIMAN, M. E., YILMAZ, M. I., CARRERO, J. J., QURESHI, A. R., SAGLAM, M., IPCIOGLU, O. M., YENICESU, M., TONG, M., HEIMBÜRGER, O., BARANY, P., ALVESTRAND, A., LINDHOLM, B. & STENVINKEL, P. 2008. Novel Links between the Long Pentraxin 3, Endothelial Dysfunction, and Albuminuria in Early and Advanced Chronic Kidney Disease. *Clin J Am Soc Nephrol*, 3, 976-985.
- SUN, Y.-S., ZHAO, Z., YANG, Z.-N., XU, F., LU, H.-J., ZHU, Z.-Y., SHI, W., JIANG, J., YAO, P.-P. & ZHU, H.-P. 2017. Risk Factors and Preventions of Breast Cancer. *Int J Biol Sci*, 13, 1387-1397.
- SUNDQVIST, A., VASILAKI, E., VOYTYUK, O., BAI, Y., MORIKAWA, M., MOUSTAKAS, A., MIYAZONO, K., HELDIN, C.-H., TEN DIJKE, P. & VAN DAM, H. 2020. TGF β and EGF signaling orchestrates the AP-1- and p63 transcriptional regulation of breast cancer invasiveness. *Oncogene*, 39, 4436-4449.
- SURH, C. D. & SPRENT, J. 2008. Homeostasis of Naive and Memory T Cells. *Immunity*, 29, 848-862.
- TAN, G., KASUYA, H., SAHIN, T. T., YAMAMURA, K., WU, Z., KOIDE, Y., HOTTA, Y., SHIKANO, T., YAMADA, S. & KANZAKI, A. J. I. J. O. C. 2015. Combination therapy of oncolytic herpes simplex virus HF10 and bevacizumab against experimental model of human breast carcinoma xenograft. 136, 1718-1730.
- TAYLOR, R. C., CULLEN, S. P. & MARTIN, S. J. 2008. Apoptosis: Controlled demolition at the cellular level. *Nature Reviews Molecular Cell Biology*, 9, 231-241.
- TEIS, D., SAKSENA, S. & EMR, S. D. 2008. Ordered Assembly of the ESCRT-III Complex on Endosomes Is Required to Sequester Cargo during MVB Formation. *Dev Cell*, 15, 578-589.
- THOMAS, D. L. & FRASER, N. W. 2003. HSV-1 therapy of primary tumors reduces the number of metastases in an immune-competent model of metastatic breast cancer. *Mol Ther*, 8, 543-551.
- THOMPSON, A. G., GRAY, E., HEMAN-ACKAH, S. M., MÄGER, I., TALBOT, K., EL ANDALOUSSI, S., WOOD, M. J. & TURNER, M. R. 2016. Extracellular vesicles in neurodegenerative disease-pathogenesis to biomarkers. *Nature Reviews Neurology*, 12, 346-357.
- THÉRY, C., AMIGORENA, S., RAPOSO, G. & CLAYTON, A. 2006. Isolation and characterization of exosomes from cell culture supernatants and biological fluids. *Current protocols in cell biology*, Chapter 3, Unit 3.22-Unit 3.22.
- TORO BEJARANO, M. & MERCHAN, J. R. 2015. Targeting tumor vasculature through oncolytic virotherapy: recent advances. *Oncolytic Virother*, 4, 169-181.
- TRAMS, E. G., LAUTER, C. J., NORMAN SALEM, JR. & HEINE, U. 1981. Exfoliation of membrane ectoenzymes in the form of micro-vesicles. *BBA - Biomembranes*, 645, 63-70.
- TYANOVA, S., TEMU, T., SINITYCYN, P., CARLSON, A., HEIN, M. Y., GEIGER, T., MANN, M. & COX, J. 2016. The Perseus computational platform for comprehensive analysis of (prote)omics data. *Nat Methods*, 13, 731-740.

- UCHE, I. K., KOUSOULAS, K. G. & RIDER, P. J. F. 2021. The effect of herpes simplex virus-type-1 (Hsv-1) oncolytic immunotherapy on the tumor microenvironment. *Viruses*, 13, 1200.
- UPADHYA, D. & SHETTY, A. K. 2021. Promise of extracellular vesicles for diagnosis and treatment of epilepsy. *Epilepsy Behav*, 121, 106499-106499.
- VAN DER VLIST, E. J., NOLTE-'T HOEN, E. N. M., STOORVOGEL, W., ARKESTEIJN, G. J. A. & WAUBEN, M. H. M. 2012. Fluorescent labeling of nano-sized vesicles released by cells and subsequent quantitative and qualitative analysis by high-resolution flow cytometry. *Nat Protoc*, 7, 1311-1326.
- VAN NIEL, G., D'ANGELO, G. & RAPOSO, G. 2018. Shedding light on the cell biology of extracellular vesicles. *Nat Rev Mol Cell Biol*, 19, 213-228.
- VAN NIEL, G., BERGAM, P., DI CICCIO, A., HURBAIN, I., LO CICERO, A., DINGLI, F., PALMULLI, R., FORT, C., POTIER, MARIE C., SCHURGERS, LEON J., LOEW, D., LEVY, D. & RAPOSO, G. 2015. Apolipoprotein E Regulates Amyloid Formation within Endosomes of Pigment Cells. *Cell Rep*, 13, 43-51.
- VAN NIEL, G., CHARRIN, S., SIMOES, S., ROMAO, M., ROCHIN, L., SAFTIG, P., MARKS, MICHAEL S., RUBINSTEIN, E. & RAPOSO, G. 2011. The Tetraspanin CD63 Regulates ESCRT-Independent and -Dependent Endosomal Sorting during Melanogenesis. *Dev Cell*, 21, 708-721.
- VERWEIJ, F. J., BEBELMAN, M. P., JIMENEZ, C. R., GARCIA-VALLEJO, J. J., JANSSEN, H., NEEFJES, J., KNOL, J. C., DE GOEIJ-DE HAAS, R., PIERSMA, S. R., BAGLIO, S. R., VERHAGE, M., MIDDELDORP, J. M., ZOMER, A., VAN RHEENEN, J., COPPOLINO, M. G., HURBAIN, I., RAPOSO, G., SMIT, M. J., TOONEN, R. F. G., VAN NIEL, G. & PEGTEL, D. M. 2018. Quantifying exosome secretion from single cells reveals a modulatory role for GPCR signaling. *Journal of Cell Biology*, 217, 1129-1142.
- VILLARROYA-BELTRI, C., BAIXAULI, F., MITTELBRUNN, M., FERNÁNDEZ-DELGADO, I., TORRALBA, D., MORENO-GONZALO, O., BALDANTA, S., ENRICH, C., GUERRA, S. & SÁNCHEZ-MADRID, F. 2016. ISGylation controls exosome secretion by promoting lysosomal degradation of MVB proteins. *Nature Communications*, 7.
- VOGEL, A., UPADHYA, R. & SHETTY, A. K. 2018. Neural stem cell derived extracellular vesicles: Attributes and prospects for treating neurodegenerative disorders. *EBioMedicine*, 38, 273-282.
- WAKS, A. G. & WINER, E. P. 2019. Breast Cancer Treatment: A Review. *JAMA*, 321, 288-300.
- WALKER, S., BUSATTO, S., PHAM, A., TIAN, M., SUH, A., CARSON, K., QUINTERO, A., LAFRENCE, M., MALIK, H., SANTANA, M. X. & WOLFRAM, J. 2019. Extracellular vesicle-based drug delivery systems for cancer treatment. *Theranostics*, 9, 8001-8017.
- WANG, H., LIU, B. & WEI, J. 2021. Beta2-microglobulin(B2M) in cancer immunotherapies: Biological function, resistance and remedy. *Cancer Lett*, 517, 96-104.
- WANG, Q. & LU, Q. 2017. Plasma membrane-derived extracellular microvesicles mediate non-canonical intercellular NOTCH signaling. *Nature Communications*, 8, 1-8.
- WANG, X., LI, Y., LIU, S., YU, X., LI, L., SHI, C., HE, W., LI, J., XU, L., HU, Z., YU, L., YANG, Z., CHEN, Q., GE, L., ZHANG, Z., ZHOU, B., JIANG, X., CHEN, S. & HE, S. 2014. Direct activation of RIP3/MLKL-dependent necrosis by herpes simplex virus 1 (HSV-1) protein ICP6 triggers host antiviral defense. *Proc Natl Acad Sci U S A*, 111, 15438-15443.
- WEI, R., ZHAO, L., KONG, G., LIU, X., ZHU, S., ZHANG, S. & MIN, L. 2020. Combination of Size-Exclusion Chromatography and Ultracentrifugation Improves the Proteomic Profiling of Plasma-Derived Small Extracellular Vesicles. *Biological procedures online*, 22, 12-12.
- WEI, Y., WANG, D., JIN, F., BIAN, Z., LI, L., LIANG, H., LI, M., SHI, L., PAN, C., ZHU, D., CHEN, X., HU, G., LIU, Y., ZHANG, C. Y. & ZEN, K. 2017. Pyruvate kinase type M2 promotes tumour cell exosome release via phosphorylating synaptosome-associated protein 23. *Nature Communications*, 8, 1-12.
- WHITLEY, R. J. & ROIZMAN, B. 2001. Herpes simplex virus infections. *Lancet*, 357, 1513-1518.

- WHITTLE, J. R., LEWIS, M. T., LINDEMAN, G. J. & VISVADER, J. E. 2015. Patient-derived xenograft models of breast cancer and their predictive power. *Breast Cancer Res*, 17, 17-17.
- WIKLANDER, O. P. B., NORDIN, J. Z., O'LOUGHLIN, A., GUSTAFSSON, Y., CORSO, G., MÄGER, I., VADER, P., LEE, Y., SORK, H., SEOW, Y., HELDRING, N., ALVAREZ-ERVITI, L., SMITH, C. I. E., LE BLANC, K., MACCHIARINI, P., JUNGBLUTH, P., WOOD, M. J. A. & ANDALOUSSI, S. E. L. 2015. Extracellular vesicle in vivo biodistribution is determined by cell source, route of administration and targeting. *J Extracell Vesicles*, 4, 1-n/a.
- WILLIAMS, C., PAZOS, R., ROYO, F., GONZÁLEZ, E., ROURA-FERRER, M., MARTINEZ, A., GAMIZ, J., REICHARDT, N.-C. & FALCÓN-PÉREZ, J. M. 2019. Assessing the role of surface glycans of extracellular vesicles on cellular uptake. *Sci Rep*, 9, 11920-14.
- WILLMS, E., JOHANSSON, H. J., MÄGER, I., LEE, Y., BLOMBERG, K. E. M., SADIK, M., ALAARG, A., SMITH, C. I. E., LEHTIÖ, J., EL ANDALOUSSI, S., WOOD, M. J. A. & VADER, P. 2016. Cells release subpopulations of exosomes with distinct molecular and biological properties. *Scientific Reports*, 6, 1-12.
- WOOD, L. W. & SHILLITOE, E. J. 2011. Effect of a caspase inhibitor, zVADfmk, on the inhibition of breast cancer cells by herpes simplex virus type 1. *Cancer Gene Ther*, 18, 685-694.
- WORTZEL, I., DROR, S., KENIFIC, C. M. & LYDEN, D. 2019. Exosome-Mediated Metastasis: Communication from a Distance. *Dev Cell*, 49, 347-360.
- WU, Q., ZHOU, W., YIN, S., ZHOU, Y., CHEN, T., QIAN, J., SU, R., HONG, L., LU, H., ZHANG, F., XIE, H., ZHOU, L. & ZHENG, S. 2019. Blocking Triggering Receptor Expressed on Myeloid Cells-1-Positive Tumor-Associated Macrophages Induced by Hypoxia Reverses Immunosuppression and Anti-Programmed Cell Death Ligand 1 Resistance in Liver Cancer. *Hepatology*, 70, 198-214.
- XAVIER, C. P. R., CAIRES, H. R., BARBOSA, M. A. G., BERGANTIM, R., GUIMARÃES, J. E. & VASCONCELOS, M. H. 2020. The Role of Extracellular Vesicles in the Hallmarks of Cancer and Drug Resistance. *Cells*, 9, 1141.
- XIE, W., SUN, Y., ZENG, Y., HU, L., ZHI, J., LING, H., ZHENG, X., RUAN, X. & GAO, M. 2022. Comprehensive analysis of PPPCs family reveals the clinical significance of PPP1CA and PPP4C in breast cancer. *Bioengineered*, 13, 190-205.
- YIP, C. C. Y., SRIDHAR, S., LEUNG, K.-H., CHENG, A. K. W., CHAN, K.-H., CHAN, J. F. W., CHENG, V. C. C. & YUEN, K.-Y. 2019. Evaluation of RealStar® Alpha Herpesvirus PCR Kit for Detection of HSV-1, HSV-2, and VZV in Clinical Specimens. *Biomed Res Int*, 2019, 5715180-6.
- YOON, Y. J., KIM, O. Y. & GHO, Y. S. 2014. Extracellular vesicles as emerging intercellular comunicasomes. *BMB reports*, 47, 531-539.
- YUAN, Z.-Y., ZHANG, L., LI, S., QIAN, X.-Z. & GUAN, Z.-Z. 2003. Safety of an E1B deleted adenovirus administered intratumorally to patients with cancer. *Ai Zheng*, 22, 310.
- YÁÑEZ-MÓ, M., BARREIRO, O., GORDON-ALONSO, M., SALA-VALDÉS, M. & SÁNCHEZ-MADRID, F. 2009. Tetraspanin-enriched microdomains: a functional unit in cell plasma membranes. *Trends Cell Biol*, 19, 434-446.
- YÁÑEZ-MÓ, M., SILJANDER, P. R. M., ANDREU, Z., BEDINA ZAVEC, A., BORRÀS, F. E., BUZAS, E. I., BUZAS, K., CASAL, E., CAPPELLO, F., CARVALHO, J., COLÁS, E., CORDEIRO-DA SILVA, A., FAIS, S., FALCON-PEREZ, J. M., GHOBRIAL, I. M., GIEBEL, B., GIMONA, M., GRANER, M., GURSEL, I., GURSEL, M., HEEGAARD, N. H. H., HENDRIX, A., KIERULF, P., KOKUBUN, K., KOSANOVIC, M., KRALJ-IGLIC, V., KRÄMER-ALBERS, E.-M., LAITINEN, S., LÄSSER, C., LENER, T., LIGETI, E., LINĚ, A., LIPPS, G., LLORENTE, A., LÖTVALL, J., MANČEK-KEBER, M., MARCILLA, A., MITTELBRUNN, M., NAZARENKO, I., NOLTE-'T HOEN, E. N. M., NYMAN, T. A., O'DRISCOLL, L., OLIVAN, M., OLIVEIRA, C., PÁLLINGER, É., DEL PORTILLO, H. A., REVENTÓS, J., RIGAU, M., ROHDE, E., SAMMAR, M., SÁNCHEZ-MADRID, F., SANTARÉM, N., SCHALLMOSER, K., STAMPE OSTENFELD, M., STOOVVOGEL, W., STUKELJ, R., VAN DER GREIN, S. G., HELENA VASCONCELOS, M., WAUBEN, M. H. M. & DE WEVER, O. 2015. Biological properties of extracellular vesicles and their physiological functions. *J Extracell Vesicles*, 4, 27066-n/a.

- ZABOROWSKI, M. P., BALAJ, L., BREAKFIELD, X. O. & LAI, C. P. 2015. Extracellular Vesicles: Composition, Biological Relevance, and Methods of Study. *Bioscience*, 65, 783-797.
- ZEELBERG, I. S., OSTROWSKI, M., KRUMEICH, S., BOBRIE, A., JANCIC, C., BOISSONNAS, A., DELCAYRE, A., PECQ, J. B. L., COMBADIÈRE, B., AMIGORENA, S. & THERY, C. 2008. Targeting tumor antigens to secreted membrane vesicles in vivo induces efficient antitumor immune responses. *Cancer Res*, 68, 1228-1235.
- ZHANG, B., ZHOU, Y. L., CHEN, X., WANG, Z., WANG, Q., JU, F., REN, S., XU, R., XUE, Q. & WU, Q. 2019. Efficacy and safety of CTLA-4 inhibitors combined with PD-1 inhibitors or chemotherapy in patients with advanced melanoma. *Int Immunopharmacol*, 68, 131-136.
- ZHANG, J. Q. & PLITAS, G. 2021. Immunotherapeutic strategies in breast cancer: A clinical update. *J Surg Oncol*, 123, 710-717.
- ZHANG, W., HU, X., LIANG, J., ZHU, Y., ZENG, B., FENG, L., ZHAO, C., LIU, S., LIU, B. & ZHANG, K. 2020. oHSV2 Can Target Murine Colon Carcinoma by Altering the Immune Status of the Tumor Microenvironment and Inducing Antitumor Immunity. *Mol Ther Oncolytics*, 16, 158-171.
- ZOMER, A., MAYNARD, C., VERWEIJ, F. J., KAMERMANS, A., SCHÄFER, R., BEERLING, E., SCHIFFELERS, R. M., DE WIT, E., BERENQUER, J., ELLENBROEK, S. I. J., WURDINGER, T., PEGTEL, D. M. & VAN RHEENEN, J. 2015. In vivo imaging reveals extracellular vesicle-mediated phenocopying of metastatic behavior. *Cell*, 161, 1046-1057.
- ZOU, P., TANG, R. & LUO, M. 2020. Oncolytic virotherapy, alone or in combination with immune checkpoint inhibitors, for advanced melanoma: A systematic review and meta-analysis. *Int Immunopharmacol*, 78, 106050-106050.
- ŁUKASIEWICZ, S., CZECZELEWSKI, M., FORMA, A., BAJ, J., SITARZ, R. & STANISŁAWEK, A. 2021. Breast cancer—epidemiology, risk factors, classification, prognostic markers, and current treatment strategies—An updated review. *Cancers*, 13, 4287.